**Title**
Investigations of Altered Proteome Dynamics in Calorie Restriction, Insulin Resistance, and Type 2 Diabetes



**Author**
Khambatta, Cyrus Farrokh

**Publication Date**
2012

Peer reviewed|Thesis/dissertation

# Investigations of Altered Proteome Dynamics in Calorie Restriction, Insulin Resistance and Type 2 Diabetes

by

**CYRUS FARROKH KHAMBATTA**

A dissertation submitted in partial satisfaction of the
requirements for the degree of

**Doctor of Philosophy**

In

**Molecular & Biochemical Nutrition**

In the

**Graduate Division of the University of California at Berkeley**

**Committee in charge:**

Professor Marc K. Hellerstein, Chair, Molecular and Biochemical Nutrition
Professor Wally Wang, Molecular and Biochemical Nutrition
Professor George A. Brooks, Integrative Biology

**Fall 2012**

# Copyright

# Abstract

Investigations of Altered Proteome Dynamics
in Calorie Restriction, Insulin Resistance
and Type 2 Diabetes

by

Cyrus Khambatta

Doctor of Philosophy in Molecular & Biochemical Nutrition

University of California, Berkeley

Professor Marc Hellerstein, M.D., Ph.D, Chair

Proteins are the ultimate laborers in biological systems. The behavior of a cell is governed by the dynamic interactions between thousands of proteins; a tissue is governed by the interactions of thousands of cells; and an organism is governed by the interaction of multiple tissues. The maintenance of protein homeostasis (proteostasis) is therefore a critical component of proper cellular function and the response to constantly changing environmental signals.

The dynamic proteomic approach used in these rodent studies involves the administration of $^{2}H_2O$ in the drinking water to achieve a target body water enrichment of 5%. During the labeling period, *in vivo* protein synthesis occurs, resulting in the creation of "heavy" proteins identical to their "light" counterparts in function, differing only in the incorporation of deuterium atoms at specific positions in the constituent amino acids from which they are comprised. These peptides are then resolved by high-affinity liquid chromatography mass spectrometry (LC-MS), resulting in the identification of hundreds to thousands of proteins from a single tissue sample. Using this experimental approach, we investigated the effect of calorie restriction (CR), insulin resistance, and diabetes on dynamic protein synthesis.

To date, CR has taken center stage as the most effective intervention in lifespan extension. Despite this, the biological mechanisms underlying increased health and longevity have yet to be fully described. While a growing body of evidence suggests that CR promotes significant gain-of-function attributes in mitochondria, a verdict on whether CR promotes mitochondrial biogenesis has not been established. In order to elucidate the controversy in the field regarding the response of mitochondria to reduced energy intake, we designed an experiment to study the effect of long-term CR on hepatic protein turnover. Our data provide conclusive evidence that mitochondrial protein turnover, concentration, and overall flux are reduced in response to CR, and may play central a role in mediating the health and longevity benefits of reduced energy intake.

Insulin resistance and islet cell failure are the two fundamental processes underlying type 2 diabetes. Alterations in mitochondrial protein turnover have been implicated in

the pathology of type 2 diabetes, however the specific effect of insulin resistance and diabetes on the intracellular dynamic islet proteome have yet to be described. We investigated the effects of insulin resistance and diabetes on the synthesis of proteins from isolated rat islets for the first time, using both $^{2}H_{2}O$ (heavy water) labeling and SILAM quantitative proteomics. Using this approach, we measured fractional and absolute synthesis rates of cytoskeletal, glycolytic, mitochondrial, ER, and ribosomal proteins, the principal pathways responsible for glucose stimulated insulin secretion (GSIS). We found that insulin resistance increased the fractional synthesis rates (FSR) of 97% of all measured islet proteins, and the subsequent transition to diabetes resulted in the selective impairment of ribosomal protein synthesis. Our findings suggest that the rapid rate of islet cell proliferation due to insulin resistance is accompanied by increased fractional and absolute synthesis of critical GSIS proteins, and that the failure of islets results mainly in impaired ribosomal pathway flux, independent of alterations in mitochondrial metabolism. Our data suggest that the rapid rate of islet cell proliferation due to insulin resistance is accompanied by increased fractional and absolute synthesis of critical GSIS components, and that the failure of islet cells in diabetes results mainly in impaired ribosomal pathway flux, independent of alterations in mitochondrial protein metabolism.

# Table of Contents

# Acknowledgements

To leave this page blank would be a sin. To pretend as though I did all the work contained within this document is an outright lie. To undermine the support given to me by friends and family during this time in my life would be selfish.
Therefore, I have no choice but to acknowledge and thank those that significantly contributed to my life as a graduate student, and to offer my gratitude for having put up with me for the past five years. I also decided to include pictures of those I am acknowledging, mainly for the humor it will provide in the future.

**Dr. Marc Hellerstein, M.D., Ph.D.**

The man, the myth, the legend. If you've ever seen the movie *Good Will Hunting*, then you understand the mental gymnastics that this man can play with the rest of the people in his life. Part genius, part athlete, part mystery – Marc Hellerstein is a true renaissance man.
I'll never forget the first time I met with Marc in his laboratory during my application process to graduate school. We talked about my research interests, the types of questions that he has investigated in the past, and touched our personal interests as athletes. Marc told me that he and his buddies in graduate school would run some god awful 17 miles a day, because they loved to run, but more importantly because they were bored. Who has time to run 17 miles a day when enrolled in a M.D. Ph.D. program? Marc Hellerstein does. The conversation continued, I started telling him about my monkey-like high carbohydrate diet, and he responded by saying that he believes that high carbohydrate diets are essential for athletic performance. I asked him what types of carbohydrates he consumes - whether they come mainly from pastas and grains, or from fruit. "Hard candy," he responded. "I get my carbohydrates mainly from candy." I laughed, thinking that he was joking, after which he stood up, rifled through his jean pocket for 10 seconds, and emerged with a collection of peppermints and butterscotch candies. He wasn't joking. The best part is that they appeared to be over a decade old, which didn't surprise me for some reason.
About a year later, I had joined his laboratory, and was developing a research plan for an upcoming fellowship application. I scheduled a meeting with him that started 3 hours late, at which point I showed him my proposal and asked for his opinion. He seemed quiet tired at the time, but shrugged off his lethargy and gave constructive feedback. About 10 minutes into our meeting, I looked down to read the requirements of the fellowship application, and then looked up at him no more than 10 seconds later. During that time, Marc had fallen into a deep sleep; his now sat slouched in his chair, his chin resting on his chest. This was the first time I had witnessed true narcolepsy firsthand. I didn't know what to do, so in an effort to not embarrass him, I put my head down started talking with a loud voice, and he woke up instantly. From that point onwards, I witnessed frequent narcoleptic episodes; in lab meeting, in seminar, in personal conversations. Anyone in need of sleep is susceptible to such episodes,

however Marc's true genius became evident after falling asleep for more than 30 minutes in the middle of a weekly seminar, violently waking up to the sound of clapping. His hand was the first to go up. "You mentioned in the beginning of your talk that bile acids are measured in the blood, however is the activity of their cognate receptors more affected by enterohepatic recycling within the gastrointestinal tract rather than from bile acids in circulation?" Marc, how the hell did you just ask such an involved question? You were asleep.

In the ensuing years, as our dynamic proteomic technology improved, Marc helped design many intelligent studies, and provided excellent feedback on my personal projects. How one man can accomplish so much in life baffles everyone that knows him. And how he can be an M.D. at UCSF, a professor at UC Berkeley, and the founder of Kinemed, Inc., a biotech startup company in Emeryville, while maintaining a suave, gracious and socially graceful demeanor is what makes Marc Hellerstein a man like no other.

**Dr. Wally Wang, Ph.D.**

When I first entered graduate school, I rotated in the laboratory of Wally Wang, and quickly realized that not only is he a scientific freight train, he is a kind and gentle man whose personality is extremely refreshing in the world of academia. Wally and I struck up an instant friendship, and often times I found myself in his office talking about NCAA basketball rather than anything even remotely science related.

Wally experienced the pleasure of watching me squirm during my qualifying exam, but instead of torturing me like a particular individual (who shall remain nameless), Wally asked me questions that allowed me to demonstrate my knowledge and preparation, and didn't attempt to flex his muscles of biochemical wisdom. Once again, he proved to me that he is a truly exceptional individual.

I know I can count on Wally to give me great feedback on my research, to guide me in the right direction, and to talk smack about wierdos in the department. He has only been a member of the department for about 6 years, and is always regarded by the students in the department as a gem, a shoe-in for what is considered a "fair" member of a qualifying exam committee, and a pleasant person to be around. If you're lucky, you can catch him in his office pretending to write a grant, watching his true love – the San Francisco Giants.

**Dr. George Brooks, Ph.D.**

If you've never heard of the godfather of exercise physiology, then allow me to introduce you to Dr. Brooks. He has authored more papers than there are countries on this planet, is the mastermind behind the sports drink Cytomax, invented a branch of exercise physiology dedicated to disproving the myth that "lactic acid hampers athletic performance," and is consistently rated by UC Berkeley students as one of their favorite professors of all time. To say that Dr. Brooks is a genius is an understatement worthy of correction.

When I first met Dr. Brooks, he had come to teach a seminar to a small group of confused first year graduate students about the basics of exercise physiology and metabolism. He lectured about lactate metabolism, glycogen depletion, whole body fuel utilization, oxidative phosphorylation, mitochondrial structure and function, and a litany of other topics that rode the fine line between fascinating and totally confusing. But of course, when Dr. Brooks lectures, you never admit that you don't understand what he's talking about. Instead, you go home, read like a madman, then return to class the next week as the resident expert in that topic. I left his first seminar thinking to myself, "Man, that guy is cool, how can I download the contents of his brain into mine?" Over the next few months I can safely say that Dr. Brooks didn't think about me even once, however our fated encounter in the RSF one day changed our relationship completely.

I saw him on the exercise bike, spinning his legs faster than I thought was humanly possible. His shirt was dripping with sweat, his gaze was complete focus, and he was breathing as if he had just been chased by a wolf. At that moment I realized that Dr. Brooks was not only a intellectual badass, but a physical specimen worthy of much respect for his ability to shame the roomful of "low intensity" undergraduate exercisers.

Over the next four years, Dr. Brooks taught me a lot about the intricacies of oxygen utilization, cardiac output, muscle contractility, fatty acid oxidation, and mitochondrial biogenesis to name a few. He served as the principal investigator on a study to measure the effect of high plasma lactate levels on $VO_2$ max, although in reality I think he just enjoyed watching macho athletes collapse from hypoxia. He allowed me to take part in the study, and found that as a type 1 diabetic my circulating lactate levels at rest and during exercise were freakishly high. As if I needed a well respected academic to confirm that I was a freak of nature.

The beauty of Dr. Brooks multidimensional - he knows more than most small nations, he is incredibly personable, he owned Floyd Landis' bike (before it was stolen from his garage), he loves to travel, and he appreciates cracking silly jokes during intense academic debate. I'll never forget the way he rescued me during my qualifying exam, amidst a series of challenging questions regarding the Michelis-Menten kinetics of two hypothetical enzymes. I was stumped. I was exhausted. I didn't understand the questions. I wanted to crawl into a hole in the ground to escape the intellectual punishment. Worst of all, I didn't care about the line of questioning, and thought that the exercise was futile. Dr. Brooks saw my frustration, my confusion, and my lack of enthusiasm, and calmly continued the line of questioning by asking me a question in

which the answer was encoded. I looked at him, said exactly what he wanted me to say, received a head nod from the entire committee, then slapped him a hypothetical high-five.

At that moment I knew that Dr. Brooks and I were on the same team. Forever.

And quite frankly, I wouldn't want to be anywhere else.

**Larry Thompson**

If you ever wanted to know what a true badass looks and smells like, look no further. Larry Thompson is your man. I had the pleasure of working with this gentleman for the first 2 years of my graduate work, until UC Berkeley made the terrible decision, and I repeat *terrible* decision at moving him from the department of Nutrition to some dysfunctional centralized purchasing office.

Practically every day I would go down to LT's office and waste my lunch hour schmoozing with this ex-navy officer, listening to stories of his escapades in Guam, Japan, and practically every country with beautiful women. He would tell me about his desire to become the lead bassist in a rock band in which I would play the role of not-so-talented-drummer.

You see, the thing that made LT the coolest man in America is a combination of many talents, which would take pages to explain. Suffice it to say that he is a one-man wrecking crew when it comes to organizing the purchases and returns of many dysfunctional labs, and he does so with a giant goofy smile on his face at all times. Unless, of course, someone is pissing him off, at which point he'll come up to you with his coined expression, "*Maaaaaaaan*." LT is the type of guy you could talk to for days before he came even close to running out of material. I wouldn't hesitate to sit in a space shuttle with this man and take a 2-month trip to the moon. That is, as long as I got more stories of what it's like to be a gangsta pimp hustla.

When Larry left the department, it got quiet. Not so awesomely quiet. Don't get me wrong the department was still a fun place to go, but without the ability to schmooze with my man, going to the ground floor lost a serious amount of excitement. It's all good though, because I quickly promoted LT to the list of life-long friends, so even if he tries to get rid of me, he'll have one hell of a difficult time.

**Dr. Matthew Bruss, Ph.D.**

I'll never forget the first few days of my rotation in the Hellerstein laboratory. I knew just about nothing, started playing with fancy looking toys, and shot the shit with this guy named Matt who reminded me of a friend from college. I could tell he was an athlete, had a lot of fun on the weekends, had a ton of friends, subscribed to the "work hard, play harder" mentality, took his work seriously but his social life more seriously, and was damn near a professional drinker. After working together for two days, I stood in front of him one day just as I was leaving to go home, and said the words, "Dude. I feel like you and I are going to get along REAL well. I'm excited to be here and work with you, because it's going to lead to some great things." He calmly smiled, nodded, and said, "I was thinking the same thing."

After spilling my feelings to this teenage heartthrob, the two of us continued to work together for four years, and made sure that the Hellerstein lab was always a place of comedic refuge. Taking anything seriously became a significant challenge, aside from the fact that keeping up with Dr. Bruss' idea factory required serious concentration. I'm not sure that any human in history has come up with more ideas than did Dr. Bruss in that four year period. Fortunately, we acted on only a few, and let the rest die a miserable death in the cemetery of lost opportunities.

Between the Mitch Hedberg standup comedy and "old timey honkey tonk" as he so often calls it, our days in the graduate department were replete with constant ridiculing, watching sports highlights, a vertical jumping contest (which I won by the way), and an ongoing tally to count the number of times a human being could say the words, "right, right, right, right, right," between words of real substance. Soon Dr. Bruss' vocabulary expanded to contain the words, "like" and "so," a shining example of the effects of graduate education.

The best part of working with Dr. Bruss, you ask? The morning weight sessions at the RSF, where we act like Olympians and compete like overly aggressive elementary school kids. What work day would be complete without a series of exhausting "burn out" sessions on the rowing machine, pushing the limits of terrible technique? Perhaps the most consistent component of my graduate school experience, our morning exercise sessions constantly proved to me that (1) even when we're butt naked in adjacent showers, we still talk about nerdy things, (2) that injuries are totally worth it if they were borne out of senseless competition, and (3) that training hard while your friend takes a three month break to father his newborn son is sometimes the only way to get ahead.

So here's to an awesome four year stint with you as my sidekick, Dr. Bruss. And to an awesome 3,000 mile road trip from Berkeley to Madison in which we proved to ourselves that gossiping like middle school girls does not have to be reserved for...middle school girls. Oh, and by the way, if by the time you're 40 you're still in science and not the high-school-drama-teacher-and-cross-country-coach you've always dreamed about, I will personally fly to Wisconsin to beat you to a pulp.

**Marcy Dalidd**

I should really give Marcy my diploma.

But instead, I'll just buy her a few mangoes to thank her for doing everything for me. It's this simple: Marcy is a one-woman wrecking crew, with more hands-on experience than an entire army of graduate students, and a cheery demeanor that is sure to leave most men drooling.

I met Marcy one day when she came into our laboratory to use a fancy piece of equipment. She was working as an assistant for Roger Wong, a fellow graduate student at the time. Roger managed a team of undergraduates, and Marcy was one of the many who thought that his style sucked. So, I did what any respectable fellow graduate student would do: I stole her. I offered her three things: (1) the ability to play (and kill) thousands of mice, (2) the ability to work in an environment where she would to most of the work (and I would take the credit), and (3) the ability to play DJ in the lab (as long as she played cheesy 80's music). She accepted, not so much because of the research temptation, but because her best friend Lindsay Roberts (below) was also working in our lab. Whatever, I'll take what I can get.

Marcy worked as my chief badass for 3+ years, and provided more help than I thought was humanly possible. Simply stated, there isn't anything that Marcy can't do. Her talents include cooking overly elaborate ethnic food items for lunch, drinking excessive beer at happy hour, gossiping with Lindsay for hours at a time, littering the lab with almost perfect crossword puzzles, and giggling at top volume for inhuman amounts of time. And let's not forget the step aerobics class that I attended with her and Lindsay on a few occasions. Apparently it had been a while since I looked like a total moron, so this was the perfect opportunity for me to fail miserably in front of 50+ women. I positioned my step behind Marcy's, hoping that from this vantage point I could easily learn the choreography. After all, how hard could it really be?

Needless to say, after no more than 10 minutes in the class, I was completely lost, having no idea how to do any of the individual sequences, and certainly clueless as to how to string them together. Marcy? She looked like she belonged in a step aerobics video as one of Richard Simmons groupies. Not only were her steps perfect, she coordinated her arm movements to match, and did it all with a cheerleader-like smile.

My favorite part about Marcy is that if she wasn't effectively married to her high school sweetheart Mac (who is a total stud by the way), she could have her pick of virtually any man. I can't even count the number of guy friends who have, at one point in our graduate student era, said something to the effect of, "Dude, that girl you work with is super hot. Is she single?" And my response was always the same, "Listen. Marcy is a badass, and is absolutely not on the market. She's practically married to her boyfriend from back in the '90's, and isn't becoming a free agent anytime soon. Oh, and by the way - she's too good for you."

## Lindsay Roberts

Lindsay, Lindsay, Lindsay. Another hard hitting scientific workhorse with the potential to take over the world. Our lab was fortunate enough to acquire this talented young lady before I had joined the lab, as she was the #1 assistant to Mark Fitch when working for Sharon Fleming. Mark did the smart thing and brought her to the third floor so that she could also enjoy listening to crappy 80's music.

When I first met Lindsay, she was very short with me. Question, answer. Question, answer. I knew that there was a silly woman underneath her formal demeanor – her smile said everything I needed to know. It wasn't until Marcy joined the lab that the two best friends began to show their incredibly talkative and goofy personalities. That's when things got fun. Our conversations went from talking about school to describing our favorite bedroom practices. Soon I was asking for advice with women, and despite her 7-year serial monogamy streak, was still able to provide insight into the dating world, and female insanity in general.

Lindsay was quickly promoted from undergraduate assistant (slave) to hourly technician (indentured servant) to salaried technician (my personal bitch). In this position, she made it very clear that (a) she was smarter than me, (b) her memory far exceeds mine, and (c) in conversation, her job was to finish my sentences. Who needs to finish a thought? When you have Lindsay around, it's her job.

After working with Lindsay for a few years, I began to realize that I had more confidence in her work as a technician than almost any graduate student in the department. Couple that with a goofy personality, another step aerobics master, a woman who speaks a mile a minute, and the Nutritional Sciences department's most qualified applicant to date, and you have yourself a hilarious and integral addition to my graduate experience.

## JC Price

I remember meeting with JC one day at Kinemed so that we could strategize for a cool story about CR that we were both excited to embark upon. In some corner office, tucked away from the rest of the world, we sat and talked about doing a study on long-term CR mice to see how being hungry your entire life affects protein turnover. We had the same idea, we had the same vision. Over the next two years, we worked hard at achieving just that, and after successfully running the project, we had cranked out one of the most in-depth explorations of CR studied to date.

Because I worked with this guy so much, we got a chance to talk about life outside of science, in which JC shared with me his views on Mitt Romney, working for arrogant bosses at previous jobs, life with an army of children while working a full time job, and how he manages to grow more fruits and vegetables in his urban backyard than most small nations. And what did I share with him, you ask? My obsession for bananas and probably a whole host of untrue stories.

Some would call him a renaissance man. Personally, I think that term belittles his creative and scientific genius. Instead, I think of him as the little (6'40") engine that could. Everything that he sets his mind to, he will achieve. Everything that he does, he does with full conviction. And every time you have a silly comment to make, he'll return it with a surprisingly sharp and witty comment.

**Airlia Thompson**

When Airlia first rotated in our lab, I played the hands-off role, because the soon-to-be Dr. Bruss was truly the man with the master plan. But I couldn't help eavesdrop on their super nerd discussions, and quickly realized that Airlia was smart. There were no two ways about it. She was just plain smart.

Before I knew it, she was talking shit to me, as if someone had told her the way to my heart. Soon I was the recipient of goofiness, attitude, and practical jokes. Lucky for her, I'm not as stuck up as I look. So over the years she played some practical jokes on me, like messing with my computer mouse so that I got continually frustrated, and I returned by pretending that my bike was stolen from the lab, giving her anxiety for a week. I'll admit, I never put my mind to pulling a long, drawn-out practical joke, but as far as I'm concerned, our friendship is only starting. Sleep with one eye open, Ms. Thompson.

On the science side of things, Airlia is fantastic. She is probably the most anal person I've ever met when it comes to performing science, which is awesome if you're working together, or if you want to mess with her workspace. I know that I can trust everything she reports because chances are, she has already kept herself up at night convincing herself that her work is legit. And as long as I got restful sleep, that's all that matters.

With her powers of mental kung-fu, Airlia may one day become the first female president of our country, and because of that I'll stay close to her. I've always wanted to work in the white house, or at least tell people that I had dinner at the white house and played with the first family dog. Maybe I'll convince her that she should hire me, so that her staff will have at least one minority. After all, it looks good for public relations.

## Mark Fitch

How one man can pack so much valuable information into a regular sized human head befuddles me. How one man can have so much experience both at science and in life, and have a story for practically every conceivable situation is the magic of Mark Fitch. A.k.a Fitchipedia. If you ever engage him on the scientific front, you'll quickly realize that no matter how much you've read, no matter how much you think you know, no matter how much experience you have, Fitch knows more. It's that simple.

Radiator busted? Call Fitch. Stuck in traffic and want some comedic relief? Call Fitch. Can't remember the last 17 super bowl winners, in reverse alphabetical order? Call Fitch. What happens at every stage in the beer brewing process, from start to finish, and how has this process changed over the course of the last 2000 years? Call Fitch.

Beyond Fitch's omnipotence, there lies a true fun loving character who loves to travel, spend time with his family backpacking through the Sierra Nevadas, recount stories of his drug-induced college days, and a man who could practically manage the Oakland A's in his spare time. For years I've been thinking of a way to shrink Mark Fitch into a 3 inch tall buddy that I could carry around on my shoulder, named Pocket Fitch. That way, whenever I needed help in life, I could consult the mini-master himself.

Working with Fitch over the past 3 years has been a pleasure, and if anything, when my turn to be a contestant on *Who Wants to be a Millionaire?* arrives, when asked an esoteric question about world history, politics, geography, pop culture, physics, meteorology, or global climate change, I know *exactly* who I'm calling. Keep that phone handy, my man, you are my ticket to financial freedom.

## Candice Allister

Without doubt, the funniest thing that ever occurred in a lab meeting happened when Candice was presenting one day during the period in Marc's life that he likes to refer to as his "tired years." Who knew narcolepsy could be so funny?

Picture the scene: Candice is presenting her story, Marc is sitting at a table with his head in his hand as he quickly enters the world of sweet dreams. Candice explains to 7 other members of our lab that she is having a difficult time understanding the phenotype of her animals, and that body weight is not a great measure of the effect of her intervention. We all realize very quickly that Marc is no longer listening given that fact that he's completely asleep, head resting heavily in the palm of his propped up hand. Violently, Marc wakes up, amidst a series of lucid images, and asks, "Did you measure their mothers?" We each look at each other, trying as hard as possible to refrain from laughing, turning red in the face, as Candice eloquently retorts in a thick southern accent, "Wha?" Realizing his blunder,

Marc then backtracks, explaining that he needed some clarification about her previous slides, when all he really had to say was, "I'm sorry, I was deep asleep. Go back."
It wasn't until years later that Marc confessed that he had no idea what Candice was talking about, and that his constant sleep deprivation was really getting in the way of work. It's OK, we're all human. Candice, without knowing it, demonstrated that when you piss her off, out comes the southern accent. From that point on, I did my best to avoid hearing that southern belle, unless there was a pitcher of beer in front of her.

**Chelsea Bidlow**

Since the day Chelsea entered our lab, I can honestly say that I have never seen a more smiley individual. If Chelsea is ever not smiling, chances are she's asleep. And even then, I wouldn't be surprised if she was cracking a subtle grin. On the outside she is inquisitive, hard-working, diligent, always willing to help out, and cheerful (to say the least). It wasn't until I started hanging out with her outside of the science world that I realized how many talents this young woman actually has.
For one, she is one of those athletes that doesn't need to practice because she has "better" things to do. How many 5'4" women weighing 115 pounds would even dare join the ranks of 5 overly-aggressive weight room junkies? Not only that, what young woman would participate in high-intensity weight training with a smile on her face, next to partners on the verge of vomiting? In the time that we worked out together on a regular basis, I was constantly approached by men in the weight room asking questions like, "Who is that girl you guys always work out with? Can I get her number?" At a certain point I stopped counting the number of admirers she had in the gym, it was making my head spin. Next, we ventured into salsa dancing territory, and had a blast pretending that we knew what we were doing. In reality, I'm sure we just looked like fools, but doing so is extremely fun when accompanied by someone who doesn't take themselves seriously even for a second.
Chelsea is the type that gets herself involved with everything under the sun – teaching class to UC Berkeley students, volunteering at San Quentin prison, and working at a lab at UCSF. You would think that all that knowledge would displace monster ballad lyrics, but after she pulled out the lyrics to "I'm All Out of Love" by Air Supply one day when searching for 80's cheese, I knew at that moment that she was worth keeping around.

**Scott Turner**

I have to admit, when I first met Scott I had a difficult time reading his personality. And I pride myself on the ability to understand people, even after short interactions. Equipped with a frank demeanor, it is difficult to tell what impact your words have on this individual, if any. It wasn't until Scott offered me a collaboration that I started to recognize his subtle humor and goofy personality that I had only heard stories about up to that point. And then when he told me that two of his passions in life are soccer and snow sports, I knew we were going to get along just fine.

Scott and I worked together on a project to determine the effect of insulin resistance and diabetes on the expression of islet cells genes, and realized that the experiment we were analyzing was very interesting, yet imperfectly designed. But that's science – no experiment is ever perfect. He taught me that putting together the pieces of a somewhat confusing story is part of the art of being a scientist. Apparently having your paper rejected three times is also an art. We worked together for the last two years of my work at UC Berkeley, and now that I'm at Kinemed, he's one of my bosses. I better not say anything here that will piss him off.

**Daniel Benjamin**

DBen. What a guy. I've known him for only about two years at this point, but man has this guy been one of my favorites. I love this guy for a thousand reasons, but the main reason is because he's as much of a gym rat as I am, and is constantly trying to get in better shape. It's like he can talk to my soul.

My favorite memory of DBen is the first time we went to the gym together. We had been talking about if for months. "Yeah, you like going to the gym? I like to deadlift, do pullups, pushups, mainly bodyweight exercises, I hate doing ab work, what about you?" Finally one day, we decided to turn out words into actions, and make the weight room our bitch. For whatever reason, I designed the workout that day, mainly because DBen was interested in learning how I liked to lift, using a faster high-intensity approach that minimized rest. So we constructed some workout that didn't provide much of anything sedentary, and 45 minutes later, we were both super tired. We returned to the weight room, slowly, then proceeded to strip down for shower time. Just as I was removing my shorts, I heard noises from the adjacent row of lockers, as if someone was puking violently. I thought to myself, "Whoa, that guy is struggling." I turned in that direction, and saw the naked backside of some guy who was bending over the trash can, returning last night's dinner to the outside world. It was DBen. "Dude, I think I got food poisoned from some fish I ate last night," he said. "I don't feel well." Sure you did. Food poisoning, the ultimate scapegoat. Way to pull that one out, tough guy.

It wasn't until many months later that he admitted to me that the workout was too intense for him at the time, and the pukage was his body's way of showing that off to his friends. At that point we admitted that we had mutual man crushes on each other, and became workout partners.

It wasn't until we played basketball one day that DBen returned the "I'll make you look like a fool" favor. He had always talked about it, and made is sound like he was pretty good, but being the skeptic that I am about white boys playing a not-white-boy game, I wasn't sure if he was all talk or not. In a pickup game one Friday morning, we decided to guard each other on both sides of the floor. Imagine a guy with the size of a boxer, the speed of a soccer player, and the moves of a ballerina. Now imagine that you're wearing the wrong shoes, that you really don't have any basketball skills to begin with, and that you're scared out of your mind. Finally, imagine that you're trying to stop him from making you look like a fool. Mission: unsuccessful. It's hard to describe what guarding DBen on the basketball court is like, but it made me realize that after playing soccer for over 25 years, I was only 1/10 the man he was on the basketball court. Perhaps I should stick to grass. To end the humiliation, I did what any real man would do. I faked an injury, and left the court to never return.

From that point onwards, DBen and I did practically everything together – talk shit about the department, leave work early to drink, watch European soccer, watch Seinfeld reruns, and theorize on why women love to give men a hard time. We didn't really come up with much, but having a right hand man makes life very fun indeed. Being friends with him has motivated me to learn every Seinfeld episode by heart, so that I can laugh at more things than I already do. In return, maybe he'll learn how to play fantasy soccer one day and provide some *real* competition.

## Family Members

### My mom and dad

### Natasha Hazel, Sabrina Hazel, Isabella Hazel, Rohan Sharma, Laila Sharma

### Persis and Kap Sharma

### Shanaz and Alex Hazel

I know it sounds cheezy, but I certainly could not have accomplished any of this without the loving support of all the jokers pictured above. My mom has always been my biggest fan, and has supported me in everything that I've set my mind to. My dad was the first to plant the Ph.D. seed in my head, and damnit, why did I listen to you? Thanks for that. Shanaz and Alex, you are both shining examples of success, and have set the bar very high for educational success. You've also raised some incredibly hilarious kids, so thanks for that. Persis and Kap, you guys also set the bar very high, and constantly offer me loving support despite the fact that you live across the country. To Natasha, Sabrina, Isabella, Rohan, and Laila – you guys are the most incredible nieces and nephews a weirdo uncle could ask for, and please be aware that your silliness has kept me sane throughout this process. I owe you guys a lot for keeping me young.

**You guys are all incredible in your own way,**
**and for that I thank you from the bottom of my heart.**

# Introduction

## Overview of Dynamic Proteomics Using $^2H_2O$ Labeling

In biological systems, proteins execute an extremely wide range of cellular activities, including (but not limited to) acting as reaction catalysts, transcription factors, chaperones, cell surface receptors, hormones, nuclear receptors, ion channels, nuclear pores, and integral components of organelle membranes. Proteins are the endpoint of biological information flow; information encoded in DNA is temporarily translated to RNA in response to environmental stimuli, resulting in the synthesis of proteins with highly specific intracellular and extracellular functions. Ultimately, the behavior of a cell is governed by the dynamic interactions between thousands of proteins; a tissue is governed by the interactions of thousands of cells; and an organism is governed by the interaction of multiple tissues. Proteins therefore are the ultimate laborers in biological systems.

Proteins play both structural and catalytic roles in cells, providing both the scaffolding and machinery necessary to regulate biological activity. They direct three fundamental cellular processes, including (a) the maintenance of DNA stability via the formation of chromatin (protein-DNA complexes), (b) the regulation of gene transcription and RNA stability, and (b) the regulation of protein translation, including initiation, elongation, and termination.

The function of a protein is regulated by a number of complex and incompletely understood processes, and is regulated by synthesis, degradation, and instantaneous interactions with enzymatic substrates, products, and neighboring proteins. These immediate regulatory controls are a result of post translational modifications, which include phosphorylation, ubiquination, glycosylation, hydroxylation, acetylation, and methylation. In addition, enzyme function is modified by direct inhibition at the active site by competitors, or by allosteric regulation at non-active sites. Proteins are also subject to folding via chaperones, and are transported to target organelles in cytoplasmic vesicles that are themselves directed by a complex orchestra of protein-protein interactions in the endoplasmic reticulum and golgi apparatus networks. Proteins that are bound for integration into the plasma membrane or into extracellular space interact with other proteins docked to the interior of the plasma membrane whose specific functions regulate constitutive and regulated exocytosis.

Overall, the process of protein synthesis, modification, and transport requires an incredibly complex series of events that are executed by preexisting cellular

proteins. Unlike DNA and RNA, proteins govern their own synthesis and breakdown. Therefore, the maintenance of protein homeostasis (proteostasis) is an absolutely critical component of proper cellular function and the response to constantly changing environmental signals.

### Proteostasis: Protein Homeostasis

Given the importance of maintaining proper protein function within the cellular environment, the term proteostasis is defined as follows:

**Proteostasis:** *The regulation of cellular protein homeostasis that controls the turnover of cellular protein, determined by the dynamic equilibrium between protein synthesis and protein breakdown.*

Characterizing biological systems at a global level has become increasingly informative in understanding fundamental cellular biology and the development of therapeutics, and is the logical progression in the development of the next generation of biomedicine. Current "-omics" techniques include genomics (DNA), transcriptomics (RNA), proteomics (protein), and metabolomics (intracellular non-protein metabolites).

In the past twenty years, a large emphasis has been placed on the simultaneous measurement of large numbers of cellular components (DNA, RNA, protein), rather than basing conclusions on a small number of traditional markers of cellular function. Advances in sophisticated "-omic" technologies have demonstrated the utility of establishing large-scale RNA and protein networks that describe cellular phenotypes in a comprehensive and definitive manner. In a comprehensive review of biological networks, Gygi et al state:

*"The reductionist approach has successfully identified most of the components and many interactions but, unfortunately, offers no convincing concepts and methods to comprehend how system properties emerge. To understand how and why cells function the way they do, comprehensive and quantitative data on component concentrations are required to quantify component interactions... the pluralism of causes and effects in biological networks is better addressed by observing, through quantitative measures, multiple components simultaneously and by rigorous data integration with mathematical models."* [1]

While "-omics" technologies are widely available to the research community, they possess an inherent limited interpretability given the measurement of static pools rather than time-dependent kinetics from which flux measurements can be made. In support of this, Anderson and Seilhamer write:

*"More knowledge about the turnover rates of the most important proteins, such as transcription factors, ribosomes and proteins of the signaling pathways would surely increase our understanding of the mechanisms of control. Moreover, in molecular biology the proteins and other macromolecules are usually and inevitably studied in an artificial milieu in vitro, whereas in reality, as is emphasized more and more, they are parts of a highly organized system."* [2]

The term proteomics refers to any study which characterizes large sets of proteins, including composition, expression,

modification, quantification, localization, and functional interaction [3–8]. Proteomics and trascriptomics are conceptually identical yet experimentally different; proteomics measures the expression of cellular proteins via mass spectrometry whereas transcriptomics measures gene expression via chip-based mRNA hybridization assays.

Our laboratory has pioneered the field of *dynamic proteomics*, a stable isotope mass spectrometric technique that combines $^2H_2O$ labeling with the measurement of hundreds to thousands of tissue proteins *in vivo*. Dynamic proteomics is useful because it combines the non-hypothesis driven approach with the interpretability of known biochemical pathways. The union of these two allow for a very accurate inference of the activity of a metabolic pathway given direct measurements of the rate of turnover many of the integral enzymes that regulate pathway flux. Unlike quantitative proteomics which measures static expression of hundreds of proteins simultaneously, dynamic proteomics measures the synthesis rate of hundreds of proteins simultaneously, which can then be used to directly measure flux through pathways of biological importance.

Dynamic proteomics can be used in two primary ways: to identify biomarkers of a disease process and to identify undiscovered protein targets involved in the pathogenesis of disease. By interrogating the dynamic behavior of the proteome, detailed information about proteome system architecture can be gathered in order to understand the underlying molecular basis of disease states. For more information, see the section entitled "Dynamic Proteomics" below.

## Limitations of Transcriptomics

*"The emphasis during the last 50 years has been reductionist, explaining biological phenomena at the atomic and molecular level. The challenge for the next 50 years is to integrate these insights into an understanding of higher levels of temporal and spatial organization..."* [9]

It is important to keep in mind that most microarray studies are performed in order to predict the expression levels of their corresponding protein counterparts, however in many physiological settings this type of cause-and-effect response is nonexistent. While transcriptomics measures the relative level of gene expression by quantifying transcript abundance, the expression of the same gene product at the protein level does not always follow a predictable pattern [10]. If the protein and gene expression are related by in direction and magnitude, the relationship is considered concordant; inverse relationships are referred to as discordant.

In complex biological systems, mRNA degradation can occur on the order of minutes as compared with proteins whose stability is generally regulated on the order of hours, days, weeks, and sometimes months. Transcript stability is affected by binding proteins such as heat shock proteins to protect against transcript degradation, or association with ribosomes to allow for protein translation [11].

Given that proteins represent the ultimate effectors of gene function, and that mRNA and protein expression are often

discordant [12], measuring protein expression reveals more valuable phenotypic information than does transcriptomics by itself [13]. While microarrays were a significant advancement in the field of network biology, subsequent advancements in proteomics have rendered the measurement of transcript abundance a complementary rather than definitive assessment of cellular phenotype. The importance of studying biological systems at the protein level is further emphasized by recent studies that clearly indicate that mRNA levels do not necessarily correlate with protein abundances [14–16].

## Protein Synthesis

The dynamic proteomic approach used in these studies involves the administration of $^2H_2O$ in the drinking water of mice or rats to achieve a target body water enrichment of 5%. During the labeling period, *in vivo* protein synthesis occurs, resulting in the creation of "heavy" proteins identical to their "light" counterparts in function, differing only in the incorporation of deuterium atoms at specific positions in the constituent amino acids from which they are comprised. Commerford et al. were the first to publish the distribution of tritium in tissue amino acids in labeled mice [17], and this quantity is integral to the calculation of fractional synthesis rate.

At the conclusion of the desired labeling period, the animal is euthanized and tissue is harvested, followed by the isolation of total cellular protein. Proteins are then alkylated under reducing conditions in order to break and cap disulfide bonds, separated by mass via SDS-PAGE, and trypsinized to resultant peptides. This peptide population contains both light and heavy species, the two of which are then resolved by high-affinity liquid chromatography mass spectrometry (LC-MS), resulting in the identification of hundreds to thousands of proteins from a single tissue sample. Using mass isotopomer distribution analysis (MIDA), the synthetic rate of each peptide identified by LC-MS is calculated by comparing the labeled mass isotopomer envelope (MIE) against the unlabeled MIE, in order to quantify the extent of $^2H$ label incorporation that occurred in the presence of $^2H_2O$ enriched body water. Proteins identified by this method are then queried against an online proteomic bioinformatic database containing gene ontology annotations for all known mammalian gene products, resulting in the creation of a dynamic network map that provides clues regarding proteomic alterations that result from either (a) a disease process, (b) nutritional intervention, or (c) therapeutic administration.

It is important to note that the dynamic range in protein abundance is estimated to be over five orders of magnitude within a cell [13]. Therefore, prior to LC-MS/MS analysis of peptides, proteins are separated by molecular weight via SDS-PAGE, and each lane is then separated into ten separate molecular weight regions. In this way, the overall complexity of proteins increases, resulting in the identification of hundreds to thousands of cellular proteins from a single tissue sample. More importantly, fractionation of proteins via SDS-PAGE increases the probability of detecting proteins expressed at low abundance, including nuclear transcription factors and secreted proteins[13]. Other acceptable fractionation techniques include

differential centrifugation to separate proteins by subcellular location [18,19].

### Protein Breakdown

The process of protein breakdown is significantly more complex than that of ribosomal protein synthesis, given the presence of multiple degradation pathways. Protein breakdown occurs in order to remove "unwanted" cellular material that may compromise normal functionality, acting on oxidized, aggregated, misfolded, and miscoded proteins. Degradation of unwanted proteins refills the intracellular free amino acid and amino acyl-tRNA pools, providing a reservoir of amino acids as substrates for subsequent rounds of protein synthesis. It is important to note that protein breakdown must also balance protein synthesis; without coordinated mechanisms, the accumulation of protein would continue infinitely [2]. The two main pathways of protein degradation include ubiquination and autophagy.

### Ubiquination

Ubiquination is the principal mechanism of controlled protein breakdown in eukaryotes, and is reliant on the "tagging" (or activation) of proteins marked for degradation by a small heat-stable ubiquitin protein. As the name implies, this protein is ubiquitously present in all cell types, and regulates the breakdown of proteins involved in cell cycle, growth, transcription, DNA repair, oncogenesis, and antigen processing [20].

Ubuiquitin is first activated by a high-energy thioester linkage, then transferred to a carrier protein via the action of an E3 ubiquitin-protein ligase. Proteins marked for degradation are typically tagged at a lysine residue at a site known as the degron, and specificity in this process is governed by the specific interaction between the E3 ubiquitin ligase and the target protein. In a typical mammalian cell there exists hundreds of E3 protein ligases, each recognizing specific degron motifs on target proteins[21]. It is appropriate to think of protein ubiquination as a type of post-translational modification.

A ubiquinated protein is then transported to the 26S proteasome, a self-contained proteolytic factory. Chaperone proteins present the tagged protein to the proteasome, which contain a collection of chymotryptic, tryptic, and caspase-like proteases, resulting in a collection of peptide fragments between 4-25 amino acids in length. In this respect, the 26S proteasome has six distinct functions, including (a) recognition of tagged proteins, (b) de-ubiquitination of presented proteins, (c) unfolding of target proteins, (d) transloation of target proteins, (e) enzymatic protein degradation, and (f) protein processing [21].

The ubiquitin protease system (UPS) is active on a wide variety of protein substrates including myofibrillar proteins, cyclins, receptors, and ion channels [2]. Moreover, the UPS occurs in all tissues, and is particularly active in muscle tissue undergoing atrophy [22–24]. Interestingly, impaired UPS function is implicated in a number of age-related neurodegenerative conditions, including parkinsons and alzheimers disease [25–28].

### Autophagy

Autophagy (self-eating) was first discovered in 1963 as a lysosome-dependent process for the removal of damaged cellular contents and entire organelles [29,30]. Autophagic digestion of

unwanted cellular material maintains cellular homeostasis by balancing the processes of organelle and protein biosynthesis [31]. Autophagic activity is high in cell types with low antioxidant activity, replicative capacity, and energy metabolism. The synthesis of reactive oxygen species (ROS) in the mitochondria of metabolically active cells presents a severe danger to neighboring proteins, lipids and nucleic acids, resulting in the formation of oxidized species which are direct targets for autophagy. The exact mechanisms underlying autophagy and mitochondrial dysfunction remain unclear, however is has been well characterized that oxidative stress influences autophagic activity [32–34]. Moreover, this process is thought to predominate due to sudden perturbations in cellular homeostasis, including cellular oxidative stress, mechanical damage, or nutrient starvation [2].

Macroautophagy is an orchestra that is conducted by over thirty participating proteins that are highly conserved between yeast and mammals [31]. In this process, a region of the cytosol is engulfed in an ER-derived vesicle devoid of ribosomes, known as an autophagic vacuole or autophagosome. The autophagosome fuses with the lysosome, and the contents are exposed to an acidic pH and a collection of proteolytic enzymes that facilitate the breakdown of a large number of proteins simultaneously. Autophagosome cargo is digested in bulk, the contents of which may contain mitochondria, ER fragments, glycogen, golgi apparatus, or structural components including actin, myosin, and tubulin. Autophagic protein breakdown is very rapid, occurring at about 9% per minute [2].

Microautophagy is a process by which lysosomes directly engulf cytosolic cargo, ingesting constituents by membrane involution [35–38]. Cytoplasmic proteins are therefore engulfed directly by lysosomal endocytosis, as opposed to macroautophagy which requires transport to the lysosomal compartment by double membrane autophagosomes. This process is thought to account for basal protein breakdown in comparison with the digestion of entire organelles via macroautophagy. Flux through these two distinct pathways is dependent on the tissue. In liver the lysosomal autophagy system predominates whereas in muscle tissue lysosomes are less abundant, therefore increasing the activity of protein ubiquination[2].

Protein breakdown is not directly measured using the dynamic proteomics method, however it is possible to calculate protein breakdown rates using the following equation:

$$\dot{Pool\ Size} = \dot{Protein\ Synthesis} - \dot{Protein\ Breakdown}$$

$$\dot{Protein\ Breakdown} = \dot{Protein\ Synthesis} - \dot{Pool\ Size}$$

where the superscript “dot” represents the protein synthetic and breakdown *rates*.

Therefore, by measuring protein synthetic rates via $^2H_2O$ labeling combined with pool size via SILAM, we can calculate protein degradation rates for all proteins with an identifiable SILAM pair. It is worthy to note that in physiological conditions at steady state, when the pool size of total proteins within a tissue is not changing over time, the rate of synthesis is equal to the rate of breakdown. *In vivo,* this is a fundamental assumption that can be made in steady state systems if body composition is unchanging over time in both the experimental and control groups.

In tissues undergoing net anabolic processes (proliferation, hyperplasia, normal adolescent growth), the rate of cellular proliferation must be measured directly, and the rate of protein synthesis can then be corrected by this factor. In tissues undergoing net catabolic processes (apoptosis, necrosis), the rate of cell death must be quantified directly, and the rate of protein synthesis can then be corrected by this factor as well.

### The Coordination of Protein Synthesis and Breakdown

In order to understand the interplay between protein synthesis and protein breakdown, it is important to conceptualize the intracellular protein pool. Conceptually, a pool represents a relatively homogenous physical entity within which mixing occurs rapidly [39]. Regardless of the physical shape of the pool (tissue fluid, circulatory system, cerebrospinal fluid), the pool can be modeled as a system with metabolite entries and exits.

When modeling the relationship between protein synthesis and breakdown, the single pool model with a single entry and exit is a safe assumption. The entry to the single pool model is the rate at which proteins are being synthesized, and the exit to the pool represents the rate at which proteins are being degraded by any of the aforementioned mechanisms, including ubiquination and autophagy.

By definition, in an animal that is considered at "steady state," protein synthesis and protein breakdown are coordinated and equal, resulting in unchanging pool sizes over time. On a global level, steady state protein homeostasis results in stable body weight and unchanging body composition over time. In contrast, at non-steady state, the size of the functional protein pool changes over time, as does the size of the intracellular free amino acid pool and the amino acid tRNA pool. In the case of positive energy balance, the size of these pools increases over time, whereas in negative energy balance pool size decreases over time.

Clearly, if protein synthesis and breakdown are coordinated systems, then there must exist some molecular link between the two pathways. Free amino acids may serve as this link, given that they are substrates for protein synthesis and are the products of protein breakdown. Little is known about the way in which these two pathways are linked, however many studies support this concept [40–42].

Pool size is not a complete determinant of protein behavior because it does not measure the rate of turnover of the protein pool, and instead reveals a static metric that may untimately not reflect important underlying metabolic processes. As an example, the synthesis rate and breakdown rate of a protein can both increase 4-fold in response to treatment without affecting the protein pool size. Therefore, without direct measurement of either the synthesis or breakdown rates, it is difficult if not impossible to determine whether the synthesis and degradation rates were affected by treatment or a disease process.

However, by determining both pool size and fractional synthetic rate via direct measurement, one can mathematically determine the absolute rate of protein synthesis using the formula:

$$r_{abs} = k * Q$$

Where $r_{abs}$ represents the absolute rate of protein synthesis (pg per day), k represents the fractional turnover rate constant (% synthesis per day), and Q represents the pool size (pg). When comparing an experimental intervention against a control state, the ratio of absolute rates can be expressed as:

$$\frac{(r_{abs})_{Exp}}{(r_{abs})_{Ctl}} = \frac{k_{Exp}}{k_{Ctl}} * \frac{Q_{Exp}}{Q_{Ctl}}$$

Where $(r_{abs})_{Exp}$ and $(r_{abs})_{Ctl}$ represent the absolute rates of protein synthesis in experimental and control animals, respectively; $k_{Exp}$ and $k_{Ctl}$ represent the fractional turnover rate constants in experimental and control animals (% per day), respectively; and $Q_{Exp}$ and $Q_{Exp}$ represent the pool size in experimental and control animals, respectively.

Turnover is determined by the rate of both synthesis and breakdown, and measuring these kinetic metrics ultimately reveals information about the flow of proteins into and out of the protein population. Figure 1 shows the three pool model for describing dynamic proteostasis.

## Dynamic Proteomics

$^2H_2O$ labeling shifts peptide mass isotopomers to heavier masses, resulting in a mass isotopomer envelope (MIE) that is perturbed from the isotope pattern observed at natural abundance. MIDA quantifies changes in the MIE by comparison against an unlabeled MIE and a fully turned over MIE, in order to derive a metric for the fractional synthetic rate of a

peptide (f, %*time$^{-1}$). Once *f* has been determined at a particular time point, a graph of *f* vs. time reveals the fractional peptide synthesis rate. Empirically, we have found that the graph of *f* vs. time reveals a one-phase exponential association, supporting our initial one-pool dynamic equilibrium assumption. By modeling this curve over multiple labeling time points, a best-fit curve can be drawn that describes the rate of protein synthesis according to *k*, the protein synthesis rate constant. Proteins can then be directly compared using *k* values in order to determine the difference in protein synthesis rates. As shown in Figure 2, the sharper the peptide synthesis curve, the higher the value of *k*. Proteins that are rapidly synthesized follow the upper curves whereas proteins with slow synthetic rates follow the lower curves. Proteins can be directly compared using this strategy by comparing the rate constant *k* between the experimental and control groups.

The fundamental concept behind the calculation of protein synthesis rates using MIDA is that a protein synthesized in the presence of a "heavy" tracer *in vivo* will be reflected by increases in isotopomeric relative abundance for all isotopomers $M_1$ trough $M_{infinity}$ detectable by LC-MS/MS. The relative abundance of the unlabeled isotopomer $M_0$ decreases as a function of protein label incorporation, resulting in a rightward shift in the isotopomer envelope. In more simplistic terms, as the peptide mass increases over time due to the incorporation of deuterium, the relative abundance of mass isotopomers $M_1$ through $M_{infinity}$ increases, and the relative abundance of mass isotopomer $M_0$ decreases. The shift towards heavier mass isotopomers therefore decreases the proportion of $M_0$ present in the labeled protein.

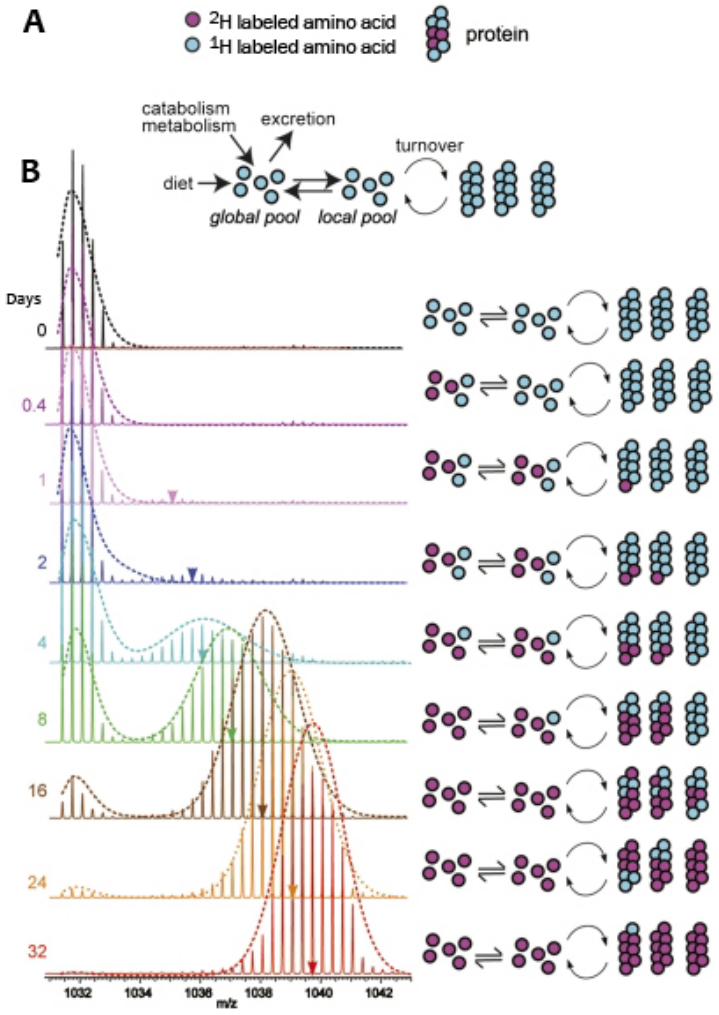


**Figure 1. Three Pool Kinetic Model Results in a Mass Isotopomer Envelope Shift.** (A) Three pool kinetic model showing the incorporation of both labeled and unlabeled amino acids into cellular proteins. Amino acids in the global pool rapidly equilibrate between local tissue amino acid pools. (B) Sample chromatographic representation of the shift in mass isotopomer envelope (MIE) over time due to the incorporation of 99.9% $^{15}$N-labeled AAs into cellular proteins. Label persistence results in an increase in the relative ratio of labeled to unlabeled peptides. Empirical data agrees well with the three pool model assumption. Mass isotopomer distribution analysis (MIDA) is used to quantify the proportion of labeled isotopomers at a given time point, and the fractional synthetic rate of the peptide can then be determined by comparison against a fully labeled peptide. Image adapted from original publication by Price et al[43].

Mathematically, a decrease in the relative abundance of the $M_0$ isotopomer is equal to the sum of the increase in relative abundance of the $M_1$ trough $M_{infinity}$ isotopomers. Therefore, measuring a decrease in the relative abundance of $M_0$ is equivalent to summing the increase in daughter isotopomers. For this reason, we quantify negative changes in $M_0$ to determine the fractional synthetic rate of a labeled peptide given that it simplifies the calculation, and is more accurate than summing a finite number of daughter isotopomers. When modeled using a non-linear one-phase exponential association regression equation, the fractional rate constant ($k$) can then be determined (Figure 2).

## Methods for Quantitative Proteomics: SILAC and SILAM

Stable Isotope Labeling with Amino Acids in Cell Culture (SILAC) is a stable isotope technique used for quantitative MS-based proteomics. SILAC was originally developed at the University of Southern Denmark in 2002 as a procedure to accurately quantify the difference in

protein expression between cell cultures, and has become a popular and inexpensive MS-based proteomic method [43].

In SILAC, labeling cells in the presence of growth media enriched with a single heavy amino acid results in the incorporation of this heavy amino acid into newly synthesized proteins. The addition of an extra neutron to a single atom of the heavy amino acid does not affect its chemical or biological properties, therefore normal metabolic processes should not be influenced by the addition of the label. Over time, labeling with a heavy amino acid results in a mass shift of newly synthesized proteins, whose monoisotopic mass can be easily resolved from its unlabeled counterpart by mass spectrometry. Importantly, the monoisotopic mass of a labeled peptide must be rightward shifted enough that the unlabeled and labeled peptides can be individually identifiable by mass spectrometry, forming a "SILAC pair."

For this reason, heavy amino acids commonly used for SILAC experiments often flank the trypsin cleavage site at the C-terminal side of both lysine and arginine except when either is covalently bound to proline. Therefore, $^{13}C_6$-Lysine and $^{13}C_6$-Arginine are commonly used in SILAC experiments. It is well classified that arginine can be converted into proline in certain cell types, therefore the use of either $^{13}C_6$-Arginine and $^{13}C_6{}^{15}N_4$-Arginine can result in the generation of $^{13}C_5$-Proline and $^{13}C_5{}^{15}N_1$-Proline, respectively. This introduces an unwanted bias that can be corrected for mathematically in all proline-containing peptides, however this is laborious and reduces quantitation accuracy. A simple solution to this problem is to label with another ubiquitous amino acid that does not interconvert in the cell type of interest, such as $^{13}C_6$-Leucine [44,45].

Using this labeling strategy, the incorporation of even a single heavy amino acid into a short peptide can shift the monoisotopic mass-to-charge ratio (m/z) significantly enough that the labeled peptide is now distinguishable from its unlabeled counterpart. Labeling with heavy amino acids results in a distinct mass difference between resultant peptides, allowing for easy detection of SILAC pairs. Peptides are then analyzed by high resolution LC-MS/MS, resulting in the identification of multiple peptides per parent protein. The median heavy-light ratio of identified peptides is then calculated, resulting in the calculation of the relative heavy:light expression ratio (Figure 4).

n a typical SILAC experiment, a cell culture is grown in the presence of either single or multiple heavy amino acids (LIST AA CHOICES HERE). The cell culture is allowed to survive for multiple generations (5+) such that the heavy amino acids are completely incorporated into the host proteome, resulting in a near complete substitution of the labeled amino acid across all cellular proteins. Generally, lysine ($^{13}C_6$-lysine) and arginine ($^{13}C_6$-arginine) are chosen as the labeled amino acids, which results in the labeling of nearly every peptide following trypsin digestion due to the presence of these two amino acids in virtually all tryptic peptides.

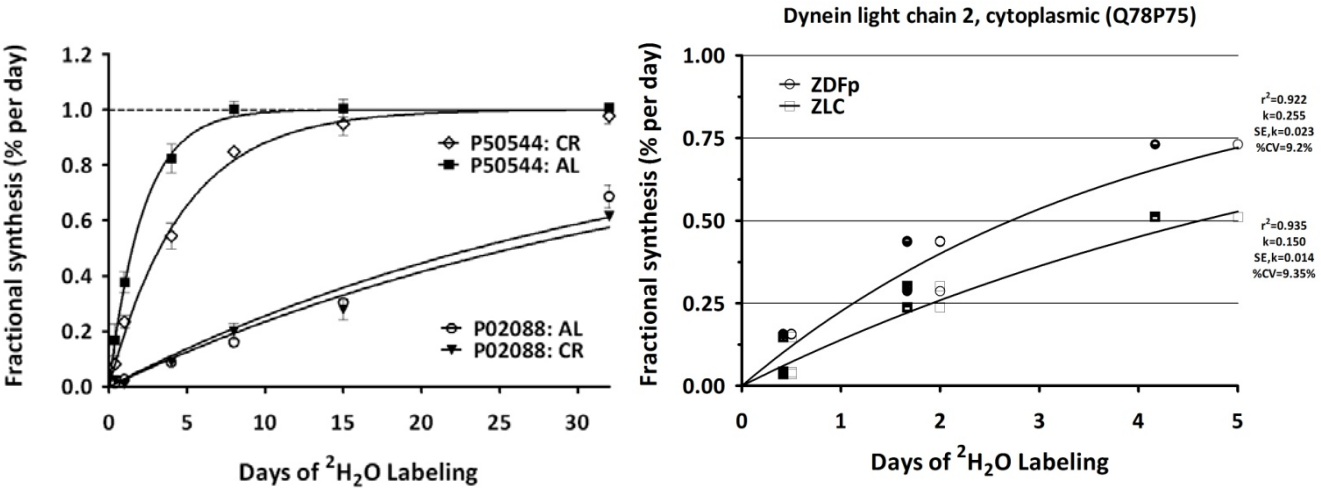


**Figure 2.** (A) Fractional replacement curves for each protein were fit using non-linear regression to calculate the replacement rate (*k*) within the population of mice labeled for various durations according to the experimental design. Shown are curves for two proteins in long-term calorie restricted (CR) and *ad libitum* (AL) mice. (B) Protein curve fits are further filtered using criteria specific to each protein, including (i) the $r^2$ value used to determine the "goodness of fit," (ii) SE(*k*) the standard error of the curve fit, and (iii) the coefficient of variation of the curve fit, calculated as %CV=SE(*k*)**k*$^{-1}$. These criteria are subsequently used as criteria for further selection against low-confidence protein identifications.

While SILAC is restricted to cell culture experiments, the Stable Isotope Labeling of Amino Acids in Mammals (SILAM) method was developed in order to label proteins in whole organisms *in vivo*. In this type of experiment, an animal is fed a diet containing the natural abundance of amino acids excepting the label, which is enriched at 99.99%. Similar to cell culture experiments, the choices for the metabolic label are numerous, including a single or double amino acid ($^{13}C_6$-lysine and/or $^{13}C_6$-arginine), or all amino acids ($^{15}$N-AAs) [46,47].

The labeled organism is allowed to replicate for multiple generations until near complete substitution of the heavy amino acid for its light counterpart has taken place (>97% AA substitution). In mice, complete proteome labeling occurs within two generations [48–50], The result of raising an organism in this manner is near-complete amino acid incorporation in many fully turned over tissues within the same organism, including extracellular proteins and those in body fluids. Protein is then isolated from the tissue of interest, and the heavy protein lysate is then mixed with the experimental light protein lysate in a known ratio (typically 1:1) prior to LC-MS/MS analysis. In this manner, labeled tissue is used as a "spike-in" standard, which allows for direct comparison between experimental samples assuming that the amount of heavy protein lysate that was added to all samples is constant.

Since the development of SILAM labeled animals is expensive and time consuming, labeled mouse tissue can be purchased directly from various retailers in the bioscience community. Often times, however, the tissue of interest is unavailable, often because specific homogenous cell populations within a tissue are laborious to isolate. Therefore,

it is possible to perform a quantitative proteomics experiment by combining the cell culture SILAC approach with the "spike in" SILAM approach. In this context, a labeled proteome is generated using the SILAC strategy *in vitro*. This cell culture is grown in the presence of heavy amino acid(s) for a minimum of 6 cell doublings, such that more than 95% of the proteome is fully labeled.

It is important to note three crucial experimental design criteria at this point. The (a) species, (b) strain, and (c) tissue of the experimental animal model must be matched to that of the labeled organism in order to ensure overlapping proteomes between the experimental model and the "spike-in" standard [51]. Neglecting either of these three may result in the identification of a low number of interpretable peptides, and create a physiological artifact due to non-overlapping proteomes between sample and standard. Using the "spike-in" standard approach, one can utilize the protein lysate from a single labeled organism in multiple downstream experiments using strains of the same species with various genetic backgrounds.

Figure 3 shows the experimental strategy for both SILAC and SILAM experiments. Some researchers have also utilized a hybrid strategy to quantify protein expression between experimental conditions using *in vitro* SILAC heavy cultures as "spike-in" standards for *in vivo* tissue protein lysates in order to accelerate the development of a labeled proteome[52].

In our experiments, we utilized two quantitative proteomics approaches. In the first study, our objective was to determine the effect of calorie restriction (CR) on hepatic proteome dynamics. Given that labeled mouse tissue was available for purchase, we used this as a "spike-in" standard. In a second experiment to determine the effect of insulin resistance (IR) and diabetes on islet cell proteome dynamics, we instead utilized a hybrid strategy in which we labeled INS-1E rat insulinoma cells in culture for six cell doublings, then used this heavy SILAC culture as a "spike-in" standard for protein lysates isolated from rats. In both cases, the number of SILAM pairs is the ultimate determinant of accurate quantitation across the entire proteome, determined by the overlap of the "spike-in" standard and unlabeled animal tissue.

### SILAM Quantitative Proteomics Analysis Method

Given the increasing use of LC-MS/MS across a wide variety of proteomics applications, the number of software applications covering all aspects of proteomics analysis has grown considerably in the last two decades. Often instrument vendors and individual laboratories develop customized software programs for specific applications, however a large number of publicly available open source applications have made the task of analyzing large proteomic datasets routine [53].

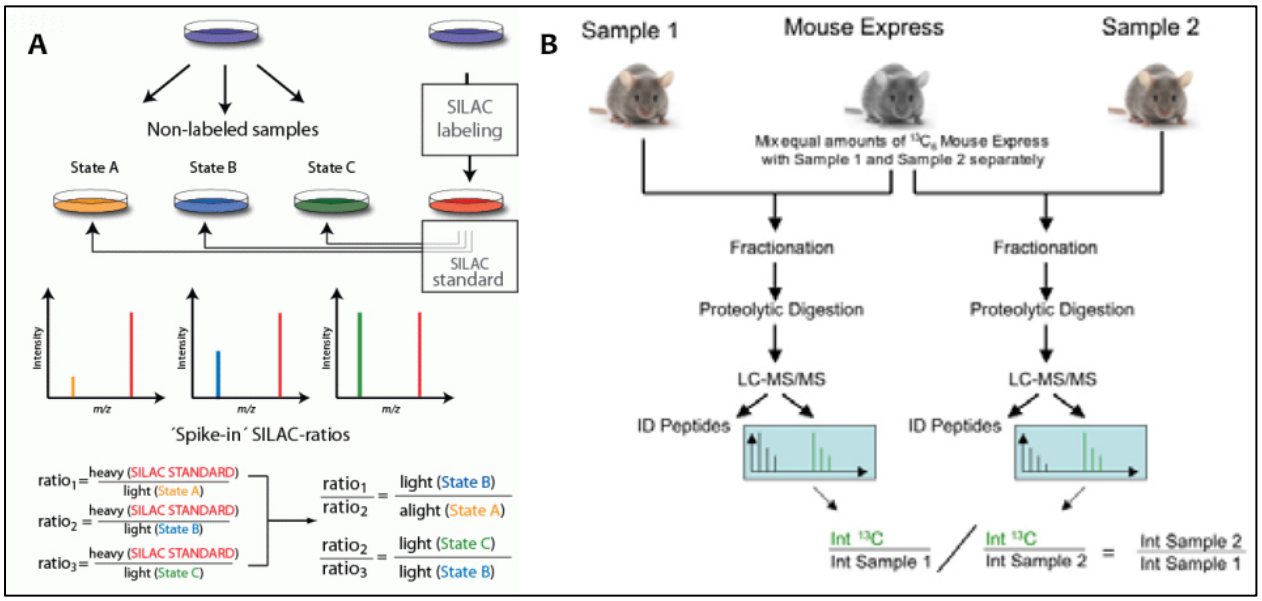


**Figure 3. SILAC and SILAM Experimental Strategies.** (A) SILAC experiments involve metabolic labeling of cells using heavy amino acids *in vitro*, followed by the mixing of this "standard" with unlabeled experimental samples. The mixed populations of peptides are then fractionated and analyzed by LC-MS/MS, resulting in the detection of heavy and light SILAC peptide pairs. Figure adapted from Geiger et al[51]. (B) SILAM experiments are performed *in vivo* by combining protein lysates from experimental models (light) and fully labeled organisms (heavy) in a known ratio. Following fractionation, trypsinization and LC-MS/MS analysis, the mixed population of peptides is then resolved into heavy and light SILAM peptide pairs. Figure adapted from Boettger[50]. In both strategies, the ratio of protein expression between experimental conditions can then be calculated using the "ratio of ratios" assuming that the amount of standard added to each condition is constant.

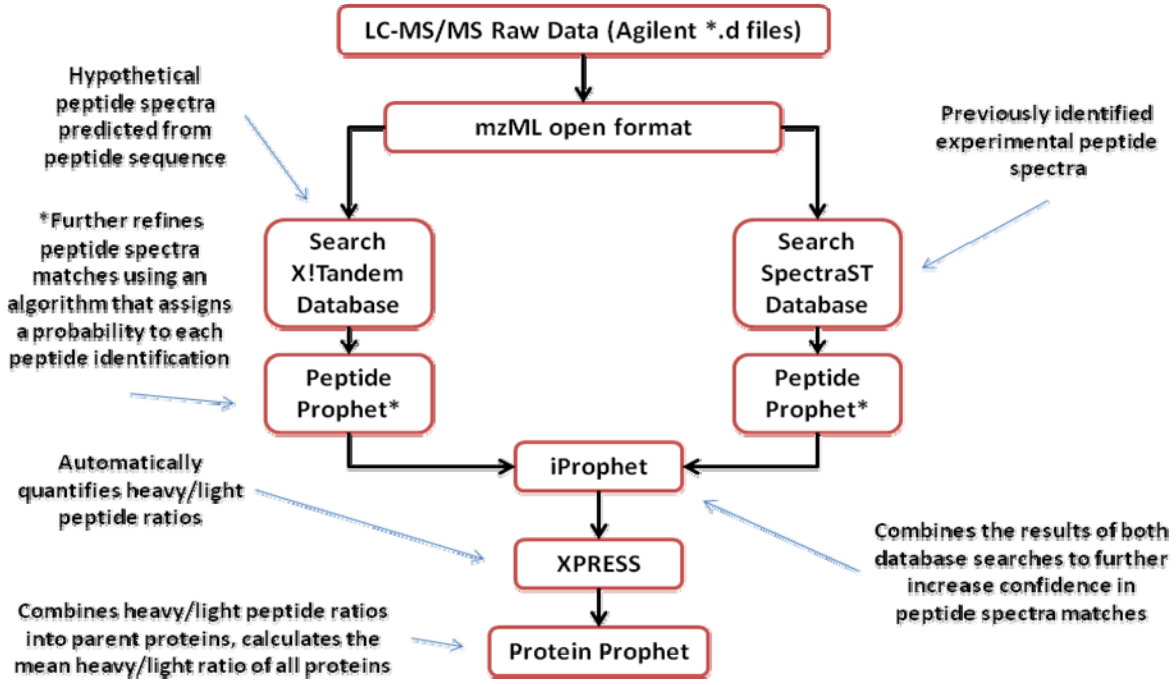


**Figure 4. Trans-Proteomic Pipeline Workflow Used for SILAM Quantitation.** For the analysis of SILAM experimental datasets, files are first converted to the mzML format, then searched against the X!Tandem database containing theoretical spectra predicted from peptide sequence and the Spectra ST database containing spectra from previously identified peptides in the species of interest. The results of both searches are then validated using the PeptideProphet algorithm, then the results of both searches are combined into a single list of high-confidence PSMs using the iProphet software tool. The quantitation of a large number of heavy:light SILAM pairs is performed using the XPRESS algorithm prior to the aggregation of peptides into parent proteins using the ProteinProphet algorithm. The final result is a list of high-confidence protein identifications with calculated heavy:light SILAM ratios.

The Trans-Proteomic Pipeline (TPP) is a suite of software tools available to the research community free of charge that allows for an in-depth analysis of many aspects of LC-MS/MS data. The TPP supports all steps of data analysis, from vendor-specific file conversion to open formats, protein-level statistical validation, empirical and theoretical database searches, and peptide quantification of stable isotope labeled SILAC/SILAM experimental data [54]. As shown in Figure 4, the TPP encompasses a number of software tools, including: (a) file conversion from Agilent *.d directories to mzML, an open mass spectrometer format, (b) search with a spectrum interpretation algorithm that attempts to match experimental spectra with all possible theoretical peptide sequences (X!Tandem), (c) search against a secondary spectral library containing previously identified spectra (SpectraST [55]), (d) validation of search results to correctly identify peptide-spectrum matches (PSMs) to minimize the probability of false discovery (PeptideProphet [56]), (e) combining the results of multiple database searches to further discriminate between correct and

incorrect PSMs (iProphet [57]), (f) analysis of stable isotope labeled SILAC/SILAM data for the identification of SILAC/SILAM pairs (as discussed above) (XPRESS [58]), and (g) combining peptide observations into a final list of proteins by assignment of multiple peptides to a single parent protein, a complex algorithm given that related proteins share peptide sequences (ProteinProphet [59,60]). Heavy protein lysate was obtained from a mouse fed a diet containing 99.9% $^{13}C_6$-Lysine for 2 generations. Data in the top left of each panel indicate the charge state, the m/z ratio, and the peak area.

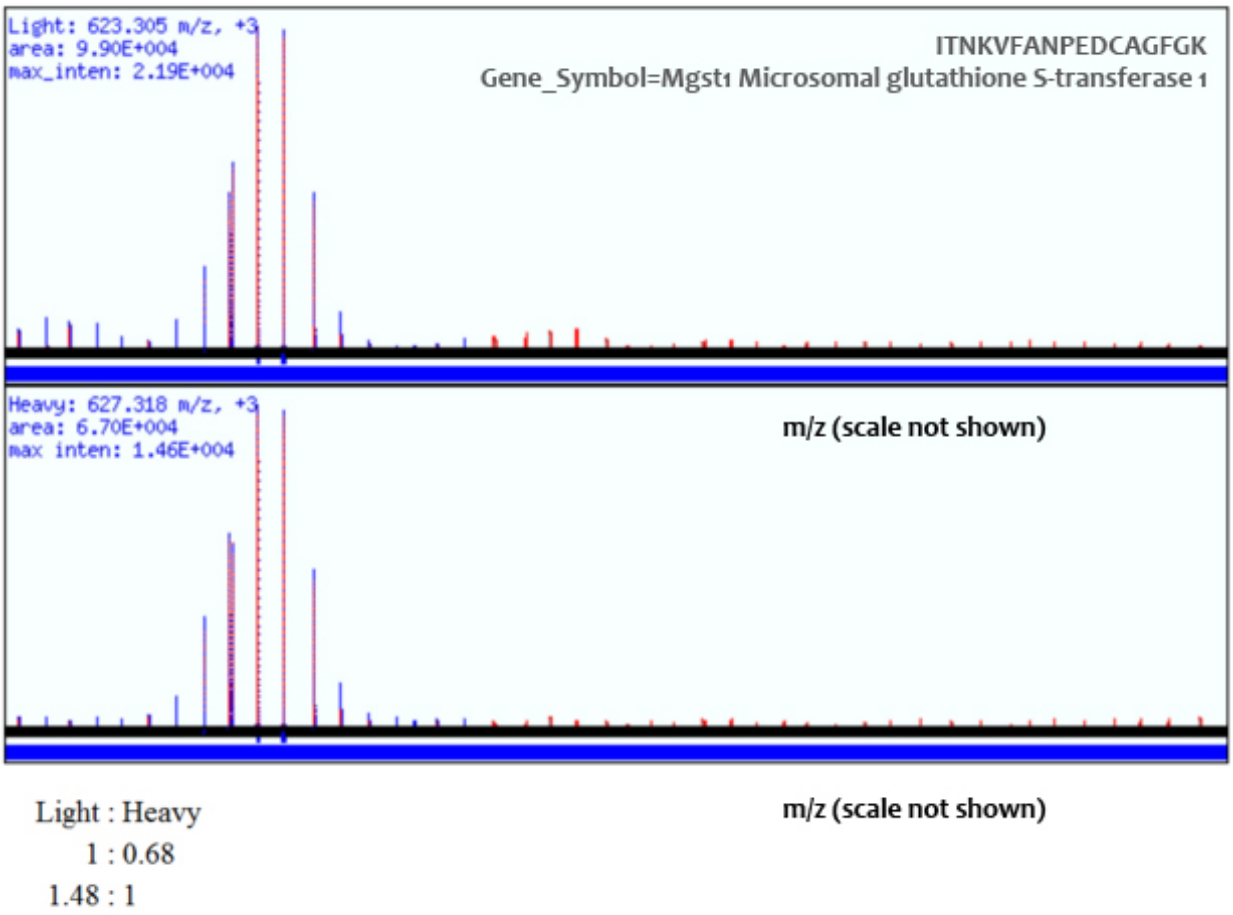


**Figure 5. Identification and Quantitation of SILAM Pair Heavy:Light Ratio.** Shown here is a sample spectra of a single peptide (ITNKVFANPEDCAGFGK) belonging to microsomal glutathione S-transferase 1 for the unlabeled (light) and labeled (heavy) SILAM peptide pair. Heavy protein lysate was obtained from a mouse fed a diet containing 99.9% $^{13}C_6$-Lysine for 2 generations. Data in the top left of each panel indicate the charge state, the m/z ratio, and the peak area. The peptide sequence demonstrates that the peptide contains 2 lysine (K) residues, shifting the mass of the peptide by 12 AMU. The charge state of these spectra is +3. The m/z shift between this SILAM pair is determined by the formula: delta m/z = (mass shift)/(charge state) = 12/3 = 4. The expected m/z shift is confirmed by subtracting the mass of the heavy peptide spectra (bottom panel) from the light peptide spectra (top panel). The heavy:light ratio is then calculated using the ratio of the peak areas.

The peptide sequence demonstrates that the peptide contains 2 lysine (K) residues, shifting the mass of the peptide by 12 AMU. The charge state of these spectra is +3. The m/z shift between this SILAM pair is determined by the formula: delta m/z = (mass shift)/(charge state) = 12/3 = 4. The expected m/z shift is confirmed by subtracting the mass of the heavy peptide spectra (bottom panel) from the light peptide spectra (top panel). The heavy:light ratio is then calculated using the ratio of the peak areas.

The ratio of the area under the curves (AUCs) represents the relative abundance ratio between light and heavy cultures (Figure 5). The heavy:light ratio within a single sample is directly comparable between samples if the amount of "spike in" standard was held constant. Therefore, when comparing between experimental and control animal models, the "ratio of ratios" ultimately reveals the relative pool size ratio between samples. An example of such equations are shown below:

$$\frac{\left(\frac{Exp_{light}}{Exp_{heavy}}\right)}{\left(\frac{Control_{light}}{Control_{heavy}}\right)} = \left(\frac{Exp_{light}}{Exp_{heavy}}\right) * \left(\frac{Control_{heavy}}{Control_{light}}\right) \text{ (ratio of ratios)}$$

$$Assume\ that\ Exp_{heavy} = Control_{heavy}\ (spike\ in\ std\ constant)$$

$$\left(\frac{Exp_{light}}{Exp_{heavy}}\right) * \left(\frac{Control_{heavy}}{Control_{light}}\right) = \left(\frac{Exp_{light}}{Control_{light}}\right) \text{ (pool size ratio)}$$

By combining both dynamic and quantitative proteomic data together, we are able to calculate both the rate of protein synthesis as well as the resultant pool size of *individual* proteins on a proteome-wide scale for the first time. Our objective in these experiments is to determine the effect of disease states, aging, and nutritional interventions on fundamental cellular mechanisms at play in the cellular proteome. A detailed understanding of subcellular protein kinetics is a significant biological undertaking, from the perspectives of instrumentation, experimentation, sample processing, data acquisition, and bioinformatic analysis. This technology represents a significant advancement in the field of proteomics, and will help elucidate the cellular mechanisms underlying many disease processes.

## Literature Cited


1. Sauer, U., Heinemann, M. & Zamboni, N. Genetics. Getting closer to the whole picture. *Science* **316**, 550–551 (2007).
2. Waterlow, J. C. *Protein turnover*. (CABI: 2006).
3. Aebersold, R. & Mann, M. Mass spectrometry-based proteomics. *Nature* **422**, 198–207 (2003).
4. Fields, S. Proteomics. Proteomics in genomeland. *Science* **291**, 1221–1224 (2001).
5. Glish, G. L. & Vachet, R. W. The basics of mass spectrometry in the twenty-first century. *Nat Rev Drug Discov* **2**, 140–150 (2003).
6. Pandey, A. & Mann, M. Proteomics to study genes and genomes. *Nature* **405**, 837–846 (2000).
7. Phan, J. H., Quo, C.-F. & Wang, M. D. Functional genomics and proteomics in the clinical neurosciences: data mining and bioinformatics. *Prog. Brain Res.* **158**, 83–108 (2006).
8. Steen, H. & Mann, M. The ABC's (and XYZ's) of peptide sequencing. *Nat. Rev. Mol. Cell Biol.* **5**, 699–711 (2004).
9. Henderson, R. Half-time in a century of molecular biology. *Excellence in Science: News from the Royal Society* 10 (2003).
10. Rogers, S. *et al.* Investigating the correspondence between transcriptomic and proteomic expression profiles using coupled cluster models. *Bioinformatics* **24**, 2894–2900 (2008).
11. Ross, J. mRNA stability in mammalian cells. *Microbiol. Rev.* **59**, 423–450 (1995).
12. Mootha, V. K. *et al.* Integrated analysis of protein composition, tissue diversity, and gene regulation in mouse mitochondria. *Cell* **115**, 629–640 (2003).
13. Maziarz, M., Chung, C., Drucker, D. J. & Emili, A. Integrating global proteomic and genomic expression profiles generated from islet alpha cells: opportunities and challenges to deriving reliable biological inferences. *Mol. Cell Proteomics* **4**, 458–474 (2005).
14. Anderson, L. & Seilhamer, J. A comparison of selected mRNA and protein abundances in human liver. *Electrophoresis* **18**, 533–537 (1997).
15. Gygi, S. P., Rochon, Y., Franza, B. R. & Aebersold, R. Correlation between protein and mRNA abundance in yeast. *Mol. Cell. Biol.* **19**, 1720–1730 (1999).
16. Wang, Y. *et al.* Precision and functional specificity in mRNA decay. *Proc. Natl. Acad. Sci. U.S.A.* **99**, 5860–5865 (2002).
17. Commerford, S. L., Carsten, A. L. & Cronkite, E. P. The distribution of tritium among the amino acids of proteins obtained from mice exposed to tritiated water. *Radiat. Res.* **94**, 151–155 (1983).
18. Pan, Y. *et al.* Identification of biochemical adaptations in hyper- or hypocontractile hearts from phospholamban mutant mice by expression proteomics. *Proceedings of the National Academy of Sciences of the United States of America* **101**, 2241–2246 (2004).
19. Kislinger, T. *et al.* PRISM, a Generic Large Scale Proteomic Investigation Strategy for Mammals. *Molecular & Cellular Proteomics* **2**, 96–106 (2003).
20. Jana, N. R. Protein homeostasis and aging: Role of ubiquitin protein ligases. *Neurochemistry International* **60**, 443–447 (2012).
21. Geng, F., Wenzel, S. & Tansey, W. P. Ubiquitin and Proteasomes in Transcription. *Annual Review of Biochemistry* **81**, null (2012).
22. Demasi, M. & Laurindo, F. R. M. Physiological and Pathological Role of the Ubiquitin-Proteasome System in the Vascular Smooth Muscle Cell. *Cardiovascular Research* (2012).doi:10.1093/cvr/cvs128

23. Yao, T. & Ndoja, A. Regulation of gene expression by the ubiquitin-proteasome system. *Seminars in Cell & Developmental Biology* (2012).doi:10.1016/j.semcdb.2012.02.006
24. Macgurn, J. A., Hsu, P.-C. & Emr, S. D. Ubiquitin and Membrane Protein Turnover: From Cradle to Grave. *Annual Review of Biochemistry* (2012).doi:10.1146/annurev-biochem-060210-093619
25. Ciechanover, A. & Brundin, P. The Ubiquitin Proteasome System in Neurodegenerative Diseases: Sometimes the Chicken, Sometimes the Egg. *Neuron* **40**, 427–446 (2003).
26. Davies, J. E., Sarkar, S. & Rubinsztein, D. C. The ubiquitin proteasome system in Huntington's disease and the spinocerebellar ataxias. *BMC Biochemistry* **8**, S2 (2007).
27. Keller, J. N., Gee, J. & Ding, Q. The proteasome in brain aging. *Ageing Research Reviews* **1**, 279–293 (2002).
28. Vernace, V. A., Schmidt-Glenewinkel, T. & Figueiredo-Pereira, M. E. Aging and regulated protein degradation: who has the UPPer hand? *Aging Cell* **6**, 599–606 (2007).
29. De Duve, C. & Wattiaux, R. Functions of lysosomes. *Annu. Rev. Physiol.* **28**, 435–492 (1966).
30. DE DUVE, C. The lysosome. *Sci. Am.* **208**, 64–72 (1963).
31. Lee, J., Giordano, S. & Zhang, J. Autophagy, mitochondria and oxidative stress: cross-talk and redox signalling. *Biochemical Journal* **441**, 523–540 (2012).
32. Gottlieb, R. A. & Carreira, R. S. Autophagy in health and disease. 5. Mitophagy as a way of life. *Am. J. Physiol., Cell Physiol.* **299**, C203–210 (2010).
33. Schneider, L. & Zhang, J. Lysosomal function in macromolecular homeostasis and bioenergetics in Parkinson's disease. *Mol Neurodegener* **5**, 14 (2010).
34. Hashimoto, M., Rockenstein, E., Crews, L. & Masliah, E. Role of protein aggregation in mitochondrial dysfunction and neurodegeneration in Alzheimer's and Parkinson's diseases. *NeuroMolecular Medicine* **4**, 21–35 (2003).
35. Mortimore, G. E., Hutson, N. J. & Surmacz, C. A. Quantitative correlation between proteolysis and macro- and microautophagy in mouse hepatocytes during starvation and refeeding. *Proc. Natl. Acad. Sci. U.S.A.* **80**, 2179–2183 (1983).
36. Mortimore, G. E., Lardeux, B. R. & Adams, C. E. Regulation of microautophagy and basal protein turnover in rat liver. Effects of short-term starvation. *J. Biol. Chem.* **263**, 2506–2512 (1988).
37. Mijaljica, D., Prescott, M. & Devenish, R. J. Microautophagy in mammalian cells: revisiting a 40-year-old conundrum. *Autophagy* **7**, 673–682 (2011).
38. Sahu, R. *et al.* Microautophagy of cytosolic proteins by late endosomes. *Dev. Cell* **20**, 131–139 (2011).
39. Wolfe, R. R. & Chinkes, D. L. *Isotope tracers in metabolic research: principles and practice of kinetic analysis*. (Wiley-IEEE: 2005).
40. Kenney, F.T. Hormonal regulation of synthesis of liver enzymes. *Mammalian Protein Metabolism* **IV**, 131–176 (1970).
41. Waterlow, J. C. The Mysteries of Nitrogen Balance. *Nutrition Research Reviews* **12**, 25–54 (1999).
42. Wurtman, R.J. Diurnal rhythms in mammalian protein metabolism. *Mammalian Protein Metabolism* **IV**, 445–479 (1970).
43. Ong, S.-E. *et al.* Stable Isotope Labeling by Amino Acids in Cell Culture, SILAC, as a Simple and Accurate Approach to Expression Proteomics. *Molecular & Cellular Proteomics* **1**, 376–386 (2002).

44. Schvartz, D., Couté, Y., Brunner, Y., Wollheim, C. B. & Sanchez, J.-C. Modulation of Neuronal Pentraxin 1 Expression in Rat Pancreatic B-Cells Submitted to Chronic Glucotoxic Stress. *Mol Cell Proteomics* (2012).doi:10.1074/mcp.M112.018051
45. Van Hoof, D. *et al.* An experimental correction for arginine-to-proline conversion artifacts in SILAC-based quantitative proteomics. *Nat. Methods* **4**, 677–678 (2007).
46. Price, J. C., Guan, S., Burlingame, A., Prusiner, S. B. & Ghaemmaghami, S. Analysis of proteome dynamics in the mouse brain. *Proc. Natl. Acad. Sci. U.S.A.* **107**, 14508–14513 (2010).
47. McClatchy, D. B. & Yates, J. R., 3rd Stable Isotope Labeling of Mammals (SILAM). *CSH Protoc* **2008**, pdb.prot4940 (2008).
48. Krüger, M. *et al.* SILAC Mouse for Quantitative Proteomics Uncovers Kindlin-3 as an Essential Factor for Red Blood Cell Function. *Cell* **134**, 353–364 (2008).
49. Sury, M. D., Chen, J.-X. X. & Selbach, M. The SILAC fly allows for accurate protein quantification in vivo. *Molecular & Cellular Proteomics* (2010).doi:10.1074/mcp.M110.000323
50. Boettger, T. *et al.* Acquisition of the contractile phenotype by murine arterial smooth muscle cells depends on the Mir143/145 gene cluster. *J. Clin. Invest.* **119**, 2634–2647 (2009).
51. Geiger, T. *et al.* Use of stable isotope labeling by amino acids in cell culture as a spike-in standard in quantitative proteomics. *Nat. Protocols* **6**, 147–157 (2011).
52. Ishihama, Y. *et al.* Quantitative mouse brain proteomics using culture-derived isotope tags as internal standards. *Nat Biotech* **23**, 617–621 (2005).
53. Jacob, R. J. Bioinformatics for LC-MS/MS-based proteomics. *Methods Mol. Biol.* **658**, 61–91 (2010).
54. Deutsch, E. W. *et al.* A guided tour of the Trans-Proteomic Pipeline. *Proteomics* **10**, 1150–1159 (2010).
55. Lam, H. *et al.* Development and validation of a spectral library searching method for peptide identification from MS/MS. *Proteomics* **7**, 655–667 (2007).
56. Keller, A., Nesvizhskii, A. I., Kolker, E. & Aebersold, R. Empirical statistical model to estimate the accuracy of peptide identifications made by MS/MS and database search. *Anal. Chem.* **74**, 5383–5392 (2002).
57. Shteynberg, D. *et al.* iProphet: multi-level integrative analysis of shotgun proteomic data improves peptide and protein identification rates and error estimates. *Mol. Cell Proteomics* **10**, M111.007690 (2011).
58. Han, D. K., Eng, J., Zhou, H. & Aebersold, R. Quantitative profiling of differentiation-induced microsomal proteins using isotope-coded affinity tags and mass spectrometry. *Nat. Biotechnol.* **19**, 946–951 (2001).
59. Nesvizhskii, A. I. & Aebersold, R. Analysis, statistical validation and dissemination of large-scale proteomics datasets generated by tandem MS. *Drug Discov. Today* **9**, 173–181 (2004).
60. Nesvizhskii, A. I., Keller, A., Kolker, E. & Aebersold, R. A statistical model for identifying proteins by tandem mass spectrometry. *Anal. Chem.* **75**, 4646–4658 (2003).

# Section 1

## Calorie Restriction, Mitochondrial Biogenesis, and Mitochondrial Protein Turnover

## Review of the Literature

Calorie restriction (CR) is considered the most robust non-genetic method to increase lifespan in a number of model organisms, including yeast [1], worms [2], flies [3], mice, rats [4], and nonhuman primates [5–7], and functions to increase both mean and maximal life span in all organisms studied to date. Calorie restriction functions to delay the onset of many age-related diseases, including cardiovascular disease, type 2 diabetes, hypertension, and cancer [8,9]. Many physiological adaptations to CR have been observed in rodent models, including a decrease in global cell proliferation, increased insulin sensitivity, reduced body weight, reduced adiposity, alterations in fatty acid synthesis and oxidation, neuroprotection, and various improvements in mitochondrial metabolism. However, despite more than 75 years of research, the underlying molecular mechanisms that confer increased resistance to disease risk remain to be fully described.

In what is considered the seminal work on calorie restriction, McCay et al. demonstrated in 1935 that restricting calories in both male and female rats retarded growth yet prolonged both mean and maximal lifespan [10]. McCay and colleagues then published three additional studies that confirmed the results of their original paper, indicating that energy reduction was solely responsible for lifespan increase rather than the reduction in any single dietary nutrient [11–13]. In the 1920s and 1930s, mean lifespan was only 53 years of age. Infant mortality and childhood diseases killed millions of children, and bacterial infections were prevalent in the population at large. For these reasons, understanding the effect of CR on growth and lifespan were very important public health issues[14]. Within the next ten years, several investigations began to elucidate the connection between CR and carcinogenesis, establishing the effect of CR in mitigating the formation of spontaneous tumors [12,15].

### Calorie Restriction Reduces Cell Proliferation

To date, no single biological mechanism has taken center stage as the most important criteria in lifespan extension. Given the complex nature of biological systems, in mammals there are a large number of physiological changes that occur in response to CR that may contribute to increased lifespan, including increased risk for the development of cancer [15–24], insulin resistance and diabetes [25–34], and cardiovascular disease

[35–42]. If CR functions by prolonging tissue lifespan, then could it be that CR reduces the fundamental rate at which an organism ages? In order to answer this question, we must first develop a biological definition of aging.

Interestingly, there exists no formal biological definition of the term *aging*, however t is very likely that cell proliferation may be related to the mechanism of aging. Evidence for this is based on the observation that increased cell proliferation rates are associated with premature aging. Mice that overexpress bovine growth hormone (BGH) experience increased postnatal growth, and are about twice the size of their wild type counterparts. These BGH transgenic mice experience a 50% reduction in lifespan, memory loss, and reduced fertility as compared with wild type controls [43]. The ATR knockout mouse is a second mouse model of premature aging in which DNA damage repair is compromised. The deletion of ATR results in the loss of proliferating cells, which stimulates increased repopulation and therefore increased cell proliferation. ATR deletion leads to premature aging in several tissues including bone marrow, intestines, spleen, and thymus [44]. The hypothesis for premature aging in the ATR deletion mouse is increased cell proliferation in response to stem cell loss, ultimately leading to premature aging and reduced lifespan.

## Macronutrient Restriction, Lifespan, and Mitochondrial Metabolism

In the 1940's, Ross and Bras conducted a series of investigations to determine the effect of restricting protein intake on longevity and spontaneous tumor formation in rats[45–50]. This collection of studies was the first to probe the connection between dietary restriction, protein metabolism, and longevity.

These studies were not designed to investigate the effect of CR on *in vivo* protein metabolism, instead they directly compared the effect of either CR or protein restriction (PR) on lifespan-extension, and concluded that the lifespan-extension effect of CR was far superior to that of PR, confirming McCay's original statement. The effect of both CR and PR on mitochondrial metabolism was an area of investigation that had yet to be explored, driven by increasing evidence that defects in mitochondrial metabolism may underlie many age-related diseases, including cardiovascular disease, type 2 diabetes, hypertension, and cancer[8,9].

CR has been shown to reduce mitochondrial oxygen radical (mtROS) production and oxidative damage to DNA in various rat tissues, two characteristics that are typical of long-lived species. To investigate whether restriction of any particular macronutrient was responsible for this effect, the group of Barja et al. systematically reduced carbohydrate, protein, and lipid intake in isolation and measured the effect on these two indicators of mitochondrial function: (a) mtROS production and (b) oxidative damage to nuclear and mtDNA. They found that reducing protein intake by 40% in male rats without significant decreases in overall calorie intake decreased mtROS production and oxidative damage to both nuclear and mitochondrial DNA by 30-40%, resulting from a decrease in the percent free radical leak and not from changes in

mitochondrial oxygen consumption. The decrease in mtROS production occurred mainly at complex I, the most significant free radical generator in the mammalian electron transport chain (REFS HERE). These results were strong evidence that PR itself may account for part of the improvements in mitochondrial metabolism, presenting a alternative to CR that may serve to increase patient compliance in CR studies conducted in humans[51].

Seven weeks of 40% Carbohydrate restriction (ChoR) without significant CR did not significantly affect mtROS production, mitochondrial oxygen consumption, percent free radical leak, or oxidative damage to nuclear or mitochondrial DNA, suggesting that carbohydrates are not the macronutrient responsible for the improvements in mitochondrial metabolism observed in CR[52]. Finally, seven weeks of 40% Lipid restriction (LR) without significant CR increased oxygen consumption with complex I-linked substrates, without affecting mitochondrial hydrogen peroxide production or oxidative damage to nuclear or mitochondrial DNA. This evidence suggests that LR does not account for the effect of CR on improvements in mitochondrial metabolism[53]. Taken together, the studies on isolated macronutrients suggest that the restriction of 40% protein is sufficient to mimic the effect of CR on mitochondrial metabolic improvements, while the restriction of 40% carbohydrates or 40% lipids by themselves do not replicate this effect.

To further investigate the connection between dietary PR, mtROS and oxidative damage to DNA, the same group of researchers then reduced only the intake of methionine (methionine restriction, MetR), and substituted 80% of dietary methionine with glutamate. MetR had been previously shown to mimic the effect of CR by extending maximal lifespan (REFS HERE), however the effect of MetR on specific makers of mitochondrial metabolism had not been investigated. Restriction of methionine by 80% had many physiological effects, including: (a) decreased mitochondrial protein oxidative damage in rat liver as measured by five markers of protein oxidation, (b) a reduced rate of mtROS production, (c) lowered membrane unsaturation, (d) Specifically decreased complex I and III content and activity in rat brain, the two electron transport chain complexes responsible for the majority of mtROS production, (e) increased uncoupling protein 4 (UCP4) expression in rat brain, increasing the resistance of the brain to metabolic and oxidative stress, and (f) decreased heart mtROS production at complex I, and lowers the rate of oxidative damage to both mitochondrial DNA and protein[54–59].

Studies were also conducted on the effect of PR independent of MetR to determine if any other dietary amino acid may play a role in mediating CR-induced longevity. Following 6-7 weeks of 40% amino acid restriction (AAR) without MetR or CR did not change mtROS production, oxidative damage to nuclear or mitochondrial DNA, mitochondrial oxygen consumption, respiratory complex I-IV content, and the expression of mitochondrial biogenesis factors PGC-1a and NRF-2 in rat liver. However, AAR decreased mitochondrial protein oxidation, the degree of mitochondrial fatty acid unsaturation while increasing SIRT-1 protein

abundance. These results strongly suggest that mtROS production and oxidative damage to DNA is controlled, in part, by a single amino acid: methionine[60].

These results suggest that MetR by itself can protect many tissues against damage to nuclear and mitochondrial DNA induced by mtROS production. Interestingly, MetR serves both a metabolic (liver) and neuroprotective (brain) effect, much in the same way that CR induces a multi-organ reprogramming resulting in improved cellular and tissue function that may contribute to a reduction in the global rate of aging at the whole-organism level.

### Calorie Restriction and Protein Synthesis

Calorie restriction has been shown to delay the rate of aging in yeast, nematodes, flies, rodents, and primates [61–63]. In addition, CR protects rodents against oxidative damage to proteins, and may acutely reduce steady state levels of oxidative stress by reducing the rate of protein oxidation [64,65]. In rats, CR decreases the fractional synthesis and fractional breakdown rates of muscle proteins [66]. Others have observed the exact opposite effect, namely increases in protein synthetic rates in response to CR [62,67–70].

### Protein Degradation Pathways

The primary pathways of protein degradation include ubiquination, autophagy, and calcium-activated proteinases. While each of these pathways has shared characteristics, the regulatory mechanisms of each system are described below.

### Autophagy

Autophagy is an intracellular catabolic process aimed at protecting the cell against the harmful effects of toxic products, including damaged macromolecules and aberrant proteins[71,72]. In macroautophagy, a region of the cytosol is engulfed in an ER-derived vesicle devoid of ribosomes, called an autophagic vacuole or an autophagosome. The autophagosome fuses with the lysosome, and the contents are exposed to an acidic pH and a collection of proteolytic enzymes that facilitate the breakdown of a large number of proteins simultaneously. Autophagosome cargo is digested in bulk, the contents of which may contain mitochondria, ER fragments, glycogen, golgi apparatus, or structural components including actin, myosin, and tubulin. This process is thought to predominate due to sudden perturbations in cellular homeostasis, including cellular oxidative stress, mechanical damage, or nutrient starvation. Similarly, microautophagy accounts for most of basal protein breakdown at steady-state[73].

### Ubiquination

Ubiquination is the principal mechanism of controlled protein breakdown in eukaryotes, and is reliant on the “tagging” (or activation) of proteins marked for degradation by a small heat-stable ubiquitin protein. As the name implies, this protein is ubiquitously present in all cell types, and regulates the breakdown of proteins involved in cell cycle, growth, transcription, DNA repair, oncogenesis, and antigen processing [74].

Ubuiquitin is first activated by a high-energy thioester linkage, then transferred to a carrier protein via the action of an E3 ubiquitin-protein ligase. Proteins marked for degradation are typically tagged at a

lysine residue at a site known as the degron, and specificity in this process is governed by the specific interaction between the E3 ubiquitin ligase and the target protein. In a typical mammalian cell there exists hundreds of E3 protein ligases, each recognizing specific degron motifs on target proteins[75]. It is appropriate to think of protein ubiquination as a type of post-translational modification.

A ubiquinated protein is then transported to the 26S proteasome, a self-contained proteolytic factory. Chaperone proteins present the tagged protein to the proteasome, which contain a collection of chymotryptic, tryptic, and caspase-like proteases, resulting in a collection of peptide fragments between 4-25 amino acids in length. In this respect, the 26S proteasome has six distinct functions, including (a) recognition of tagged proteins, (b) de-ubiquitination of presented proteins, (c) unfolding of target proteins, (d) transloation of target proteins, (e) enzymatic protein degradation, and (f) protein processing [75].

The ubiquitin protease system (UPS) is active on a wide variety of protein substrates including myofibrillar proteins, cyclins, receptors, and ion channels [73]. Moreover, the UPS occurs in all tissues, and is particularly active in muscle tissue undergoing atrophy [76–78]. Interestingly, impaired UPS function is implicated in a number of age-related neurodegenerative conditions, including parkinsons and alzheimers disease [79–82].

## Aging and Protein Degradation

It has been well documented that aging reduces the expression, transcription, and translation of genes across the genome in many species, however the absolute amount (pool size) of most proteins remain relatively constant over time [83]. Since protein synthesis and degradation are linked processes, these observations would predict a decline in protein degradation with age, which is indeed the case [84–86]. In the brain of aged mice, the amount of ubiquitin-protein conjugates is increased in comparison with young controls, suggesting that the efficiency of protein degradation decreases with age [87]. The decline in proteasomal activity results in increased protein half-life, allowing for the persistence of oxidized proteins [88].

In addition, molecular chaperone activity is reduced with increased age. These proteins are responsible for maintaining the native conformation of both proteins and RNA, and their protective role in the cell is vital to survival. In long-lived nematode and fly mutants, increased levels of stress-induced chaperones are present, arguing that the ability to respond to acute stress is a key indicator of longevity [89–92].

## The Effect of Calorie Restriction on *in vivo* Mitochondrial Metabolism

Dysfunctional mitochondrial function has been implicated in a number of age-related diseases [93], and age-related diseases are associated with the accumulation of improperly folded proteins and cross-linked protein aggregates [83,94]. Mitochondrial metabolism in muscle and liver has become an increasingly important area of investigation in CR, given that mitochondria are implicated in a number of age-related metabolic and neurodegenerative diseases. Therefore, the measurement of hepatic protein homeostasis may provide insight into the molecular mechanisms underlying

prolonged lifespan and reduced disease risk.

## The Effect of CR on Mitochondrial Biogenesis: Controversy in the Literature

Mitochondrial biogenesis may play a role in mediating the effects of CR, although this argument remains controversial. Given that full oxidation of fuel substrates takes place exclusively in the mitochondrial compartment, increased dependence on fatty acids for fuel may provide a metabolic signal for the biosynthesis of mitochondria in skeletal muscle[95]. To this effect, several studies have shown mitochondrial biogenesis in response to CR. In a recent study conducted in vitro and in vivo, CR induced proliferation of mitochondria with reduced membrane potential and rate of reactive oxygen species (ROS) production[96], while in another investigation CR promoted increases in oxidative capacity concomitant with decreases in triglyceride content in rat skeletal muscle[97].

Another study reported that CR promoted mitochondrial biogenesis in mice through a signaling pathway activating endothelial nitric oxide synthase[98]. CR has also been shown to induce increases in citrate synthase acvitity (CS, a marker for total mitochondrial mass), PGC-1a, COX-IV, and Mfn-2 expression, in conjunction with increased eNOS and Akt phosphorylation[99]. In humans, it was observed that 6-months of CR and 6-months of CR combined with exercise (CREX) demonstrated increased expression of genes involved in mitochondrial metabolism including PGC1a, TFAM, eNOS, SIRT1, and PARL. In addition, mtDNA content increased by 35% in the CR group vs. 21% in the CREX group. Interestingly, despite these changes, there were no observable differences in the activity of enzymes involved in the TCA cycle, beta oxidation pathway, and electron transport chain[100]. Taken together, these investigations support the hypothesis that CR promotes bioenergetic efficiency via increases in mitochondrial density.

## Fuel Selection May Influence Mitochondrial Metabolism

In support of these findings, observations by our laboratory indicate that mice fed on a CR regimen experience a dramatic change in feeding pattern, resulting in prolonged periods of fatty acid availability[101]. CR mice consume their entire daily allotment of food within the span of four hours, followed by a twenty hour daily fast. Glucose oxidation predominates during the feeding period (RER $\geq$ 0.9), followed by a rapid shift to fatty acid oxidation in the post-absorptive state (RER $\leq$ 0.8). We also found that CR mice oxidized four times as much fat per day as ad libitum (AL)-fed controls (367 ± 19 vs. 97 ± 14 mg/day, $P < 0.001$) despite reduced energy intake from fat, demonstrating that CR dramatically increases the total energy derived directly from FA oxidation compared with AL controls. This increase in FA oxidation was balanced by a threefold increase in adipose tissue FA synthesis compared with AL. In contrast, CR did not alter the accumulation of any endogenously synthesized FA in the liver. When extrapolated to total fat mass, CR mice synthesized and retained in adipose tissue and liver a total of 212 ± 13 mg FA/day compared with 91 ± 9 mg/day for AL controls. These data suggest that CR

induces a surprising metabolic pattern characterized by periods of elevated FA synthesis alternating with periods of FA oxidation disproportionate to dietary FA intake.

Furthermore, given that fatty acid oxidation takes place in the mitochondrial compartment, increased availability of fatty acids as a fuel substrate may in itself provide a metabolic signal for the biosynthesis of mitochondria in skeletal muscle. In support of our observations, recent studies in rodents demonstrated that increased reliance on fatty acids for energy production results in mitochondrial biogenesis and increases in lipid oxidative enzymes. In the first study, mice fed a high fat diet experienced increases in the activity of enzymes involved in fatty acid oxidation, the TCA cycle, and the respiratory chain, as well as increases in mtDNA copy number per diploid nuclear genome [102]. In the second study, mice fed a high fat diet demonstrated increases in lipid oxidative capacity without the induction of insulin resistance via ectopic lipid accumulation [103]. Fuel selection therefore seems to play a significant role in mediating mitochondrial function, providing a link between daily feeding dynamics and mitochondrial biogenesis.

## Does Calorie Restriction Promote Mitochondrial Biogenesis?

While a growing body of evidence suggests that CR promotes significant gain-of-function attributes in mitochondria, a verdict on whether CR promotes mitochondrial biogenesis has not been established. In fact, the effect of CR on mitochondrial biogenesis is conflicting, and the research on this topic is not definitive.

Interventions known to alter substrate metabolism and provide a signal for increased ATP production are expected to result in increased mitochondrial content. Exercise, as an example, increases the need for maximal ATP production and therefore promotes mitochondrial biogenesis in skeletal muscle [104–106]. Unpublished data from our lab clearly indicates that forced treadmill running in mice subjected to a progressive resistance protocol for 3 weeks results in a profound perturbation in the heart, soleus (red muscle), and gastrocnemius (white muscle) mitochondrial proteome, resulting in increased synthesis rates of mitochondrial proteins involved in fatty acid metabolism, oxidative phosphorylation, and the TCA cycle.

A second intervention that promotes increased mitochondrial substrate flux is cold exposure. Animals subjected to cold adapt by increasing heat production, resulting in large increases in the expression of uncoupling protein 1 (UCP1) in brown adipose tissue (BAT), together with increased mitochondrial density [107,108].

By definition, CR is achieved via a reduction in energy intake. Why then would CR lead to increases in mitochondrial biogenesis in the face of reduced macronutrient availability? While the findings of Nisoli et al. in particular seem to be very well accepted in the CR community, two findings in particular raise question. The first of these concerns centers around the finding that mitochondrial biogenesis is increased in cardiac muscle in response to 30% CR. In a 2010 review, Hancock et al. state,

*"The heart has a very high content of mitochondria, and a further increase in*

*mitochondria resulting from overexpression of PGC-1α in transgenic mice is maladaptive, causing disruption of myofibrillar architecture and heart failure. Therefore, the finding of Nisoli et al. that CR resulted in large increases in mitochondria and respiration in heart muscle seemed particularly surprising, as it does not fit with the evidence that CR results in maintenance of good diastolic cardiac function into old age* [109]*."* [110]

If experimental manipulation to increase heart mitochondrial content does in fact unfavorably disrupt normal cardiac function, then the finding that CR promotes cardiac mitochondrial biogenesis is either an exception to that rule, or presents a biologically counterintuitive argument.

The second perplexing result is that CR increases oxygen consumption and ATP production at steady-state. This suggests that an increase in mitochondrial content *per se* increases ATP production despite reduced nutrient flux. It has been known for years that exercise-induced mitochondrial biogenesis does not alter the rate of oxygen consumption and ATP production *at rest*, rather permits for an increased rate of *maximal* ATP production during exercise. Therefore, the metabolic demand of the tissue at any moment in time uniquely determines the rate of instantaneous ATP production. Increased mitochondrial content is therefore an insurance policy to protect against the exercise-induced demand for ATP production[111].

Therefore, the discovery that CR results in increased oxygen consumption and ATP production at steady-state is indeed controversial. Hancock et al. further demonstrates that 30% CR in rats had no effect on (a) heart mitochondrial content or (b) brain mitochondrial content, as evidenced by no changes in the expression of key protein complexes in the respiratory chain required to induce mitochondrial biogenesis. Moreover, Hancock et al. demonstrate that in skeletal muscle, CR did not change the expression levels of 6 key mitochondrial marker proteins or the coordinately regulated GLUT4 transporter. Finally, CS activity was found to be unchanged in muscle, liver, and heart, suggesting that total mitochondrial content was unaffected by CR in multiple tissues [110], findings that are also supported by Sreekumar et al [112].

In another well-accepted study conducted in humans, Civitaresse found that 6 months of 25% CR resulted in a 35% increase in muscle mtDNA content despite no changes in CS content, or the activity levels of CS, COXII, or beta-HAD [100]. Hancock et al. write,

*"In our opinion, it is not possible to have an increase in functional mitochondria without increases in these mitochondrial enzymes"* [110].

The discrepancy between these studies highlights not only conflicting data, but conflicting opinions about the physiology of mitochondrial metabolism as a whole. Given conflicting results between studies, it is difficult to determine whether artifacts in experimental analysis may be responsible for erroneous conclusions, or whether species or strain-specific differences can explain opposing conclusions. Regardless, Hancock et al. provide a strong argument refuting the possibility of increased mitochondrial density in response to reduced calorie intake, citing that the basic physiological

premise that ATP production at rest should remain constant in most states. Differences in the rate of maximal ATP production occur in response to exercise, and return to the steady state rate of ATP production at rest. In addition, exercise most likely provides a significantly stronger stimulus for mitochondrial biogenesis than does CR, suggesting that alterations in steady state ATP production at rest in CR is not possible from a physiological point of view.

**Dynamic Proteomics To The Rescue**

In light of this controversy in the literature, is it possible for CR to induce mitochondrial biogenesis given a state of chronic nutrient scarcity? If so, what is the mitochondrial biogenic impetus in response to reduced energy intake?

In order to further elucidate the controversy in the field regarding the response of mitochondria to reduced energy intake, we designed an experiment to study the effect of long-term CR on hepatic protein turnover. We hypothesized that using the dynamic proteomics approach, we could determine the steady-state kinetics of hundreds of mitochondrial and non-mitochondrial proteins proteins in the liver of C57BL6 male mice, which would lend evidence regarding the difference in basal turnover rate of hepatic proteins in response to CR.

The importance of our study design is highlighted by the investigation of eighteen-month old mice fed either ad libitum (AL) their entire life or CR for the last fourteen months of life. This model allows us to measure steady-state hepatic protein turnover rates independent of transient perturbations that occur in the first few weeks of CR, as evidenced by a host of immediate physiological adaptations, including a reduction in body weight, adiposity, tissue weight, core temperature, and an increase in voluntary activity most likely associated with foraging behavior.

Moreover, using this experimental design we are able to probe the entire cellular proteome, providing the freedom to measure the turnover rates of proteins both in the mitochondrial reticulum as well as in extra-mitochondrial compartments, cell membranes, and the nucleus. Importantly, using this approach in combination with quantitative Stable Isotope Labeling of Animals (SILAM) quantitative proteomics, we are able to measure (a) the absolute turnover rates (protein flux), (b) the protein pool size (protein concentration), and (c) the replacement rates of individual proteins. To our knowledge, no studies have combined these proteomics techniques together, and therefore our study represents a significant advancement in the field of protein biology in that it merges both kinetic and quantitative data together.

In support of Hancock's previous statement, we are able to measure the effect of long-term CR on mitochondrial proteins considered *essential* for mitochondrial biogenesis, including those located in the electron transport chain and matrix. Based on the literature, we hypothesized that long-term CR would increase mitochondrial protein turnover, giving rise to a newer, more biologically efficient mitochondrial reticulum that produced fewer mtROS, reducing the rate of macromolecular oxidative damage and protein aggregates.

## Literature Cited


1. Guarente, L. Calorie restriction and SIR2 genes--towards a mechanism. *Mech. Ageing Dev.* **126**, 923–928 (2005).
2. Houthoofd, K. & Vanfleteren, J. R. The longevity effect of dietary restriction in Caenorhabditis elegans. *Exp. Gerontol.* **41**, 1026–1031 (2006).
3. Partridge, L., Piper, M. D. W. & Mair, W. Dietary restriction in Drosophila. *Mech. Ageing Dev.* **126**, 938–950 (2005).
4. Ramsey, J. J., Harper, M. E. & Weindruch, R. Restriction of energy intake, energy expenditure, and aging. *Free Radic. Biol. Med.* **29**, 946–968 (2000).
5. Colman, R. J. *et al.* Caloric Restriction Delays Disease Onset and Mortality in Rhesus Monkeys. *Science* **325**, 201 –204 (2009).
6. Das, S. K. *et al.* Long-term effects of 2 energy-restricted diets differing in glycemic load on dietary adherence, body composition, and metabolism in CALERIE: a 1-y randomized controlled trial. *The American Journal of Clinical Nutrition* **85**, 1023 –1030 (2007).
7. Mattison, J. A., Roth, G. S., Lane, M. A. & Ingram, D. K. Dietary restriction in aging nonhuman primates. *Interdiscip Top Gerontol* **35**, 137–158 (2007).
8. Anderson, R. M., Shanmuganayagam, D. & Weindruch, R. Caloric restriction and aging: studies in mice and monkeys. *Toxicol Pathol* **37**, 47–51 (2009).
9. Masoro, E. J. Caloric restriction and aging: an update. *Exp. Gerontol.* **35**, 299–305 (2000).
10. MCCAY, C., CROWELL, M. & MAYNARD, L. NUTRITION METABOLISM CLASSIC - THE EFFECT OF RETARDED GROWTH UPON THE LENGTH OF LIFE-SPAN AND UPON THE ULTIMATE BODY SIZE (REPRINTED FROM JOURNAL OF NUTRITION, VOL 10, PG 63-79, 1935). *Nutrition* **5**, 155–171 (1989).
11. McCay, C. M., Maynard, L. A., Sperling, G. & Barnes, L. L. Retarded Growth, Life Span, Ultimate Body Size and Age Changes in the Albino Rat after Feeding Diets Restricted in Calories. *The Journal of Nutrition* **18**, 1 –13 (1939).
12. McCay, C. M., Ellis, G. H., Barnes, L. L., Smith, C. a. H. & Sperling, G. Chemical and Pathological Changes in Aging and after Retarded Growth. *The Journal of Nutrition* **18**, 15 –25 (1939).
13. Lowry, O. H., McCay, C. M., Hastings, A. B. & Brown, A. N. Histochemical Changes Associated with Aging. *Journal of Biological Chemistry* **143**, 281 –284 (1942).
14. McDonald, R. B. & Ramsey, J. J. Honoring Clive McCay and 75 Years of Calorie Restriction Research. *The Journal of Nutrition* **140**, 1205 –1210 (2010).
15. Tannenbaum, A. The Genesis and Growth of Tumors. II. Effects of Caloric Restriction per se. *Cancer Research* **2**, 460 –467 (1942).
16. Heuson, J. C. & Legros, N. Influence of insulin deprivation on growth of the 7,12-dimethylbenz(a)anthracene-induced mammary carcinoma in rats subjected to alloxan diabetes and food restriction. *Cancer Res.* **32**, 226–232 (1972).
17. Klurfeld, D. M., Welch, C. B., Lloyd, L. M. & Kritchevsky, D. Inhibition of DMBA-induced mammary tumorigenesis by caloric restriction in rats fed high-fat diets. *Int. J. Cancer* **43**, 922–925 (1989).
18. Klurfeld, D. M., Weber, M. M. & Kritchevsky, D. Inhibition of chemically induced mammary and colon tumor promotion by caloric restriction in rats fed increased dietary fat. *Cancer Res.* **47**, 2759–2762 (1987).
19. Kritchevsky, D. Caloric restriction and experimental carcinogenesis. *Hybrid. Hybridomics* **21**, 147–151 (2002).
20. Kritchevsky, D. Caloric restriction and cancer. *J. Nutr. Sci. Vitaminol.* **47**, 13–19 (2001).

21. Kritchevsky, D. Caloric restriction and experimental carcinogenesis. *Toxicol. Sci.* **52**, 13–16 (1999).
22. Rous, P. THE INFLUENCE OF DIET ON TRANSPLANTED AND SPONTANEOUS MOUSE TUMORS. *J. Exp. Med.* **20**, 433–451 (1914).
23. Sylvester, P. W., Aylsworth, C. F., Van Vugt, D. A. & Meites, J. Influence of underfeeding during the 'critical period' or thereafter on carcinogen-induced mammary tumors in rats. *Cancer Res.* **42**, 4943–4947 (1982).
24. TANNENBAUM, A. & SILVERSTONE, H. The genesis and growth of tumors; effects of varying the proportion of protein (casein) in the diet. *Cancer Res.* **9**, 162–173 (1949).
25. Redman, L. M. & Ravussin, E. Caloric restriction in humans: impact on physiological, psychological, and behavioral outcomes. *Antioxid. Redox Signal.* **14**, 275–287 (2011).
26. Ravussin, E. & Redman, L. M. Adiposity and comorbidities: favorable impact of caloric restriction. *Nestle Nutr Workshop Ser Pediatr Program* **63**, 135–146; discussion 147–150, 259–268 (2009).
27. Liang, F., Kume, S. & Koya, D. SIRT1 and insulin resistance. *Nat Rev Endocrinol* **5**, 367–373 (2009).
28. Huang, P. *et al.* Calorie restriction and endurance exercise share potent anti-inflammatory function in adipose tissues in ameliorating diet-induced obesity and insulin resistance in mice. *Nutr Metab (Lond)* **7**, 59 (2010).
29. Wing, R. R. *et al.* Caloric restriction per se is a significant factor in improvements in glycemic control and insulin sensitivity during weight loss in obese NIDDM patients. *Diabetes Care* **17**, 30–36 (1994).
30. Williams, K. V., Mullen, M. L., Kelley, D. E. & Wing, R. R. The effect of short periods of caloric restriction on weight loss and glycemic control in type 2 diabetes. *Diabetes Care* **21**, 2–8 (1998).
31. Hughes, T. A., Gwynne, J. T., Switzer, B. R., Herbst, C. & White, G. Effects of caloric restriction and weight loss on glycemic control, insulin release and resistance, and atherosclerotic risk in obese patients with type II diabetes mellitus. *Am. J. Med.* **77**, 7–17 (1984).
32. Hanefeld, M. & Weck, M. Very low calorie diet therapy in obese non-insulin dependent diabetes patients. *Int J Obes* **13 Suppl 2**, 33–37 (1989).
33. Capstick, F. *et al.* Very low calorie diet (VLCD): a useful alternative in the treatment of the obese NIDDM patient. *Diabetes Res. Clin. Pract.* **36**, 105–111 (1997).
34. Kelley, D. E. *et al.* Relative effects of calorie restriction and weight loss in noninsulin-dependent diabetes mellitus. *J. Clin. Endocrinol. Metab.* **77**, 1287–1293 (1993).
35. Weiss, E. P. & Fontana, L. Caloric restriction: powerful protection for the aging heart and vasculature. *Am. J. Physiol. Heart Circ. Physiol.* **301**, H1205–1219 (2011).
36. Sung, M. M. Y. & Dyck, J. R. B. Age-related cardiovascular disease and the beneficial effects of calorie restriction. *Heart Fail Rev* **17**, 707–719 (2012).
37. Omodei, D. & Fontana, L. Calorie restriction and prevention of age-associated chronic disease. *FEBS Lett* **585**, 1537–42 (2011).
38. Kemnitz, J. W. Calorie restriction and aging in nonhuman primates. *ILAR J* **52**, 66–77 (2011).
39. Han, X. *et al.* Influence of long-term caloric restriction on myocardial and cardiomyocyte contractile function and autophagy in mice. *The Journal of nutritional biochemistry* (2012).doi:10.1016/j.jnutbio.2011.11.002
40. Dolinsky, V. W. & Dyck, J. R. B. Calorie restriction and resveratrol in cardiovascular health and disease. *Biochim. Biophys. Acta* **1812**, 1477–1489 (2011).
41. Dai, D.-F., Rabinovitch, P. S. & Ungvari, Z. Mitochondria and cardiovascular aging. *Circ. Res.* **110**, 1109–1124 (2012).
42. Ahmet, I., Tae, H.-J., de Cabo, R., Lakatta, E. G. & Talan, M. I. Effects of calorie

restriction on cardioprotection and cardiovascular health. *J. Mol. Cell. Cardiol.* **51**, 263–271 (2011).
43. Bartke, A. *et al.* Neuroendocrine and reproductive consequences of overexpression of growth hormone in transgenic mice. *Proc. Soc. Exp. Biol. Med.* **206**, 345–359 (1994).
44. Ruzankina, Y. *et al.* Deletion of the developmentally essential gene ATR in adult mice leads to age-related phenotypes and stem cell loss. *Cell Stem Cell* **1**, 113–126 (2007).
45. Ross, J. mRNA stability in mammalian cells. *Microbiol. Rev.* **59**, 423–450 (1995).
46. Ross, M. & Bras, G. Food preference and length of life. *Science* **190**, 165 –167 (1975).
47. Ross, M. H. Length of life and caloric intake. *The American Journal of Clinical Nutrition* **25**, 834 –838 (1972).
48. Ross, M. H., Bras, G. & Ragbeer, M. S. Influence of Protein and Caloric Intake upon Spontaneous Tumor Incidence of the Anterior Pituitary Gland of the Rat. *The Journal of Nutrition* **100**, 177 –189 (1970).
49. Ross, M. H. Length of Life and Nutrition in the Rat. *The Journal of Nutrition* **75**, 197 – 210 (1961).
50. ROSS, M. H. Protein, calories and life expectancy. *Fed. Proc.* **18**, 1190–1207 (1959).
51. Sanz, A., Caro, P. & Barja, G. Protein restriction without strong caloric restriction decreases mitochondrial oxygen radical production and oxidative DNA damage in rat liver. *J. Bioenerg. Biomembr.* **36**, 545–552 (2004).
52. Sanz, A., Gómez, J., Caro, P. & Barja, G. Carbohydrate restriction does not change mitochondrial free radical generation and oxidative DNA damage. *J. Bioenerg. Biomembr.* **38**, 327–333 (2006).
53. Sanz, A., Caro, P., Sanchez, J. G. & Barja, G. Effect of lipid restriction on mitochondrial free radical production and oxidative DNA damage. *Ann. N. Y. Acad. Sci.* **1067**, 200–209 (2006).
54. Caro, P. *et al.* Forty percent and eighty percent methionine restriction decrease mitochondrial ROS generation and oxidative stress in rat liver. *Biogerontology* **9**, 183–196 (2008).
55. López-Torres, M. & Barja, G. Lowered methionine ingestion as responsible for the decrease in rodent mitochondrial oxidative stress in protein and dietary restriction possible implications for humans. *Biochim. Biophys. Acta* **1780**, 1337–1347 (2008).
56. Naudí, A. *et al.* Methionine restriction decreases endogenous oxidative molecular damage and increases mitochondrial biogenesis and uncoupling protein 4 in rat brain. *Rejuvenation Res* **10**, 473–484 (2007).
57. Pamplona, R. & Barja, G. Mitochondrial oxidative stress, aging and caloric restriction: the protein and methionine connection. *Biochim. Biophys. Acta* **1757**, 496–508 (2006).
58. Sanchez-Roman, I. *et al.* Forty percent methionine restriction lowers DNA methylation, complex I ROS generation, and oxidative damage to mtDNA and mitochondrial proteins in rat heart. *J. Bioenerg. Biomembr.* **43**, 699–708 (2011).
59. Sanz, A. *et al.* Methionine restriction decreases mitochondrial oxygen radical generation and leak as well as oxidative damage to mitochondrial DNA and proteins. *FASEB J.* **20**, 1064–1073 (2006).
60. Caro, P. *et al.* Effect of 40% restriction of dietary amino acids (except methionine) on mitochondrial oxidative stress and biogenesis, AIF and SIRT1 in rat liver. *Biogerontology* **10**, 579–592 (2009).
61. Merry, B. J. & Holehan, A. M. Onset of Puberty and Duration of Fertility in Rats Fed a Restricted Diet. *J Reprod Fertil* **57**, 253–259 (1979).
62. Holehan, A. M. & Merry, B. J. THE EXPERIMENTAL MANIPULATION OF AGEING BY DIET. *Biological Reviews* **61**, 329–368 (1986).

63. Sohal, R. S. & Weindruch, R. Oxidative stress, caloric restriction, and aging. *Science* **273**, 59–63 (1996).
64. Youngman, L. D., Park, J. Y. & Ames, B. N. Protein Oxidation Associated with Aging Is Reduced by Dietary Restriction of Protein or Calories. *PNAS* **89**, 9112–9116 (1992).
65. Dubey, A., Forster, M. J., Lal, H. & Sohal, R. S. Effect of Age and Caloric Intake on Protein Oxidation in Different Brain Regions and on Behavioral Functions of the Mouse. *Archives of Biochemistry and Biophysics* **333**, 189–197 (1996).
66. Goldspink, D. F., El Haj, A. J., Lewis, S. E. M., Merry, B. J. & Holehan, A. M. The influence of chronic dietary intervention on protein turnover and growth of the diaphragm and extensor digitorum longus muscles of the rat. *Experimental Gerontology* **22**, 67–78 (1987).
67. Lewis, S. E. M., Goldspink, D. F., Phillips, J. G., Merry, B. J. & Holehan, A. M. The effects of aging and chronic dietary restriction on whole body growth and protein turnover in the rat. *Experimental Gerontology* **20**, 253–263 (1985).
68. Merry, B. J. & Holehan, A. M. Effect of age and restricted feeding on polypeptide chain assembly kinetics in liver protein synthesis in vivo. *Mechanisms of Ageing and Development* **58**, 139–150 (1991).
69. Ward, W. & Richardson, A. Effect of age on liver protein synthesis and degradation. *Hepatology* **14**, 935–948 (1991).
70. Jazwinski, S. M. Metabolic control and ageing. *Trends in Genetics* **16**, 506–511 (2000).
71. Petrovski, G. & Das, D. K. Does autophagy take a front seat in lifespan extension? *J. Cell. Mol. Med.* **14**, 2543–2551 (2010).
72. Salminen, A. & Kaarniranta, K. Regulation of the aging process by autophagy. *Trends Mol Med* **15**, 217–224 (2009).
73. Waterlow, J. C. *Protein turnover*. (CABI: 2006).
74. Jana, N. R. Protein homeostasis and aging: Role of ubiquitin protein ligases. *Neurochemistry International* **60**, 443–447 (2012).
75. Geng, F., Wenzel, S. & Tansey, W. P. Ubiquitin and Proteasomes in Transcription. *Annual Review of Biochemistry* **81**, null (2012).
76. Demasi, M. & Laurindo, F. R. M. Physiological and Pathological Role of the Ubiquitin-Proteasome System in the Vascular Smooth Muscle Cell. *Cardiovascular Research* (2012).doi:10.1093/cvr/cvs128
77. Yao, T. & Ndoja, A. Regulation of gene expression by the ubiquitin-proteasome system. *Seminars in Cell & Developmental Biology* (2012).doi:10.1016/j.semcdb.2012.02.006
78. Macgurn, J. A., Hsu, P.-C. & Emr, S. D. Ubiquitin and Membrane Protein Turnover: From Cradle to Grave. *Annual Review of Biochemistry* (2012).doi:10.1146/annurev-biochem-060210-093619
79. Ciechanover, A. & Brundin, P. The Ubiquitin Proteasome System in Neurodegenerative Diseases: Sometimes the Chicken, Sometimes the Egg. *Neuron* **40**, 427–446 (2003).
80. Davies, J. E., Sarkar, S. & Rubinsztein, D. C. The ubiquitin proteasome system in Huntington's disease and the spinocerebellar ataxias. *BMC Biochemistry* **8**, S2 (2007).
81. Keller, J. N., Gee, J. & Ding, Q. The proteasome in brain aging. *Ageing Research Reviews* **1**, 279–293 (2002).
82. Vernace, V. A., Schmidt-Glenewinkel, T. & Figueiredo-Pereira, M. E. Aging and regulated protein degradation: who has the UPPer hand? *Aging Cell* **6**, 599–606 (2007).
83. Tavernarakis, N. & Driscoll, M. Caloric restriction and lifespan: a role for protein turnover? *Mechanisms of Ageing and Development* **123**, 215–229 (2002).
84. Lee, C. K., Klopp, R. G., Weindruch, R. & Prolla, T. A. Gene expression profile of aging and its retardation by caloric restriction. *Science* **285**, 1390–1393 (1999).

85. Rattan, S. I. & Clark, B. F. Intracellular protein synthesis, modifications and aging. *Biochem. Soc. Trans.* **24**, 1043–1049 (1996).
86. Rattan, S. I. Synthesis, modifications, and turnover of proteins during aging. *Exp. Gerontol.* **31**, 33–47 (1996).
87. Ohtsuka, H., Takahashi, R. & Goto, S. Age-Related Accumulation of High-Molecular-Weight Ubiquitin Protein Conjugates in Mouse Brains. *The Journals of Gerontology Series A: Biological Sciences and Medical Sciences* **50A**, B277–B281 (1995).
88. Sitte, N., Merker, K., von Zglinicki, T. & Grune, T. Protein oxidation and degradation during proliferative senescence of human MRC-5 fibroblasts. *Free Radical Biology and Medicine* **28**, 701–708 (2000).
89. Lithgow, G. J., White, T. M., Melov, S. & Johnson, T. E. Thermotolerance and Extended Life-Span Conferred by Single-Gene Mutations and Induced by Thermal Stress. *PNAS* **92**, 7540–7544 (1995).
90. Murakami, S. & Johnson, T. E. Life extension and stress resistance in Caenorhabditis elegans modulated by the tkr-1 gene. *Curr. Biol.* **8**, 1091–1094 (1998).
91. Walker, G. A., Walker, D. W. & Lithgow, G. J. Genes That Determine Both Thermotolerance and Rate of Aging in Caenorhabditis elegansa. *Annals of the New York Academy of Sciences* **851**, 444–449 (1998).
92. Yang, Y. & Wilson, D. L. Isolating aging mutants: a novel method yields three strains of the nematode Caenorhabditis elegans with extended life spans. *Mechanisms of Ageing and Development* **113**, 101–116 (2000).
93. Mao, P. & Reddy, P. H. Aging and amyloid beta-induced oxidative DNA damage and mitochondrial dysfunction in Alzheimer's disease: implications for early intervention and therapeutics. *Biochim. Biophys. Acta* **1812**, 1359–1370 (2011).
94. Hekimi, S. & Guarente, L. Genetics and the specificity of the aging process. *Science* **299**, 1351–1354 (2003).
95. Civitarese, A. E., Smith, S. R. & Ravussin, E. Diet, energy metabolism and mitochondrial biogenesis. *Curr Opin Clin Nutr Metab Care* **10**, 679–687 (2007).
96. Barazzoni, R. *et al.* Moderate caloric restriction, but not physiological hyperleptinemia per se, enhances mitochondrial oxidative capacity in rat liver and skeletal muscle--tissue-specific impact on tissue triglyceride content and AKT activation. *Endocrinology* **146**, 2098–2106 (2005).
97. López-Lluch, G. *et al.* Calorie restriction induces mitochondrial biogenesis and bioenergetic efficiency. *Proc. Natl. Acad. Sci. U.S.A.* **103**, 1768–1773 (2006).
98. Nisoli, E. *et al.* Calorie restriction promotes mitochondrial biogenesis by inducing the expression of eNOS. *Science* **310**, 314–317 (2005).
99. Cerqueira, F. M., Laurindo, F. R. M. & Kowaltowski, A. J. Mild mitochondrial uncoupling and calorie restriction increase fasting eNOS, akt and mitochondrial biogenesis. *PLoS ONE* **6**, e18433 (2011).
100. Civitarese, A. E. *et al.* Calorie Restriction Increases Muscle Mitochondrial Biogenesis in Healthy Humans. *PLoS Med* **4**, e76 (2007).
101. Bruss, M. D., Khambatta, C. F., Ruby, M. A., Aggarwal, I. & Hellerstein, M. K. Calorie restriction increases fatty acid synthesis and whole body fat oxidation rates. *Am. J. Physiol. Endocrinol. Metab.* **298**, E108–116 (2010).
102. Garcia-Roves, P. *et al.* Raising plasma fatty acid concentration induces increased biogenesis of mitochondria in skeletal muscle. *Proc. Natl. Acad. Sci. U.S.A.* **104**, 10709–10713 (2007).
103. Turner, N. *et al.* Excess lipid availability increases mitochondrial fatty acid oxidative capacity in muscle: evidence against a role for reduced fatty acid oxidation in lipid-induced insulin resistance in rodents. *Diabetes* **56**, 2085–2092 (2007).

104. Baar, K. *et al.* Adaptations of skeletal muscle to exercise: rapid increase in the transcriptional coactivator PGC-1. *FASEB J.* **16**, 1879–1886 (2002).
105. Booth F. W., Baldwin K. M. Muscle plasticity: energy demanding and supply processes. *Handbook of Physiology, Sect. 12: Exercise Regulation and Integration of Multiple Systems* 1075–1123
106. Holloszy, J. O. & Coyle, E. F. Adaptations of skeletal muscle to endurance exercise and their metabolic consequences. *J Appl Physiol* **56**, 831–838 (1984).
107. Cao, W. *et al.* p38 mitogen-activated protein kinase is the central regulator of cyclic AMP-dependent transcription of the brown fat uncoupling protein 1 gene. *Mol. Cell. Biol.* **24**, 3057–3067 (2004).
108. Puigserver, P. *et al.* A cold-inducible coactivator of nuclear receptors linked to adaptive thermogenesis. *Cell* **92**, 829–839 (1998).
109. Taffet, G. E., Pham, T. T. & Hartley, C. J. The age-associated alterations in late diastolic function in mice are improved by caloric restriction. *J. Gerontol. A Biol. Sci. Med. Sci.* **52**, B285–290 (1997).
110. Hancock, C. R., Han, D.-H., Higashida, K., Kim, S. H. & Holloszy, J. O. Does calorie restriction induce mitochondrial biogenesis? A reevaluation. *The FASEB Journal* **25**, 785 –791 (2011).
111. Constable, S. H. *et al.* Energy metabolism in contracting rat skeletal muscle: adaptation to exercise training. *Am. J. Physiol.* **253**, C316–322 (1987).
112. Sreekumar, R. *et al.* Effects of caloric restriction on mitochondrial function and gene transcripts in rat muscle. *Am. J. Physiol. Endocrinol. Metab.* **283**, E38–43 (2002).

# Chapter 1

## The Effect of Long-Term Calorie Restriction on *In Vivo* Hepatic Proteostasis: A Novel Combinaion of Dynamic and Quantitative Proteomics

John C. Price†‡, Cyrus F. Khambatta*‡, Kelvin W. Li†, Matthew D. Bruss*, Mahalakshmi Shankaran†, Marcy Dalidd*, Nicholas A. Floreani†, Lindsay S. Roberts*, Scott M. Turner†, William E. Holmes†, and Marc K. Hellerstein*

‡ These authors contributed to this work equally

*Department of Nutritional Sciences and Toxicology, University of California at Berkeley, Berkeley, California 94720

† KinemedInc, Emeryville, CA 94608

**Abstract**

Calorie restriction without malnutrition (CR) is considered the "gold standard" longevity-promoting intervention. A frequently cited hypothesis is that CR increases protein degradation, including the autophagic digestion of mitochondria (mitophagy)and removal of damaged proteins while promoting mitochondrial biogenesis and protein replacement. To test this hypothesis, we used stable isotope metabolic labeling and exogenously labeled SILAM standards to measure (a) the turnover kinetics and (b) the concentrations of hundreds of proteins *in vivo* in long-term CR mice and age matched *ad libitum* (AL)-fed controls. We found that CR causes a general reduction in the rate of hepatic cell proliferation and protein turnover. In particular, mitophagy and mitochondrial biogenesis were greatly reduced, as were ribosomal protein synthesis and breakdown. We also observed that proteins with related functions experienced similar perturbations in both turnover rate and concentration, allowing identification of potential regulatory nodes. We propose that the reduced global protein synthetic burden may contribute to improved cellular fitness and health benefits in CR.

**Keywords**

Calorie Restriction, Protein turnover, Proteome Dynamics, Mitochondrial Biogenesis, Isotopic Labeling.

**Abbreviations**

CR, Calorie restriction; AL, Ad libitum; ROS, Reactive Oxygen Species; DNA, mtDNA, Mitochondrial DNA; $f$ = fractional replacement, $k$=turnover rate constant, $p$=precursor pool enrichment, $n$=number of sites within peptide capable of incorporating label, $n_{AA}$=number of sites within amino acid capable of incorporating label, RMS=root mean square error, MPE=molar percent excess, LC-MS/MS=liquid chromatography tandem mass spectrometry, BW=body water, m/z = mass to charge ratio, M0=monoisotopic mass, EM0=absolute value of change in M0 intensity, D0= time point at day 0, AAPP=amino acid precursor pool, MIDA=mass isotopomer distribution analysis, NIA=National Institute on Aging.

## Introduction

Calorie restriction (CR) is a dietary intervention in which calorie intake is reduced without malnutrition [1]. CR is considered the most robust non-genetic method for increasing lifespan in yeast [2], worms [3], flies [4], mice, rats [5,6], and nonhuman primates [1,7–9], and has been shown to protect against the development of age-related diseases including cancer, diabetes, hypertension, and cardiovascular disease in mammalian models [1,9,10]. Beyond the prevention of disease, CR also reduces the age related decline in cognitive function and the development of sarcopenia [7]. The longevity extending effects of CR were first demonstrated in rats in 1934, yet despite more than 75 years of research the underlying cellular mechanisms are not understood [5,6].

The mechanism of increased longevity induced by CR is unknown, however current hypotheses invoke the reprogramming of cellular metabolism through the activation of master genetic regulators [7]. CR induces a host of physiological changes, including reduced reactive oxygen species (ROS) production [11,12], reduced core body temperature [13], and reduced global cell proliferation rates [14,15]. In contrast, increased mitochondrial function [16,17], fatty acid synthesis, fatty acid oxidation [14], mitochondrial DNA (mtDNA) content, oxygen consumption, and ATP production have been reported in CR, suggesting that CR may promote mitochondrial efficiency and mitochondrial biogenesis [18]. Therefore CR may function to directly oppose age-related mitochondrial dysfunction [19].

Age-related diseases are often accompanied by the accumulation of misfolded or cross-linked protein aggregates [20,21]. Autophagy is an intracellular catabolic mechanism that attenuates this accumulation of toxins via the digestion of damaged macromolecules, including protein aggregates and entire organelles [22,23]. The combined observations of CR-dependent increases in mitochondrial biogenesis [17,24,25], and increased protein catabolism [22,23,26,27] should result in increased protein turnover and shorter protein half-life. In this study, we directly tested this hypothesis by measuring hepatic proteome kinetics in response to long-term CR, using a recently developed

technique for measuring proteome dynamics [28]. Combining proteome dynamics with the measurement of protein concentrations (Fig. 1), we are able to measure both absolute synthesis rates and fractional replacement rates (half-lives)in both CR and AL-fed controls [29–31].

In this paper, we report the effect of long-term CR the turnover rates of hundreds of hepatic proteins in C57BL6 mice from the CR colony maintained by the National Institutes on Aging (NIA). Similar to earlier reports, we found that the turnover of functionally related proteins are regulated coordinately [32]. In contrast to expectations, we found that CR (a) reduced global protein turnover as measured by heavy water labeling, and (b) reduced protein concentrations as measured by SILAM quantitative proteomics. Together these two measurements show that CR significantly reduced global protein flux in comparison with AL-fed controls. Interestingly, we found that mitochondrial proteins were most affected at the level of protein turnover with greatly increased half-lives, while the concentration of ribonuclear proteins was most affected. Our findings suggest that individual protein groups/ontologies/complexes (categories sounds unscientific) are selectively regulated by multiple mechanisms in CR to reduce the absolute protein synthetic burden. In light of this data, we propose that reduced protein synthesis coupled with increased proteostatic quality control may play important roles in mediating the beneficial effects of CR.

## Materials and Methods

### Animals

Eighteen-month old CR male C57/BL6 mice (n=12) and age-matched AL controls (n=12) were purchased from Charles River (Wilmington, MA) where the NIA Caloric Restricted Mouse Colony is maintained (Fig. 2).Following one week of acclimation, animals in each group were labeled with an intraperitoneal injection of 100% $^2H_2O$ saline (0.35mL/10 g body weight) and were subsequently provided 8% $^2H_2O$ drinking water for the remainder of the study to maintain body $^2H_2O$ enrichments of approximately 5%, as described previously [33]. Animals in the CR group were fed 3.0 grams of the NIH-31/NIA fortified diet at 5pm daily, and animals in the AL group were provided unrestricted access to the NIH-31 diet (Fig. 2). Animals were sacrificed following 0.5, 1, 4, 8, 15 or 32 days of heavy water labeling (Fig 2A). Body weight and food intake were monitored on a weekly basis, and at the time of euthanasia (Fig. 2B). Animals were anesthetized with isoflurane and euthanized by cardiac puncture. All experiments were performed under the approval of the Institutional Animal Care and Use Committees of the University of California at Berkeley.

### Measurement of $^2H$ Enrichment In Body Water

Enrichment of $^2H_2O$ in body water (blood) was measured by chemical conversion to tetrabromoethane as described previously [33,34]. Briefly, the hydrogen atoms in $H_2O$ were transferred to acetylene by addition of 2–5 µl water via syringe to a chip of calcium carbide in a sealed vial, equipped with a 3 ml syringe inserted into the septum. The resulting acetylene gas was drawn into the 3 ml syringe and expelled into another sealed vial containing 0.5 ml

$Br_2$ (0.1 mM) dissolved in $CCl_4$. After 2 h of incubation at room temperature, the remaining $Br_2$ was reacted with cyclohexene dissolved in $CCl_4$ (10% solution). This solution was injected into the GC/MS for analysis. GC/MS analysis was performed with a DB-225, 30 m column at 220 °C, using methane chemical ionization with selected ion monitoring. The $C_2H_2Br_3^+$ fragment ($m/z$ 265 and 266, representing the $M_0$ and the $M_{+1}$ ion of the $^{79}Br^{79}Br^{81}Br$ isotopologue), was used for calculating $^2H$ enrichment, by comparison to standard curves generated by mixing 100% $^2H_2O$ with natural abundance $H_2O$ in known proportions.

### In Vivo Cell Proliferation Measurement

DNA was extracted from 30-50ug liver tissue using the DNeasy kit (Qiagen, Valencia, CA), and was enzymatically hydrolyzed to free deoxyribonucleosides by overnight incubation at 37°C with S1 nuclease and potato acid phosphatase. Hydrolysates were reacted with pentafluorobenzyl hydroxylamine and acetic acid and then acetylated with acetic anhydride and 1-methylimidazole. Dichloromethane extracts were dried, resuspended in ethyl acetate, and analyzed by gas chromatography-mass spectrometry on a DB-17 column with negative chemical ionization, using He as carrier and $CH_4$ as reagent gas. The fractional molar isotope abundances at $m/z$ 435 ($M_0$ mass isotopomer) and 436 ($M_1$) of the pentafluorobenzyl triacetyl derivative of purine dR were quantified using ChemStation software. Excess fractional $M_{+1}$ enrichment ($EM_1$) was calculated as

$$EM_1 = \frac{(AbundanceM_1)_{sample}}{(AbundanceM_0 + M_1)_{sample}} - \frac{(AbundanceM_1)_{standard}}{(AbundanceM_0 + M_1)_{standard}}$$

where sample and standard refer to the analyzed sample and an unenriched pentafluorobenzyl triacetyl purine dR derivative standard, respectively. The fractional replacement rate ($f$) was calculated by a comparison of $EM_1$ to the theoretical maximum $EM_1$ of a fully turned over tissue at the measured body water enrichment according to the following equation:

$$f = \frac{EM_{1\,sample}}{EM_{1\,maximum}}$$

### Protein Isolation and In-Gel Trypsin Digestion

At each time-point for collection, 2 mice were anesthetized under isoflurane gas and were then euthanized cardiac puncture and cervical dislocation. Tissues were harvested and snap-frozen in liquid nitrogen. For analysis liver samples were thawed and homogenized for 75 s in PBS containing 1 mM PMSF using a Mini-BeadBeater 8 (BioSpec, Bartlesville, OK) placed on ice for 1 min. This procedure was repeated twice and the resulting homogenate was diluted to 10% (w/v) in PBS containing 1 mM PMSF. Cultured cells were homogenized in 1ml of M-PER reagent (Pierce, Rockford, IL) containing protease inhibitors (When did we do cultured cells?). Protein from prepared homogenates was uniformly reduced by incubation in 10 mM DTT and SDS-PAGE sample loading buffer for 5 min at 95 °C. The reduced samples were then alkylated by incubating in 15 mM iodoacetamide for 1 h at room temperature. Proteins were then fractionated by SDS-PAGE

(Invitrogen). Using in-gel molecular weight markers, each sample was divided into molecular weight regions and subjected to overnight trypsin digestion at 37°C (Trypsin Gold, Promega, Madison, WI).

### LCMS Data Acquisition

The isotopic distributions of peptides were measured using an Agilent 6520 QToF with Chip Nano source (Agilent, Santa Clara CA). Injection volumes of extracted peptides were normalized according to the staining density of the original regions of the gel. Each sample was injected two times per analysis. During the first injection, data dependent MSMS fragmentation spectra were collected for peptide identification. No MSMS fragmentations were performed during the second injection, and a longer dwell time (1 spectrum per second) was used in the full scan acquisition. The longer dwell time increased the signal to noise ratio for the observed isotopomer patterns.

### Extraction of Kinetic Labeling Information

MSMS fragmentation data was analyzed using the Agilent software package Spectrum Mill and protein identifications were based on the Uniprot/Swissprot database (08/2010) where species=mouse, trypsin digest, and carbamidomethylation of cysteine were used as restrictions on the search. Isotopomer patterns were extracted from the MS scan data using the MassHunter software package from Agilent. The peptide list with calculated neutral mass, elemental formula, and retention time was used to filter the observed isotope clusters. A visual basic application was used to calculate peptide elemental composition from lists of peptide sequences and calculate isotopomer patterns over a range of precursor body $^2H_2O$ enrichments (***p***), for the number (***n***) of C-H positions actively incorporating H/D from body water (see below). Subsequent data handling was performed using Microsoft Excel.

### Measurement of Amino Acid Enrichments By GC/MS

Protein components of tissue homogenate were precipitated from a 200 ul aliquot by dilution into cold acetone (800 ul) followed by incubation at -20 °C for 1 hour. Free amino acids were isolated from the organic supernatant after evaporation of the solvent under reduced pressure. Dried amino acids were resuspended in 1 ml of 50% acetonitrile, 50 mM $K_2HPO_4$, pH 11. Pentafluorobenzyl bromide (20 uL) was added, and the sample was sealed and incubated at 100 °C for 1 hour. After cooling to room temperature, ethyl acetate (600 ul) was added to each sample followed by mixing. The top layer was then transferred to a fresh tube containing $Na_2SO_4$. The anhydrous organic solution was injected directly onto a DB-17MS (30m x 0.25mmID x 0.25µm film thickness), J&W. Scientific, Santa Clara CA). The data was acquired on an Agilent 6890N using CI source maintained at 280 °C. The oven temperature was cycled from 140 °Cto 280 °C over a 7.5 minute run. Data was collected in SIM mode with a 15 second dwell time using the ions listed in table S1.

### Calculation of Turnover Rate

Fractional replacement (***f***) is the proportion of newly synthesized proteins in a population, expressed as a fraction of the total pool. The kinetic interpretation

of the time-dependent replacement of pre-existing protein molecules by newly synthesized molecules requires an knowledge of the mass isotope pattern of newly-synthesized species as compared to unlabeled species [28,35]. The mass isotopomer pattern of peptides synthesized in the presence of an stable-isotope enriched precursor pool can be calculated based on the elemental composition of the peptide. Each protein (and by extension, each tryptic peptide) acquires isotopic enrichment from the precursor pool at the rate of protein turnover (***k***), the $^2$H-isotopic enrichment in the body water (***p***), and the number of sites in the peptide capable of incorporating H/D from water(***n***). Therefore,***p*** and ***n*** must both be known to calculate ***k***.In these experiments, we have measured ***p***directly (Fig S1). At the $^2$H enrichments used in this study the mass spectra of newly synthesized protein will occupy the same m/z range as the unlabeled species, but knowing ***p*** and ***n*** we can deconvolute the isotopomer patterns.

In order to calculate peptide specific ***n*** values, literature-derived estimates of ***n*** were calculated for each amino acid (AA) [36]. We confirmed these literature values of $n_{AA}$ for each AA in two ways, first by directly measuring the relative deuterium incorporation in soluble AA's, then by comparison against the mass isotopomer pattern of peptides isolated from the labeled tissue to theoretical values for ***n*** and established the best fit value (Fig S2).

Due to the rapid equilibration of water in the body (Fig S1A), ***p*** can be measured from any accessible bodily fluid. In this study we used blood plasma collected from each mouse at each time point. Since body water enrichment was slightly different for each animal (Fig. S1B), the amino acid precursor pool (AAPP)$^2$H-enrichment used to calculate fractional replacement was different in each animal.

For a ***f*** between 0-100% (i.e. a mixed protein pool), deconvoluting the two subpopulations is carried out by treating each peptide as a biochemical polymer and calculating quantitative changes in the relative isotopic abundance pattern using the Mass Isotopomer Distribution Analysis (MIDA) [35]. As described previously [28], the mass isotopomer of each peptide was normalized to the total intensity of the isotopomer envelope, typically 4 masses (M0-M3). Peptides with a mass greater than ~2,400 Da exhibit a larger isotopomer envelope, so 5 masses (M0-M4) were used. We have based our calculations of ***f*** on the change in intensity of the normalized monoisotopic peak (EM0). We find that the signal to noise is most favorable for EM0, because of the larger change in fractional abundance for this isotopomer (EM0 decreases while labeled species distribute from EM1 to EM4). Peptides which met our criteria for inclusion had signal intensity >30,000 counts, an RMS error against the theoretical natural abundance spectra of less than 1.5% for the day 0 (D0) sample, and had a LC elution time within 30 seconds of the unlabeled control. The ***f*** of each peptide was calculated using the ***n*** specific for that sequence and the ***p*** measured for the mouse. Each peptide was considered as a replicate measurement of the fractional replacement for the protein of origin. Therefore the protein ***f*** in each mouse was calculated as the median ***f*** of the peptide population from that protein. A time-depended fractional replacement curve was constructed for each protein, by

plotting the protein ***f*** for the each mouse in each feeding regime against the time of exposure to $^{2}H_2O$ (Fig. S3). Proteins which were observed in fewer than 3 mice were removed from the data set. The ***k*** for each protein was calculated using a regression fit for the single pool model ($f=1-e^{(-kt)}$) in the Prism software package (Graph Pad, La Jolla CA). A coefficient of variation (CV) was calculated for each protein as the ratio of standard deviation reported for the regression over the rate constant. Proteins which had a %CV of more than 30 for either the CR or AL feeding regime were removed from the data set.

### Stable Isotope Labeling in Mammals (SILAM) Quantitation

In order to validate the LC-MS/MS based quantitation method, to test the range of quantifiable concentration differences, and assess the variability within the measurement, a standard curve of labeled cell lysate was constructed. Rat neural stem cells ((EMD Millipore, Billerica, MA) were grown as a mono-layer in flasks coated with poly-ornithine and laminin. Two different media containing DMEM/F-12 medium with B-27 serum-free supplement and 20 ng/ml FGF (EMD Millipore, Billerica, MA) were used, either unlabeled lysine and arginine (light) or $^{13}C_6$ lysine and $^{13}C_6$ arginine (heavy), as previously described [37]. The total protein content of cell lysates from these cultures was measured using bicinchoninic acid (BCA, Pierce, Rockford, IL). Light and heavy cell lysates were mixed to form a curve of protein isotopic ratios at1:1, 1:3, 1:6, and 1:10 light:heavy protein. The mixtures of crude cell lysates were fractionated using SDS-page. The 37-50kD molecular weight range of the gel was digested using trypsin and analyzed by LCMS as described above. The same peptide identification and isotopomer extraction methods described for the kinetic analysis were used in this experiment. Relative protein concentrations were calculated as the average of ratios of light/heavy isotopomer intensity measured for all peptides belonging to the same protein.

For application of the quantitation method in mammalian tissue or SILAM, ($^{13}C_6$) lysine labeled mouse liver (MouseExpress Liver, Cambridge Isotope, Andover MA) was used as the heavy standard for LC-MS/MS quantitation. The protein was quantified in D0 experimental tissue from each feeding group. Total protein content of the experimental and SILAM tissue lysates were measured using BCA (Pierce, Rockford, IL). Sample and standard protein were mixed in a 1:1 ratio prior to SDS-PAGE and trypsinization. Our protocol was modeled after literature reports [29–31]. Ratios of light to heavy peptides were calculated independently using two different software packages: (a) MassHunter Qualitative Analysis (Agilent) and (b) the Trans-Proteomic Pipeline [38]. Protein concentration was calculated as the weighted average of the measurements from both software packages, where the number of peptides measured for a given protein was used as the weighting factor.

### Calculation of Absolute Synthesis Rates

In the kinetic labeling experiment we calculate the turnover rate constant(***k***) from the change in ***f*** over time using the relationship, $f=1-e^{(-kt)}$. In order to directly compare the CR and AL experiments we

also calculated the absolute flux into and out of each specific protein pool. Protein flux is calculated as the turnover rate (***k***) multiplied by the pool size (**V**), Flux=***k*****V**. For this calculation we assumed protein homeostasis, so although **V** may be different between the AL and CR experiments, it is constant over the duration of the experiment. Therefore the flux into the system (synthesis) is equal to the flux out (degradation). For the synthesis calculation, we normalized all concentration measurements to the AL pool size. This results in a unitless mass per day synthesis rate, that is directly comparable between experimental groups.

### Gene Ontology and Pathway Analysis

Gene annotation, and gene ontology information and biochemical pathway information were obtained from the Database for Annotation, Visualization and Integrated Discovery (DAVID) v6.7 from the National Institute of Allergy and Infectious Diseases (NIAID), at the National Institutes of Health (NIH) [39,40]. Mitochondrial proteins were cross referenced against the Mitocarta database [41]. The network analysis testing expression control of protein dynamics was done using both the Ingenuity IPA (version 12402621) and the GeneGo Metacore database. Parallel pathway analyses methods were used to assess for correlation between predicted transcriptional control of protein and measured changes in replacement rate and concentration. For this analysis we considered a 5% difference in replacement rate and 10% in concentration necessary to be considered changed. Special emphasis was placed on testing the recently proposed hypothesis that peroxisome proliferator-activated receptor gamma coactivator 1-alpha (PGC-1alpha) is a central regulator of the mitochondrial adaptation to CR [42].

## Results

### CR Model and Cell Proliferation

CR mice gained weight at a rate similar to the AL fed controls maintaining the ~30% difference throughout the course of our experiment (Fig. 2B). AL mice consumed an average of 5 grams per day, and CR mice were therefore provided 3 grams per day to maintain 40% CR (Fig. 2C) as per the NIA protocol.

In order to validate our experimental model, we measured hepatic cell proliferation rates following 15 and 32 days of $^{2}H_2O$ labeling (Fig 2D). As expected, the percentage of new cells increased from day 15 to day 32, allowing the use of both time points to calculate hepatic cell proliferation rates.. New cell synthesis rates were reduced ~50% in the CR animals relative to the AL, resulting in proliferation rates of 0.002 and 0.004 $day^{-1}$ respectively, in agreement with previous observations [15,43,44].

### Body Water Labeling

The bolus injection used to initiate isotopic labeling results in a rapid equilibration of the body water (BW) at the target isotopic enrichment of 5% (Fig S1). In order to measure the rate of isotopic equilibration, in a separate experiment we serially sampled the BW enrichment in C57BL6 mice every 60 minutes for a total of 240 minutes following a fixed volume bolus injection of $H_2{}^{18}O$.. We confirmed that *in vivo* $^{2}H_2O$ isotopic equilibrium was established within 60 minutes, and isotopic

enrichment was dependent on body weight (Fig S1A). A common assumption for kinetic experiments is that it takes 5 half-lives for a kinetic process to achieve equilibrium. This would suggest that the body water equilibration has a half-life of at most 12 minutes in an animal the size of a mouse. This means that BW equilibration has a rate constant of at least 86 $Day^{-1}$ in our experiment. A similar bolus injection was used to initiate labeling of the CR and AL mice, and BW enrichments were measured at the time of tissue collection throughout the duration of the experiment (Fig. S1B). The enrichments we observed were comparable between CR and AL mice. We also observed that the enrichment was very stable within the CR group, while the AL group had a slight decline in enrichment as the experiment progressed. The general decline in the AL BW enrichments over time may be related to the catabolism of a proportion higher of dietary fatty acids resulting in the production of unlabeled metabolic water, or the lower lean body mass within these mice.

**Validation of literature n**

Each peptide ***n*** is the sum of its individual amino acid ***n***'s ($n_{AA}$). As previously described [28], using literature values for tritium incorporation into amino acids we calculated ***n*** values for each amino acid as a ratio of the validated ***n*** for alanine (4) [45,46]. We tested the validity of these ***n*** values in two different ways. First, we isolated free amino acids from tissue which had been labeled for 32 days to measure maximal deuterium incorporation (Table S1). We observed a strong linear correlation between the measured isotopic enrichment and the theoretical value predicted by the literature ***n*** at the measured ***p*** (Fig S2A). Next, we compared experimental peptide spectra against theoretical predictions for isotopomer patterns from proteins expected to be fully labeled (Fig. S2B, C). We evaluated deviations between measured mass isotopomer patterns for these peptides and a family of theoretical spectra where ***n*** varied around the literature value (Fig. S2B). We found that for most peptides the best fit ***n*** matched literature values closely. Some random variation was observed, however a minimum Root Mean Square Error (RMS) was observed over a range of ***n*** values extending from 90% to 100% of the expected value for ***n***.

**Rate of Precursor Pool Enrichment**

Rate of Precursor Intracellular amino acids are the link between the BW isotopic enrichment and peptide isotopic enrichment (Fig. 1). In order to determine whether the maximal enrichment of the AAPP was changing over time, we measured the stability of peptide ***n*** over time. To do this, we calculated the best fit ***n*** value for several different peptides at each time point of the experiment (Fig S2C). We targeted peptides from multiple proteins with rate constants fast enough to result in measureable labeled peptide population at 9 hours (>30% $Day^{-1}$), and which were observed in both AL and CR animals. By comparing each peptide at each time point against a family of theoretical spectra (as per S1B), we found that the observed best fit ***n*** value was within 10% of the literature value throughout the time course. Observing the stable ***n*** at 9 hours suggests that the precursor pool has achieved equilibrium. If, as suggested by this data, 9 Hrs is

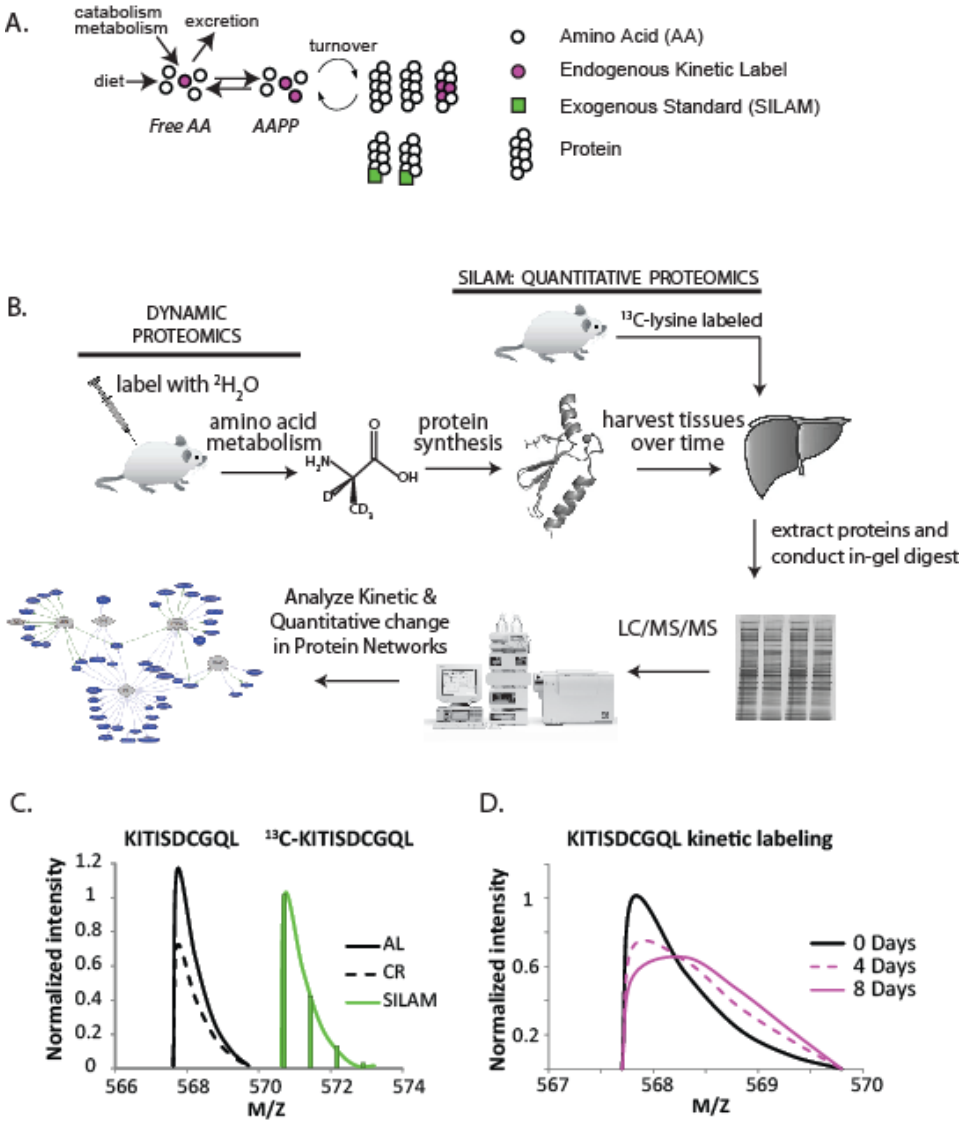


**Figure 1. Dynamic proteomics workflow.** (A) Two techniques for isotopic labeling were used to concurrently measure protein concentration and protein turnover. Turnover was measured by utilizing AA metabolism to isotopically label (purple) the amino acid precursor pool (AAPP). Protein concentration was measured through addition of exogenous labeled protein (green). (B) Mice were labeled with $^2H_2O$ via bolus injection and labeled drinking water. Tissues are harvested following euthanasia, and protein homogenates, with addition of SILAM protein standards to selected samples,are separated by SDS-PAGE, followed by in-gel trypsinization. LC-MS/MS is performed on tryptic peptides, and peptide isotopomer distributions are thenanalyzed using mass isotopomer distribution analysis (MIDA) to quantify the fractional replacement rates(***f***) of hundreds or thousands of newly synthesized peptides and, thus, their parent proteins.(C) For each lysine containing peptide, ratios of SILAM-labeled peptides (green) to endogenous peptides (black) allow differences in protein concentrations to be measured.For clarity a curve joining the peak of each isotopomer is shown. (D) Fractional replacement causes distinct changes in the isotope pattern of each peptide, these time dependent changes allowed f and k to be measured for each protein from multiple peptides.For clarity only curves joining the peak of each isotopomer is shown.

Each peptide *i* is the sum of its individual

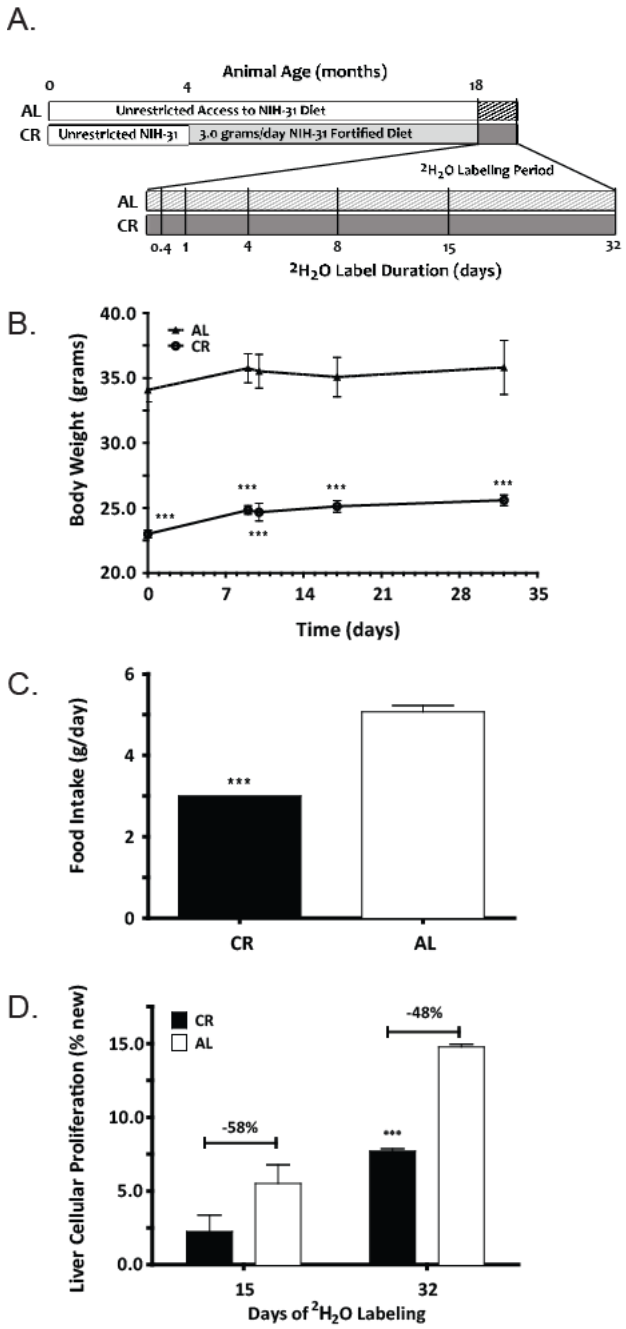


**Figure 2. Confirmation of physiologic response in the chronic CR model**A) 18 month old CR (n=12) and AL (n=12) mice were purchased from the NIA calorie restricted colony and labeled with $^2H_2O$ for 0.4 Days, 1 day, 4 days, 8 days, 15 days and 32 days(n=2 animals per group per timepoint). (B) Mouse body weight was monitored over the course of the experiment. Although there was modest weight gain in both CR and AL groups, CR mice were significantly smaller than the AL fed controls.(C) Food intake was monitored during labeling, AL mice consumed an average of 5 grams, while the CR mice were administered 3 grams per day as per NIA protocol. (D) The rate of liver cell proliferation was measured following 15 and 32 days of $^2H_2O$ labeling. Values are means $\pm$ SEM, and significance was calculated by a two-tailed student's t-test vs. AL animals (****, $p<0.001$).

longer than 5 half-lives for precursor pool turnover, the half-life of precursor pool is at most 1.8 hours. This means that the rate constant for turnover of the amino acid precursor pool is at least 13.3 $Day^{-1}$. These results are consistent with literature values for intracellular amino acid turnover [47].

## Liver Proteome Dynamics

We used four selection criteria to remove low confidence protein information from the analysis: each peptide measurement signal intensity (>30,000 counts), RMS error for peptide mass isotopomer abundance measurements in an unlabeled sample of less than 1.5%, 2 or more peptides must be observed for each protein in each mouse, and a rate constant that could be defined with less than 30% coefficient of variation from the incorporation curve. While the number and proportion of peptides that finally yielded kinetic information varied between groups, we identified 2769 AL peptides and 3939 CR peptides. These peptides were heterogeneously distributed amongst proteins, with up to 120 peptides identified for the same protein. Measurements of protein ***f*** were assembled into a time dependent isotope incorporation curve for each protein (Fig S3). A non-linear regression fit through the measured enrichments was used to calculate a unique turnover rate constant

(***k***), and fit statistics for each protein in each experiment. The difference in the number of unique peptides between the two
groups, resulted in AL having fewer proteins overall (384) than CR (447). There were 288 shared proteins which could be compared between groups (Fig S4).
The proteomic data demonstrates that CR induced a general reduction in total intracellular hepatic protein replacement (Fig.3A, 4). Comparison of the median protein replacement rate for the proteins which made the final filter, results in more than 80% of shared proteins with reduced rate in CR. We calculated the rate ratio (CR/AL), and categorized proteins into three broad categories (Table 1): reduced (CR/AL<0.90), unchanged (0.90<CR/AL<1.10), and increased replacement rates (CR/AL>1.10).

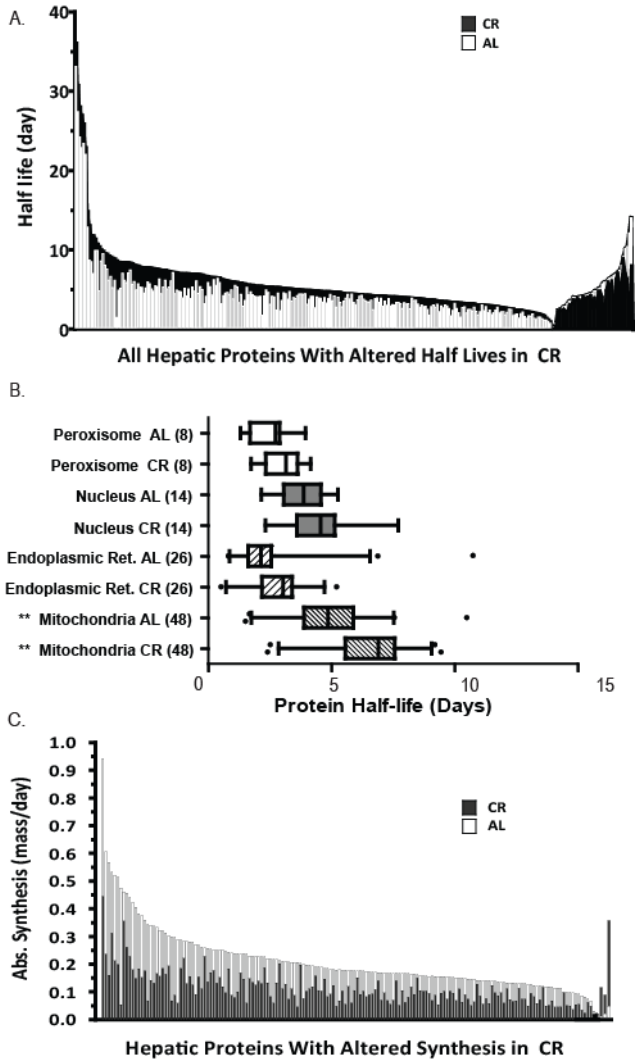


**Figure 3.** CR results in broad scale reductions in hepatic protein metabolism (**A**) Direct comparison of fractional replacement rates (***f***) for all proteins observed in this study shows that CR (black) reduced the replacement rates relative to AL (open) for 85% of proteins observed. (**B**) Comparison of the half-life (t ½, calculated as ln(2)/k) for proteins associated with specific organelles. Boxes show the inter quartile range for protein turnover in the organelle bars extend to 5 and 95% of the data. Only proteins which were solely and unambiguously assigned to the indicated organelle were used. Although the median half-life was systematically longer in CR, only the mitochondrial proteins were statistically significant (Students 2 tailed heteroscetatic ttest, ** $p < 0.005$) (**C**) Absolute synthesis rates for each protein were calculated from the replacement rate and the SILAM concentration measurement, differences between CR and AL mice were more distinct on this absolute scale, with CR mice producing substantially less of each protein daily.

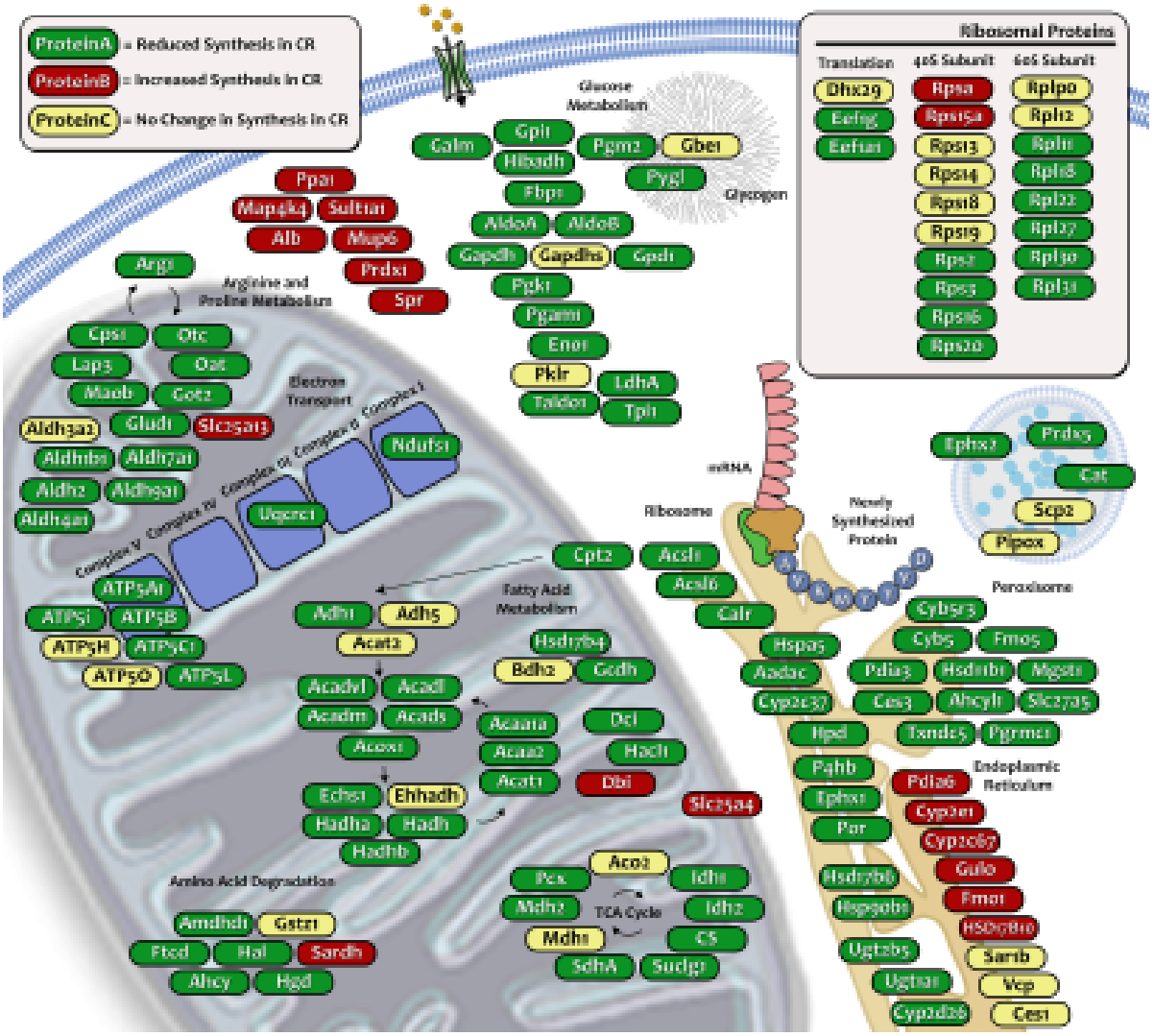


**Figure 4.** Throughout the cell, protein turnover is slower in CR mice compared to AL. Selected functional classes like the 40S ribosomal subunit and some classes of cytosolic proteins are less perturbed than the average, while the mitochondrial proteins are affected to a greater degree.

Various regions of the cell were enriched for proteins from these broad rate categories (Fig. 4). Proteins associated with the mitochondria where changed most significantly with 94% (80/85) proteins reduced more than 25% ($p<0.0005$). We measured significantly lower replacement rates for proteins associated with TCA, fatty acid metabolism, and ATP synthesis. Although the median replacement rates of proteins from the endoplasmic reticulum and the golgi apparatus were also slower in CR, neither shift was statistically significant (Fig 3B, Table S3). Interestingly, although less than 15 percent of observed proteins had rates which were faster in CR (**Table Sx**), half of the observed 40S

ribosomal proteins have either the same or faster turnover rate (Fig 4, 5, **Table Sx**).

### SILAM Quantitation

The standard curve of heavy to light cell lysates validated the quantitation method. We measured the ratios for approximately 50 peptides belonging to seven different proteins throughout a series of dilutions from 1:1 to 1:10 heavy to light ratio (Fig.S5, **Table Sx**). Every protein and all associated peptides showed a highly linear correlation between the measured and the expected ratio. The deviation from the mean was approximately 10% of the measured ratio, resulting in an increasing spread among the population of proteins as the expected ratio increased with dilution.

Initial analysis of the experimental liver samples used the Agilent MassHunter software program which identified2832 peptides with high confidence, of these only 36% contained lysine, the majority were arginine terminal peptides. We measured SILAM ratios for 979 peptides in CR and 1117 peptides in AL corresponding to 223 and 203 proteins, respectively. These data were then analyzed again using the Trans Proteomic Pipeline (TPP) software package which measured SILAM ratios for 2010 peptides yielding 163 proteins observed in both the AL and CR groups. There were 123 proteins which were common to both analysis methods, with 41 unique to the TPP analysis and 72 to the Agilent analysis. For proteins common to both analyses there was good agreement in the measurement, with a median deviation of 10 percent. For these shared proteins, a heavy:light ratio weighted average was calculated, weighted by the number of peptides observed in each method. To facilitate data analysis all CR protein measurements were normalized to the AL pool. This resulted in quantitation ratios (CR/AL) for 236 proteins in total.

We observed a general shift towards lower protein concentration in the CR mice, with 82% (194/236) of the proteins exhibiting a >20% decrease in pool size. Based on the 10% deviation observed in the standard curve, any ratios between 0.9 and 1.1 were to be designated as unchanged. Within this group of proteins there was a significant enrichment ($p=0.008$) for the proteins involved in carboxylic acid metabolism and valine metabolism (Table Sx). There were a number of proteins (19% of total) with significantly reduced concentrations (<50% CR/AL), ribonuclear proteins were enriched ($p=0.04$) among this group.

### Calculation of Absolute Synthesis Rates

Flux into the protein pool (synthesis) is an integrated measurement of both fractional replacement (measured by heavy water labeling) and concentration (measured by SILAM). Therefore, synthesis calculations could only be performed for proteins which were observed in both the kinetic and SILAM proteomic experiments (Fig 1C-D). Comparison of the protein specific synthesis exaggerated the changes between the AL and the CR groups (Fig. 3C, **Table Sx**). We normalized measured SILAM protein concentrations in the CR group to the AL group such that CR flux is corrected by the ratio of CR/AL, whereas AL protein flux is equal to the measured

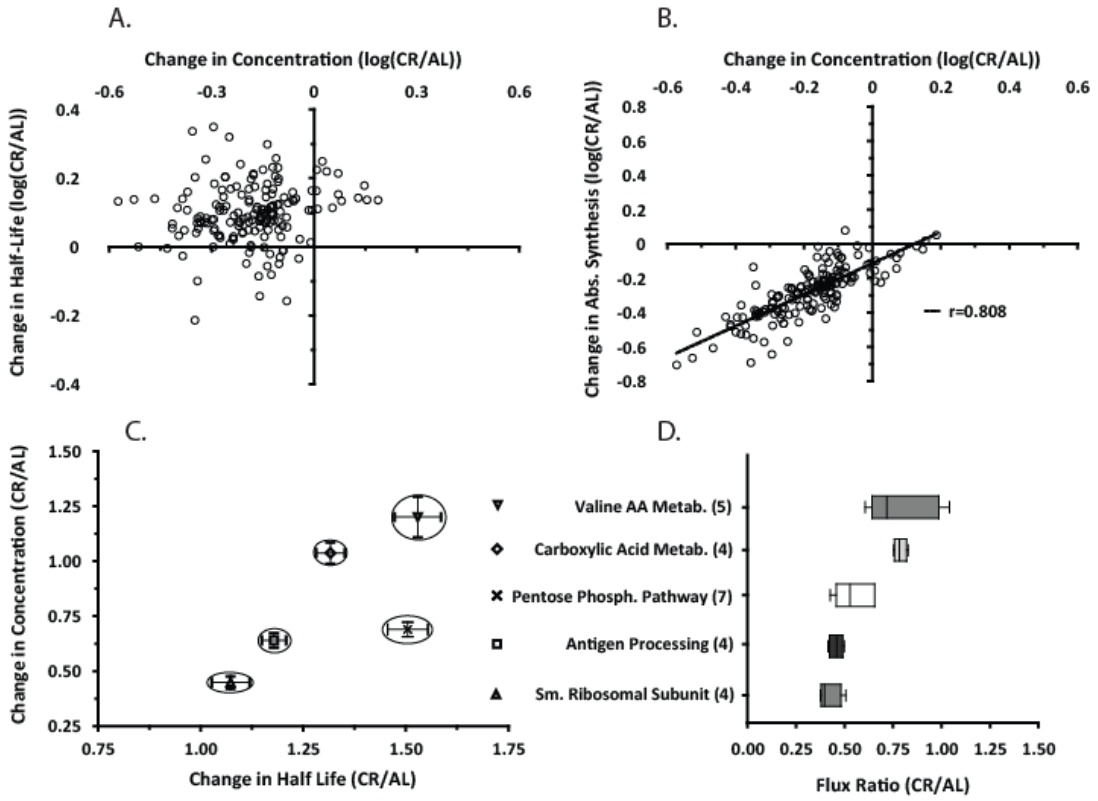


**Figure 5**. (A) Distribution and comparison of change in half-lives to the change in concentration for each protein (open circles). The great majority of proteins detected exhibited lower concentrations in liver from CR compared to AL mice; and these were almost all associated with longer half-lives, not shorter half-lives. There was no correlation between t ½ and protein concentrations.(B) Distribution and comparison of change in total synthesis rates (calculated as the product of k and concentration), to the change in concentration for each protein (open circles). As noted in A, the great majority of proteins detected exhibited lower concentrations in liver for CR compared to AL mice; and almost all were associated with lower total synthesis rates. Thus, most proteins were in the lower left quadrant (lower concentration, lower total synthesis rate). (C)Proteins belonging to the selected Gene Ontology(GO) categories experienced similarchanges in both concentration and half-life.(D)As shown here, changes in total synthesis rates for CR/AL mice for proteins within functionally related selected GO categories. Proteins within a pathway tended to exhibit coordinated changes in total synthesis rates in response to CR.

turnover rate (k). We observed that the CR concentrations were 70% of the AL pool. For the same subset of proteins the average turnover rate constant in CR was on 81% of the rate observed in the AL experiment, resulting in an average flux for the CR experiment which was 55% of the flux observed in the AL experiment.

There was a general trend toward slower replacement and lower concentration (Fig5A). When proteins belonging to specific gene ontologies were considered, we observed that they tended to have similar changes in turnover and pool size (Fig 5C).

### Gene Ontology

In order to identify protein networks with differentially regulated flux, we analyzed both functional and spatial interconnectivity between proteins in groups defined by the change in turnover and protein concentration. As has been previously shown, we found evidence that protein turnover is regulated at three distinct levels: the organelle, the multi-protein complex, and the protein itself (Fig 6).

### Expression Pathway Analysis

Both IPA and Metacore databases suggested that four transcription factors (MYC, HNF4A, PPAR-gamma, and MYCN) were connected to approximately half of the proteins with measured replacement rates (Fig 6A). The predicted directionality of the expression profiles (Table Sxx) were negatively correlated for MYC (z=-2.3), HNF4A (z=-2.1), MYCN (-3.0), and PPAR-gamma (z=-3.1). MYC, MYCN and PPAR-gamma were also negatively correlated with the changes in protein concentration (z= -2.9, -2.2, and -2.1 respectively). We tested whether PGC-1alpha control of transcription could account for the correlations observed with the 4 transcription factors, as recently proposed [42]. HNF4A and PPAR-gamma are known targets of PGC-1alpha, while MYC, and MYCN are known to be under the control of HNF4A. We also tested the hypothesis that PGC-1alpha was involved in the transcriptional regulation of proteins involved in mitochondrial biogenesis, including ERR1, ERR3, NRF1, and NRF2. We found that PGC-1alpha may directly control the expression of these genes, and that reduced PGC-1alpha expression may explain reduced mitochondrial protein flux in CR (Fig 6B).

### Discussion

Although the efficacy of increased longevity due to CR has been well established in animal models, human subjects are resistant to dietary restriction. If the mechanism of action can be identified, the beneficial effects of CR may still be achieved in humans using less extreme lifestyle and/or pharmacological interventions [48]. A popular mechanistic hypothesis for CR focuses on mitochondrial fitness [49,50], suggesting that mitochondrial biogenesis (synthesis) [17,24] and autophagy (degradation) [22,23,26,51] are both increased in CR, resulting in increased protein turnover and increased mitochondrial efficiency (Fig 7).

To investigate this turnover-dependent hypothesis, we have directly measured protein turnover in mice from the well validated NIA CR mouse colony and compared to age-matched AL-fed controls. In measuring kinetic processes such as protein turnover, the measurement of the isotopic enrichment of the AAPP and the change in protein concentration are critical parameters for proper interpretation of the measurements. In cell culture experiments the concentration of labeled amino acids in the media can be used as the precursor concentration [52,53]. *In vivo,* the AAPP is not easily sampled, and the enrichment between tissues is variable [54]. We and others have recently shown in mice that if the AAPP enrichment approaches 100%, precursor enrichment can be measured independent of the protein turnover rate within the MS spectrum. These experiments required a complete exchange of the protein component of the mouse feed for ubiquitously labeled protein [32,55]. Since

diet composition and calorie content are the main experimental variables in a CR experiment, introducing a uniquely formulated labeled diet presented an obstacle to maintaining the accepted CR model. We have recently shown that using very low $^2H_2O$ enrichment we can measure protein turnover in humans [28]. In the current study, we employed a similar$^2H_2O$ labeling strategy to measure proteome dynamics in mice from the commonly accepted NIA CR colony (Fig. 2).

$^2H_2O$ "heavy water" has been described as a universal label for the study *in vivo* metabolism [56] and has been successfully used for a variety of biological molecules [57]. In our study, *in vivo* labeled amino acids were generated through normal cellular metabolism (Fig 1). It is well established that each type of amino acid will incorporate different numbers of isotopic labels [28,36,56,58]. By isolating the most abundant individual free amino acids from the liver tissue of 32 day labeled AL and CR mice, we directly measured the isotopic enrichments. We found that there was good agreement between the CR and AL free AA, and that there was a strong correlation (r=0.92) with the predicted deuterium enrichments (Fig S2A).

The true precursor pool for protein synthesis is the charged intracellular tRNA pool. Sampling this pool specifically to measure AAPP enrichments is very challenging. We saw that at late time points free AA enrichments were consistent with literature; however it was important for us to establish how fast the enrichment of this precursor pool was achieved. A powerful component of the MIDA method is that if the isotopic enrichment $\boldsymbol{p}$ changes slowly relative the analyte turnover a unique $\boldsymbol{n}$ can be calculated from the measured isotopic pattern[35]. By comparing the measured peptide isotopomer against a family of theoretical patterns to find the best fit for each peptide at each time point, we show that the best fit $\boldsymbol{n}$ is within 10% of the predicted value (Fig. S2B). Importantly this $\boldsymbol{n}$ value is established by 9 hours, the earliest point within our experimental time course (Fig. S2C). Therefore in the current experiment, the peptide $\boldsymbol{n}$ value is considered a constant.

The experimental design places upper and lower boundaries on the protein turnover rates we were able to measure. It is commonly estimated that 5 half-lives are required before equilibrium is established. By this measure we found that the rate of BW enrichment following a bolus injection is faster than 86 $Day^{-1}$. By similar approximation the rate of amino acid pool enrichment, which will define the upper rate limit in this experiment, is faster than 13 $Day^{-1}$. This fast rate of precursor enrichment is a distinct advantage over the use of labeled algae protein where a distinct lag in the delivery of isotopic label was observed in the experiment [32,59]. The slowest rates of protein turnover will be dominated by the synthesis of new cells within the tissue. A second advantage of the $^2H_2O$ labeling is that every newly synthesized molecule in the body will incorporate label. Therefore in the same group of mice we measured the cell proliferation rate [33,60] at 0.002 and 0.004 $Day^{-1}$ for CR and AL respectively, giving us the lower limit for possible protein rates. The protein turnover rates measured in this experiment are well within the range imposed by the experimental conditions, with a rates ranging from ~4 $Day^{-1}$ for the

major urinary proteins (P11588, P11580, P02762) and ~0.02 $Day^{-1}$for hemoglobin subunits (P01942, P06467, P02088).

We designed this study to ensure that both the CR and AL mice were at a condition of steady state proteostasis, indicated by stable body weight and unchanging body composition (Fig 2).These mice were healthy adults of stable weight, and the CR mice had been maintained for 14 months on the NIH-31 Fortified diet at the NIA (Fig. 2). In spite of the observation that CR reduces cell proliferation [43,44], our expectation was that mitochondrial biogenesis and protein turnover would be increased in long term CR animals, in support of recent studies [9,22–24,26,27] (Fig. 7). Instead, we observed a general slowing of protein turnover (Fig 4), and a reduction in general protein concentration, resulting in significantly lower protein flux in the CR mice as compared with AL-fed controls (Fig. 5, 6).

The effect of CR on mitochondrial biogenesis remains controversial. Several CR studies have demonstrated that CR induced mitochondrial biogenesis. In a recent study conducted *in vitro* and *in vivo*, CR induced proliferation of mitochondria with reduced membrane potential and rate of reactive oxygen species (ROS) production [61], while in another investigation CR promoted increases in oxidative capacity concomitant with decreases in triglyceride content in rat skeletal muscle [62]. A third study reported that CR promoted mitochondrial biogenesis in mice through a signaling pathway activating endothelial nitric oxide synthase (eNOS) [17], while in humans CR has been implicated in increased mitochondrial DNA [24,25]. Taken together, these investigations support the hypothesis that CR promotes bioenergetic efficiency via increases in mitochondrial density. In our study, mitochondrial proteins showed a significant decrease in absolute synthesis. In support of this, others have challenged the idea that CR increases mitochondrial biogenesis [63], and our data provide strong evidence that mitochondrial biogenesis, turnover, and concentration are all reduced in response to CR. Interestingly, many functionally related proteins experienced similar changes in turnover rate and pool size (Fig. 5, 6B) suggesting that a broader investigation of the proteome may elucidate mechanisms of CR fitness.

Understanding the molecular mechanisms that maintain the CR homeostasis and differentiate it from the AL state may provide framework for the development of therapeutics to combat age-related diseases [48]. Our data suggest that HNF4A, MYC, PPAR-gamma, and MYCN, which are all associated with cellular proliferation, are inhibited by long term CR. PGC-1alpha has been suggested as a master regulator of the CR effect [42]. PGC-1a activation of HNF4A and PPAR-gamma is known, which in turn activate MYC and MYCN (Fig 6A). PGC-1alpha also activates transcription factors responsible for mitochondrial biogenesis (Fig 6B), and these transcription factors are significantly downregulated lower during CR (Fig 5). Expression patterns of some targets (PPAR-alpha etc) of this promiscuous co-activator were not strongly correlated with our data. Other routes of control of protein metabolism, like modulation of catabolic rates, could be used to vary the effect of PGC-1alpha inhibition.

Multiple observations show that the CR-extended lifespan results from multiple interacting processes. CR has been shown

to protect from oxidative stress, but overexpression of antioxidant proteins is insufficient to extend lifespan [64]. We show that CR slows cell proliferation and protein turnover, and others have shown that CR lowers core body temp [13], all of which suggest that general cellular metabolism is slower. Yet several studies have shown that CR improves the livers ability to recover from injury, showing significantly increased cell proliferation during tissue repair relative to AL controls [65,66]. We have shown here that protein turnover is slower, yet in *in vitro* activity assays of proteasome activity show that CR increases the activity of the proteasome relative to age matched controls [67]. These factors suggest that although the global cellular metabolism is slower in CR, the dynamic modulation of cellular response to outside stimuli is more sensitive. Our data suggest that the activity of "quality control" mechanisms increase the efficiency and maintain the function of proteins longer to allow for slower protein turnover and longer protein half-lives. We also observe that although the concentration is lower the turnover of ribosomal subunits is not affected by CR. The ribosome is a first response element in the production of new protein and the relatively unchanged rate of ribosomal turnover suggests that pool size is prepared to expand rapidly under the right conditions. This would then supply sufficient ribosomes to ensure a quick response to newly synthesized mRNA as an efficient biological switch. This suggests that there are key transcription factors or stored mRNA which sense the available caloric levels and actuate the production of new proteins based on caloric intake or other signals. A similar strategy has been shown to regulate the hypoxia response through the degradation of the HIF-1alpha transcription factor [68,69].

**Conclusion**

Here we lay out a strategy to investigate the *in vivo* metabolism of proteins across the entire proteome. We investigated the effect of CR and show that the cell modulates protein flux by regulating both the rate of protein turnover and total protein concentration, at the level of the functional group and individual protein. These data also provide conclusive evidence that hepatic mitochondrial biogenesis is not increased due to caloric restriction; instead we propose that mitochondrial protein turnover, concentration, and overall flux are reduced in response to CR, and may play central a role in mediating the health and longevity benefits of reduced energy intake.

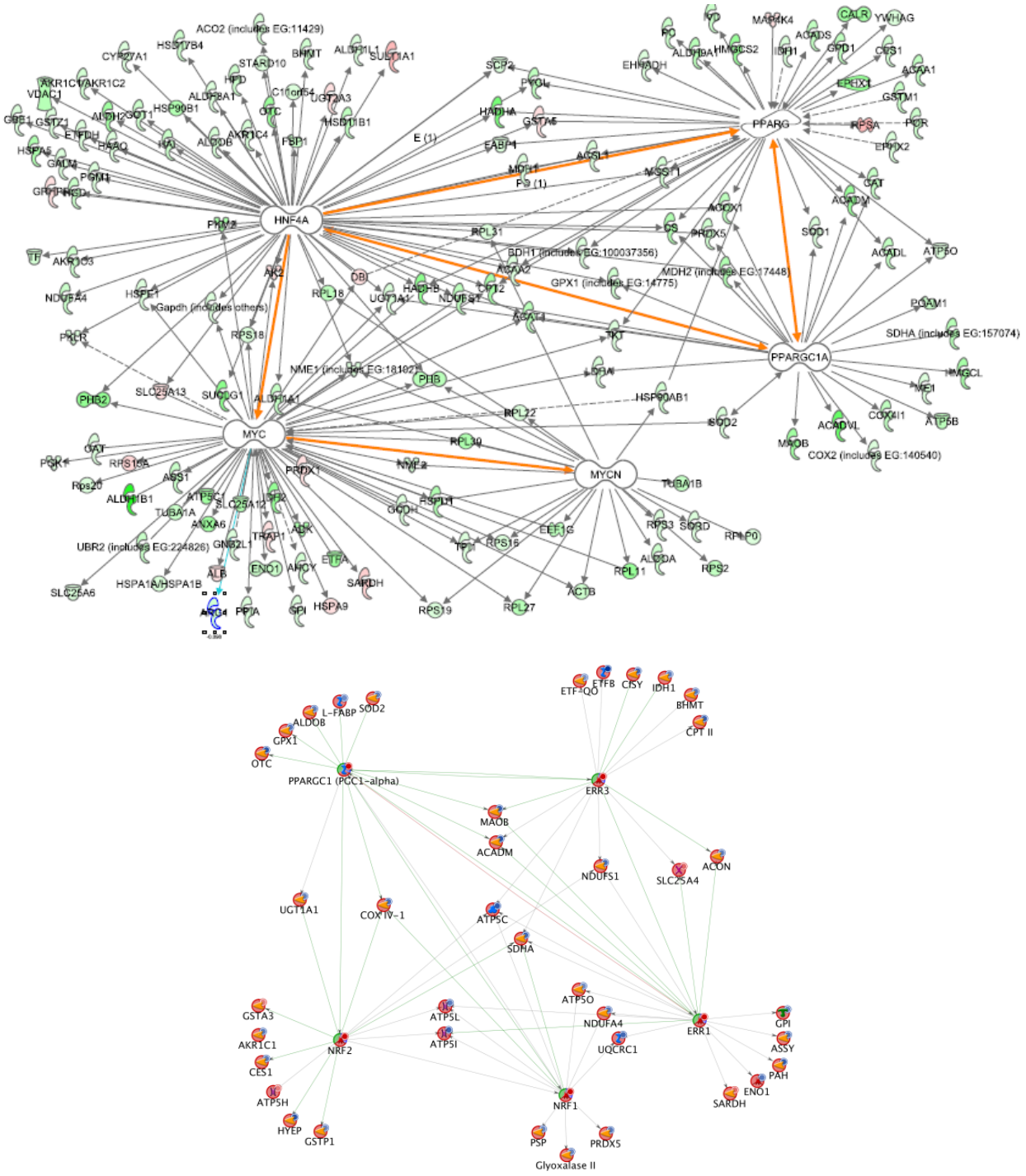


**Figure 6.** Significant expression networks within our data set. (A) Expression patterns for proteins regulated by MYC, HNF4A, PPAR□, and MYCN were significantly correlated for inhibition of these transcription factors. Each transcription factor is linked (highlighted connection) and PGC-1a is known as an upstream regulator influencing these expression patterns. (B) Transcription factors involved in mitochondrial biogenesis are also known targets of PGC-1a.

**Contributions**

JCP, CFK, MDB, MKH, participated in study design; CFK, MDB, MD, NAF, LSR executed the experiments; JCP, KWL, MS, WH provided new reagents or tools; JCP, CFK, KWL, WH analyzed data; JCP, CFK, MKH wrote the paper.

**Acknowledgements**

We thank Joan Protasio, and Chancy Fessler for their assistance in collecting the gas chromatography data. We thank Antonio Moreno for his behind the scenes work in making the laboratory environment a comfortable place to work. We also thank the Berkeley Laboratory Animal Research and Care facility, including Bob Williams, Julio Gonzalez, and Joan Wallace for their assistance with the labeling and animal maintenance. We also thank Leonie Waanders for her generous assistance in graphical representation of our data.

**Conflict of Interest**

JCP, NAF, KWL, MS, WH, and MKH have a financial interest in KineMed Inc.

## Literature Cited


1. Anderson, R. M., Shanmuganayagam, D. & Weindruch, R. Caloric restriction and aging: studies in mice and monkeys. *Toxicol Pathol* **37**, 47–51 (2009).
2. Guarente, L. Calorie restriction and SIR2 genes--towards a mechanism. *Mech. Ageing Dev.* **126**, 923–928 (2005).
3. Houthoofd, K. & Vanfleteren, J. R. The longevity effect of dietary restriction in Caenorhabditis elegans. *Exp. Gerontol.* **41**, 1026–1031 (2006).
4. Partridge, L., Piper, M. D. W. & Mair, W. Dietary restriction in Drosophila. *Mech. Ageing Dev.* **126**, 938–950 (2005).
5. McCay, C. M., Crowell, M. F. & Maynard, L. A. The effect of retarded growth upon the length of life span and upon the ultimate body size. *Nutrition* **5**, 155–71; discussion 172 (1935).
6. McCay, C. M., Maynard, L. A., Sperling, G. & Barnes, L. L. Retarded Growth, Life Span, Ultimate Body Size and Age Changes in the Albino Rat after Feeding Diets Restricted in Calories. *The Journal of Nutrition* **18**, 1 –13 (1939).
7. Colman, R. J. *et al.* Caloric Restriction Delays Disease Onset and Mortality in Rhesus Monkeys. *Science* **325**, 201 –204 (2009).
8. Das, S. K. *et al.* Long-term effects of 2 energy-restricted diets differing in glycemic load on dietary adherence, body composition, and metabolism in CALERIE: a 1-y randomized controlled trial. *The American Journal of Clinical Nutrition* **85**, 1023 –1030 (2007).
9. Masoro, E. J. Caloric restriction and aging: an update. *Exp. Gerontol.* **35**, 299–305 (2000).
10. Omodei, D. & Fontana, L. Calorie restriction and prevention of age-associated chronic disease. *FEBS Lett* **585**, 1537–42 (2011).
11. Caro, P. *et al.* Forty percent and eighty percent methionine restriction decrease mitochondrial ROS generation and oxidative stress in rat liver. *Biogerontology* **9**, 183–196 (2008).
12. Hagopian, K. *et al.* Caloric restriction influences hydrogen peroxide generation in mitochondrial sub-populations from mouse liver. *J Bioenerg Biomembr* **43**, 227–36 (2011).
13. Soare, A., Cangemi, R., Omodei, D., Holloszy, J. O. & Fontana, L. Long-term calorie restriction, but not endurance exercise, lowers core body temperature in humans. *Aging (Albany NY)* **3**, 374–9 (2011).
14. Bruss, M. D., Khambatta, C. F., Ruby, M. A., Aggarwal, I. & Hellerstein, M. K. Calorie restriction increases fatty acid synthesis and whole body fat oxidation rates. *Am. J. Physiol. Endocrinol. Metab.* **298**, E108–116 (2010).
15. Varady, K. A. & Hellerstein, M. K. Alternate-day fasting and chronic disease prevention: a review of human and animal trials. *Am J Clin Nutr* **86**, 7–13 (2007).
16. Lin, S. J. *et al.* Calorie restriction extends Saccharomyces cerevisiae lifespan by increasing respiration. *Nature* **418**, 344–8 (2002).
17. Nisoli, E. *et al.* Calorie restriction promotes mitochondrial biogenesis by inducing the expression of eNOS. *Science* **310**, 314–317 (2005).
18. Sohal, R. S. & Weindruch, R. Oxidative stress, caloric restriction, and aging. *Science* **273**, 59–63 (1996).
19. Mao, P. & Reddy, P. H. Aging and amyloid beta-induced oxidative DNA damage and mitochondrial dysfunction in Alzheimer's disease: implications for early intervention and therapeutics. *Biochim. Biophys. Acta* **1812**, 1359–1370 (2011).
20. Hekimi, S. & Guarente, L. Genetics and the specificity of the aging process. *Science* **299**, 1351–1354 (2003).
21. Kirkwood, T. B. L. A systematic look at an old problem. *Nature* **451**, 644–647 (2008).

22. Petrovski, G. & Das, D. K. Does autophagy take a front seat in lifespan extension? *J. Cell. Mol. Med.* **14**, 2543–2551 (2010).
23. Salminen, A. & Kaarniranta, K. Regulation of the aging process by autophagy. *Trends Mol Med* **15**, 217–224 (2009).
24. Civitarese, A. E., Smith, S. R. & Ravussin, E. Diet, energy metabolism and mitochondrial biogenesis. *Curr Opin Clin Nutr Metab Care* **10**, 679–687 (2007).
25. Civitarese, A. E. *et al.* Calorie Restriction Increases Muscle Mitochondrial Biogenesis in Healthy Humans. *PLoS Med* **4**, e76 (2007).
26. Lee, C. K., Klopp, R. G., Weindruch, R. & Prolla, T. A. Gene expression profile of aging and its retardation by caloric restriction. *Science* **285**, 1390–1393 (1999).
27. Matecic, M. *et al.* A microarray-based genetic screen for yeast chronological aging factors. *PLoS Genet.* **6**, e1000921 (2010).
28. Price, J. C. *et al.* Measurement of human plasma proteome dynamics with 2H2O and liquid chromatography tandem mass spectrometry. *Analytical Biochemistry* **420**, 73–83 (2012).
29. Aebersold, R. & Mann, M. Mass spectrometry-based proteomics. *Nature* **422**, 198–207 (2003).
30. Pandey, A. & Mann, M. Proteomics to study genes and genomes. *Nature* **405**, 837–846 (2000).
31. Wu, C., MacCoss, M., Howell, K., Matthews, D. & Yates, J. Metabolic labeling of mammalian organisms with stable isotopes for quantitative proteomic analysis. *Anal. Chem.* **76**, 4951–4959 (2004).
32. Price, J. C., Guan, S., Burlingame, A., Prusiner, S. B. & Ghaemmaghami, S. Analysis of proteome dynamics in the mouse brain. *Proc. Natl. Acad. Sci. U.S.A.* **107**, 14508–14513 (2010).

## Supplemental Figures

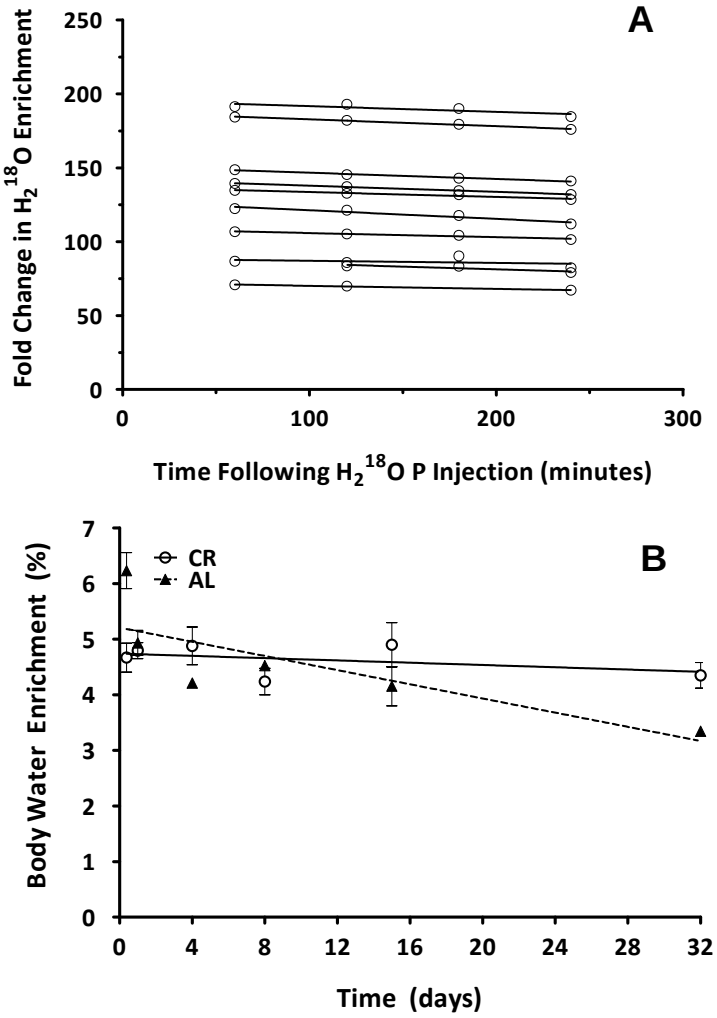


**Figure S1: Establishing isotopic enrichment stability in mice.**(A) Change in body water following a bolus injection of isotopically enriched water ($H_2{}^{18}O$), enrichment was measured repeatedly in mice over a 3 Hr timespan. Target body water enrichment was achieved 60 minutes after the bolus injection. (B) Isotopic enrichments were maintained over the 32 Day experiment, both AL and CR mice achieved similar enrichments, with slightly lower values in AL

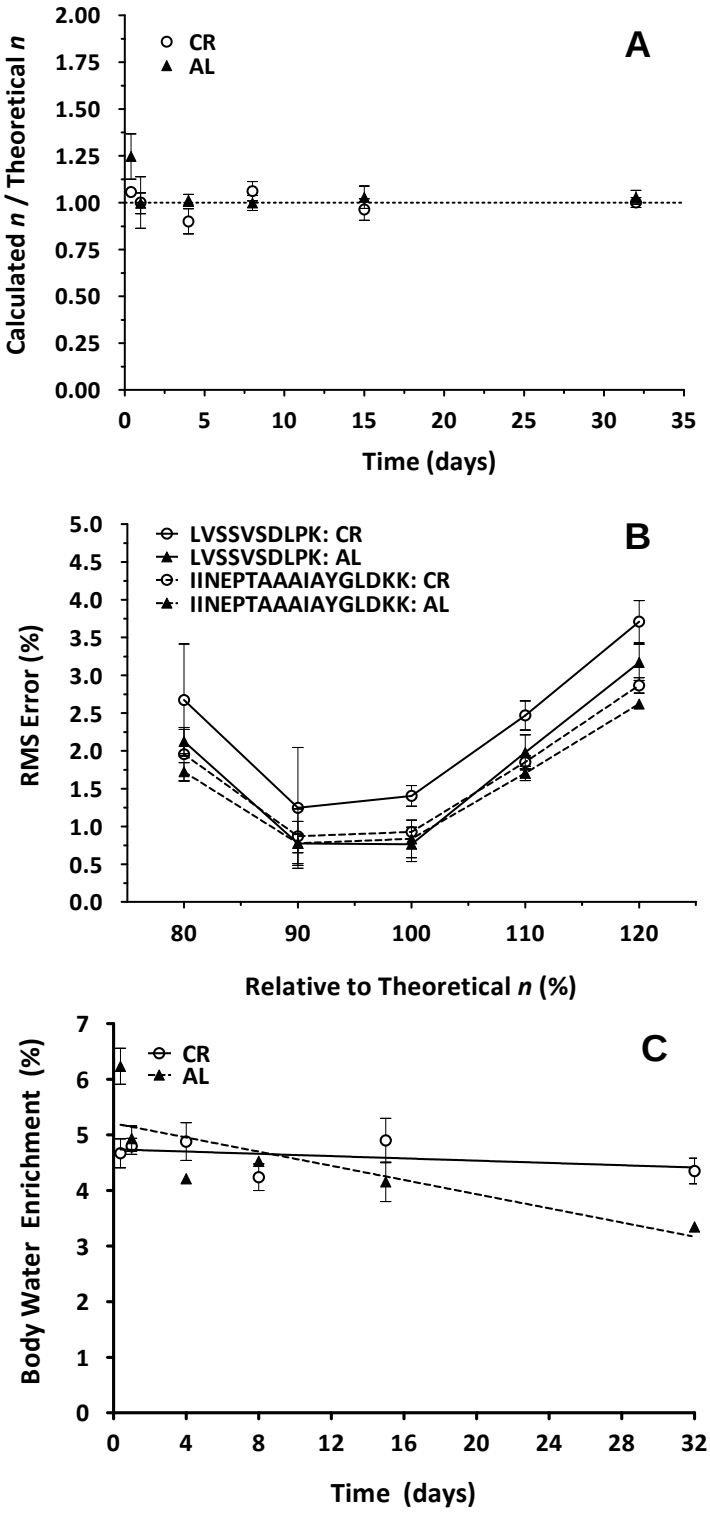


**Figure S2: Validation of sequence-specific peptide number of active H-atoms(*n*)during $^2H_2O$ labeling** (A) After 32 days of $^2H_2O$ labeling, maximal deuterium enrichments for free hepatic amino acids were measured in 2 AL and 2 CR mice.The measured values correlated strongly with theoretically expected values ($R^2$=0.92). (B) Deviations between measured spectra and a family of theoretical spectra where measured (*n*) is varied from 80% to 120% of the literature value. Two representative peptides from heat shock related protein 70 kDaprotein 2 (P17156) are shown. We observed a minimum for deviations (RMS error) at 90%-100% of the literature *n* in both CR and AL mice. (C) Four peptides from different proteins were used to test for stability of ***n*** over time of $^2H_2O$ labeling. Best fit ***n*** values were typically within 10% of the literature ***n*** value even at the earliest time points.

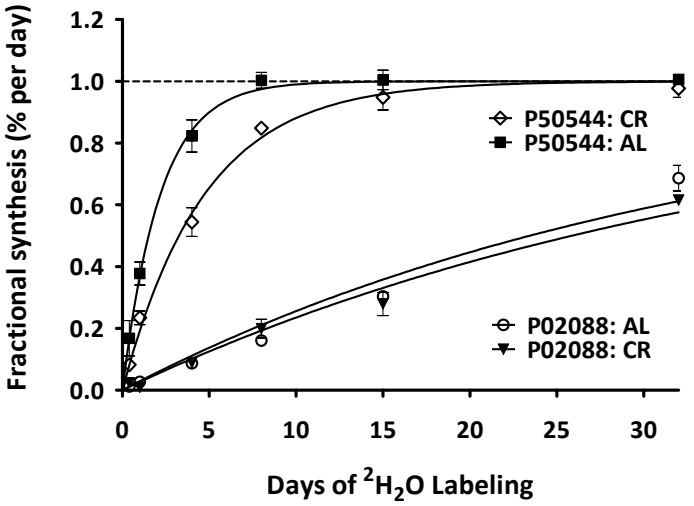


**Figure S3:** Fractional replacement curves for each protein were fit using non-linear regression to calculate the replacement rate (k) within the population of mice. Shown are curves for two proteins in CR and AL groups. For a majority of proteins, the CR animals had a reduced k relative to the AL animals.

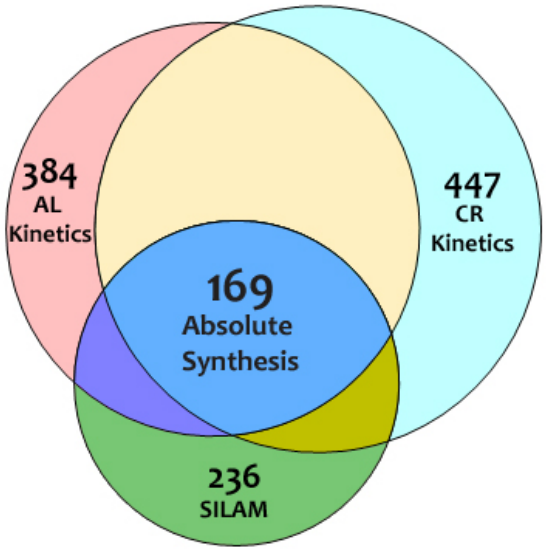


**Figure S4**: Absolute synthesis rates were determined for 169 proteins due to incomplete overlap of protein measurements in CR and AL groups and protein quantitation by SILAM.

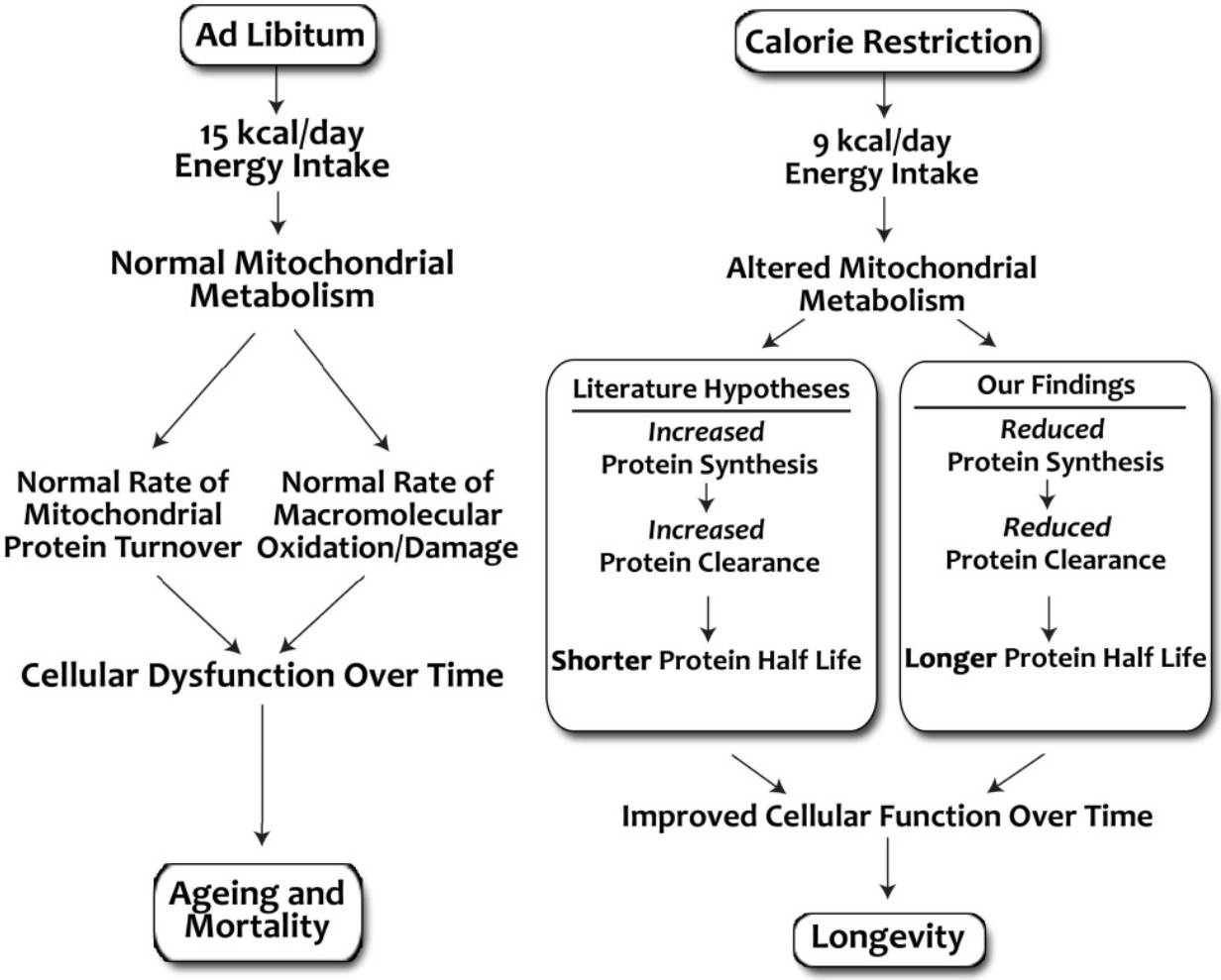


**Figure S5**: **Modeling the Effects of Calorie Restriction and *Ad Libitum* Feeding on Mitochondrial Metabolism.** Our proposed model for the effect of CR on mitochondrial metabolism in comparison with the effect of *ad libitum* feeding. Our findings are contrasted against hypotheses proposed in the literature on protein synthesis, clearance, and half life.

| AA | GCMS ion | Non-Labile H/mole | rel. 3H specific activity | Labeled H (n) | Theo EM1 (CR1) | Exp EM1 (CR1) | Theo EM1 (CR2) | Exp EM1 (CR2) | Theo EM1 (AL1) | Exp EM1 (AL1) | Theo EM1 (AL2) | Theo EM1 (AL2) |
|---|---|---|---|---|---|---|---|---|---|---|---|---|
| Ala | 448 | 4 | 1 | 4 | 11.67% | 10.06% | 10.51% | 9.15% | 8.61% | 8.30% | 8.85% | 7.98% |
| Arg | | 7 | 0.49 | 3.43 | | | | | | | | |
| Asn | | 3 | 0.63 | 1.89 | 5.83% | 8.21% | 5.21% | 7.66% | 4.21% | 6.63% | 4.34% | 6.56% |
| Asp | 672 | 3 | 0.63 | 1.89 | | | | | | | | |
| Cys | 480 | 3 | 0.54 | 1.62 | 5.05% | 6.37% | 4.51% | 5.69% | 3.64% | 4.69% | 3.75% | 4.94% |
| Glu | 686 | 5 | 0.79 | 3.95 | 9.92% | 10.16% | 8.93% | 9.30% | 7.30% | 8.37% | 7.50% | 8.44% |
| Gln | | 5 | 0.79 | 3.95 | | | | | | | | |
| Gly | 434 | 2 | 1.03 | 2.06 | 6.56% | 5.07% | 5.87% | 4.59% | 4.75% | 4.28% | 4.89% | 4.29% |
| His | | 4 | 0.72 | 2.88 | | | | | | | | |
| Ile | 490 | 10 | 0.1 | 1 | 3.08% | 2.99% | 2.74% | 2.35% | 2.21% | 2.30% | 2.27% | 2.34% |
| Leu | 490 | 10 | 0.06 | 0.6 | 1.85% | 3.32% | 1.65% | 2.68% | 1.32% | 2.43% | 1.36% | 2.51% |
| Lys | 685 | 9 | 0.06 | 0.54 | 1.63% | 0.64% | 1.45% | 0.38% | 1.17% | 0.46% | 1.20% | 0.41% |
| Met | 328 | 8 | 0.14 | 1.12 | 6.38% | 4.22% | 5.71% | 3.46% | 4.62% | 3.39% | 4.75% | 3.53% |
| Phe | 524 | 8 | 0.04 | 0.32 | 1.06% | 1.84% | 0.94% | 1.35% | 0.76% | 1.47% | 0.78% | 1.44% |
| Pro | 294 | 7 | 0.37 | 2.59 | 8.66% | 5.84% | 7.77% | 4.11% | 6.32% | 3.80% | 6.50% | 3.42% |
| Ser | | 3 | 0.87 | 2.61 | | | | | | | | |
| Thr | 478 | 5 | 0.04 | 0.2 | | | | | | | | |
| Tyr | 540 | 7 | 0.06 | 0.42 | 1.23% | 2.27% | 1.09% | 1.87% | 0.88% | 1.76% | 0.91% | 1.74% |
| Trp | | | | 0.08 | 0.25% | 0.17% | 0.23% | 0.09% | 0.18% | 0.08% | 0.19% | 0.16% |
| Val | 476 | 8 | 0.07 | 0.56 | 1.76% | 2.46% | 1.57% | 1.99% | 1.26% | 1.86% | 1.30% | 1.98% |

**Table S1:** Amino acid '***n***' values based on the Commerford et al. measurements. Also listed is the GCMS ion which is monitored from the penta-fluoro benzyl bromide (PFBr) derivative of the amino acid used in the analysis. The number of exchangeable hydrogens on each AA are listed with the relative specific activity of tritium labeled AA as measured using long-term labeling of mice with $^{3}H_2O$. The $\boldsymbol{n_{AA}}$ value was calculated from the specific activity in relation to the number of non-exchangable hydrogens. These ***n*** values were used to calculate theoretical enrichments at the measured ***p***for each mouse. Experimentally observed enrichment values in free AA in liver tissue from these mice are compared.

| Accession | %CV AL | AL (k) | %CV CR | CR (k) | SILAM (CR/AL) |
|---|---|---|---|---|---|
| Q921H8 | 9.39 | 0.34 | 8.56 | 0.25 | 0.27 |
| P13707 | 28.60 | 0.21 | 12.90 | 0.15 | 0.30 |
| P06801 | 6.15 | 0.18 | 17.99 | 0.18 | 0.31 |
| Q9ET01 | 18.65 | 0.24 | 9.13 | 0.17 | 0.34 |
| P62264 | 9.88 | 0.10 | 7.86 | 0.10 | 0.37 |
| P16015 | 6.85 | 0.18 | 6.44 | 0.16 | 0.38 |
| P16858 | 9.56 | 0.17 | 7.33 | 0.14 | 0.39 |
| Q05920 | 11.56 | 0.17 | 12.03 | 0.13 | 0.40 |
| P53657 | 10.07 | 0.18 | 10.56 | 0.17 | 0.40 |
| P35980 | 9.53 | 0.08 | 13.68 | 0.06 | 0.41 |
| Q8BWQ1 | 26.20 | 0.16 | 12.78 | 0.17 | 0.41 |
| P12710 | 4.86 | 0.17 | 8.06 | 0.15 | 0.42 |
| Q99LX0 | 9.83 | 0.24 | 29.35 | 0.19 | 0.43 |
| Q8VCU1 | 7.15 | 0.30 | 17.25 | 0.21 | 0.43 |
| Q63880 | 4.80 | 0.29 | 21.84 | 0.13 | 0.44 |
| P48962 | 20.02 | 0.07 | 10.81 | 0.11 | 0.45 |
| P16331 | 19.68 | 0.57 | 22.32 | 0.36 | 0.45 |
| Q9DB20 | 9.09 | 0.12 | 20.54 | 0.11 | 0.45 |
| P14131 | 6.04 | 0.13 | 9.12 | 0.11 | 0.46 |
| Q9QXX4 | 21.53 | 0.09 | 13.26 | 0.12 | 0.46 |
| P70694 | 5.57 | 0.22 | 6.10 | 0.18 | 0.46 |
| P62908 | 22.03 | 0.11 | 5.25 | 0.10 | 0.46 |
| P29758 | 8.89 | 0.61 | 16.69 | 0.51 | 0.46 |
| Q91VS7 | 5.52 | 0.20 | 10.35 | 0.16 | 0.46 |
| P60867 | 4.76 | 0.09 | 5.98 | 0.07 | 0.47 |
| Q80XN0 | 11.10 | 0.11 | 6.91 | 0.10 | 0.48 |
| Q9WUM5 | 20.19 | 0.18 | 10.18 | 0.10 | 0.48 |
| O55125 | 18.77 | 0.14 | 11.69 | 0.12 | 0.48 |
| Q64471 | 22.92 | 0.17 | 19.73 | 0.14 | 0.49 |
| P34914 | 4.41 | 0.24 | 12.51 | 0.20 | 0.50 |
| P62301 | 16.68 | 0.10 | 5.61 | 0.10 | 0.51 |
| Q8VC30 | 17.97 | 0.30 | 11.58 | 0.13 | 0.51 |
| P06151 | 5.11 | 0.21 | 6.44 | 0.17 | 0.51 |
| P06745 | 10.30 | 0.15 | 9.69 | 0.14 | 0.51 |

| | | | | | |
|---|---|---|---|---|---|
| P55264 | 14.23 | 0.27 | 9.94 | 0.18 | 0.51 |
| O08709 | 6.04 | 0.18 | 11.64 | 0.16 | 0.51 |
| Q91YI0 | 6.37 | 0.25 | 8.66 | 0.18 | 0.52 |
| Q01853 | 6.57 | 0.32 | 9.21 | 0.30 | 0.52 |
| Q62425 | 3.11 | 0.38 | 17.11 | 0.29 | 0.53 |
| P32020 | 8.64 | 0.36 | 11.26 | 0.33 | 0.53 |
| P60710 | 7.31 | 0.17 | 10.03 | 0.13 | 0.53 |
| P28474 | 17.97 | 0.15 | 8.46 | 0.14 | 0.53 |
| P08113 | 25.25 | 0.41 | 19.01 | 0.28 | 0.54 |
| P97872 | 12.05 | 0.34 | 8.53 | 0.24 | 0.54 |
| P05064 | 9.36 | 0.42 | 28.97 | 0.33 | 0.54 |
| Q91VR2 | 19.44 | 0.15 | 7.33 | 0.09 | 0.55 |
| P42125 | 12.37 | 0.16 | 5.56 | 0.10 | 0.55 |
| Q9EQ20 | 7.74 | 0.15 | 5.82 | 0.11 | 0.55 |
| Q9DCW4 | 19.56 | 0.22 | 6.27 | 0.10 | 0.56 |
| Q64374 | 4.89 | 0.16 | 6.22 | 0.16 | 0.57 |
| P10126 | 7.45 | 0.17 | 11.06 | 0.14 | 0.57 |
| O55022 | 16.57 | 0.52 | 22.44 | 0.35 | 0.57 |
| P08228 | 8.81 | 0.13 | 7.70 | 0.12 | 0.58 |
| P14152 | 8.47 | 0.19 | 8.92 | 0.18 | 0.58 |
| P51881 | 4.88 | 0.14 | 7.11 | 0.13 | 0.58 |
| Q921I1 | 29.17 | 0.94 | 23.14 | 0.76 | 0.58 |
| Q06185 | 4.38 | 0.11 | 11.63 | 0.08 | 0.59 |
| P99029 | 5.46 | 0.17 | 8.68 | 0.14 | 0.60 |
| P00329 | 4.06 | 0.17 | 7.74 | 0.15 | 0.60 |
| Q8BWT1 | 15.14 | 0.10 | 4.08 | 0.08 | 0.60 |
| P15532 | 3.62 | 0.20 | 7.67 | 0.17 | 0.61 |
| P97328 | 11.33 | 0.21 | 7.69 | 0.12 | 0.61 |
| Q8QZT1 | 7.24 | 0.12 | 4.41 | 0.08 | 0.61 |
| Q9WVL0 | 5.07 | 0.16 | 11.88 | 0.14 | 0.62 |
| P02088 | 6.87 | 0.03 | 5.38 | 0.03 | 0.62 |
| O88844 | 4.33 | 0.18 | 6.20 | 0.15 | 0.62 |
| P35700 | 9.44 | 0.24 | 10.29 | 0.27 | 0.63 |
| Q91Y97 | 6.46 | 0.31 | 9.16 | 0.26 | 0.64 |
| P40142 | 4.30 | 0.12 | 8.11 | 0.10 | 0.64 |
| P63038 | 6.02 | 0.15 | 7.85 | 0.10 | 0.64 |
| Q8CHT0 | 5.06 | 0.12 | 8.08 | 0.09 | 0.64 |

| | | | | | |
|---|---|---|---|---|---|
| Q8BVI4 | 21.75 | 0.19 | 23.27 | 0.16 | 0.65 |
| O35215 | 2.86 | 0.15 | 6.72 | 0.16 | 0.65 |
| P27773 | 6.32 | 0.25 | 8.13 | 0.18 | 0.65 |
| Q921G7 | 7.95 | 0.16 | 15.89 | 0.16 | 0.65 |
| P13745 | 4.82 | 0.16 | 8.67 | 0.16 | 0.65 |
| P63017 | 7.29 | 0.34 | 13.46 | 0.22 | 0.65 |
| Q9CZS1 | 6.59 | 0.47 | 7.10 | 0.08 | 0.66 |
| P62962 | 6.29 | 0.23 | 9.33 | 0.19 | 0.66 |
| Q9R092 | 29.04 | 0.52 | 10.74 | 0.32 | 0.66 |
| Q99LC5 | 10.33 | 0.14 | 4.45 | 0.09 | 0.66 |
| Q01768 | 5.26 | 0.21 | 12.56 | 0.17 | 0.66 |
| P20029 | 3.31 | 0.28 | 11.11 | 0.19 | 0.67 |
| P09411 | 3.03 | 0.16 | 8.46 | 0.14 | 0.67 |
| Q9QXD6 | 4.66 | 0.26 | 7.19 | 0.20 | 0.68 |
| O09173 | 8.09 | 0.25 | 12.55 | 0.19 | 0.68 |
| Q64105 | 22.93 | 0.17 | 11.18 | 0.20 | 0.69 |
| Q9DCG6 | 19.28 | 0.12 | 6.79 | 0.17 | 0.69 |
| Q91X83 | 15.60 | 0.46 | 9.97 | 0.38 | 0.69 |
| P52760 | 3.46 | 0.16 | 7.25 | 0.14 | 0.69 |
| Q8BH00 | 10.47 | 0.17 | 22.50 | 0.15 | 0.69 |
| Q99KI0 | 6.12 | 0.13 | 3.90 | 0.11 | 0.69 |
| P17182 | 3.69 | 0.17 | 15.35 | 0.13 | 0.70 |
| Q9JII6 | 6.96 | 0.18 | 6.45 | 0.15 | 0.70 |
| Q5FW57 | 27.94 | 0.17 | 7.52 | 0.10 | 0.71 |
| Q61176 | 7.18 | 0.20 | 7.84 | 0.16 | 0.71 |
| P30115 | 5.72 | 0.16 | 6.81 | 0.16 | 0.71 |
| Q91ZJ5 | 14.00 | 0.28 | 9.24 | 0.22 | 0.71 |
| Q91V76 | 14.09 | 0.18 | 8.41 | 0.17 | 0.72 |
| P35505 | 4.49 | 0.15 | 7.47 | 0.13 | 0.72 |
| Q8K009 | 13.31 | 0.32 | 7.75 | 0.26 | 0.72 |
| P17742 | 7.76 | 0.24 | 8.89 | 0.20 | 0.72 |
| P05202 | 4.62 | 0.13 | 6.73 | 0.09 | 0.72 |
| Q9R0H0 | 7.66 | 0.44 | 10.86 | 0.32 | 0.72 |
| Q64442 | 6.64 | 0.19 | 7.64 | 0.16 | 0.72 |
| Q8BMS1 | 19.24 | 0.24 | 19.09 | 0.12 | 0.73 |
| P31786 | 4.25 | 0.19 | 13.95 | 0.22 | 0.73 |
| P52196 | 9.77 | 0.15 | 6.66 | 0.10 | 0.73 |

| | | | | | |
|---|---|---|---|---|---|
| Q63886 | 6.67 | 0.21 | 5.82 | 0.18 | 0.73 |
| Q91VA0 | 4.10 | 0.13 | 8.00 | 0.10 | 0.73 |
| Q9D0F9 | 5.86 | 0.16 | 8.26 | 0.14 | 0.73 |
| P38647 | 3.62 | 0.28 | 16.84 | 0.30 | 0.74 |
| P17751 | 9.41 | 0.17 | 6.11 | 0.14 | 0.75 |
| Q9DBJ1 | 25.06 | 0.17 | 9.42 | 0.13 | 0.75 |
| Q9CPQ8 | 3.46 | 0.09 | 8.44 | 0.07 | 0.75 |
| Q91Z53 | 7.23 | 0.14 | 20.03 | 0.17 | 0.75 |
| O35490 | 3.53 | 0.22 | 7.55 | 0.18 | 0.75 |
| Q9WTP7 | 8.96 | 0.21 | 15.98 | 0.15 | 0.75 |
| P16460 | 5.48 | 0.23 | 8.64 | 0.17 | 0.76 |
| Q8VCT4 | 8.37 | 0.23 | 6.19 | 0.18 | 0.76 |
| P26443 | 3.73 | 0.13 | 8.18 | 0.08 | 0.76 |
| P08249 | 9.60 | 0.13 | 5.51 | 0.09 | 0.76 |
| P50247 | 4.45 | 0.22 | 7.61 | 0.17 | 0.76 |
| P15105 | 5.55 | 0.27 | 9.51 | 0.20 | 0.76 |
| P41216 | 5.59 | 0.29 | 7.39 | 0.24 | 0.76 |
| P47738 | 7.25 | 0.38 | 8.03 | 0.24 | 0.77 |
| Q9CPY7 | 7.66 | 0.26 | 26.85 | 0.14 | 0.77 |
| P24270 | 7.99 | 0.53 | 9.25 | 0.40 | 0.78 |
| O35945 | 24.42 | 0.28 | 12.24 | 0.17 | 0.78 |
| P52825 | 7.67 | 0.18 | 9.65 | 0.12 | 0.78 |
| P01942 | 6.82 | 0.03 | 5.86 | 0.02 | 0.79 |
| P24549 | 10.12 | 0.23 | 7.11 | 0.17 | 0.79 |
| P14211 | 8.27 | 0.33 | 7.15 | 0.21 | 0.79 |
| Q8R0Y6 | 5.12 | 0.25 | 6.12 | 0.21 | 0.79 |
| P07724 | 6.59 | 0.26 | 13.65 | 0.29 | 0.79 |
| A2ASS6 | 17.87 | 0.13 | 25.94 | 0.14 | 0.79 |
| P11352 | 10.22 | 0.17 | 12.06 | 0.13 | 0.80 |
| Q64433 | 6.00 | 0.13 | 7.99 | 0.12 | 0.80 |
| Q99KB8 | 27.92 | 0.25 | 8.01 | 0.22 | 0.81 |
| P35979 | 8.13 | 0.07 | 4.21 | 0.08 | 0.81 |
| P10649 | 7.53 | 0.17 | 9.09 | 0.17 | 0.81 |
| P56480 | 2.86 | 0.12 | 5.67 | 0.09 | 0.82 |
| P17563 | 9.93 | 0.18 | 6.94 | 0.15 | 0.83 |
| Q99LB7 | 24.96 | 0.07 | 5.36 | 0.10 | 0.83 |
| P19157 | 6.46 | 0.15 | 9.17 | 0.13 | 0.83 |

| | | | | | |
|---|---|---|---|---|---|
| Q61133 | 6.22 | 0.15 | 12.63 | 0.11 | 0.84 |
| P19783 | 9.83 | 0.14 | 7.99 | 0.10 | 0.87 |
| Q9CQ62 | 15.81 | 0.14 | 6.34 | 0.10 | 0.87 |
| Q9QXF8 | 6.88 | 0.23 | 6.39 | 0.17 | 0.87 |
| P09103 | 5.66 | 0.30 | 13.44 | 0.22 | 0.88 |
| Q9WTP6 | 5.14 | 0.10 | 15.30 | 0.11 | 0.90 |
| Q9DBM2 | 7.73 | 0.18 | 10.43 | 0.17 | 0.91 |
| Q9QXE0 | 5.98 | 0.24 | 12.65 | 0.19 | 0.96 |
| Q8VCC2 | 16.45 | 0.21 | 12.35 | 0.21 | 0.98 |
| Q99L13 | 29.76 | 0.12 | 6.89 | 0.08 | 0.98 |
| P49429 | 10.99 | 0.46 | 11.52 | 0.36 | 0.99 |
| Q03265 | 2.72 | 0.14 | 6.69 | 0.09 | 1.02 |
| P54869 | 5.20 | 0.25 | 7.69 | 0.15 | 1.02 |
| P05201 | 5.18 | 0.18 | 12.70 | 0.14 | 1.02 |
| Q99JY0 | 14.92 | 0.18 | 9.12 | 0.10 | 1.06 |
| P11725 | 10.64 | 0.16 | 4.98 | 0.09 | 1.09 |
| Q8C196 | 6.71 | 0.13 | 4.08 | 0.10 | 1.13 |
| Q91ZA3 | 25.10 | 0.14 | 10.46 | 0.08 | 1.18 |
| Q91XD4 | 4.34 | 0.23 | 7.89 | 0.16 | 1.18 |
| P51174 | 9.05 | 0.14 | 7.28 | 0.10 | 1.20 |
| Q8VCN5 | 5.90 | 0.20 | 8.17 | 0.15 | 1.35 |
| Q9DBF1 | 10.63 | 0.16 | 6.34 | 0.11 | 1.40 |
| Q8BH95 | 11.36 | 0.10 | 6.84 | 0.08 | 1.43 |
| P56395 | 5.90 | 0.31 | 7.60 | 0.23 | 1.54 |
| Q91X91 | 27.46 | 0.40 | 15.06 | 0.13 | |
| P50544 | 7.17 | 0.46 | 6.17 | 0.21 | |
| Q8R086 | 8.97 | 0.14 | 28.04 | 0.07 | |
| Q99PG0 | 26.12 | 0.40 | 9.32 | 0.19 | |
| Q922Q1 | 14.37 | 0.42 | 15.00 | 0.21 | |
| Q8K1Z0 | 13.90 | 0.22 | 6.04 | 0.11 | |
| O35129 | 19.71 | 0.14 | 4.32 | 0.08 | |
| Q9D379 | 12.29 | 0.39 | 7.90 | 0.23 | |
| Q4LDG0 | 10.35 | 0.50 | 14.49 | 0.29 | |
| P54071 | 3.15 | 0.15 | 5.26 | 0.09 | |
| P45952 | 9.25 | 0.22 | 7.99 | 0.13 | |
| Q9CXW4 | 6.71 | 0.10 | 17.44 | 0.06 | |
| P14824 | 8.89 | 0.25 | 8.05 | 0.15 | |

| | | | | | |
|---|---|---|---|---|---|
| Q8BW75 | 8.68 | 0.17 | 11.15 | 0.10 | |
| Q80SW1 | 15.76 | 0.31 | 9.94 | 0.20 | |
| P38060 | 10.19 | 0.19 | 3.95 | 0.12 | |
| P52480 | 9.05 | 0.22 | 7.59 | 0.14 | |
| P63101 | 13.60 | 0.26 | 21.01 | 0.17 | |
| Q61425 | 11.44 | 0.14 | 7.47 | 0.09 | |
| P62889 | 8.75 | 0.08 | 17.02 | 0.05 | |
| P50580 | 12.01 | 0.13 | 17.33 | 0.09 | |
| Q9CZU6 | 9.92 | 0.15 | 9.54 | 0.10 | |
| Q8BH59 | 23.94 | 0.16 | 11.00 | 0.11 | |
| P17156 | 5.67 | 0.39 | 7.09 | 0.26 | |
| Q9CZ13 | 6.15 | 0.14 | 5.67 | 0.10 | |
| Q60932 | 10.62 | 0.24 | 12.66 | 0.17 | |
| Q8K2B3 | 3.81 | 0.20 | 5.99 | 0.14 | |
| Q8CIM7 | 15.63 | 0.61 | 13.24 | 0.43 | |
| P61358 | 4.55 | 0.11 | 13.81 | 0.08 | |
| Q91W90 | 12.97 | 0.33 | 8.24 | 0.23 | |
| Q9JLJ2 | 6.48 | 0.19 | 7.70 | 0.14 | |
| P67778 | 15.50 | 0.13 | 8.19 | 0.09 | |
| Q9D8N0 | 9.48 | 0.13 | 14.26 | 0.09 | |
| Q91VD9 | 4.59 | 0.13 | 21.39 | 0.09 | |
| P62737 | 9.11 | 0.16 | 8.55 | 0.12 | |
| P50172 | 11.64 | 0.31 | 9.61 | 0.23 | |
| Q9DBA8 | 6.74 | 0.13 | 6.42 | 0.10 | |
| Q07417 | 7.60 | 0.11 | 7.61 | 0.08 | |
| P25444 | 28.52 | 0.13 | 13.53 | 0.10 | |
| Q9CZ30 | 19.07 | 0.18 | 10.37 | 0.14 | |
| P05213 | 22.37 | 0.17 | 10.27 | 0.13 | |
| Q6TXD4 | 13.52 | 0.12 | 11.28 | 0.09 | |
| Q9DCT1 | 24.13 | 0.17 | 14.99 | 0.13 | |
| Q6WKZ8 | 8.43 | 0.16 | 7.89 | 0.12 | |
| P15626 | 22.14 | 0.21 | 17.05 | 0.16 | |
| P68369 | 10.75 | 0.19 | 8.54 | 0.15 | |
| P35492 | 8.94 | 0.30 | 10.19 | 0.23 | |
| Q9JHI5 | 23.26 | 0.12 | 8.02 | 0.09 | |
| Q8K023 | 15.91 | 0.18 | 15.66 | 0.14 | |
| Q93092 | 19.80 | 0.28 | 11.89 | 0.22 | |

| | | | | | |
|---|---|---|---|---|---|
| P51660 | 12.85 | 0.27 | 9.90 | 0.21 | |
| P37040 | 13.28 | 0.41 | 19.12 | 0.32 | |
| Q8BFZ3 | 12.00 | 0.16 | 9.91 | 0.12 | |
| P61922 | 6.36 | 0.16 | 8.43 | 0.13 | |
| P11499 | 14.30 | 0.36 | 15.72 | 0.29 | |
| Q91WR5 | 9.23 | 0.20 | 8.84 | 0.16 | |
| Q9JM62 | 8.58 | 0.33 | 9.18 | 0.27 | |
| Q9D6Y7 | 6.47 | 0.22 | 17.67 | 0.18 | |
| P17717 | 6.71 | 0.29 | 9.75 | 0.24 | |
| P09671 | 3.87 | 0.11 | 8.96 | 0.09 | |
| Q61696 | 7.39 | 0.35 | 9.96 | 0.29 | |
| P00405 | 6.45 | 0.11 | 9.98 | 0.09 | |
| Q91WC3 | 11.27 | 0.21 | 13.49 | 0.17 | |
| Q9DCU9 | 21.26 | 0.10 | 8.80 | 0.08 | |
| Q6ZQ58 | 7.04 | 0.03 | 8.10 | 0.03 | |
| P56654 | 22.39 | 0.72 | 10.76 | 0.61 | |
| P68040 | 26.51 | 0.08 | 23.99 | 0.07 | |
| Q8VCR7 | 7.90 | 0.18 | 15.79 | 0.16 | |
| P02089 | 8.65 | 0.03 | 7.40 | 0.02 | |
| Q60759 | 14.83 | 0.19 | 9.41 | 0.16 | |
| Q99J08 | 7.39 | 0.25 | 8.29 | 0.22 | |
| Q64331 | 21.24 | 0.05 | 8.52 | 0.05 | |
| P62900 | 15.72 | 0.07 | 8.42 | 0.06 | |
| Q8VCX1 | 18.38 | 0.15 | 6.91 | 0.13 | |
| Q9JMD3 | 7.79 | 0.22 | 7.10 | 0.20 | |
| Q9DCN2 | 5.91 | 0.23 | 9.64 | 0.20 | |
| P67984 | 8.62 | 0.09 | 12.26 | 0.08 | |
| Q9R0P3 | 3.68 | 0.16 | 6.12 | 0.14 | |
| Q9D6Y9 | 21.99 | 0.13 | 11.36 | 0.12 | |
| Q6PGC1 | 4.33 | 0.02 | 5.08 | 0.02 | |
| P62270 | 15.58 | 0.07 | 6.09 | 0.06 | |
| Q64467 | 6.53 | 0.16 | 8.69 | 0.15 | |
| Q78JT3 | 9.37 | 0.19 | 7.05 | 0.18 | |
| P40936 | 9.26 | 0.18 | 12.21 | 0.17 | |
| Q9D826 | 10.50 | 0.24 | 9.01 | 0.23 | |
| Q8K157 | 4.58 | 0.17 | 8.33 | 0.16 | |
| P61982 | 26.08 | 0.11 | 15.62 | 0.11 | |

| | | | | | |
|---|---|---|---|---|---|
| P06467 | 11.40 | 0.03 | 9.75 | 0.03 | |
| P14869 | 19.10 | 0.07 | 4.20 | 0.07 | |
| Q9EQF5 | 15.84 | 0.25 | 23.26 | 0.24 | |
| Q9DBG1 | 13.50 | 0.28 | 12.79 | 0.28 | |
| Q9CZX8 | 8.28 | 0.11 | 15.49 | 0.11 | |
| Q9CQC9 | 5.17 | 0.27 | 20.63 | 0.27 | |
| Q80UF4 | 11.72 | 0.23 | 6.55 | 0.23 | |
| Q9CQN1 | 23.57 | 0.27 | 8.22 | 0.27 | |
| Q8JZV9 | 23.18 | 0.11 | 28.75 | 0.11 | |
| Q9JHW2 | 11.09 | 0.13 | 5.81 | 0.14 | |
| Q80W21 | 7.46 | 0.16 | 11.42 | 0.17 | |
| P47740 | 10.95 | 0.17 | 20.08 | 0.18 | |
| Q9DCX2 | 6.87 | 0.10 | 10.16 | 0.11 | |
| Q8CAY6 | 10.07 | 0.17 | 22.57 | 0.18 | |
| Q9D819 | 25.97 | 0.16 | 6.45 | 0.18 | |
| P97820 | 28.84 | 0.17 | 19.16 | 0.19 | |
| Q8VC12 | 5.09 | 0.19 | 15.93 | 0.22 | |
| O08756 | 12.19 | 0.11 | 18.18 | 0.13 | |
| Q8VC28 | 26.95 | 0.11 | 11.31 | 0.14 | |
| Q922R8 | 21.80 | 0.23 | 16.59 | 0.30 | |
| P62245 | 10.65 | 0.09 | 7.13 | 0.12 | |
| Q8VCR2 | 7.53 | 0.21 | 26.02 | 0.29 | |
| Q05421 | 21.23 | 0.86 | 18.21 | 1.35 | |
| Q9QX47 | 15.02 | 0.15 | 15.55 | 0.25 | |
| P52840 | 27.15 | 0.14 | 8.54 | 0.24 | |
| P14206 | 14.93 | 0.05 | 24.73 | 0.09 | |
| P02762 | 11.20 | 2.32 | 28.27 | 4.35 | |
| P50285 | 9.63 | 0.10 | 12.51 | 0.22 | |
| P58710 | 24.48 | 0.06 | 12.07 | 0.28 | |
| P56657 | 10.53 | 0.12 | 12.48 | 0.65 | |

**Table S2**: List of final filtered measurements for each protein with the uniprot/swissprot accession numbers (column b, c). The confidence value of the fit for each protein is listed in as %CV. The turnover rates (k) obtained from the fit of the fractional synthesis curves as shown in Figure S3 (column d), SILAM Quantitation ratio for CR mice (AL = 1) is listed in column j. Calculated flux in both CR and AL mice.

| Accession# | Mean No. Peptides | 1 | 3 | 6 | 10 | Var 1:1 | Var 1:3 | Var 1:6 | Var 1:10 | No. 1:1 | No. 1:3 | No. 1:6 | No. 1:10 |
|---|---|---|---|---|---|---|---|---|---|---|---|---|---|
| P04797 | 4.00 | 0.92 | 3.21 | 6.57 | 8.63 | 0.27 | 0.02 | 0.00 | 0.04 | 3.00 | 5.00 | 4.00 | 4.00 |
| P05065 | 3.00 | 0.88 | 2.77 | 6.04 | 9.98 | 0.21 | 0.04 | | 0.00 | 6.00 | 3.00 | 1.00 | 2.00 |
| P07335 | 13.25 | 1.07 | 3.10 | 5.53 | 10.16 | 0.25 | 0.03 | 0.04 | 0.02 | 20.00 | 15.00 | 8.00 | 10.00 |
| P38983 | 3.50 | 1.24 | 3.25 | 6.61 | 11.22 | 0.04 | 0.04 | 0.00 | 0.00 | 5.00 | 3.00 | 2.00 | 4.00 |
| P60711 | 12.75 | 1.03 | 2.85 | 5.81 | 10.16 | 0.05 | 0.05 | 0.01 | 0.01 | 21.00 | 16.00 | 7.00 | 7.00 |
| P62738 | 11.00 | 0.98 | 2.86 | 5.65 | 7.72 | 0.06 | 0.02 | 0.01 | 0.06 | 16.00 | 12.00 | 9.00 | 7.00 |
| Q5XI22 | 2.25 | 1.24 | 3.03 | 5.76 | 9.87 | 0.04 | 0.08 | | | 4.00 | 3.00 | 1.00 | 1.00 |
| | **Mean** | **1.05** | **3.01** | **6.00** | **9.68** | | | | | | | | |
| | **Std Dev** | **0.14** | **0.19** | **0.43** | **1.15** | | | | | | | | |

**Table S4:** The standard curve of quantitation ratios measured for peptides belonging to 7 proteins. Samples were formulated at the ratios indicated from unlabeled liver cell lysate or lysate from cells labeled with the heavy amino acid, U-$^{13}C_6$-L-arginine U-$^{13}C_6$-L-lysine. The average measured ratio for the spectral intensities of the heavy to light peptide agreed well with the expected value.

| Accession | Genes in dataset | Transcription Factor | Literature Expectation (# of citations) | Experimental Log Ratio | Prediction |
|---|---|---|---|---|---|
| P17751 | TPI1 | MYCN | Upregulates (1) | -0.071 | Inhibited |
| Q64442 | SORD | MYCN | Upregulates (1) | -0.075 | Inhibited |
| P62908 | RPS3 | MYCN | Upregulates (1) | -0.053 | Inhibited |
| P25444 | RPS2 | MYCN | Upregulates (1) | -0.132 | Inhibited |
| Q9CZX8 | RPS19 | MYCN | Upregulates (1) | -0.004 | Inhibited |
| P14131 | RPS16 | MYCN | Upregulates (1) | -0.069 | Inhibited |
| P14869 | RPLP0 | MYCN | Upregulates (1) | -0.014 | Inhibited |
| P62900 | RPL31 | MYCN | Upregulates (1) | -0.059 | Inhibited |
| P62889 | RPL30 | MYCN | Upregulates (1) | -0.175 | Inhibited |
| P61358 | RPL27 | MYCN | Upregulates (1) | -0.155 | Inhibited |
| P67984 | RPL22 | MYCN | Upregulates (1) | -0.047 | Inhibited |
| P35980 | RPL18 | MYCN | Upregulates (1) | -0.140 | Inhibited |
| Q9CXW4 | RPL11 | MYCN | Upregulates (1) | -0.224 | Inhibited |
| Q01768 | NME2 | MYCN | Upregulates (2) | -0.093 | Inhibited |
| P15532 | NME1 (includes EG:18102) | MYCN | Upregulates (3) | -0.070 | Inhibited |
| P63038 | HSPD1 | MYCN | Upregulates (2) | -0.168 | Inhibited |
| P11499 | HSP90AB1 | MYCN | Upregulates (1) | -0.096 | Inhibited |
| Q9D8N0 | EEF1G | MYCN | Upregulates (1) | -0.143 | Inhibited |
| P05064 | ALDOA | MYCN | Upregulates (1) | -0.106 | Inhibited |
| P24549 | ALDH1A1 | MYCN | Upregulates (1) | -0.124 | Inhibited |
| P05213 | TUBA1B | MYCN | Downregulates (1) | -0.128 | Activated |
| P60710 | ACTB | MYCN | Downregulates (1) | -0.106 | Activated |
| P67778 | PHB | MYCN | Regulates (1) | -0.150 | |
| P08228 | SOD1 | PPAR gamma | Upregulates (3) | -0.024 | Inhibited |
| P14206 | RPSA | PPAR gamma | Downregulates (1) | 0.236 | Inhibited |
| Q05920 | PC | PPAR gamma | Upregulates (24) | -0.113 | Inhibited |
| Q91VS7 | MGST1 | PPAR gamma | Upregulates (2) | -0.088 | Inhibited |
| P14152 | MDH1 | PPAR gamma | Upregulates (3) | -0.022 | Inhibited |
| Q9JHI5 | IVD | PPAR gamma | Upregulates (2) | -0.113 | Inhibited |
| P54869 | HMGCS2 | PPAR gamma | Upregulates (3) | -0.224 | Inhibited |
| Q99JY0 | HADHB | PPAR gamma | Upregulates (2) | -0.249 | Inhibited |
| Q8BMS1 | HADHA | PPAR gamma | Upregulates (2) | -0.298 | Inhibited |

| | | | | | |
|---|---|---|---|---|---|
| P13707 | GPD1 | PPAR gamma | Upregulates (7) | -0.138 | Inhibited |
| P12710 | FABP1 | PPAR gamma | Upregulates (8) | -0.048 | Inhibited |
| Q9DBM2 | EHHADH | PPAR gamma | Upregulates (10) | -0.022 | Inhibited |
| Q9CZU6 | CS | PPAR gamma | Upregulates (3) | -0.170 | Inhibited |
| P52825 | CPT2 | PPAR gamma | Upregulates (5) | -0.189 | Inhibited |
| Q8VCT4 | CES1 | PPAR gamma | Upregulates (1) | -0.092 | Inhibited |
| P24270 | CAT | PPAR gamma | Upregulates (8) | -0.122 | Inhibited |
| P14211 | CALR | PPAR gamma | Upregulates (1) | -0.198 | Inhibited |
| Q80XN0 | BDH1 (includes EG:100037356) | PPAR gamma | Upregulates (2) | -0.073 | Inhibited |
| Q9DB20 | ATP5O | PPAR gamma | Upregulates (2) | -0.040 | Inhibited |
| P41216 | ACSL1 | PPAR gamma | Upregulates (5) | -0.076 | Inhibited |
| Q9R0H0 | ACOX1 | PPAR gamma | Upregulates (16) | -0.145 | Inhibited |
| Q07417 | ACADS | PPAR gamma | Upregulates (3) | -0.135 | Inhibited |
| P45952 | ACADM | PPAR gamma | Upregulates (3) | -0.224 | Inhibited |
| Q8BWT1 | ACAA2 | PPAR gamma | Upregulates (2) | -0.075 | Inhibited |
| Q921H8 | ACAA1 | PPAR gamma | Upregulates (3) | -0.132 | Inhibited |
| Q9D379 | EPHX1 | PPAR gamma | Downregulates (1) | -0.232 | Activated |
| P51174 | ACADL | PPAR gamma | Regulates (3) | -0.134 | |
| Q9JLJ2 | ALDH9A1 | PPAR gamma | Regulates (1) | -0.152 | |
| P13745 | GSTA5 | PPAR gamma | Regulates (1) | 0.001 | |
| Q9ET01 | PYGL | PPAR gamma | Regulates (4) | -0.140 | |
| P32020 | SCP2 | PPAR gamma | Regulates (2) | -0.033 | |
| P40142 | TKT | PPAR gamma | Regulates (2) | -0.049 | |
| P61982 | YWHAG | PPAR gamma | Regulates (2) | -0.017 | |
| P17751 | TPI1 | MYC | Upregulates (4) | -0.071 | Inhibited |
| P51881 | SLC25A6 | MYC | Upregulates (1) | -0.030 | Inhibited |
| P60867 | Rps20 | MYC | Upregulates (1) | -0.069 | Inhibited |
| Q9CZX8 | RPS19 | MYC | Upregulates (2) | -0.004 | Inhibited |
| P62270 | RPS18 | MYC | Upregulates (1) | -0.032 | Inhibited |
| P14131 | RPS16 | MYC | Upregulates (1) | -0.069 | Inhibited |
| P62889 | RPL30 | MYC | Upregulates (1) | -0.175 | Inhibited |
| P61358 | RPL27 | MYC | Upregulates (1) | -0.155 | Inhibited |
| P67984 | RPL22 | MYC | Upregulates (1) | -0.047 | Inhibited |
| P17742 | PPIA | MYC | Upregulates (1) | -0.070 | Inhibited |
| P53657 | PKLR | MYC | Upregulates (2) | -0.032 | Inhibited |
| P67778 | PHB | MYC | Upregulates (3) | -0.150 | Inhibited |

| | | | | | |
|---|---|---|---|---|---|
| P09411 | PGK1 | MYC | Upregulates (4) | -0.046 | Inhibited |
| Q01768 | NME2 | MYC | Upregulates (1) | -0.093 | Inhibited |
| P15532 | NME1 (includes EG:18102) | MYC | Upregulates (2) | -0.070 | Inhibited |
| P06151 | LDHA | MYC | Upregulates (12) | -0.080 | Inhibited |
| Q64433 | HSPE1 | MYC | Upregulates (6) | -0.029 | Inhibited |
| P63038 | HSPD1 | MYC | Upregulates (11) | -0.168 | Inhibited |
| P06745 | GPI | MYC | Upregulates (4) | -0.047 | Inhibited |
| P16858 | Gapdh (includes others) | MYC | Upregulates (1) | -0.067 | Inhibited |
| P17182 | ENO1 | MYC | Upregulates (9) | -0.109 | Inhibited |
| P16460 | ASS1 | MYC | Upregulates (2) | -0.118 | Inhibited |
| P07724 | ALB | MYC | Downregulates (1) | 0.050 | Inhibited |
| P50247 | AHCY | MYC | Upregulates (1) | -0.096 | Inhibited |
| Q63886 | UGT1A1 | MYC | Downregulates (1) | -0.078 | Activated |
| Q9CQN1 | TRAP1 | MYC | Upregulates (1) | 0.007 | Activated |
| P09671 | SOD2 | MYC | Downregulates (1) | -0.081 | Activated |
| Q99LB7 | SARDH | MYC | Upregulates (1) | 0.158 | Activated |
| P62245 | RPS15A | MYC | Upregulates (1) | 0.135 | Activated |
| P38647 | HSPA9 | MYC | Upregulates (1) | 0.021 | Activated |
| P31786 | DBI | MYC | Upregulates (1) | 0.056 | Activated |
| P52825 | CPT2 | MYC | Downregulates (1) | -0.189 | Activated |
| Q9WTP6 | AK2 | MYC | Upregulates (6) | 0.034 | Activated |
| P60710 | ACTB | MYC | Downregulates (1) | -0.106 | Activated |
| Q8QZT1 | ACAT1 | MYC | Regulates (5) | -0.152 | |
| P55264 | ADK | MYC | Regulates (5) | -0.184 | |
| P14824 | ANXA6 | MYC | Regulates (5) | -0.207 | |
| Q61176 | ARG1 | MYC | Regulates (1) | -0.098 | |
| Q61696 | HSPA1A/HSPA1B | MYC | Regulates (1) | -0.079 | |
| P54071 | IDH2 | MYC | Regulates (5) | -0.229 | |
| O35129 | PHB2 | MYC | Regulates (5) | -0.234 | |
| P52480 | PKM2 | MYC | Regulates (2) | -0.193 | |
| P40142 | TKT | MYC | Regulates (5) | -0.049 | |
| Q63886 | UGT1A1 | HNF4A | Upregulates (1) | -0.078 | Inhibited |
| P32020 | SCP2 | HNF4A | Upregulates (2) | -0.033 | Inhibited |
| Q9ET01 | PYGL | HNF4A | Upregulates (1) | -0.140 | Inhibited |
| P53657 | PKLR | HNF4A | Upregulates (10) | -0.032 | Inhibited |

| | | | | | |
|---|---|---|---|---|---|
| P11725 | OTC | HNF4A | Upregulates (9) | -0.219 | Inhibited |
| P49429 | HPD | HNF4A | Upregulates (1) | -0.106 | Inhibited |
| P16858 | Gapdh (includes others) | HNF4A | Upregulates (1) | -0.067 | Inhibited |
| P12710 | FABP1 | HNF4A | Upregulates (7) | -0.048 | Inhibited |
| Q80XN0 | BDH1 (includes EG:100037356) | HNF4A | Upregulates (1) | -0.073 | Inhibited |
| Q91Y97 | ALDOB | HNF4A | Upregulates (3) | -0.086 | Inhibited |
| P47738 | ALDH2 | HNF4A | Upregulates (11) | -0.206 | Inhibited |
| P41216 | ACSL1 | HNF4A | Upregulates (1) | -0.076 | Inhibited |
| Q8QZT1 | ACAT1 | HNF4A | Upregulates (1) | -0.152 | Inhibited |
| Q8BWT1 | ACAA2 | HNF4A | Regulates (1) | -0.075 | |
| Q99KI0 | ACO2 (includes EG:11429) | HNF4A | Regulates (1) | -0.086 | |
| Q9R0H0 | ACOX1 | HNF4A | Regulates (1) | -0.145 | |
| Q9WTP6 | AK2 | HNF4A | Regulates (1) | 0.034 | |
| Q91WR5 | AKR1C1/AKR1C2 | HNF4A | Regulates (1) | -0.095 | |
| Q8K023 | AKR1C3 | HNF4A | Regulates (1) | -0.109 | |
| P70694 | AKR1C4 | HNF4A | Regulates (3) | -0.083 | |
| P24549 | ALDH1A1 | HNF4A | Regulates (1) | -0.124 | |
| Q8R0Y6 | ALDH1L1 | HNF4A | Regulates (1) | -0.074 | |
| Q8BH00 | ALDH8A1 | HNF4A | Regulates (1) | -0.075 | |
| O35490 | BHMT | HNF4A | Regulates (1) | -0.098 | |
| Q91V76 | C11orf54 | HNF4A | Regulates (1) | -0.029 | |
| P52825 | CPT2 | HNF4A | Regulates (1) | -0.189 | |
| Q9CZU6 | CS | HNF4A | Regulates (1) | -0.170 | |
| Q9QXD6 | FBP1 | HNF4A | Regulates (1) | -0.109 | |
| Q9D6Y9 | GBE1 | HNF4A | Regulates (1) | -0.046 | |
| P05201 | GOT1 | HNF4A | Regulates (1) | -0.110 | |
| P11352 | GPX1 (includes EG:14775) | HNF4A | Regulates (1) | -0.103 | |
| Q91Z53 | GRHPR | HNF4A | Regulates (1) | 0.081 | |
| Q9WVL0 | GSTZ1 | HNF4A | Regulates (1) | -0.040 | |
| Q78JT3 | HAAO | HNF4A | Regulates (1) | -0.027 | |
| Q8BMS1 | HADHA | HNF4A | Regulates (1) | -0.298 | |
| Q99JY0 | HADHB | HNF4A | Regulates (1) | -0.249 | |
| P35492 | HAL | HNF4A | Regulates (1) | -0.114 | |

| | | | | | |
|---|---|---|---|---|---|
| O09173 | HGD | HNF4A | Regulates (1) | -0.116 | |
| P50172 | HSD11B1 | HNF4A | Regulates (1) | -0.137 | |
| P51660 | HSD17B4 | HNF4A | Regulates (1) | -0.108 | |
| P08113 | HSP90B1 | HNF4A | Regulates (1) | -0.166 | |
| P20029 | HSPA5 | HNF4A | Regulates (1) | -0.175 | |
| Q64433 | HSPE1 | HNF4A | Regulates (1) | -0.029 | |
| P08249 | MDH2 (includes EG:17448) | HNF4A | Regulates (1) | -0.168 | |
| Q91VS7 | MGST1 | HNF4A | Regulates (1) | -0.088 | |
| Q62425 | NDUFA4 | HNF4A | Regulates (1) | -0.116 | |
| Q91VD9 | NDUFS1 | HNF4A | Regulates (1) | -0.141 | |
| P15532 | NME1 (includes EG:18102) | HNF4A | Regulates (1) | -0.070 | |
| Q9D0F9 | PGM1 | HNF4A | Regulates (1) | -0.049 | |
| P67778 | PHB | HNF4A | Regulates (1) | -0.150 | |
| O35129 | PHB2 | HNF4A | Regulates (1) | -0.234 | |
| P52480 | PKM2 | HNF4A | Regulates (1) | -0.193 | |
| P99029 | PRDX5 | HNF4A | Regulates (1) | -0.099 | |
| P35980 | RPL18 | HNF4A | Regulates (1) | -0.140 | |
| P62900 | RPL31 | HNF4A | Regulates (1) | -0.059 | |
| P62270 | RPS18 | HNF4A | Regulates (1) | -0.032 | |
| Q9QXX4 | SLC25A13 | HNF4A | Regulates (1) | 0.100 | |
| Q9JMD3 | STARD10 | HNF4A | Regulates (1) | -0.057 | |
| Q9WUM5 | SUCLG1 | HNF4A | Regulates (1) | -0.255 | |
| P52840 | SULT1A1 | HNF4A | Regulates (1) | 0.233 | |
| Q921I1 | TF | HNF4A | Regulates (1) | -0.091 | |
| Q8BWQ1 | UGT2A3 | HNF4A | Regulates (1) | 0.027 | |
| Q60932 | VDAC1 | HNF4A | Regulates (1) | -0.158 | |

**Table S5**: Predicted expression profiles from the literature were compared against the measured kinetic perturbationsof proteins in the Liver. Four transcription factors were significantly negatively correlated with the data found in the Ingenuity IPA data base.

# Chapter 2

## Calorie Restriction Increases Fatty Acid Synthesis and Whole Body Fat Oxidation Rates

Matthew D. Bruss[1], Cyrus F. Khambatta[1], Maxwell A. Ruby[2],
Ishita Aggarwal[1] and Marc K. Hellerstein[1]

[1]Department of Nutritional Sciences and Toxicology,
University of California at Berkeley, Berkeley, California 94720
[2]Children's Hospital Oakland Research Institute, Oakland, CA 94609

**Abstract**

Calorie restriction (CR) increases longevity and retards the development of many chronic diseases, but the underlying metabolic signals are poorly understood. Increased fatty acid (FA) oxidation and reduced FA synthesis have been hypothesized to be important metabolic adaptations to CR. At metabolic steady state, however, FA oxidation must match FA intake plus synthesis; moreover, FA intake is low, not high, during CR. It is therefore not clear how FA dynamics are altered during CR. Accordingly, we measured food intake patterns, whole-body fuel selection, endogenous FA synthesis and gene expression in mice on CR. Within two days of starting CR, a shift occurred to a cyclic, diurnal pattern of whole-body FA metabolism, with an initial phase of elevated endogenous FA synthesis (respiratory exchange ratio [RER]>1.10, lasting 4-6 hours after food provision), followed by a prolonged phase of FA oxidation (RER=0.70, lasting 18-20 hours). CR mice oxidized four times as much fat per day as *ad libitum* fed (AL) controls (367 ± 19 vs 97 ± 14 mg/d, P< O.001) despite reduced energy intake from fat. This increase in FA oxidation was balanced by a 3-fold increase in adipose tissue FA synthesis compared to

AL. Expression of fatty acid synthase and acetyl-CoA carboxylase mRNA were increased in adipose and liver in a time-dependent manner. We conclude that CR induces a surprising metabolic pattern characterized by periods of elevated FA synthesis alternating with periods of FA oxidation disproportionate to dietary FA intake. This pattern may have implications for oxidative damage and disease risk.

**Key words**

Fat oxidation, fat synthesis, lipogenesis, palmitoleate, heavy water

## Introduction

Calorie restriction (CR) delays the development of chronic disease and prolongs lifespan in mice (1, 17, 27, 34). These effects correlate with a rapid induction in the expression of certain genes that persist as long as animals remain on CR (10, 36), even after energy balance is restored. These observations suggest the presence of a chronic signal of reduced energy availability that persists after energy balance has been reestablished. However, the underlying metabolic signals and adaptations responsible are not fully understood.

Mice on CR regimens have been reported to exhibit increased expression of genes for fatty acid (FA) oxidation and decreased expression of genes for FA synthesis compared to *ad libitum* fed (AL) controls (6, 7, 30, 38). Due to differential entry points into the electron transport chain, a metabolic shift from carbohydrate to FA oxidation may reduce the production of reactive oxygen species (ROS) (15). A shift to FA oxidation thereby represents a potential mechanism for reduced oxidative damage, which has been proposed as a potential explanation for the health benefits of CR (14, 15, 29, 35). It has also been proposed that reduced rates of FA synthesis may inhibit tumor formation (30, 38). Thus, changes in macronutrient metabolism – specifically, FA oxidation or synthesis - may be an important metabolic mediator of the health benefits of CR.

A problem with the FA oxidation hypothesis, however, relates to a basic principle of energetics and macronutrient balance in whole organisms. At metabolic steady state, i.e., when body composition is stable, fuel selection must match dietary macronutrient composition (13, 44). In other words, the respiratory quotient (RQ) over each 24-hour period is usually identical to the net daily "food quotient" (FQ). Since the macronutrient composition of the diets fed to CR and AL mice are typically identical (FQ = 0.94) and total energy intake is lower on CR, neither relative nor absolute FA intake is elevated in CR animals. On the surface, these considerations argue against a role for increased FA oxidation rates as a signal mediating health benefits in CR mice.

The goal of this study was to determine whole body FA oxidation and synthesis rates in CR and AL mice, using a combination of indirect calorimetry and stable isotope labeling, and to compare these metabolic changes to gene expression in white adipose tissue and liver. We report here a rapidly induced diurnal pattern of FA synthesis and oxidation in mice on CR regimens. We hypothesize that this pattern of macronutrient metabolism could provide signals linking CR to health benefits.

## Methods

### Mice and diets

Nine-week-old C57BL/6J male mice were obtained from Charles River Breeding Laboratories, housed individually, and maintained under temperature and light controlled conditions (12 hour light/dark cycle: lights on at 7 AM and off at 7 PM) for 1 week. During this acclimation period, mice were given free access to water and a semipurified AIN-93M diet (Bio-Serv), and the daily amount of food consumed by each mouse was recorded.

At 10 weeks of age, mice were randomly assigned to either the CR or the AL control group. Mice in the AL group were provided free access to food throughout the day, while mice in the CR group were provided 70% of the calories consumed by the AL group. Food was provided to the CR group daily at 6 PM. Mice were maintained on CR or AL for at least 5 weeks before any experimental studies were carried out. Upon completion of each experiment, mice were anesthetized under 3% isoflurane and blood was collected via cardiac puncture, followed by cervical dislocation. All procedures and protocols received approval from the University of California Berkeley Animal Use Committee.

### Food Consumption

Food consumption was determined by 24-hour automatic food monitoring system in Environment Controlled CLAMS metabolic cages (Columbus Scientific). Total food consumption was measured six times per hour and averaged to determine hourly food consumption.

### Respiratory Exhange Ratio (RER), Energy Expenditure (EE), FA Oxidation and Fuel Selection

We determined RER, EE, FA oxidation and fuel selection in environment controlled CLAMS metabolic cages, equipped with an indirect open circuit calorimeter (Oxymax Equal Flow System). The system measures carbon dioxide produced and oxygen consumed over a one-minute period, six times per hour. These values were averaged to determine the rate of carbon dioxide produced ($VCO_2$) and oxygen consumed ($VO_2$) in milliliters per hour. EE, RER and FA oxidation were calculated using the following equations (25):

$$RER = \frac{V_{CO_2}}{V_{O_2}}$$

$$EE = 3.815 + 1.232 * 1000 * RER * V_{O_2}$$

$$FA\ Oxidation = EE * \left(\frac{1 - RER}{0.3}\right)$$

Daily FA oxidation was calculated from the 24-hour area under the curve (AUC) of hourly FA oxidation. Daily carbohydrate plus protein oxidation was calculated from total daily EE, determined from the AUC of hourly EE, minus daily FA oxidation.

### FA Synthesis

FA synthesis was measured by stable isotope incorporation, with analysis by gas chromatography-mass spectrometry (GC-MS). Mice were labeled with an intraperitoneal injection of 100% $^2H_2O$ (0.35ml/ 10g body weight) and then provided 8% $^2H_2O$ as drinking water for 6–24 hours, as described previously (40). Upon completion of labeling, mice were euthanized and tissue or serum was

collected and homogenized in 2:1 chloroform/methanol solution. Pentadecanoic acid (10mg/mL) was added to solutions as an internal control. Lipid was extracted in methanol/chloroform overnight and methylated with 5% methanolic acid with heating at 50°C for 1 hour. The FA methyl esters were extracted via the Folch technique with hexane after the addition of water.

Total FA concentrations were measured via gas chromatography-flame ionization detection using an Agilent 6890N GC (Agilent Technologies, Palo Alto, CA) and a DB-225MS column. Hydrogen was used as carrier gas at a constant flow rate of 40mL/min. The temperature of the GC oven was set to 110°C for 2 minutes, increased to 220°C for 8min and held at 240°C for 5 minutes. HP Chemstation software was used for data analysis.

The fraction of newly synthesized non-essential saturated FA formed during the $^2H_2O$ labeling period was assessed using a combinatorial model of polymerization biosynthesis, as described previously (37, 39). Briefly, mass isotopomer distribution analysis (MIDA) was used to determine the number (n) of hydrogen atoms in FA C–H bonds that were derived from cellular water during endogenous synthesis of FA. Enrichments, or excess fractional molar abundances ($EM_x$) above baseline, were measured for the parent ($EM_0$), single-labeled ($EM_1$) and double-labeled ($EM_2$) mass isotopomers in the FA by GC-MS. Specifically, the fractional abundances of molecular anions m/z 270, 271 and 272 (for 16:0, palmitate), and m/z 298, 299 and 300 (for 18:0, stearate) were determined in natural abundance (baseline) samples and in $^2H_2O$ labeled samples. The measured body $^2H_2O$ enrichment was then used to represent the isotopic enrichment of hydrogen atoms entering C-H bonds in the FA synthetic pathway, i.e., the true precursor pool (p) (37, 39), and n was calculated from $EM_2/EM_1$ ratios, as described previously (22). The maximal or asymptotic $^2H$ excess mass +1 isotopomeric enrichment ($A^*_1$) possible in the FA at this p and n, representing the $EM_1$ value if 100% of the FA were newly synthesized from this body water pool was then calculated (37, 39). The measured $EM_1$ value was divided by the asymptotic value to calculate the fraction (f) of FA that was endogenously synthesized during the labeling period.

$$Fraction endogenously synthesized\ FA(f) = EM_1/A_1^*$$

This approach was modified to determine the fractional synthesis of palmitoleate (16:1) and oleate (18:1). The double bonds were saturated by reacting 10mg of FA methyl esters with 5mg of bromine in 400uL of carbon tetrachloride for 30 minutes. The resultant dibromo methyl ester-FAs were analyzed by positive chemical ionization and, after loss of bromine, anions m/z 347 and 348 (for 16:1) and m/z 377, 378 and 379 (for 18:1) were compared to determine $EM_1$ and $EM_2$ values.

Whole-body fat mass, used to calculate total adipose FA synthesis, was estimated at 15% body weight for CR and 32% body weight for AL, based on literature values (3, 4, 9, 16, 18, 26).

### Gene Expression

RNA was isolated from snap frozen inguinal and epididymal adipose tissue and liver tissue using RNeasy kit (Qiagen) and reverse transcribed with M-MulV reverse transcriptase (New England

Biolabs). Next, 25ng of diluted cDNA was run on an ABI 7500 Fast Real-Time PCR System, using TaqMan gene expression master mix and probed with fatty acid synthase (FAS, Mm01253300_g1), acetyl-coA carboxylase 1 (ACC1, Mm01304289_m1), beta-2 microglobulin (B2M, Mm00437762_m1), sterol regulatory element-binding protein 1 (SREBP-1; Mm00550338_m1), peroxisome proliferator-activated receptor gamma (PPARγ; Mm00440945_m1) and glyceraldeyde-3-phosphate dehydrogenase (GAPDH, Pre-developed TaqMan assay reagent) according to manufacturers instructions (Applied Biosystems). To account for potential time dependent changes in any single reference gene, the expression of FAS, ACC1, SREBP-1 and PPARγ mRNA were divided by the expression of two reference genes (GAPDH and B2-microglobin) in each tissue and these values were then averaged. Data from all groups were expressed as means ± SEM, relative to AL control animals at 6 PM.

### Serum Lipids

Serum non-esterified fatty acid (NEFA) and triglyceride (TG) concentrations were determined by HR Series NEFA-HR and L-Type TG M methods (Wako Diagnostics), respectively.

### Statistical Analysis

All results are presented as mean ± SEM. The area under the curve for Fig. 3 was calculated with a baseline of 0 and from x =0 to x= 24. Differences between groups were analyzed by two-way ANOVA with Bonferroni *post hoc* test or T-test. Data were analyzed by Prism Graphpad software (version 5.0a).

## Results

### Body weights and food intake pattern.

The most obvious changes in response to CR in rodents are lower body weights and reduced adiposity. Another major adaptation that we have observed is a dramatic alteration in feeding pattern. Mice fed AL maintained relatively constant energy intake throughout the day (0.69 ± 0.07 kcal/h; Fig. 1A). In contrast, CR mice given food each day at 6 PM consumed their entire daily allotment of food in approximately one hour, at an average rate of 8.7 kcal/h, followed by a nearly twenty-three hour daily absence of food energy intake (Fig. 1A).

### Fuel selection

To determine whether this pattern of feeding and fasting influences fuel selection throughout the day and to determine the duration of CR needed to induce a potential change, the RER was calculated after various durations of CR. We observed that CR immediately led to a dramatic change in the daily pattern of fuel selection (Fig. 2). While AL mice maintained an RER of approximately 0.9 - 1.0, representing primarily carbohydrate oxidation (Fig. 2A), as expected from the predominance of carbohydrate energy in the diet, CR mice exhibited two distinct phases of fuel selection each day (Fig. 2B-F). In the first phase, immediately following provision of food, the CR mice exhibited RER values significantly greater than 1.0, which is generally taken to represent both carbohydrate oxidation and endogenous FA synthesis (33). In the second phase, beginning approximately six hours after food is presented each day, RER values rapidly fell to ~0.7,

representing exclusively FA oxidation. This pattern became more pronounced over the course of the first 7 days of CR (Fig. 2A-D) and the circadian pattern continued for the remainder of the CR feeding regimen (Fig. 2F). Thus, it appears that CR rapidly and significantly alters whole body fuel selection, leading to a metabolically unusual pattern of both increased FA oxidation and increased FA synthesis, on the whole-body level.

### Total fat oxidation in the whole body

The energy derived from FA oxidation was calculated from a combination of RER (Fig. 3A) and energy expenditure (Fig. 3B). Both the hourly and daily FA oxidation rates are shown (Fig. 3C & 3D; see calculations). CR mice oxidized almost four times as much fat as AL mice per day (3.3 ± 0.17 vs. 0.87 ± 0.13 kcal/d, or 367 ± 19 and 97 ± 14 mg/d, respectively; Fig. 3D). CR mice derived 37% of their daily energy needs from fat oxidation, compared to only 7% for AL mice (Fig. 3D). Fat content of the diet fed to both groups was identical (9.7% of metabolizable energy). These data demonstrate that CR dramatically increases the total energy derived directly from FA oxidation compared to AL controls.

CR mice oxidized over 300mg of fat per day, but they only consumed 92 mg of fat per day. Over the last 28 days of the 35 day CR regimen, CR mice were in neutral or positive energy balance (Fig. 1B). To establish whether increased FA synthesis can be detected biochemically and whether this synthesis can account for the higher FA oxidation rates in the whole body, we measured endogenous FA synthesis from $^2H$ incorporation into FAs in adipose and liver tissue after endogenous labeling with $^2H_2O$.

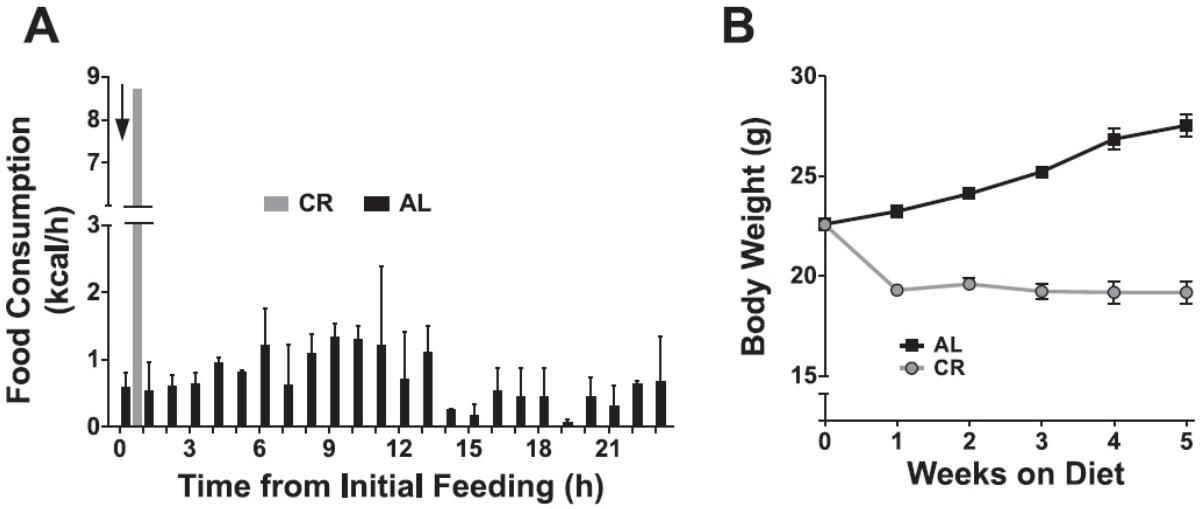


**Figure 1. Altered feeding pattern and body weight in response to calorie restriction.** Food was provided to CR and AL mice at 6 PM. Food consumption was recorded hourly, using food balance in metabolic cages, over the next twenty-four hours (A). Mice were weighed weekly (B). Values are means ± SEM for 6 mice per group. ↓ indicates time when daily food was provided to CR mice.

### Endogenous fatty acid synthesis

CR led to a 15.8-, 26.8-, 30- and 3.2-fold increase in the daily accumulation of endogenously synthesized palmitate, palmitoleate, stearate and oleate (mg/g adipose tissue), respectively, in adipose tissue relative to AL controls (Fig. 4A).

In contrast, CR did not alter the accumulation of any endogenously synthesized FA in the liver (Fig. 4B). When extrapolated to total fat mass, CR mice synthesized and retained in adipose tissue and liver a total of 212 ± 13 mg FA/day as compared to 91 ± 9 mg/day for AL controls (Fig. 4C). Thus, endogenous FA synthesis that was retained in the adipose tissue and liver (212 mg/day) accounts for a substantial proportion of the whole body FA oxidation that was in excess of food intake (~270 mg/day). Endogenous FAs that were synthesized and directly oxidized, rather than mixing into the general adipose TG pool, would not accrue or be measured in adipose depots, and could account for the remainder of FA oxidation in excess of intake.

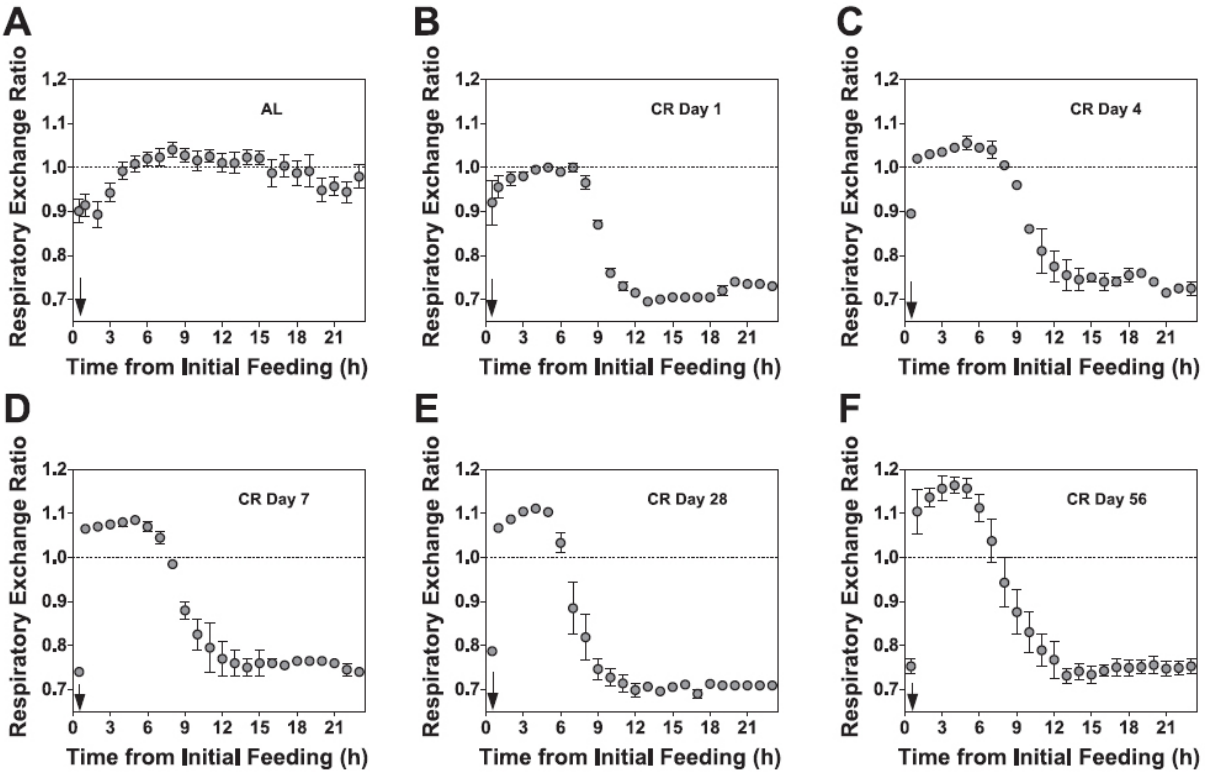


**Figure 2. Time course of effect of CR on fuel selection pattern.** AL fed mice were placed in metabolic cages before starting a CR diet (A) and again at day 1 (B), 4 (C), 7 (D), 28 (E) and 56 (F) of calorie restriction. Gas exchange was monitored for twenty-four hours each time mice were placed in metabolic cages. Respiratory exchange ratios (RER) were recorded six times per hour, then averaged to give RER for each hour. Values are means ± SEM for 4 mice per diet. ↓ indicates time when daily food was provided to CR mice.

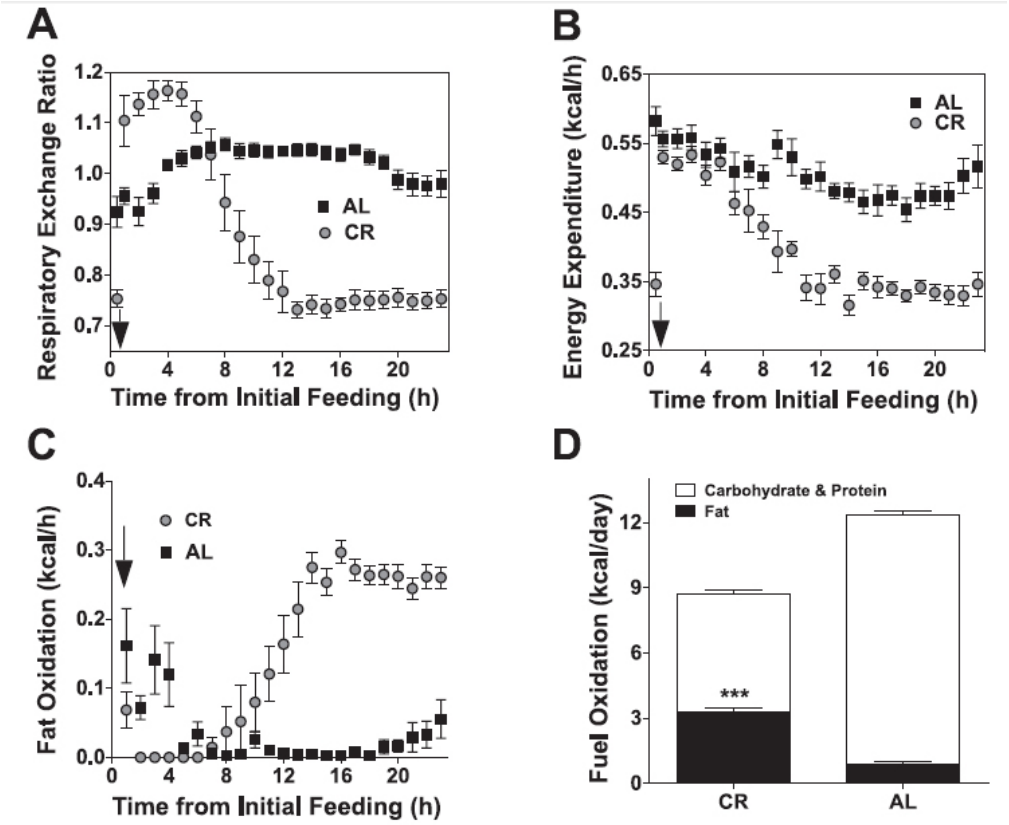


**Figure 3. Higher rates of whole body fat oxidation in response to CR.** Mice were adapted to CR or AL feeding for at least five weeks and were then placed in metabolic cages for twenty-four hours to determine respiratory exchange ratio (A) and energy expenditure (B) at each hour of the day. Hourly fat oxidation (C) and summed daily macronutrient oxidation (D) were calculated as described in "Methods". Values are means ± SEM (n=4-8 mice per group). ***P<0.001 difference from AL values, by ANOVA and Bonferroni *post hoc* test. ↓ indicates time when daily food was provided to CR mice.

To determine whether the endogenous synthesis of FAs occurred in the adipose tissue directly or were transported to the adipose following synthesis in the liver, we measured $^2H$ incorporation into palmitate in adipose (subcutaneous and epididymal depots), liver and VLDL throughout the first day after exposure to $^2H_2O$ (Fig. 5). In the first 3 hours after food was provided, a 5-fold increase was observed in the accumulation of newly synthesized palmitate in the subcutaneous depot (14.1 ± 1.2 vs 2.7 ± 0.2 mg/depot) and a 2-fold increase was observed in the epididymal depot (2.9 ± 0.1 vs 1.5 ± 0.1 mg/depot) in CR mice relative to AL controls, after which accumulation occurred at a much slower rate (Fig. 5A & B). This circadian pattern of FA synthesis parallels the pattern seen in the RER data (Fig. 2). In contrast, there was no increase in the accumulation of endogenously synthesized palmitate in the liver at any time point (Fig. 5C) and only a small increase in plasma VLDL of CR mice six hours after feeding (Fig. 5D). The magnitude and timing of the accumulation of endogenously synthesized palmitate in the adipose tissue relative to the liver suggests that

adipose tissue is the major site of FA synthesis in response to CR.

### Gene expression

To determine whether changes in gene expression reflected these striking changes in flux through FA synthetic pathways, we measured FAS, ACC1, SREBP-1 and PPARY mRNA levels in liver and adipose tissue at several time points throughout the day (Fig. 6 & Fig. 7). In the liver, FAS and ACC1 expression were widely variable throughout the day in CR mice, exhibiting 51- and 16-fold differences, respectively, between 6 PM and 9 PM (0.05 vs 2.55 RU and 0.09 vs 1.44 RU, respectively; Fig. 6A & B). In contrast, the expression of these genes varied little in AL controls over the same time period (1.00 vs 0.87 and 1.00 vs 0.72 RU; Fig. 6A & B). SREBP-1 followed a similar, but less dramatic, pattern between 6 PM and 9 PM in livers of CR mice (0.42 vs. 1.46 RU, respectively; Fig. 6C), and again, there was very little change in control values (1.00 vs 0.97 RU). There was a trend for decreased PPARY expression in CR livers at all time points (Fig. 6D).

In the adipose tissue, FAS and ACC1 expression were 4 and 3-fold higher, respectively, in CR than AL mice at 6 PM (3.97 vs 1.00 RU; 2.92 vs 1.00 RU; Fig. 7A & B), and this difference was maintained throughout the day. While there was no difference in SREBP-1 expression in adipose tissue of CR mice at 6 PM, there was a 2-fold increase at 9 PM (2.02 vs 1.03 RU; Fig. 7C). There was no difference in PPARY expression in the adipose between CR and AL mice at any time point (Fig. 7D).

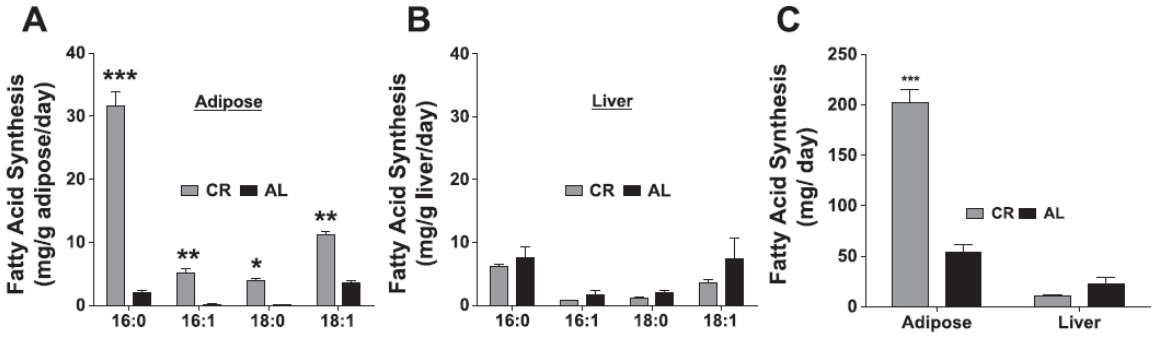


**Figure 4. Effect of CR on FA synthesis in adipose tissue and liver.** Daily FA synthesis was calculated for the 4 most abundant fatty acids: palmitate (16:0), palmitoleate (16:1), stearate (18:0) and oleate (18:1) in the subcutaneous adipose depot (A) and the liver (B) in CR and AL mice, values are expressed as milligrams per gram of tissue. Total adipose and liver FA that was synthesized during the period of $^2H_2O$ exposure and remained in the tissue was calculated from values in (A) and (B) and adjusted for estimated whole-body fat mass (as described in "Methods") and measured liver weights, respectively (C). Values are means ± SEM (n=8-14 mice per dietary group). ***P<0.001, **P<0.01, *P<0.05 difference from AL values, by ANOVA and Bonferroni *post hoc* test.

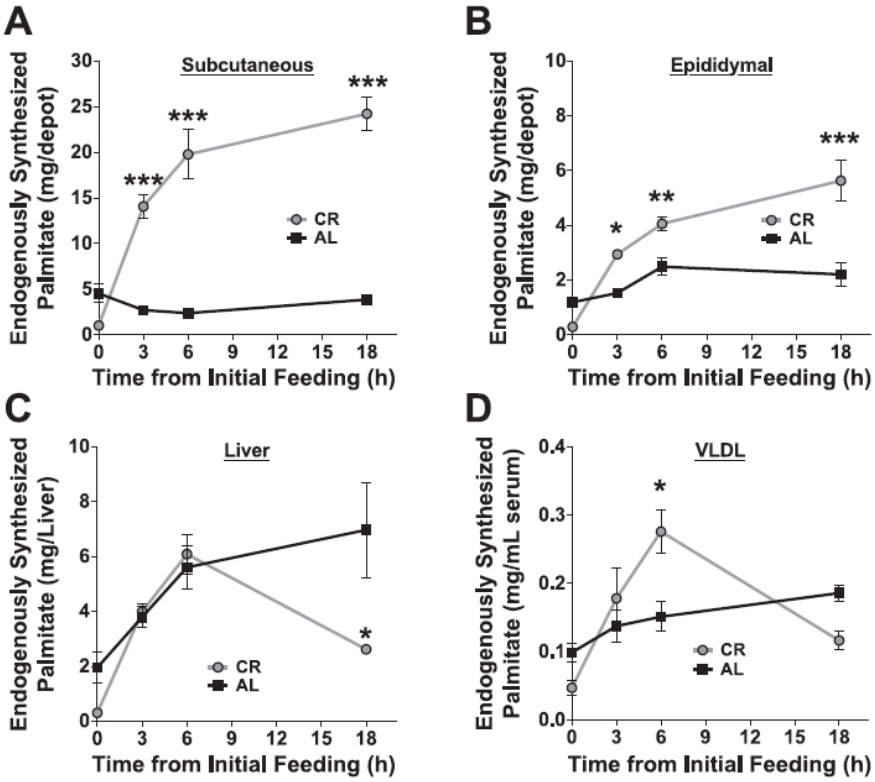


**Figure 5. Endogenous synthesis of palmitate in various tissues throughout the day.** Mice were labeled with $^2H_2O$ at 12 PM and tissues were collected and endogenous palmitate synthesis was calculated at various times after provision of daily food: 6 PM (0h), 9 PM (3h), 12 AM (6h) and 12 PM (18h) in subcutaneos (A) and epididymal (B) adipose depots and in liver (C). Endogenously synthesized palmitate was also calculated in plasma VLDL at 6 PM, 9 PM, 12 AM and 12 PM in the same mice (D). Values represent palmitate synthesis in the total subcutaneous and epididymal depots as well as in the total liver. Palmitate synthesis in VLDL is expressed per milliliter of serum. Values are means ± SEM (n= 6 mice per dietary group). ***P<0.001, **P<0.01, *P<0.05 difference from AL values, by ANOVA and Bonferroni *post hoc* test. ↓ indicates time when daily food was provided to CR mice.

### Serum Palmitoleate Leves in Mice

It has recently been suggested that increased rates of FA synthesis in adipose tissue result in a particular accumulation of palmitoleate, which is an insulin sensitizing FA (5, 11), in adipose tissue as well as in serum (5, 19, 20, 32, 42, 43). To determine if there was an increase in palmitoleate accumulation in our CR mice, we used gas chromatography coupled to flame ionization detection to measure FA composition in the inguinal and epidymal adipose depots and in the liver. We found a significant increase in palmitate concentration in both adipose depots, but no increase in palmitoleate concentration in adipose tissue or the liver (Table 1).

### Serum lipids in CR mice

To determine if changes in serum lipids reflect the pattern of feeding and fasting in CR mice, we measured serum NEFA and TG in CR and AL mice at 6 PM, before food was provided to CR mice, and 9 PM, 3h after food was provided. We found a significant increase in serum NEFA of CR

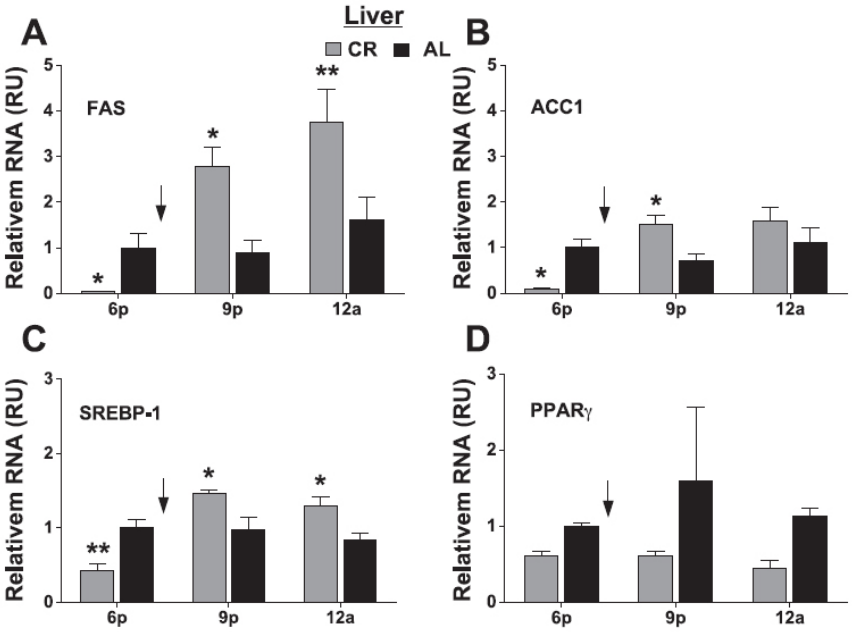


**Figure 6. Effect of CR on lipogenic gene expression in liver.** FAS (A), ACC1 (B), SREBP-1 (C) and PPARγ (D) gene expression was measured in the liver of CR and AL mice at 6 PM, 9 PM or 12 AM. Expression was normalized first to both GAPDH and b2m and then these normalized values were averaged. Values are shown relative to AL values measured at 6 PM (Relative Units; RU). Values are means ± SEM (n=6 mice per dietary group). ***P<0.001, **P<0.01, *P<0.05 difference from time-matched AL values, by ANOVA and Bonferroni *post hoc* test. ↓ indicates time when daily food was provided to CR mice.

mice compared to AL mice at 6 PM (0.87 ± .10 vs 0.45 ± .02 mEq/L), but no difference at 9 PM. In contrast, for serum TG, we found a significant increase in CR mice at 9 PM (81.0 ± 3.8 vs 39.3 ± 1.9 mg/dL), but no difference at 6 PM. These data are consistent with a prolonged fasting period in CR mice until 6 PM when food was provided and then a rapid feeding phase immediately following.

## Discussion

The experiments presented here demonstrate that CR, administered by daily feeding, leads to a unique pattern of fuel selection in mice, characterized by a brief period of markedly increased endogenous FA synthesis in adipose tissue followed by a prolonged period of elevated whole body FA oxidation. This pattern is consistent with previous reports demonstrating diurnal changes in RER in calorie restricted rats (12, 28). Here we confirm these metabolic effects with indirect calorimetry, stable isotope labeling, FA composition and to some extent gene expression, and demonstrate that the pattern is induced rapidly and persists as long as the mouse remains calorie restricted.

The metabolic adaptations to CR described here have implications for current hypotheses about the mechanisms mediating the effects of CR. In addition, our data provide insight into a time dependence of experimental designs for studying genetic adaptations to CR.

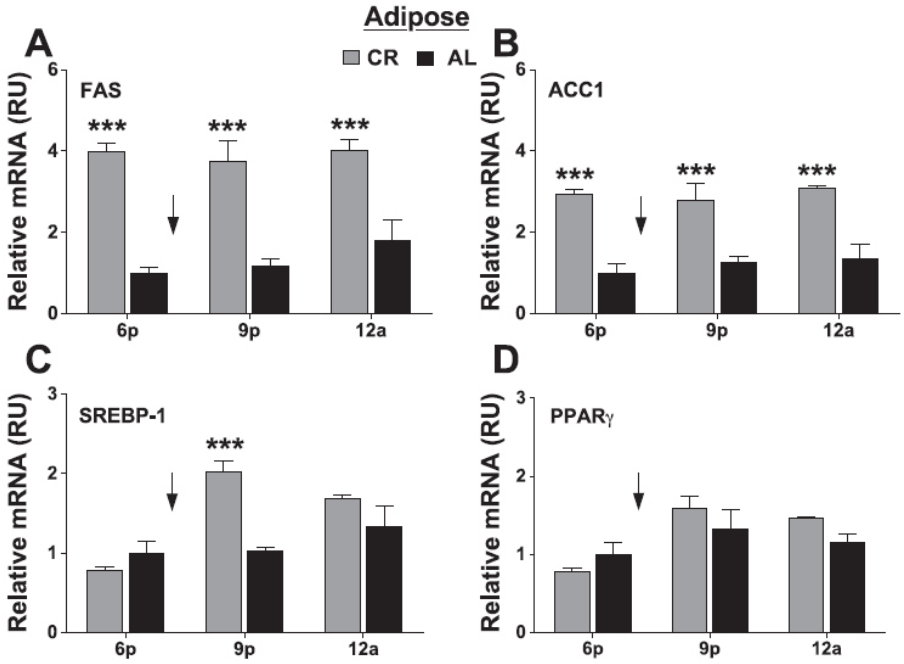


**Figure 7. Effect of CR on lipogenic gene expression in adipose tissue.** FAS (A), ACC1 (B), SREBP-1 (C) and PPARγ (D) gene expression was measured in the adipose tissue of CR and AL mice at 6 PM, 9 PM or 12 AM. Expression was normalized first to both GAPDH and b2m and then these normalized values were averaged. Values are shown relative to AL values measured at 6 PM (Relative Units; RU). Values are means ± SEM (n=6 mice per dietary group). ***P<0.001 difference from time-matched AL values, by ANOVA and Bonferroni *post hoc* test. ↓ indicates time when daily food was provided to CR mice.

The data confirm the view that the absolute amount of whole-body FA oxidation is higher in CR mice than AL controls (15, 23, 38). This is, in fact, a remarkable result, in context of classic principles of whole-body macronutrient balances (13, 44). After an initial 1-2 week period of weight loss, CR mice reestablish a state of energy balance in which fat mass is preserved or even increased. The energy intake from fat in CR mice is ~92 mg/day (2.3g food/day x 4% fat in diet by weight), yet we measured by indirect calorimetry 367mg fat oxidized/day in CR mice. The majority of fat oxidation occurred during the 12 hours after feeding when mice were oxidizing exclusively fat (RER= 0.7, Fig. 3). While there are limitations to estimating fat oxidation from indirect calorimetry (46), given that it only accounts for net changes, in this case, where RER values are 0.7 for so long, alternate interpretations are unlikely. Thus, the question remains, if CR mice oxidize a much greater quantity of FAs per day than dietary intake but remain weight stable, where does the FA substrate come from?

"Very nice," he whispers appreciatively, and my nipples harden even more. He blows very gently on one as his hand moves to my other breast, and his thumb slowly rolls the end of my nipple elongating it. I groan, feeling the sweet sensation all the way to my groin. He pinches me hard, and my body writhes

convulsively against his front. I gasp at the acute pleasure/pain. I feel him against me. I moan and my hands clench in his hair pulling harder. I moan loudly. He moves, pounding into me, a fast, intense pace against my sore behind. The feeling is beyond exquisite, raw and debasing and mind-blowing. He slides his leg in between mine, pushing my feet father apart, widening my stance, and runs my hands over my sex, one hand at a time in turn, setting up a rhythm. It's so erotic. Truly I am a marionette and he is the master puppeteer. I groan. Parting my legs, he cuffs first my right ankle and then my left so I am staked out, spread-eagled, and totally vulnerable to him.

He releases me and turns me around. "Hold on to the sink," he orders and pulls my hips back again, like he did in the playroom, so I'm bending down. He reaches between my legs and pulls on the blue string… what! And… a gently pulls my tampon out and tosses it into the nearby toilet. Holy fuck. Sweet mother of all… Jeez. And then he's inside me… ah! Skin against skin… moving slowly at first… easily, testing me, pushing me… oh my. I grip on to the sink, panting, forcing myself back on him, feeling him inside me. Oh the sweet agony… his hands clasp my hips. He sets a punishing rhythm – in, out, and he reaches around and finds my clitoris, massaging me… oh jeez. I can feel myself quicken.

"That's right, baby," he rasps as he grinds into me, angling his hips, and it's enough to send me flying, flying high. Whoa… and I come, loudly, gripping for dear life onto the sink as I spiral down through my orgasm, everything spinning and clenching at once. He follows, clasping me tightly, his front on my back as he climaxes and calls my name like it's a litany or a prayer. "Oh, Ana!" His breathing is ragged in my ear, in perfect synergy with mine. "Oh, baby, will I ever get enough of you?" he whispers. Will it always be like this? So overwhelming, so all-consuming, so bewildering and beguiling. I wanted to talk, but I'm crippled.

Quantitatively, we demonstrate that the increase in FA oxidation is almost entirely accounted for by an increase in endogenous FA synthesis in CR mice. Some previous reports had suggested that CR reduces endogenous FA synthesis, based on FAS and/or ACC1 expression in the liver (6, 7, 30, 38). Our stable isotope based measurements of flux through the FA synthetic pathway support the opposite conclusion. It should be noted that our calculations for endogenous FA synthesis are based on literature values for percent body fat in CR and AL from similarly aged and restricted C57BL/6 male mice. The literature values for percent body fat range from 15-30% for CR mice and 22-42% for AL mice. For a conservative estimate of FA synthesis in CR mice we used the lower value of 15%. For the estimation of AL FA synthesis we used the median value of 32%. In addition, any endogenously synthesized FAs that are oxidized rather than being stored in adipose tissue will not be detected by measurements on adipose tissue triglycerides. Thus, our measurements represent a lower bound estimate of FA synthesis in CR mice, yet accounted for the great majority of whole body FA oxidation in excess of dietary fat intake.

Adipose tissue, as opposed to the liver, may be the primary site for whole body endogenous FA synthesis in CR mice. Within three hours of feeding there was

an accumulation of 14mg of endogenously synthesized palmitate in the subcutaneous depot and another 3mg in the epididymal tissue. In contrast, only 4mg of endogenously synthesized palmitate accumulated in the liver over the same time period. In addition, in the first three hours post-feeding, endogenously synthesized palmitate accumulated in the subcutaneous depot five times faster in CR mice than AL controls, whereas in the liver and VLDL there was no difference in newly synthesized FA accumulation between these groups (Fig. 5C & D). It is possible, though quantitatively unlikely, that a dramatic increase in VLDL-TG delivery to adipose tissue in CR mice could account for the accumulation of endogenously synthesized fatty acids in this tissue. This possibility may warrant further investigation. Glucose is likely the predominant substrate for FA synthesis in the adipose tissue. Consistent with adipose playing a role in FA synthesis, Wetter et al. (45) demonstrated that glucose uptake is increased in adipose tissue of calorie restricted rats.

Several recent reports (5, 19, 20, 32, 42, 43) have proposed that palmitoleate (16:1) accumulates in adipose tissue or serum during times of increased FA synthesis, and that increased palmitoleate content is a marker of FA synthesis in adipose tissue. While we saw an increase in palmitate (16:0) content in adipose of CR mice, we did not observe an increase in palmitoleate content. Consistent with these data, the rate of palmitate synthesis was six times higher than the rate of palmitoleate in adipose tissue of CR mice (Fig. 4A). To our knowledge, this is the first report to compare palmitate and palmitoleate synthesis rates under conditions of increased FA synthesis. Palmitoleate accumulation does not appear to be a universal marker of endogenous FA synthesis. It is possible that the increase in palmitoleate accumulation observed in previous reports was specifically related to a change in diet, since animals were switched from a high fat diet to a high carbohydrate diet, which may alter SCD-1 activity (2, 8).

Liver FAS, ACC1 gene expression at a single time point did not necessarily reflect the expression pattern in CR mice throughout the day. This previously unreported circadian pattern may have implications for future genomic studies in CR mice. We observed that at 6 PM, just before food was provided, FAS and ACC1 expression were 20- & 10-fold lower in CR than AL mice (Fig. 6A & B). This is the same trend reported in several previous publications (6, 7, 30, 38) and has led to the conclusion that FA synthesis is decreased in CR. However, immediately after food was provided, FAS expression increased 50-fold in CR mice, leading to values nearly 3-fold higher than AL controls (Fig. 6A). In the same period, ACC1 expression increased 16-fold in CR mice, leading to values 2-fold higher than the AL group (Fig. 6B). This increase in FAS and ACC1 expression correlated with a relatively small, but statistically significant increase in FA synthesis in the livers of CR mice. Unfortunately, most studies investigating the changes in gene expression patterns in response to CR have measured expression at one time point, and in some cases animals were fasted overnight (6, 30), masking the time-dependent gene expression pattern. Furthermore, it is likely that the expression of other metabolic genes are influenced by this unique circadian

pattern. We believe that future studies into the physiologic, metabolic and genomic adaptations to CR must take into account this cyclical metabolic pattern.

A larger question is whether this diurnal fuel selection pattern plays a role in mediating the effects of CR on health and longevity. The pattern of food intake observed in response to CR is, in fact, a form of intermittent fasting. Other intermittent fasting protocols, most notably alternate day fasting, have been shown to slow tumor growth, decrease cell proliferation, improve insulin sensitivity and increase longevity, perhaps without a concomitant decrease in body weight (41). It should be noted that Nelson & Halberg (31) demonstrated that CR provided as six meals per day increased longevity to an equal extent as CR provided as one meal per day. Yet, it is possible that some of the effects of CR may be mediated by intermittent energy intake rather than or in addition to altered body composition.

One potential effect of CR that may be mediated by intermittent fasting is a reduced production of ROS. It has been hypothesized that an increased reliance on FA oxidation could lead to decreased ROS production, because FA oxidation increases the FADH/NADH ratio compared to carbohydrate oxidation (15). While NADH donates electrons to complex I of the electron transport chain, FADH donates electrons directly to complex II, the electron transfer flavoprotein dehydrogenase (ETF), which then passes the electrons to complex III via ubiquinone. FADH oxidation therefore bypasses complex I, which is a major contributor to cellular ROS production (21, 24). An interesting question for future research is whether effects of CR on ROS production depend upon the cyclic stimulation of FA synthesis.

In conclusion, we have characterized a unique feeding and macronutrient metabolic pattern in CR mice associated with a dramatic increase in whole body FA oxidation and a marked increase in adipose tissue FA synthesis. This pattern is rapidly induced, influences the daily pattern of gene expression, and may provide a metabolic switch that translates the dietary changes of CR into a program of health and survival.

**Acknowledgements**

The authors would like to thank Richard Neese, Mark Fitch, Simply Floracruz, Robby Pixton, Alicia White and DJ Rhook for their outstanding technical support. We would also like to thank Larry Thompson for his amazing commitment and help. The authors have no conflicts of interest to report.

## Literature Cited


1. Anderson RM, Shanmuganayagam D, and Weindruch R. Caloric restriction and aging: studies in mice and monkeys. *Toxicol Pathol* 37: 47-51, 2009.
2. Bassilian S, Ahmed S, Lim SK, Boros LG, Mao CS, and Lee WN. Loss of regulation of lipogenesis in the Zucker diabetic rat. II. Changes in stearate and oleate synthesis. *Am J Physiol Endocrinol Metab* 282: E507-513, 2002.
3. Berrigan D, Lavigne JA, Perkins SN, Nagy TR, Barrett JC, and Hursting SD. Phenotypic effects of calorie restriction and insulin-like growth factor-1 treatment on body composition and bone mineral density of C57BL/6 mice: implications for cancer prevention. *In Vivo* 19: 667-674, 2005.
4. Brochmann EJ, Duarte ME, Zaidi HA, and Murray SS. Effects of dietary restriction on total body, femoral, and vertebral bone in SENCAR, C57BL/6, and DBA/2 mice. *Metabolism* 52: 1265-1273, 2003.
5. Cao H, Gerhold K, Mayers JR, Wiest MM, Watkins SM, and Hotamisligil GS. Identification of a lipokine, a lipid hormone linking adipose tissue to systemic metabolism. *Cell* 134: 933-944, 2008.
6. Cao SX, Dhahbi JM, Mote PL, and Spindler SR. Genomic profiling of short- and long-term caloric restriction effects in the liver of aging mice. *Proc Natl Acad Sci U S A* 98: 10630-10635, 2001.
7. Chen D, Bruno J, Easlon E, Lin SJ, Cheng HL, Alt FW, and Guarente L. Tissue-specific regulation of SIRT1 by calorie restriction. *Genes Dev* 22: 1753-1757, 2008.
8. Chong MF, Hodson L, Bickerton AS, Roberts R, Neville M, Karpe F, Frayn KN, and Fielding BA. Parallel activation of de novo lipogenesis and stearoyl-CoA desaturase activity after 3 d of high-carbohydrate feeding. *Am J Clin Nutr* 87: 817-823, 2008.
9. Colman RJ, Nam G, Huchthausen L, Mulligan JD, and Saupe KW. Energy restriction-induced changes in body composition are age specific in mice. *J Nutr* 137: 2247-2251, 2007.
10. Dhahbi JM, Kim HJ, Mote PL, Beaver RJ, and Spindler SR. Temporal linkage between the phenotypic and genomic responses to caloric restriction. *Proc Natl Acad Sci U S A* 101: 5524-5529, 2004.
11. Dimopoulos N, Watson M, Sakamoto K, and Hundal HS. Differential effects of palmitate and palmitoleate on insulin action and glucose utilization in rat L6 skeletal muscle cells. *Biochem J* 399: 473-481, 2006.
12. Duffy PH, Feuers RJ, Leakey JA, Nakamura K, Turturro A, and Hart RW. Effect of chronic caloric restriction on physiological variables related to energy metabolism in the male Fischer 344 rat. *Mech Ageing Dev* 48: 117-133, 1989.
13. Flatt JP. Body composition, respiratory quotient, and weight maintenance. *Am J Clin Nutr* 62: 1107S-1117S, 1995.
14. Gredilla R and Barja G. Minireview: the role of oxidative stress in relation to caloric restriction and longevity. *Endocrinology* 146: 3713-3717, 2005.
15. Guarente L. Mitochondria--a nexus for aging, calorie restriction, and sirtuins? *Cell* 132: 171-176, 2008.
16. Hamrick MW, Ding KH, Ponnala S, Ferrari SL, and Isales CM. Caloric restriction decreases cortical bone mass but spares trabecular bone in the mouse skeleton: implications for the regulation of bone mass by body weight. *J Bone Miner Res* 23: 870-878, 2008.
17. Heilbronn LK and Ravussin E. Calorie restriction and aging: review of the literature and implications for studies in humans. *Am J Clin Nutr* 78: 361-369, 2003.

18. Hong J, Stubbins RE, Smith RR, Harvey AE, and Nunez NP. Differential susceptibility to obesity between male, female and ovariectomized female mice. *Nutr J* 8: 11, 2009.
19. Kunesova M, Braunerova R, Hlavaty P, Tvrzicka E, Stankova B, Skrha J, Hilgertova J, Hill M, Kopecky J, Wagenknecht M, Hainer V, Matoulek M, Parizkova J, Zak A, and Svacina S. The influence of n-3 polyunsaturated fatty acids and very low calorie diet during a short-term weight reducing regimen on weight loss and serum fatty acid composition in severely obese women. *Physiol Res* 55: 63-72, 2006.
20. Kunesova M, Hainer V, Tvrzicka E, Phinney SD, Stich V, Parizkova J, Zak A, and Stunkard AJ. Assessment of dietary and genetic factors influencing serum and adipose fatty acid composition in obese female identical twins. *Lipids* 37: 27-32, 2002.
21. Kushnareva Y, Murphy AN, and Andreyev A. Complex I-mediated reactive oxygen species generation: modulation by cytochrome c and NAD(P)+ oxidation-reduction state. *Biochem J* 368: 545-553, 2002.
22. Lee WN, Bassilian S, Guo Z, Schoeller D, Edmond J, Bergner EA, and Byerley LO. Measurement of fractional lipid synthesis using deuterated water (2H2O) and mass isotopomer analysis. *Am J Physiol* 266: E372-383, 1994.
23. Lopez-Lluch G, Irusta PM, Navas P, and de Cabo R. Mitochondrial biogenesis and healthy aging. *Exp Gerontol* 43: 813-819, 2008.
24. Lopez-Torres M, Gredilla R, Sanz A, and Barja G. Influence of aging and long-term caloric restriction on oxygen radical generation and oxidative DNA damage in rat liver mitochondria. *Free Radic Biol Med* 32: 882-889, 2002.
25. Lusk G. Analysis of the oxidation of mixtures of carbohydrate and fat: A Correction. *J Biol Chem* 59: 2, 1924.
26. Mai V, Colbert LH, Berrigan D, Perkins SN, Pfeiffer R, Lavigne JA, Lanza E, Haines DC, Schatzkin A, and Hursting SD. Calorie restriction and diet composition modulate spontaneous intestinal tumorigenesis in Apc(Min) mice through different mechanisms. *Cancer Res* 63: 1752-1755, 2003.
27. Masoro EJ. Caloric restriction and aging: an update. *Exp Gerontol* 35: 299-305, 2000.
28. Masoro EJ, McCarter RJ, Katz MS, and McMahan CA. Dietary restriction alters characteristics of glucose fuel use. *J Gerontol* 47: B202-208, 1992.
29. Merry BJ. Molecular mechanisms linking calorie restriction and longevity. *Int J Biochem Cell Biol* 34: 1340-1354, 2002.
30. Mulligan JD, Stewart AM, and Saupe KW. Downregulation of plasma insulin levels and hepatic PPARgamma expression during the first week of caloric restriction in mice. *Exp Gerontol* 43: 146-153, 2008.
31. Nelson W and Halberg F. Meal-timing, circadian rhythms and life span of mice. *J Nutr* 116: 2244-2253, 1986.
32. Parks EJ, Skokan LE, Timlin MT, and Dingfelder CS. Dietary sugars stimulate fatty acid synthesis in adults. *J Nutr* 138: 1039-1046, 2008.
33. Schutz Y. Concept of fat balance in human obesity revisited with particular reference to de novo lipogenesis. *Int J Obes Relat Metab Disord* 28 Suppl 4: S3-S11, 2004.
34. Sinclair DA. Toward a unified theory of caloric restriction and longevity regulation. *Mech Ageing Dev* 126: 987-1002, 2005.
35. Sohal RS and Weindruch R. Oxidative stress, caloric restriction, and aging. *Science* 273: 59-63, 1996.
36. Spindler SR and Dhahbi JM. Conserved and tissue-specific genic and physiologic responses to caloric restriction and altered IGFI signaling in mitotic and

postmitotic tissues. *Annu Rev Nutr* 27: 193-217, 2007.
37. Strawford A, Antelo F, Christiansen M, and Hellerstein MK. Adipose tissue triglyceride turnover, de novo lipogenesis, and cell proliferation in humans measured with 2H2O. *Am J Physiol Endocrinol Metab* 286: E577-588, 2004.
38. Tsuchiya T, Dhahbi JM, Cui X, Mote PL, Bartke A, and Spindler SR. Additive regulation of hepatic gene expression by dwarfism and caloric restriction. *Physiol Genomics* 17: 307-315, 2004.
39. Turner SM, Murphy EJ, Neese RA, Antelo F, Thomas T, Agarwal A, Go C, and Hellerstein MK. Measurement of TG synthesis and turnover in vivo by 2H2O incorporation into the glycerol moiety and application of MIDA. *Am J Physiol Endocrinol Metab* 285: E790-803, 2003.
40. Varady KA, Allister CA, Roohk DJ, and Hellerstein MK. Improvements in body fat distribution and circulating adiponectin by alternate-day fasting versus calorie restriction. *J Nutr Biochem*, 2009.
41. Varady KA and Hellerstein MK. Alternate-day fasting and chronic disease prevention: a review of human and animal trials. *Am J Clin Nutr* 86: 7-13, 2007.
42. Volek JS, Phinney SD, Forsythe CE, Quann EE, Wood RJ, Puglisi MJ, Kraemer WJ, Bibus DM, Fernandez ML, and Feinman RD. Carbohydrate restriction has a more favorable impact on the metabolic syndrome than a low fat diet. *Lipids* 44: 297-309, 2009.
43. Watkins SM, Reifsnyder PR, Pan HJ, German JB, and Leiter EH. Lipid metabolome-wide effects of the PPARgamma agonist rosiglitazone. *J Lipid Res* 43: 1809-1817, 2002.
44. Westerterp KR. Food quotient, respiratory quotient, and energy balance. *Am J Clin Nutr* 57: 759S-764S; discussion 764S-765S, 1993.
45. Wetter TJ, Gazdag AC, Dean DJ, and Cartee GD. Effect of calorie restriction on in vivo glucose metabolism by individual tissues in rats. *Am J Physiol* 276: E728-738, 1999.
46. Wolfe RR. *Isotope Tracers in Metabolic Research*: Wiley & Sons, 2005.

# Section 2

## The Transcriptomic and Proteomic Basis of Islet Cell Proliferation and Failure in Type 2 Diabetes

## Review of the Literature

Type 2 diabetes (T2D) is a condition of increasing global prevalence, which affected an estimated 150 million people worldwide in the year 2000, and is estimated to grow to 300 million individuals by the year 2025 [1]. In the United States alone, 25.8 million adults and children suffer from T2D, comprising 8.3% of the population. Contributing to this population are 79 million prediabetic individuals, diagnosed at a staggering rate of 1.9 million cases per year. According to current estimates, the total number of diabetic patients in the United States will nearly double, to 44.1 million adults by 2034 [2,3]. In 2007, the total cost of diabetes in the United States was $218 billion, with a 2.3 times higher medical care cost per individual in comparison with nondiabetics [4]. According to conservative estimates, annual diabetes related spending is expected to increase to $336 billion by 2034, adding a significant strain to the already overburdened health care system [3].

While diabetes *per se* does not increase the risk of death, peripheral organ damage that occurs in response to fluctuating blood glucose levels presents increased risk for the development of cardiovascular disease (CVD), high blood pressure, retinopathy, nephropathy, neuropathy, macular degeneration, hypercholesterolemia, blindness, limb amputation, and atherosclerosis [4,5]. The risk for stroke in adults with diabetes is 2-4 times that of healthy individuals, reflected by a 2-4 times increase in the death rate of diabetics due to CVD. More than two-thirds of diabetics are hypertensive or use hypertensive medication to control elevated blood pressure. In addition, diabetes is the leading cause of blindness among all adults, and accounted for nearly 50% of kidney failures in 2008. More than 60-70% of diabetics in the United States suffer from mild to severe neuropathy, partially accounting for 60% of all lower-limb amputations [4].

### The Relationship Between Obesity and Type 2 Diabetes

Following World War II obesity rates have grown exponentially, and now more than 50 years after the start of the "gastronomic revolution," 35% of Americans are obese [6], 65% are overweight, and 40% suffer from the metabolic syndrome [7]. While there is no international definition of the metabolic syndrome, this condition is a cluster of increasingly prevalent metabolic

dysfunctions, including (a) impaired glucose tolerance (IGT), or T2D, (b) hypertension, (c) hypertriglyeridemia, (d) low HDL cholesterol, and (e) central obesity. Within 20 years an estimated 100 million Americans will have the metabolic syndrome [8,9].

To say that obesity is associated with the development of T2D underestimates the impact of adiposity on adverse glucose metabolism. In fact, obesity is now classified as *the most important determinant* of insulin resistance (IR) and is the single most important risk factor for T2D and the metabolic syndrome [10]. In the human population, overweight is defined as having a body mass index (BMI, the ratio of weight (kg) to the square of height ($m^2$)) between 25-30, and obesity is defined as having a BMI greater than 30. There are now more overweight individuals than underweight individuals worldwide [11].

As shown in Figure 1, in 1985, the highest proportion of obese individuals per state was 10-14%, and was prevalent in a total of 8 states. By 2010, the picture had changed dramatically as the number of obese individuals increased significantly; *every state* had a prevalence of obesity greater than 20%. More specifically, thirty-six states had an obesity prevalence of 25% or more, and 12 states had an obesity prevalence of 30% or more [12].

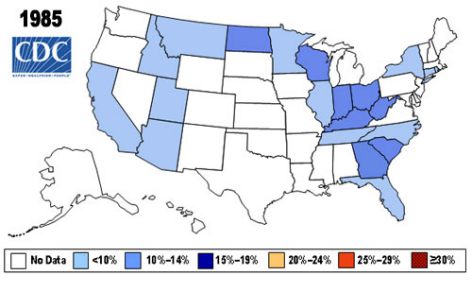


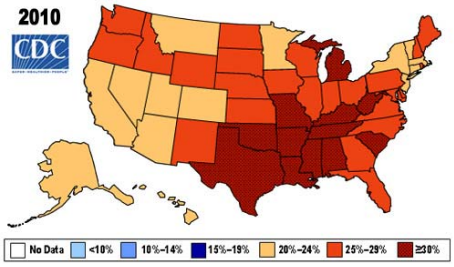


**Figure 1. Obesity Pevalence in the United States between 1985 and 2010.** In the past quarter century, the prevalence of obese individuals in the United States has more than tripled. A geographical representation of the proportion of obese individuals by state is shown for 1985 (left) and 2010 (right).

While obesity increases the risk for developing T2D, not all obese individuals are diabetic, arguing against a causal relationship between the two conditions. Interestingly, a subset of obese individuals exhibit classic symptoms of IR while remaining resistant to the development of T2D despite prominent central adiposity. While the exact mechanism that protects these individuals from diabetes is unknown, both mouse and rat models of obesity, IR, and T2D are commonly used to investigate the molecular basis of the response of pancreatic islets to obesity.

Obesity is a multi-factorial disease of dysregulated energy metabolism that results from genetic, lifestyle and psycosocial factors. In obese animals and humans, excessive weight gain is the result of an imbalance between energy intake and energy expenditure. The physiological mechanisms underlying energy imbalance are numerous, and differ between individuals, cultures, and geographical location. Environmental factors contributing to the obesity epidemic include insufficient energy expenditure, excess caloric intake, and

excess dietary lipid. These lifestyle determinants of obesity have been well classified, however the interaction between lifestyle and genetic makeup differs between individuals, increasing the importance of understanding the genetic basis of this complicated metabolic disorder.

Support for the genetic basis of obesity originally came from a study conducted on overfed monozygotic twins. The results of inducing positive energy balance in many pairs of twins indicated that the tendency for weight gain between twins was remarkably similar, while the degree of weight gain between sets of twins varied widely [13]. Similarly, studies on human subpopulations show that the risk for developing obesity and obesity-related disorders is in part determined by genetic factors. Studies on Pima Indians clearly show accelerated risk for the development of obesity, due to reduced basal metabolic rate and not to sedentary behavioral factors alone [14].

In the mid-1990s, leptin was discovered as an adipocyte-derived hormone that controlled central feeding behavior in proportion to the size of peripheral fat stores. Leptin deficiency was soon discovered to play a major role in the central control of energy intake, and paramount studies in obese (ob/ob) and diabetic (db/db) mice demonstrated that mutations in both the leptin gene and its cognate receptor in the brain have significant negative impacts on energy metabolism, increasing the risk for the development of obesity and diabetes [15–18]. In some humans and rodents however, obesity persists despite high levels of circulating leptin, creating a state of "leptin resistance" which is not affected by the administration of additional exogenous leptin. Evolutionarily, leptin resistance may have been selected for due to an increased ability to store energy in times of feast [6].

In addition, extensive research on uncoupling proteins (UCPs), inner mitochondrial membrane proton-leak proteins that specifically uncouple the generation of a proton gradient from the production of ATP, has shown that these proteins promote adaptive thermogenesis primarily in brown adipose tissue (BAT) and skeletal muscle [19–23]. Conflicting research has led to the conclusion that none of the UCPs alone can singlehandedly fight against the development of obesity, but that specific combinatorial expression patterns across many tissues can have a significant effect on ameliorating dysregulated energy balance [6]. Further studies identified many genes as playing a causative role in the development of obesity, including ADD/SREBP1 [24,25], as well as PGC-1a and PPAR-alpha [26].

## The Pathogenesis of Type 2 Diabetes

Type 2 diabetes is characterized by two principal mechanisms: (a) IR and (b) islet failure (IF); the failure of the islets of Langerhans in the pancreas to adequately secrete insulin in response to elevations in blood glucose levels. Maintenance of islet cell mass and function over the lifetime of an organism therefore protects against the development of T2D, and nutritional and therapeutic interventions to maintain normal islet cell function are therefore of great interest.

## Islet Cell Morphology

Islet cells are clusters of endocrine cells in the pancreas with a highly specialized role

in regulating insulin secretion in response to nutrient intake. The term *islet cell* refers to a cluster of pancreatic tissue containing between 400-4000 cells [27] whose primary metabolic activity is the secretion of insulin in response to increases in circulating glucose (glucose-stimulated insulin secretion, GSIS). Islet cells are a heterogeneous collection of cell types, containing about 15-20% alpha cells (glucagon producing), 65%-80% beta cells (insulin producing), 5-10% delta cells (somatostatin producing), 3-5% PP cells (pancreatic polypeptide producing), and <1% epsilon cells (grehlin producing) in rats [28–30]. Each of these secreted peptide hormones affect glucose homeostasis independently, and have either direct or indirect actions on the promotion of insulin secretion or the inhibition of insulin secretion [31].

Glucagon is a peptide hormone whose action indirectly opposes that of insulin. Glucagon is released by the alpha cells in response to hypoglycemic conditions, and signals for an increase in hepatic glucose production (HGP) by the liver via the breakdown of stored glycogen. Increased HGP results in a transient increase in blood glucose values. Thus, glucagon and insulin play opposing yet coordinated roles in regulating blood glucose concentrations. Somatostatin is a peptide hormone released by the delta cells, and functions to reduce smooth muscle contractions and blood flow in the intestine, slow the rate of gastric emptying, suppress the release of insulin from the beta cells, inhibit the release of glucagon from the alpha cells, and suppress the secretory action of the exocrine pancreas [32]. Figure 2 shows a visual schematic and immunohistochemical distribution of islet cell types.

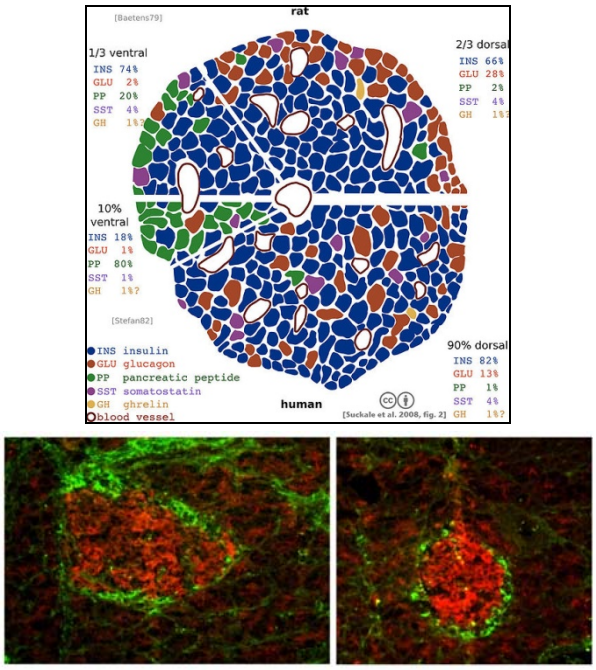


**Figure 2. Distribution of Cell Types in the Islet Cell.** Top panel: schematic representation of the distribution of alpha, beta, delta, PP, and epsilon cell types in rat (above) and human (below) islets. Image adapted from [30]. Bottom panels: immunohistochemical staining of rat islets, stained for glucagon (alpha cell, green) and insulin (beta cell, red). Glucagon-positive cells are distributed towards the periphery of the islet cell, whereas insulin-positive cells cluster towards the core of the islet cell.

The regulation of GSIS is the primary metabolic role of the beta cells. In response to an increase in systemic blood glucose concentrations, the flux of glucose into the beta cell is facilitated by GLUT2 transporters at the plasma membrane. Intracellular metabolism of glucose via the glycolytic pathway results in an increase in ATP concentrations, and a coordinate decrease in ADP. ATP-sensitive potassium channels embedded

in the membrane close in response to increased ATP availability, decreasing the permeability of the cell to potassium ($K^+$). In response to channel closure, the membrane undergoes depolarization, causing the opening of voltage-gated calcium ($Ca^{2+}$) channels and a subsequent influx of extracellular $Ca^{2+}$. Cytosolic vesicles containing insulin located adjacent to the plasma membrane then fuse with the plasma membrane in response to increased $Ca^{2+}$, resulting in a pulsatile exocytosis of insulin [33–39].

### Peripheral Insulin Resistance

In humans and in rodents, IR often proceeds islet failure. IR is a condition characterized by reduced insulin action predominantly in skeletal muscle and liver, which in turn increases the demand for insulin production by islet cells [40].

There are numerous causes underlying the development of IR, and in humans this condition can precede the onset of frank diabetes by 10-20 years. In peripheral tissues including skeletal muscle, adipose, and liver, the accumulation of ectopic lipid has been shown to reduce glucose disposal and increase the prevalence of IR [9,41].

Randle et al. were the first to postulate a mechanism by which fatty acid exposure impairs insulin-stimulated glucose oxidation in muscle tissue [42]. According to the Randle Hypothesis, as it became known, glycolytic enzymes are inhibited by alterations in cellular metabolism that result from fatty acid oxidation. First, the oxidation of fatty acids results in an increase in both the ratio of mitochondrial NADH/NAD+ and the ratio of mitochondrial Acetyl-CoA/CoA, directly inhibiting pyruvate dehydrogenase located at the inner mitochondrial membrane. In parallel, increases in cytosolic citrate resulting from increased fatty acid oxidation inhibits phosphofructokinase-1 (PFK-1), increasing intracellular glucose-6-phosphate (G6P), in turn inhibiting the activity of hexokinase at the plasma membrane. In effect, this theory provides a mechanism by which the oxidation of fatty acids directly reduces glycolytic flux and subsequently impairs glucose uptake in muscle tissue.

Continued research in uncovering the mechanism of lipid-induced IR has resulted in a new hypothesis that has gained significant support in the IR community. According to this theory, the accumulation of muscular fatty acids reduces the ability of insulin receptor substrate-1 (IRS-1) to stimulate phosphatidylinositol 3-kinase (PI3 kinase), reducing the net activation of glucose transport 4 (GLUT4) proteins to the plasma membrane to promote insulin-stimulated glucose uptake. Intramuscular fatty acids also activate a serine kinase signaling cascade in which the theta subunit of protein kinase C (PKC-theta) and the inhibitor of nuclear factor kappa-B kinase subunit *beta* (IKK-beta) stimulate a local inflammatory response, and impair insulin-stimulated muscle glycogen synthesis [11,41].

The careful work of Kelley and Goodpaster et al. in humans has uncovered interesting findings relating skeletal muscle lipid content and the development of IR, and has recently uncovered a paradox in endurance-trained athletes. Ectopic storage of lipid in skeletal muscle is associated with IR in the settings of obesity [43–47], and T2D [48,49] in human subjects. Animal models of

obesity and T2D also support this hypothesis [50–52]. Importantly, the storage of lipid intracellularly may differ from the storage of lipid in muscle-resident adipocytes, however experimental techniques to study this pool of lipids have proven technically challenging. Recent studies using magnetic resonance spectroscopy (MRS) have found that intramyocellular lipid (IMCL) promotes IR in obese and T2D subjects, but does not impair insulin sensitivity in endurance trained athletes [53].

The effects of insulin resistance on skeletal muscle fatty acid oxidation and mitochondrial metabolism are numerous. To address the effect of fatty acid availability on skeletal muscle mitochondrial metabolism, one must consider two important variables: (a) the development of IR, and (b) mitochondrial mass. Conflicting results from many research groups have led to a somewhat contradictory state of affairs, namely that high fat diets cause IR and either stimulate or impair muscle mitochondrial metabolism.

The connection between IR and mitochondrial metabolism is a classic chicken-and-egg story. Two important questions predominate:

***Question 1:***

*Do mitochondrial defects precede the onset of T2D and thus play a role in the development of T2D?*

***Question 2:***

*Is mitochondrial dysfunction a consequence of T2D?*

Kelley et al. showed that mitochondrial oxidative capacity is decreased in skeletal muscle of obese individuals and is highly correlated with IR [54]. In addition, they showed that obese and type 2 diabetic individuals show a reduction in the density of subsarcolemmal mitochondria independent of alterations to intermyofibrillar mitochondria [54]. Subsarcolemmal mitochondria are located adjacent to the sarcolemma and play a role in signal transduction, ion exchange, substrate transport – all processes which are relevant to insulin action [55]. However, in order to determine whether defects in mitochondrial metabolism are a cause or effect of IR, many groups devised experiments to determine the effect of increased fatty acid availability on mitochondrial structure and function.

Turner et al. showed that excess lipid availability increases mitochondrial fatty acid oxidative capacity in skeletal muscle, as evidenced by increased activity of beta-HAD, MCAD, CPT1, and citrate synthase. In addition, they found that high fat diets increased the protein expression of PGC-1a, and UCP3. They argue that the increased capacity for fatty acid oxidation is merely a compensatory mechanism to protect against the storage of fatty acids in muscle tissue, and instead promote increased oxidation due to increased circulating fatty acid supply [40]. This finding was supported by two other papers from the research group of John Holloszy. They found that raising circulating fatty acid concentrations by high fat feeding or by daily heparin infusions resulted in augmented mitochondrial function, including increased protein expression of MCAD, LCAD and VLCAD, and mitochondrial DNA copy number. In addition, they found that elevations in circulating fatty acid concentrations induced insulin resistance, as supported by both the

Randle Theory and the protein kinase C theory, arguing against the fact that insulin resistance causes defects in muscle mitochondrial metabolism. Instead, this body of work supports the idea that increased fatty acid availability due to high fat feeding results in a macronutrient "switch," from a glucose-centric to a lipid-centric economy, despite the development of IR.

In direct contradiction, Kelley et al. found that IR and elevated skeletal muscle lipid content lowers the oxidative capacity of skeletal muscle for fatty acid oxidation [56–58]. In these studies, it was found that the deposition of ectopic lipid in skeletal muscle results in IR, and impairs mitochondrial function, opposing the findings of Turner, Hancock and Garcia-Roves. They further demonstrated that in the insulin resistant state, weight loss reduces IMCL and improves skeletal muscle insulin action, but does not stimulate mitochondrial biogenesis independent of increased physical activity [59,60]. Together, these studies set the stage for conflicting viewpoints on the effects of IR on mitochondrial metabolism.

## Treatment of Insulin Resistance Via Diet and Exercise

In both rodents and humans, insulin resistance can be treated by lifestyle interventions, including increased energy expenditure via exercise [5,61–65], reduced lipid intake [10,66], and calorie restriction (CR) [67–76]. Impaired islet cell function can be reversible, particularly at early stages of the disease process before an intangible and highly individual threshold has been crossed, preventing the return to normal GSIS [77].

Exercise stimulates increased mitochondrial substrate oxidation in muscle tissue, increasing basal fatty acid oxidation rates [47,78–81], and enhances glucose disposal and insulin sensitivity [82–85]. Exercise training is considered the gold standard for maintaining insulin sensitivity, yet the sedentary proportion of the American population is increasing with time. According to a recent review article citing potential causes of T2D, Unger and Scherer stated:

*The 16-h of daily physical activity, previously allocated for productive human activities, have been drastically reduced or eliminated by technologies that require virtually no muscular contraction. This has created an unprecedented challenge for maintenance of metabolic homeostasis, for which no defense has had time to evolve* [9].

Figure 3 shows a county-level map of the age-adjusted estimates of the percentage of adults over 20 years old who were physically inactive in 2008. These data indicate that in more than 25 states, 20% or more of the population was considered sedentary [86].

The overconsumption of dietary fat results in a sustained deposition of fatty acids in adipose tissue. After the storage capacity of the adipose tissue has reached a physiological maximum, ectopic lipid accumulation begins. The consequences of ectopic lipid storage depend on the ability of extra-adipose tissues such as the skeletal muscle and liver to store excess fat as a neutral lipid. Excess lipid accumulation in these peripheral tissues beyond storage capacity results in impaired tissue function and the production of inflammatory cytokines, a condition known as lipotoxicity. Reduction of lipid intake may reverse

ectopic lipid deposition, restoring normal metabolic function to lipotoxic tissues [9].

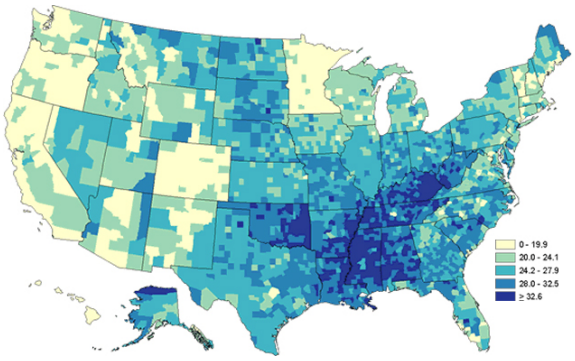


**Figure 3. Age-Adjusted Estimates for the Percentage of Inactive Adults.** The percentage of sedentary individuals in 2008 is represented by on the county level. States with the highest inactive proportion of the population include Oklahoma, Arkansas, Louisiana, Alabama, Mississippi, Tennessee, and Kentucky, and states with the lowest proportion of inactivity include Minnesota, Colorado, Oregon and Hawaii.

In addition to the effect of reducing total lipid intake, substitution of saturated dietary fat with both omega-3 and omega-6 unsaturated fatty acids has been shown to improve insulin sensitivity [87,88]. Calorie restriction (CR) results in reduced total body adiposity, reduced ectopic lipid accumulation, altered mitochondrial fatty acid oxidation, and reduces inflammation in white adipose tissue [89], together resulting in significant improvements in glucose tolerance and insulin sensitivity [90,91].

## Pharmacological Interventions

Antidiabetic drugs have become increasingly prevalent in western society, and function to improve dysregulated glucose homeostasis via a number of different mechanisms. Each medication is designed to function independently of changes in diet (energy intake) and exercise (energy expenditure).

The most commonly prescribed antidiabetic medication is Metformin (Glucophage, Riomet, Fortamet), and is recommended as the first-line oral therapy for T2D. Thousands of papers document the cellular and molecular effects of Metformin action, given its effectiveness in the clinical setting at reducing hyperglycemia. Metformin functions primarily via direct targeting of complex I in the respiratory chain of the liver, and secondarily through activation of the cellular low energy sensor AMP-activated protein kinase (AMPK). Together, these two pathways converge by reducing hepatic glucose production (HGP) primarily by inhibition of the gluconeogenic pathway, thereby reducing circulating glucose concentrations [92,93]. In addition, Metformin increases AMPK activation in muscle tissue, increasing the rate of glucose disposal and muscle glycogen content [94]. Sulfonylureas (Glucotrol, DiaBeta, Glynase, Micronase, Amaryl),and meglitinides (Starlix, Prandin)

It has been known for over 30 years that an oral glucose load increases insulin production over an intravenous glucose load due to the effects of neuro-hormonal incretin release from the intenstine in the presence of carbohydrates. Two of these incretins, glucagon-like peptide 1 (GLP-1) and glucose dependent insulinotrophic peptide (GIP), promote insulin secretion, and are therefore a focus of the pharmaceutical industry in developing new targets for the treatment of T2D. These “gliptin” drugs (Sitagliptin, Vidagliptin) are prescribed for human use, and result in a reduction of glycosylated

hemoglobin (HbA1c, a circulating marker of 3-month glycemia) by 0.5-1.1% [95–99].

Rosiglitazone and Pioglitazone are members of the thiazolidinedione (TZD) class of anti-diabetic compounds, and function as agonists of the peroxisomal proliferator-activated receptor gamma (PPAR-gamma) nuclear receptor superfamily of ligand-activated transcription factors. PPAR-gamma is widely expressed in many human and rodent tissues, including adipose, skeletal muscle, cardiac muscle, endothelium, kidney, pancreas and bone, and is expressed in the beta cells of both humans and rodents [100–103].

The insulin sensitizing action of rosiglitazone is mainly attributed to the activation of PPAR-gamma in peripheral tissues, yet recent *in vitro* and *in vivo* evidence suggest that TZDs may exert an effect on islet function and proliferation directly. In cultured primary rat islets and insulinomas, PPAR-gamma activation directly promotes the expression of Glut2 and glucokinase, and reduces cell proliferation in cancerous cultures of pancreatic acinar tissue [104–106]. In addition, treatment of prediabetic humans and rodents with PPAR-gamma agonists improves glucose-stimulated insulin secretion (GSIS), increases beta cell insulin content, inhibits islet cell apoptosis [77], and prevents against dysfunctions in islet architecture [107,108]. In prediabetic Zucker Diabetic Fatty rats (ZDF), a leptin receptor deficient obese, hyperglycemic and glucose intolerant rat model of T2D, PPAR-gamma activation protects against islet hyperplasia and necrosis, attenuates defects in GSIS, and prevents against the loss of beta cell mass by preventing an increase in net beta cell death [52,101,103,109–112]. *In vivo,* targeted knockout of murine beta cell PPAR-gamma blunts islet hyperplasia in response to high fat feeding [107]. In 2008, two large meta-analysis studies reported that the usage of glitazones (Rosiglitazone and Pioglitazone) increased the incidence of myocardial infarction by 40%. This greatly reduced the use of these antidiabetic agents, and as a result Rosiglitazone is now only available as a dual therapy with other medications, and is strongly unadvised in patients with ischaemic heart disease [113–115].

## Islet Cell Hyperplasia

In addition to the deleterious effects of IR on peripheral tissue, islet cells are known to acquire direct functional impairments resulting from abnormal glucose homeostasis. A fundamental question in the pathogenesis of T2D is the mechanism of islet failure due to prolonged periods of IR. The proliferation of islet cell mass due to IR is present in many animal models [116,117], and decreases in islet cell mass likely underlies islet cell failure [118–122]. Glucotoxicity, lipotoxicity, proinflammatory cytokines, and islet cell amyloid protein result in impaired GSIS, ultimately contributing to the development of islet failure [77]. Islet cell hyperplasia is driven primarily by chronic elevations in blood glucose, and is a compensatory mechanism to increase insulin production in an effort to reduce circulating glucose concentrations. In order to perform this, islet cells respond to IR by (a) transient increases in islet cell mass, and (b) increased insulin output.

Increased islet cell mass can occur via a number of mechanisms, which include replication of preexisting islet cells, neogenesis of islet cell precursors [123–125],

and inhibition of islet cell apoptosis [126]. It still remains unclear which of these mechanisms results in increased islet cell mass in response to IR, however the net effect results in 2-5-fold elevations in islet cell mass and insulin production [127]. In rodents, however, pre-existing terminally-differentiated islet cells have been shown to be the source of new islet cells, arguing against the hypothesis that neogenic differentiation of pluripotent stem cells significantly contributes to islet cell mass expansion in response to IR [128,129].

Many studies have investigated the physiological behavior of islet cells in order to identify genes and proteins underlying mass expansion. Three rat models are commonly used to investigate these effects: the Zucker Fatty (ZF), Zucker Diabetic Fatty (ZDF), and the Zucker Lean Control (ZLC) rat. ZF rats are an obese, hyperlipidemic, glucose intolerant, insulin resistant strain that demonstrate severe peripheral insulin resistance in skeletal muscle and reduced insulin-stimulated glucose disposal.

ZF rats are hyperphagic as compared with ZLC controls, yet they are resistant to hyperglycemia and the development of diabetes. Studies show that islet proliferation in ZF rats far exceeds those of ZLC rats in response to IR, suggesting that resistance to T2D originates from an ability to increase islet mass via either preexisting islet cell proliferation or by islet neogenesis [121,130–135].

The ZDF rat is obese, severely insulin resistant, and demonstrates islet cell hyperplasia prior to the onset of diabetes at eight to twelve weeks of age [136]. Studies have shown that ZDF rat islet failure occurs despite high rates of islet cell proliferation as compared with ZF rats, suggesting that a high rate of islet cell apoptosis is responsible for islet cell mass reduction and the transition to T2D [121].

ZLC rats are heterozygous for a mutation in the leptin receptor (fa/+), and are used as a lean control strain against which ZF and ZDF rat models are compared. ZLC rats are a non-obese, non-IR, non-diabetic model with the same genetic background as the obese ZF and ZDF phenotypes.

The length of time in which islet cell hyperproliferation can occur is strain dependent. In ZF rats, this physiological response to IR can last for long periods of time, protecting against islet failure. In ZDF rats, however, islet hyperproliferation is temporally programmed independent of interventions that delay the transition to T2D, including oral antidiabetic drugs and exercise. In our investigations, we used this temporal transition to diabetes to our advantage in designing experiments to study the genetic and proteomic mechanisms that may control the onset of T2D.

## Experimental Methods to Measure Islet Cell Hyperplasia

The most ubiquitously utilized method for measuring the rate of cell proliferation in many tissues is labeling with 5-bromodeoxyuridine (BrdU), a thymine analog that is readily incorporated into newly synthesized DNA and detected by immunofluoresence or flow cytometry [137–140]. Despite the ease of use of BrdU, this non-radioactive agent has cytotoxic effects and chronic exposure can affect the rate of cell proliferation independent of external influences [141]. Furthermore, BrdU administration depends on the usage of semiquantitative methods to determine the rate of cell proliferation.

We have developed a technique for measuring cell proliferation rates *in vivo*, based on non-toxic $^2H_2O$ labeling and mass spectrometric analysis, which has been applied to the measurement of the proliferation of numerous cell types in experimental animals and humans, including islet cell proliferation in rats [142,143]. This method is well suited for the measurement of cell proliferation in slow turnover tissues because $^2H_2O$ can be conveniently administered for long periods of time in drinking water, combined with the high sensitivity of mass spectrometric analysis of the deoxyribose (dR) moiety of DNA [144].

Studies from our laboratory were conducted to determine the basal turnover rate of islet cells in a healthy rat pancreas using $^2H_2O$ labeling. In this paper, Chen et al. found that BrdU administration suppressed islet cell proliferation, creating an experimental artifact that alters physiological islet cell proliferative dynamics that was detectable following only 7 days of labeling [143]. Others have observed the same effect in various tissues [141,145,146], supporting the use of $^2H_2O$ labeling for the measurement of cell proliferation in slow turnover tissues.

## Islet Cell Failure

In most cases, IR-induced compensatory insulin production over time results in the sudden and coordinated failure of islet cells, resulting in sharp reductions in islet cell mass, insulin secretory failure, and the transition to type 2 diabetes. Compensated IR is generally a finite process; the duration of time in which an animal can sustain insulin resistance before transitioning to diabetes is strain-dependent.

In mice, this strain-dependent physiology is evident when comparing ob/ob and db/db mice. Both strains exhibit classic symptoms of dysregulated lipidemia, including hypercholesterolemia, obesity, insulin resistance, hyperglycemia, and glucose intolerance. Ob/ob mice suffer from leptin deficiency, and are resistant to the development of diabetes, while leptin receptor-deficient db/db mice develop diabetes at an early age [147].

In rats, a similar difference in physiology exists between Zucker Fatty (ZF) rats, and ZDF rats. Similar to obese mouse models, the ZF and ZDF rat models are hyperlipidemic, hypercholesterolemic, obese, insulin resistant, hyperglycemic, and glucose intolerant. Leptin-deficient ZF rats are resistant to diabetes, and remain insulin resistant their entire life, while ZDF rats experience a temporally programmed transition to diabetes due to the failure of islet cell compensation [148,149].

In humans, the failure of islet cell compensation to IR also occurs, resulting in T2D. The temporal nature of islet cell compensation is highly individual, and dependent on lifestyle-related factors including genetic predisposition, diet, and exercise as discussed above [1].

## Gene Expression Profiles of Hyperplastic and Failed Islets

While hundreds to thousands of scientific papers have been written about the mechanisms underlying the pathogenesis of islet cell dysfunction in T2D, the underlying genetic mechanisms of islet cell hyperproliferation and failure remain elusive. The effects of hyperglycemia-induced islet proliferation and failure on the islet cell gene expression profile is an area of significant interest.

### *In Vitro* Islet Genomic Approaches

The first human islet genome was published in 2002 and investigated the effect of low and high concentrations of glucose on the gene expression of primary human islets. Hyperglycemic conditions increased the expression of Txnip, Iapp, and Pc1/Pc3. Two members of the TGF-beta superfamily were highly regulated by high glucose concentrations, including BMP5 and PDF [150].

In order to evaluate the effect of various glucose concentrations on key GSIS signaling pathway gene expression, Bensellam et al. performed a series of *in vitro* experiments followed by gene expression profiling using Affymetrix Rat 230 2.0 microarrays. Rat primary islets were incubated in either 2mM, 5mM, 10mM, or 30mM glucose concentrations in culture followed by hybridization of mRNA to gene chips and downstream expression analysis. They found a total of 40 differentially expressed genes, of which 16 were upregulated and 19 were downregulated. Upregulated genes include Txnip, AldoB, Crem, and Fos, and downregulated genes include Dbp, Ddit3, and Trib3. Many other pro-apoptotic, ER stress, cholesterol-regulated, and glucose metabolic genes were identified by this analysis, and often in ways that were not predicted *a priori*, resulting in a complex interaction of gene transcripts that does not follow the two-state (high vs. low glucose concentration) model [151].

Webb et al. found that the expression of genes encoding proteins involved in ribosome docking, intermediary metabolism, amino acid metabolism, and urea metabolism were all significantly affected by high glucose concentrations *in vitro* [152]. Tsuboi et al. also found that the expression of the Glut2 and glucokinase genes were significantly downregulated due to high glucose concentrations *in vitro*, concomitant with abnormal termination of insulin release by inhibiting normal glucose sensing. In other words, islet cells incubated at high glucose concentrations in culture exhibit decreased GSIS due to reductions in insulin signaling [153]. Genes involved in the differentiation of pancreatic AR42J cells into insulin producing cells include thymosin 10, PTHrP, SPP-24 precursor, Carboxypeptidase E, Amyloid precursor-like protein, and Keratin D [154].

### *In Vivo* Islet Transcriptomic Profiling

While the *in vitro* approach to discover islet-specific genes regulated by IR and islet failure are informative, a thorough understanding of the *in vivo* response to these conditions ultimately reveals a physiologically relevant set of target genes. In the search for these *in vivo* gene targets, many microarray studies have begun to elucidate a set of transcription factors and genes that principally regulate GSIS, including the gene products of DNA-binding genes, ER-stress related genes, genes involved in ribosomal translation, protein and peptide vesicular transport, vesicle docking at the plasma membrane, glycolytic genes, as well as negative and positive regulators of apoptosis.

Thanks to the efforts of researchers committed to centralizing information regarding transcriptomic profiling of both *in vitro* and *in vivo* pancreatic cell types, in 2007 the freely available EPConDB database (http://www.cbil.upenn.edu/EPConDB) was published by the Beta Cell Biology

Consortium. The results contained in this database are obtained from studies investigating the gene expression profiles of mature pancreatic tissue, during development and growth, *in vitro* differentiation of insulin-producing cells, in response to beta cell injury, and genetic models of impaired beta cell function. Furthermore, the database allows researchers to explore the relationship between a specified gene, upstream transcriptional regulators, and downstream protein interactions [155]. In this database, a number of studies have identified important genes involved in the maintenance of normal beta cell biology.

Ferrer et al. found a total of 42 differentially expressed genes in human islet cells in comparison with exocrine tissue *in vivo* [156,157]. Rafaeloff et al. identified a number of novel genes expressed during islet neogenesis in the hamster pancreas *in vivo*, including Cytochrome c oxidase, Ubiquitin conjugating enzyme, Elastase I, the Reg gene family, and Pancreatitis Associated Protein (Pap) [158]. In a series of transcriptional profiling experiments, FoxA2 has been described as a critical determinant of vesicular trafficking, membrane targeting, and fuel-secretion pathways [159]. HNF-1alpha (also known as Tcf1) has been established as a central node in the regulation of downstream genes required for the maintenance of normal beta cells; microarray studies in HNF-1alpha knockout mice identified a HNF-1alpha promoter binding site in the transmembrane protein-27 (Tmem27), a cell surface glycosylated protein that is required for beta cell proliferation [160]. In addition, transcriptional profiling has identified Pdx-1 as an upstream regulator of ER-related genes involved in disulfide bond formation, protein folding, and the unfolded protein response, including Mafa, Slc2a2, Pax4, Ero1lb, and Nnat [161].

Garnett et al found that reduced EGR-1 expression may contribute to a decrease in beta cell proliferation and failure observed in later stages of type 2 diabetes [162]. A recent article in Goto-Kakizaki rats showed that genes involved in glucose sensing, phosphorylation, incretin action, glucocorticoid handling, ion transport, mitogenesis, and apoptosis [163].

In human microarray studies, genes responsible for the regulation of normal GSIS include HNF-4alpha, insulin receptor, IRS2, Akt2, G6PI, Aldo, PFK, PGM, and the transcription factor aryl hydrocarbon receptor nuclear translocator (ARNT, also known as HIF-1beta) [164]. Further analysis of the transcriptomes of human alpha, beta, large duct, small duct, and acinar cells identified Hopx, Hdac9, and MafB as genes that play a central role in beta cell biology [165].

### Islet Proteommic Approaches Using Animal Disease Models

Despite a growing body of research discussing the effect of IR and IF on individual proteins, the underlying global proteomic effects of IR and IF have yet to be described in detail. Significant advances in liquid chromatography mass spectrometry (LCMS) in the past decade has allowed for detailed analyses of the islet proteome that was not possible before the advent of such sophisticated instrumentation.

In 2001, the mouse SWISS-2D PAGE database was created to document the results of two(2)-Dimensional PolyAcrylamide Gel Electrophoresis on the quantitative expression of islet cell

proteins, and identified a limited set of 44 proteins [166].

In 2008, Petyuk et al. published the first comprehensive proteomic dataset of mouse islet cells, and identified 2,612 proteins, containing 133 highly expressed islet cell proteins [31]. This dataset became the first publicly available mouse islet proteome, and is available online (http://ncrr.pnl.gov). Of the 133 islet-specific proteins identified in this study, high abundance proteins include those (a) involved in the regulation of secretion, including Chga, Chgb, Scg2, Scg3, and Scg5, (b) islet-specific peptide hormones, including Gcg, Iapp, Ins1, Ins2, Pdyn, Ppy, Pyy, Sst, and Ucn3. These proteins are not only highly expressed in islet cells, they are expressed at very low levels in peripheral tissues.

Waanders et al. published a more comprehensive repository of islet proteins in 2009 by quantifying the relative expression level of 6,873 proteins isolated from a *single* islet cell. Using this approach, Waanders et al. found that the most highly expressed proteins in the islet proteome included insulin-1, insulin-2, glucagon, and the family of secretogranins. More than half of the islet proteome are proteins that regulate housekeeping functions and cell adhesion. Proteins enriched more than 4-fold above bulk pancreas protein expression includes G protein coupled receptors, cAMP regulators, receptor tyrosine kinases, and ion channels. Treatment of islet cells with high glucose concentrations *in vitro* resulted in the identification of increased protein expression of the mitochondrial stress regulator Park7, and a general upregulation of proteins involved in glycolysis, the TCA cycle, and ATP transport [27].

Interesting findings from this study include increased expression of antioxidant proteins, including ERO1l-alpha, Prdx3, Park7, Sod2, and a decreased expression of proteins that regulate vesicle secretion, including VAMP-2, Sytl-4, Rab3b, and the endoplasmic reticulum calcium ATPase SERCA complex. Importantly, 24-hour glucose stimulation also stimulated the expression of proteins involved in cytoskeletal remodeling and cell proliferation, including Villin 1, Gelsolin, alpha actinin 1, alpha actinin 4, and integrin beta-1.

In animal models of diabetes, protein profiling has also been performed [167]. The BioBreeding (BB-DP) rat is a model for type 1 insulin dependent diabetes (T1D), and islet proteomic profiling has revealed that IL-1beta significantly influenced the expression of proteins related to carbohydrate metabolism, DNA synthesis, protein synthesis, cell differentiation and apoptosis [168–171]. In the NOD mouse, another model of autoimmune T1D, the expression of intracellular stress regulators was higher when compared with the alloxan-resistant (ALR) mouse [172].

The proteomic expression of islet cells from animal models of T2D has also been studied. Included in these models is the obese lep/lep mouse in which oxidative stress proteins glutathione S-transferase and calgranulin B were downregulated in comparison with lean litter mates [173]. In the IR non-diabetic MKR mouse model, proteins related to insulin secretory defects, unfolded protein response (Erp72, Erp44, Erp29, Ppib, Fkbp2,

Fkbp11, Dnajb11), ER-associated protein degradation (Vcp and Ufm1) and mitochondrial metabolism (Ndufa9, Uqcrh, Cox2, Cox4l1, Cox5a, ATP6v1b2, ATP6v1h, Ant1, Ant2, Etfa, and Etfb) were found to be differentially expressed in comparison with control mice. The authors also performed gene expression profiling to determine the crossover between mRNA and protein datasets, and found that 46% of the proteins were represented by detectable transcripts, suggesting that post-translational modifications may underlie changes in protein function in the context of IR [174].

While these studies are excellent classifications of the islet proteome in response to either IR, T1D, or T2D, each of these studies classifies the static quantitative expression of islet proteins through either physical (2D-PAGE) or bioinformatic quantitative methods. Determining the kinetics of protein expression in insulin sensitive, insulin resistant hyperplastic islets, and failed islet cells represents the next generation of islet proteome analysis, and we hypothesize that the combination of $^2H_2O$ labeling and LCMS analysis will contribute a significant advancement in the field of islet cell kinetic biology.

## Combining Genomic and Proteomic Datasets

Given that transcriptomic and proteomic datasets are often large and only interpretable as a molecular network, there is a significant interest in combining the two types of data together to uncover both transcriptional and translational control of protein synthesis in response to IR and diabetes. Experimentally, this can be performed using mRNA and protein homogenates from the same animals (ideal), or by performing parallel experiments (less ideal). The goal of such an approach is to determine the degree of overlap between genomic and proteomic datasets, creating a single *proteogenomic* dataset that can be further used to explain underlying islet cell behavior. The degree of overlap between genomic and proteomic datasets is determined by the experimental design, the degree of post-translational modifications, and the bioinformatic analysis method used to determine statistical significance.

Experimentally, comparing between experiments often yields a low degree of overlap, as found in a recent study in which the genomic and proteomic datasets of mouse models of T1D were compared. This cross-comparison resulted in 18% commonality between identified transcripts and protein [171,175]. Comparing within experiments increases genomic and proteomic overlap, however a large proportion of identified transcripts are frequently unidenfitied in the proteomic datasets, or the transcript and protein expression are discordant [167]. In a study to investigate proteogenomic expression in the MKR mouse model of T2D, 45% of differentially regulated genes also demonstrated differentially regulated protein partners concordantly, yet in 54% of the differentially expressed proteins a corresponding mRNA transcript was not detected [174]. This approach minimized the proportion of discordant proteogenomic changes (1%). In a recent study, a parallel proteogenomic approach was applied to human beta cells *in vitro*, resulting in 65% concordant overlap between differentially expressed transcripts and proteins, representing 54% concordant expression and 14% discordant expression [176].

## Conclusions

While much work has been done to classify the effect of insulin resistance and diabetes on the expression of islet cell proteins, techniques to study the dynamic synthesis and breakdown of a large number of islet-specific proteins remains to be performed. Our objective in these studies is to contribute to this body of knowledge and identify the groups of proteins whose synthesis is markedly influenced by the ambient insulin secretory burden present in early and late stage type 2 diabetes. This knowledge will help pinpoint the regulatory networks associated with islet cell hyperplasia in response to peripheral insulin resistance, and islet cell failure. We hope that this knowledge may help drive the development of therapeutics aimed at delaying or preventing the onset of type 2 diabetes in the future.

## Literature Cited


1. Zimmet, P., Alberti, K. G. & Shaw, J. Global and societal implications of the diabetes epidemic. *Nature* **414**, 782–787 (2001).
2. Diabetes expected to double, costs to triple by 2034 | Healthland | TIME.com. *TIME.com* at <http://healthland.time.com/2009/11/27/diabetes-expected-to-double-costs-to-triple-by-2034/>
3. Huang, E. S., Basu, A., O'Grady, M. & Capretta, J. C. Projecting the Future Diabetes Population Size and Related Costs for the U.S. *Diabetes Care* **32**, 2225 –2229 (2009).
4. CDC - 2011 National Diabetes Fact Sheet - Publications - Diabetes DDT. at <http://www.cdc.gov/diabetes/pubs/factsheet11.htm?utm_source=WWW&utm_medium=ContentPage&utm_content=CDCFactsheet&utm_campaign=CON#citation>
5. Kelley, D. E. & Goodpaster, B. H. Effects of exercise on glucose homeostasis in Type 2 diabetes mellitus. *Med Sci Sports Exerc* **33**, S495–501; discussion S528–529 (2001).
6. Spiegelman, B. M. & Flier, J. S. Obesity and the regulation of energy balance. *Cell* **104**, 531–543 (2001).
7. Ford, E. S. Prevalence of the Metabolic Syndrome Defined by the International Diabetes Federation Among Adults in the U.S. *Diabetes Care* **28**, 2745 –2749 (2005).
8. Riccardi, G., Giacco, R. & Rivellese, A. A. Dietary fat, insulin sensitivity and the metabolic syndrome. *Clin Nutr* **23**, 447–456 (2004).
9. Unger, R. H. & Scherer, P. E. Gluttony, sloth and the metabolic syndrome: a roadmap to lipotoxicity. *Trends in Endocrinology & Metabolism* **21**, 345–352 (2010).
10. Riccardi, G., Giacco, R. & Rivellese, A. . Dietary fat, insulin sensitivity and the metabolic syndrome. *Clinical Nutrition* **23**, 447–456 (2004).
11. Samuel, V. T., Petersen, K. F. & Shulman, G. I. Lipid-induced insulin resistance: unravelling the mechanism. *Lancet* **375**, 2267–2277 (2010).
12. Obesity and Overweight for Professionals: Data and Statistics: U.S. Obesity Trends | DNPAO | CDC. at <http://www.cdc.gov/obesity/data/trends.html>
13. Bouchard, C. *et al.* The response to long-term overfeeding in identical twins. *N. Engl. J. Med.* **322**, 1477–1482 (1990).
14. Ravussin, E. Metabolic differences and the development of obesity. *Metab. Clin. Exp.* **44**, 12–14 (1995).
15. Chen, H. *et al.* Evidence that the diabetes gene encodes the leptin receptor: identification of a mutation in the leptin receptor gene in db/db mice. *Cell* **84**, 491–495 (1996).
16. Friedman, J. M. & Halaas, J. L. Leptin and the regulation of body weight in mammals. *Nature* **395**, 763–770 (1998).
17. Halaas, J. L. *et al.* Weight-reducing effects of the plasma protein encoded by the obese gene. *Science* **269**, 543–546 (1995).
18. Zhang, Y. *et al.* Positional cloning of the mouse obese gene and its human homologue. *Nature* **372**, 425–432 (1994).
19. Clapham, J. C. *et al.* Mice overexpressing human uncoupling protein-3 in skeletal muscle are hyperphagic and lean. *Nature* **406**, 415–418 (2000).
20. Kozak, L. P. & Koza, R. A. Mitochondria uncoupling proteins and obesity: molecular and genetic aspects of UCP1. *Int. J. Obes. Relat. Metab. Disord.* **23 Suppl 6**, S33–37 (1999).
21. Kozak, U. C. *et al.* An upstream enhancer regulating brown-fat-specific expression of the mitochondrial uncoupling protein gene. *Mol. Cell. Biol.* **14**, 59–67 (1994).
22. Lowell, B. B. & Flier, J. S. Brown adipose tissue, beta 3-adrenergic receptors, and obesity. *Annu. Rev. Med.* **48**, 307–316 (1997).
23. Ricquier, D. & Bouillaud, F. Mitochondrial uncoupling proteins: from mitochondria to the regulation of energy balance. *J. Physiol. (Lond.)* **529 Pt 1**, 3–10 (2000).

24. Kim, J. B. & Spiegelman, B. M. ADD1/SREBP1 promotes adipocyte differentiation and gene expression linked to fatty acid metabolism. *Genes Dev.* **10**, 1096–1107 (1996).
25. Shimano, H. *et al.* Overproduction of cholesterol and fatty acids causes massive liver enlargement in transgenic mice expressing truncated SREBP-1a. *J. Clin. Invest.* **98**, 1575–1584 (1996).
26. Puigserver, P. *et al.* A cold-inducible coactivator of nuclear receptors linked to adaptive thermogenesis. *Cell* **92**, 829–839 (1998).
27. Waanders, L. F. *et al.* Quantitative proteomic analysis of single pancreatic islets. *Proc. Natl. Acad. Sci. U.S.A.* **106**, 18902–18907 (2009).
28. Elayat AA, el-Naggar MM, Tahir M & Elayat AA, el-N. M. An immunocytochemical and morphometric study of the rat pancreatic islets. *Journal of Anatomy* **(Pt 3)**, 629–37 (1995).
29. Guz, Y., Nasir, I. & Teitelman, G. Regeneration of pancreatic beta cells from intra-islet precursor cells in an experimental model of diabetes. *Endocrinology* **142**, 4956–4968 (2001).
30. Suckale, J. & Solimena, M. Pancreas islets in metabolic signaling - focus on the beta-cell RID E-1275-2011. *Front. Biosci.* **13**, 7156–7171 (2008).
31. Petyuk, V. A. *et al.* Characterization of the mouse pancreatic islet proteome and comparative analysis with other mouse tissues. *J. Proteome Res.* **7**, 3114–3126 (2008).
32. Costoff A & A, C. Endocrinology: The Endocrine Pancreas. *Sect. 5, Ch. 4: Structure, Synthesis, and Secretion of Somatostatin* pp. page 16at <http://www.lib.mcg.edu/edu/eshuphysio/program/section5/5ch4/s5ch4_16.htm>
33. Ashcroft, F. M., Harrison, D. E. & Ashcroft, S. J. Glucose induces closure of single potassium channels in isolated rat pancreatic beta-cells. *Nature* **312**, 446–448 (1984).
34. Ashcroft, F. M. ATP-sensitive potassium channelopathies: focus on insulin secretion. *Journal of Clinical Investigation* **115**, 2047–2058 (2005).
35. Dunne, M. J., Cosgrove, K. E., Shepherd, R. M., Aynsley-Green, A. & Lindley, K. J. Hyperinsulinism in infancy: from basic science to clinical disease. *Physiol. Rev.* **84**, 239–275 (2004).
36. Gloyn, A. L. *et al.* Activating mutations in the gene encoding the ATP-sensitive potassium-channel subunit Kir6.2 and permanent neonatal diabetes. *N. Engl. J. Med.* **350**, 1838–1849 (2004).
37. Koster, J. C., Marshall, B. A., Ensor, N., Corbett, J. A. & Nichols, C. G. Targeted overactivity of beta cell K(ATP) channels induces profound neonatal diabetes. *Cell* **100**, 645–654 (2000).
38. Miki, T. *et al.* Defective insulin secretion and enhanced insulin action in KATP channel-deficient mice. *Proc. Natl. Acad. Sci. U.S.A.* **95**, 10402–10406 (1998).
39. Seghers, V., Nakazaki, M., DeMayo, F., Aguilar-Bryan, L. & Bryan, J. Sur1 knockout mice. A model for K(ATP) channel-independent regulation of insulin secretion. *J. Biol. Chem.* **275**, 9270–9277 (2000).
40. Turner, N. *et al.* Excess lipid availability increases mitochondrial fatty acid oxidative capacity in muscle: evidence against a role for reduced fatty acid oxidation in lipid-induced insulin resistance in rodents. *Diabetes* **56**, 2085–2092 (2007).
41. Perseghin, G., Petersen, K. & Shulman, G. I. Cellular mechanism of insulin resistance: potential links with inflammation. *Int J Obes Relat Metab Disord* **27**, S6–S11 (0000).
42. Randle, P. J., Garland, P. B., Hales, C. N. & Newsholme, E. A. THE GLUCOSE FATTY-ACID CYCLE ITS ROLE IN INSULIN SENSITIVITY AND THE METABOLIC DISTURBANCES OF DIABETES MELLITUS. *The Lancet* **281**, 785–789 (1963).

43. Forouhi, N. G. *et al.* Relation of triglyceride stores in skeletal muscle cells to central obesity and insulin sensitivity in European and South Asian men. *Diabetologia* **42**, 932–935 (1999).
44. Goodpaster, B. H., Thaete, F. L., Simoneau, J. A. & Kelley, D. E. Subcutaneous abdominal fat and thigh muscle composition predict insulin sensitivity independently of visceral fat. *Diabetes* **46**, 1579 –1585 (1997).
45. Kelley, D. E., Goodpaster, B. H. & Storlien, L. Muscle triglyceride and insulin resistance. *Annu. Rev. Nutr.* **22**, 325–346 (2002).
46. Pan, D. A. *et al.* Skeletal muscle triglyceride levels are inversely related to insulin action. *Diabetes* **46**, 983 –988 (1997).
47. Phillips, D. I. *et al.* Intramuscular triglyceride and muscle insulin sensitivity: evidence for a relationship in nondiabetic subjects. *Metab. Clin. Exp.* **45**, 947–950 (1996).
48. Falholt, K. *et al.* Carbohydrate and lipid metabolism of skeletal muscle in type 2 diabetic patients. *Diabet. Med.* **5**, 27–31 (1988).
49. Standl, E., Lotz, N., Dexel, T., Janka, H. U. & Kolb, H. J. Muscle triglycerides in diabetic subjects. Effect of insulin deficiency and exercise. *Diabetologia* **18**, 463–469 (1980).
50. Dobbins, R. L. *et al.* Prolonged Inhibition of Muscle Carnitine Palmitoyltransferase-1 Promotes Intramyocellular Lipid Accumulation and Insulin Resistance in Rats. *Diabetes* **50**, 123 –130 (2001).
51. Oakes, N. D., Camilleri, S., Furler, S. M., Chisholm, D. J. & Kraegen, E. W. The insulin sensitizer, BRL 49653, reduces systemic fatty acid supply and utilization and tissue lipid availability in the rat. *Metab. Clin. Exp.* **46**, 935–942 (1997).
52. Shimabukuro, M. *et al.* Direct antidiabetic effect of leptin through triglyceride depletion of tissues. *Proc. Natl. Acad. Sci. U.S.A.* **94**, 4637–4641 (1997).
53. Goodpaster, B. H., He, J., Watkins, S. & Kelley, D. E. Skeletal muscle lipid content and insulin resistance: evidence for a paradox in endurance-trained athletes. *J. Clin. Endocrinol. Metab.* **86**, 5755–5761 (2001).
54. Kelley, D. E., He, J., Menshikova, E. V. & Ritov, V. B. Dysfunction of mitochondria in human skeletal muscle in type 2 diabetes. *Diabetes* **51**, 2944–2950 (2002).
55. Hood, D. A. Invited Review: Contractile activity-induced mitochondrial biogenesis in skeletal muscle. *Journal of Applied Physiology* **90**, 1137–1157 (2001).
56. Kelley, D. E., Goodpaster, B., Wing, R. R. & Simoneau, J. A. Skeletal muscle fatty acid metabolism in association with insulin resistance, obesity, and weight loss. *Am. J. Physiol.* **277**, E1130–1141 (1999).
57. Simoneau, J., Colberg, S., Thaete, F. & Kelley, D. Skeletal muscle glycolytic and oxidative enzyme capacities are determinants of insulin sensitivity and muscle composition in obese women. *The FASEB Journal* **9**, 273 –278 (1995).
58. Simoneau, J.-A., Veerkamp, J. H., Turcotte, L. P. & Kelley, D. E. Markers of capacity to utilize fatty acids in human skeletal muscle: relation to insulin resistance and obesity and effects of weight loss. *The FASEB Journal* **13**, 2051 –2060 (1999).
59. He, J., Goodpaster, B. H. & Kelley, D. E. Effects of weight loss and physical activity on muscle lipid content and droplet size. *Obes. Res.* **12**, 761–769 (2004).
60. Toledo, F. G. S. *et al.* Mitochondrial capacity in skeletal muscle is not stimulated by weight loss despite increases in insulin action and decreases in intramyocellular lipid content. *Diabetes* **57**, 987–994 (2008).
61. Goldberg, R. B. Prevention of type 2 diabetes. *Med. Clin. North Am.* **82**, 805–821 (1998).
62. Ivy, J. L. Role of exercise training in the prevention and treatment of insulin resistance and non-insulin-dependent diabetes mellitus. *Sports Med* **24**, 321–336 (1997).

63. Kriska, A. M. & Bennett, P. H. An epidemiological perspective of the relationship between physical activity and NIDDM: from activity assessment to intervention. *Diabetes Metab Rev* **8**, 355–372 (1992).
64. Kriska, A. M., Blair, S. N. & Pereira, M. A. The potential role of physical activity in the prevention of non-insulin-dependent diabetes mellitus: the epidemiological evidence. *Exerc Sport Sci Rev* **22**, 121–143 (1994).
65. Kriska, A. Physical activity and the prevention of type 2 diabetes mellitus: how much for how long? *Sports Med* **29**, 147–151 (2000).
66. Zaman, M.-Q. *et al.* Lipid profile and insulin sensitivity in rats fed with high-fat or high-fructose diets. *Br. J. Nutr.* **106**, S206–S210 (2011).
67. Armeno, M. L., Krochik, A. G. & Mazza, C. S. Evaluation of two dietary treatments in obese hyperinsulinemic adolescents. *J. Pediatr. Endocrinol. Metab.* **24**, 715–722 (2011).
68. Cartee, G. D. & Dean, D. J. Glucose transport with brief dietary restriction: heterogenous responses in muscles. *American Journal of Physiology - Endocrinology And Metabolism* **266**, E946 – E952 (1994).
69. Cartee, G. D., Kietzke, E. W. & Briggs-Tung, C. Adaptation of muscle glucose transport with caloric restriction in adult, middle-aged, and old rats. *American Journal of Physiology - Regulatory, Integrative and Comparative Physiology* **266**, R1443 – R1447 (1994).
70. Davidson, R. T., Arias, E. B. & Cartee, G. D. Calorie restriction increases muscle insulin action but not IRS-1-, IRS-2-, or phosphotyrosine-PI 3-kinase. *American Journal of Physiology - Endocrinology And Metabolism* **282**, E270 –E276 (2002).
71. Dean, D. J. & Cartee, G. D. Brief dietary restriction increases skeletal muscle glucose transport in old Fischer 344 rats. *J. Gerontol. A Biol. Sci. Med. Sci.* **51**, B208–213 (1996).
72. Dean, D. J., Brozinick, J. T., Cushman, S. W. & Cartee, G. D. Calorie restriction increases cell surface GLUT-4 in insulin-stimulated skeletal muscle. *American Journal of Physiology - Endocrinology And Metabolism* **275**, E957 –E964 (1998).
73. McCurdy, C. E. & Cartee, G. D. Akt2 Is Essential for the Full Effect of Calorie Restriction on Insulin-Stimulated Glucose Uptake in Skeletal Muscle. *Diabetes* **54**, 1349 –1356 (2005).
74. McCurdy, C. E., Davidson, R. T. & Cartee, G. D. Brief calorie restriction increases Akt2 phosphorylation in insulin-stimulated rat skeletal muscle. *American Journal of Physiology - Endocrinology And Metabolism* **285**, E693 –E700 (2003).
75. Sharma, N. *et al.* Mechanisms for increased insulin-stimulated Akt phosphorylation and glucose uptake in fast- and slow-twitch skeletal muscles of calorie-restricted rats. *American Journal of Physiology - Endocrinology And Metabolism* **300**, E966 – E978 (2011).
76. Sharma, N. *et al.* Improved insulin sensitivity with calorie restriction does not require reduced JNK1/2, p38, or ERK1/2 phosphorylation in skeletal muscle of 9-month-old rats. *Am. J. Physiol. Regul. Integr. Comp. Physiol.* **302**, R126–136 (2012).
77. Wajchenberg, B. L. beta-cell failure in diabetes and preservation by clinical treatment. *Endocr. Rev.* **28**, 187–218 (2007).
78. Coggan, A. R. *et al.* Skeletal muscle adaptations to endurance training in 60- to 70-yr-old men and women. *Journal of Applied Physiology* **72**, 1780–1786 (1992).
79. Gollnick, P. D. *et al.* Effect of training on enzyme activity and fiber composition of human skeletal muscle. *Journal of Applied Physiology* **34**, 107–111 (1973).
80. Hurley, B. F. *et al.* Muscle triglyceride utilization during exercise: effect of training. *Journal of Applied Physiology* **60**, 562–567 (1986).
81. Phillips, S. M. *et al.* Effects of training duration on substrate turnover and oxidation

during exercise. *Journal of Applied Physiology* **81**, 2182–2191 (1996).
82. Bogardus, C. *et al.* Effects of physical training and diet therapy on carbohydrate metabolism in patients with glucose intolerance and non-insulin-dependent diabetes mellitus. *Diabetes* **33**, 311–318 (1984).
83. DeFronzo, R. A., Sherwin, R. S. & Kraemer, N. Effect of physical training on insulin action in obesity. *Diabetes* **36**, 1379–1385 (1987).
84. Dela, F., Mikines, K. J., Larsen, J. J. & Galbo, H. Training-induced enhancement of insulin action in human skeletal muscle: the influence of aging. *J. Gerontol. A Biol. Sci. Med. Sci.* **51**, B247–252 (1996).
85. Ross, R. *et al.* Reduction in Obesity and Related Comorbid Conditions after Diet-Induced Weight Loss or Exercise-Induced Weight Loss in Men. *Annals of Internal Medicine* **133**, 92–103 (2000).
86. Centers for Disease Control Centers for Disease Control and Prevention: National Diabetes Surveillance System. (2012).
87. Summers, L. K. M. *et al.* Substituting dietary saturated fat with polyunsaturated fat changes abdominal fat distribution and improves insulin sensitivity. *Diabetologia* **45**, 369–377 (2002).
88. Vessby, B. *et al.* Substituting dietary saturated for monounsaturated fat impairs insulin sensitivity in healthy men and women: The KANWU Study. *Diabetologia* **44**, 312–319 (2001).
89. Huang, P. *et al.* Calorie restriction and endurance exercise share potent anti-inflammatory function in adipose tissues in ameliorating diet-induced obesity and insulin resistance in mice. *Nutr Metab (Lond)* **7**, 59 (2010).
90. Redman, L. M. & Ravussin, E. Endocrine alterations in response to calorie restriction in humans. *Molecular and Cellular Endocrinology* **299**, 129–136 (2009).
91. Roth, G. S. *et al.* Biomarkers of Caloric Restriction May Predict Longevity in Humans. *Science* **297**, 811 (2002).
92. Kirpichnikov, D., McFarlane, S. I. & Sowers, J. R. Metformin: an update. *Ann. Intern. Med.* **137**, 25–33 (2002).
93. Viollet, B. *et al.* Cellular and molecular mechanisms of metformin: an overview. *Clin. Sci.* **122**, 253–270 (2012).
94. Musi, N. *et al.* Metformin increases AMP-activated protein kinase activity in skeletal muscle of subjects with type 2 diabetes. *Diabetes* **51**, 2074–2081 (2002).
95. Bosi, E., Lucotti, P., Setola, E., Monti, L. & Piatti, P. M. Incretin-based therapies in type 2 diabetes: a review of clinical results. *Diabetes Res. Clin. Pract.* **82 Suppl 2**, S102–107 (2008).
96. Hare, K. J. & Knop, F. K. Incretin-based therapy and type 2 diabetes. *Vitam. Horm.* **84**, 389–413 (2010).
97. Janosz, K. E. N., Zalesin, K. C., Miller, W. M. & McCullough, P. A. Treating type 2 diabetes: incretin mimetics and enhancers. *Ther Adv Cardiovasc Dis* **3**, 387–395 (2009).
98. Mikhail, N. Incretin mimetics and dipeptidyl peptidase 4 inhibitors in clinical trials for the treatment of type 2 diabetes. *Expert Opin Investig Drugs* **17**, 845–853 (2008).
99. Wajchenberg, B. L. Clinical approaches to preserve beta-cell function in diabetes. *Adv. Exp. Med. Biol.* **654**, 515–535 (2010).
100. Cavaghan, M. K., Ehrmann, D. A., Byrne, M. M. & Polonsky, K. S. Treatment with the oral antidiabetic agent troglitazone improves beta cell responses to glucose in subjects with impaired glucose tolerance. *J. Clin. Invest.* **100**, 530–537 (1997).
101. Fujiwara, T., Yoshioka, S., Yoshioka, T., Ushiyama, I. & Horikoshi, H. Characterization of new oral antidiabetic agent CS-045. Studies in KK and ob/ob mice and Zucker fatty rats. *Diabetes* **37**, 1549–1558 (1988).
102. Nolan, J. J., Ludvik, B., Beerdsen, P., Joyce, M. & Olefsky, J. Improvement in glucose tolerance and insulin resistance in obese

subjects treated with troglitazone. *N. Engl. J. Med.* **331**, 1188–1193 (1994).
103. Sreenan, S., Sturis, J., Pugh, W., Burant, C. F. & Polonsky, K. S. Prevention of hyperglycemia in the Zucker diabetic fatty rat by treatment with metformin or troglitazone. *Am. J. Physiol.* **271**, E742–747 (1996).
104. Kim, H. *et al.* Peroxisomal proliferator-activated receptor-gamma upregulates glucokinase gene expression in beta-cells. *Diabetes* **51**, 676–685 (2002).
105. Kim, H. I. *et al.* Identification and functional characterization of the peroxisomal proliferator response element in rat GLUT2 promoter. *Diabetes* **49**, 1517–1524 (2000).
106. Elnemr, A. *et al.* PPARgamma ligand (thiazolidinedione) induces growth arrest and differentiation markers of human pancreatic cancer cells. *Int. J. Oncol.* **17**, 1157–1164 (2000).
107. Rosen, E. D. *et al.* Targeted elimination of peroxisome proliferator-activated receptor gamma in beta cells leads to abnormalities in islet mass without compromising glucose homeostasis. *Mol. Cell. Biol.* **23**, 7222–7229 (2003).
108. Buckingham, R. E. *et al.* Peroxisome proliferator-activated receptor-gamma agonist, rosiglitazone, protects against nephropathy and pancreatic islet abnormalities in Zucker fatty rats. *Diabetes* **47**, 1326–1334 (1998).
109. Lehmann, J. M. *et al.* An antidiabetic thiazolidinedione is a high affinity ligand for peroxisome proliferator-activated receptor gamma (PPAR gamma). *J. Biol. Chem.* **270**, 12953–12956 (1995).
110. Saltiel, A. R. & Olefsky, J. M. Thiazolidinediones in the treatment of insulin resistance and type II diabetes. *Diabetes* **45**, 1661–1669 (1996).
111. Spiegelman, B. M. PPAR-gamma: adipogenic regulator and thiazolidinedione receptor. *Diabetes* **47**, 507–514 (1998).
112. Willson, T. M., Lambert, M. H. & Kliewer, S. A. Peroxisome proliferator-activated receptor gamma and metabolic disease. *Annu. Rev. Biochem.* **70**, 341–367 (2001).
113. Phillips, P. J. & Twigg, S. M. Oral hypoglycaemics - a review of the evidence. *Aust Fam Physician* **39**, 651–653 (2010).
114. Nissen, S. E. & Wolski, K. Effect of rosiglitazone on the risk of myocardial infarction and death from cardiovascular causes. *N. Engl. J. Med.* **356**, 2457–2471 (2007).
115. Singh, S., Loke, Y. K. & Furberg, C. D. Long-term risk of cardiovascular events with rosiglitazone: a meta-analysis. *JAMA* **298**, 1189–1195 (2007).
116. Butler, A. E. *et al.* Beta-cell deficit and increased beta-cell apoptosis in humans with type 2 diabetes. *Diabetes* **52**, 102–110 (2003).
117. Klöppel, G., Löhr, M., Habich, K., Oberholzer, M. & Heitz, P. U. Islet pathology and the pathogenesis of type 1 and type 2 diabetes mellitus revisited. *Surv Synth Pathol Res* **4**, 110–125 (1985).
118. Brüning, J. C. *et al.* Development of a novel polygenic model of NIDDM in mice heterozygous for IR and IRS-1 null alleles. *Cell* **88**, 561–572 (1997).
119. Chua, S., Jr *et al.* Differential beta cell responses to hyperglycaemia and insulin resistance in two novel congenic strains of diabetes (FVB- Lepr (db)) and obese (DBA-Lep (ob)) mice. *Diabetologia* **45**, 976–990 (2002).
120. Coleman, D. L. Obese and diabetes: two mutant genes causing diabetes-obesity syndromes in mice. *Diabetologia* **14**, 141–148 (1978).
121. Pick, A. *et al.* Role of apoptosis in failure of beta-cell mass compensation for insulin resistance and beta-cell defects in the male Zucker diabetic fatty rat. *Diabetes* **47**, 358 – 364 (1998).
122. Tokuyama, Y. *et al.* Evolution of beta-cell dysfunction in the male Zucker diabetic fatty rat. *Diabetes* **44**, 1447–1457 (1995).
123. Bonner-Weir, S., Baxter, L. A., Schuppin, G. T. & Smith, F. E. A second pathway for

regeneration of adult exocrine and endocrine pancreas. A possible recapitulation of embryonic development. *Diabetes* **42**, 1715–1720 (1993).
124. Bonner-Weir, S. Life and death of the pancreatic beta cells. *Trends Endocrinol. Metab.* **11**, 375–378 (2000).
125. Finegood, D. T., Scaglia, L. & Bonner-Weir, S. Dynamics of beta-cell mass in the growing rat pancreas. Estimation with a simple mathematical model. *Diabetes* **44**, 249–256 (1995).
126. Lee, S.-H., Hao, E. & Levine, F. β-Cell replication and islet neogenesis following partial pancreatectomy. *Islets* **3**, 188–195 (2011).
127. Zhou, Y. P., Cockburn, B. N., Pugh, W. & Polonsky, K. S. Basal insulin hypersecretion in insulin-resistant Zucker diabetic and Zucker fatty rats: role of enhanced fuel metabolism. *Metab. Clin. Exp.* **48**, 857–864 (1999).
128. Dor, Y., Brown, J., Martinez, O. I. & Melton, D. A. Adult pancreatic [beta]-cells are formed by self-duplication rather than stem-cell differentiation. *Nature* **429**, 41–46 (2004).
129. Georgia, S. & Bhushan, A. Beta cell replication is the primary mechanism for maintaining postnatal beta cell mass. *J. Clin. Invest.* **114**, 963–968 (2004).
130. Bray, G. A. The Zucker-fatty rat: a review. *Fed. Proc.* **36**, 148–153 (1977).
131. Cleary, M. P., Phillips, F. C. & Morton, R. A. Liver, serum and adipose tissue fatty acid composition in suckling Zucker rats. *Lipids* **29**, 753–758 (1994).
132. Phillips, M. S. *et al.* Leptin receptor missense mutation in the fatty Zucker rat. *Nat. Genet.* **13**, 18–19 (1996).
133. Takaya, K. *et al.* Molecular cloning of rat leptin receptor isoform complementary DNAs--identification of a missense mutation in Zucker fatty (fa/fa) rats. *Biochem. Biophys. Res. Commun.* **225**, 75–83 (1996).
134. Truett, G. E., Walker, J. A. & Harris, R. B. S. A developmental switch affecting growth of fatty rats. *American Journal of Physiology - Regulatory, Integrative and Comparative Physiology* **279**, R1956 –R1963 (2000).
135. Williams, G. *et al.* The hypothalamus and the control of energy homeostasis: different circuits, different purposes. *Physiol. Behav.* **74**, 683–701 (2001).
136. Finegood, D. T. *et al.* Beta-cell mass dynamics in Zucker diabetic fatty rats. Rosiglitazone prevents the rise in net cell death. *Diabetes* **50**, 1021–1029 (2001).
137. Teta, M., Long, S. Y., Wartschow, L. M., Rankin, M. M. & Kushner, J. A. Very Slow Turnover of β-Cells in Aged Adult Mice. *Diabetes* **54**, 2557–2567 (2005).
138. Bonner-Weir, S. Islet growth and development in the adult. *J. Mol. Endocrinol.* **24**, 297–302 (2000).
139. Goldberg, I. D. *et al.* Vascular smooth muscle cell kinetics: a new assay for studying patterns of cellular proliferation in vivo. *Science* **205**, 920–922 (1979).
140. Bonhoeffer, S., Mohri, H., Ho, D. & Perelson, A. S. Quantification of Cell Turnover Kinetics Using 5-Bromo-2'-deoxyuridine1. *The Journal of Immunology* **164**, 5049–5054 (2000).
141. Tapscott, S., Lassar, A., Davis, R. & Weintraub, H. 5-bromo-2'-deoxyuridine blocks myogenesis by extinguishing expression of MyoD1. *Science* **245**, 532 – 536 (1989).
142. Busch, R., Neese, R. A., Awada, M., Hayes, G. M. & Hellerstein, M. K. Measurement of cell proliferation by heavy water labeling. *Nat Protoc* **2**, 3045–3057 (2007).
143. Chen, S. *et al.* Measurement of pancreatic islet cell proliferation by heavy water labeling. *Am. J. Physiol. Endocrinol. Metab.* **293**, E1459–1464 (2007).
144. Neese, R. A. *et al.* Measurement in vivo of proliferation rates of slow turnover cells by 2H2O labeling of the deoxyribose moiety of DNA. *Proc. Natl. Acad. Sci. U.S.A.* **99**, 15345–15350 (2002).
145. Jecker, P., Beuleke, A., Dressendörfer, I., Pabst, R. & Westermann, J. Long-term oral

application of 5-bromo-2-deoxyuridine does not reliably label proliferating immune cells in the LEW rat. *J. Histochem. Cytochem.* **45**, 393–401 (1997).

146. Weghorst, C. M., Henneman, J. R. & Ward, J. M. Dose response of hepatic and renal DNA synthetic rates to continuous exposure of bromodeoxyuridine (BrdU) via slow-release pellets or osmotic minipumps in male B6C3F1 mice. *J. Histochem. Cytochem.* **39**, 177–184 (1991).
147. Ktorza, A. *et al.* Are animal models of diabetes relevant to the study of the genetics of non-insulin-dependent diabetes in humans? *Diabetes Metab.* **23 Suppl 2**, 38–46 (1997).
148. Leonard, B. L., Watson, R. N., Loomes, K. M., Phillips, A. R. J. & Cooper, G. J. Insulin resistance in the Zucker diabetic fatty rat: a metabolic characterisation of obese and lean phenotypes. *Acta Diabetol* **42**, 162–170 (2005).
149. Schmidt, R. E., Dorsey, D. A., Beaudet, L. N. & Peterson, R. G. Analysis of the Zucker Diabetic Fatty (ZDF) type 2 diabetic rat model suggests a neurotrophic role for insulin/IGF-I in diabetic autonomic neuropathy. *Am. J. Pathol.* **163**, 21–28 (2003).
150. Shalev, A. *et al.* Oligonucleotide microarray analysis of intact human pancreatic islets: identification of glucose-responsive genes and a highly regulated TGFbeta signaling pathway. *Endocrinology* **143**, 3695–3698 (2002).
151. Bensellam, M., Van Lommel, L., Overbergh, L., Schuit, F. C. & Jonas, J. C. Cluster analysis of rat pancreatic islet gene mRNA levels after culture in low-, intermediate- and high-glucose concentrations. *Diabetologia* **52**, 463–476 (2009).
152. Webb, G. C., Akbar, M. S., Zhao, C. & Steiner, D. F. Expression profiling of pancreatic beta cells: glucose regulation of secretory and metabolic pathway genes. *Proc. Natl. Acad. Sci. U.S.A.* **97**, 5773–5778 (2000).
153. Tsuboi, T., Ravier, M. A., Parton, L. E. & Rutter, G. A. Sustained exposure to high glucose concentrations modifies glucose signaling and the mechanics of secretory vesicle fusion in primary rat pancreatic beta-cells. *Diabetes* **55**, 1057–1065 (2006).
154. Mashima, H. *et al.* Genes expressed during the differentiation of pancreatic AR42J cells into insulin-secreting cells. *Diabetes* **48**, 304–309 (1999).
155. Mazzarelli, J. M. *et al.* EPConDB: a web resource for gene expression related to pancreatic development, beta-cell function and diabetes. *Nucleic Acids Res.* **35**, D751–755 (2007).
156. Ferrer, J. *et al.* Mapping novel pancreatic islet genes to human chromosomes. *Diabetes* **46**, 386–392 (1997).
157. Bernal-Mizrachi, E., Cras-Méneur, C., Ohsugi, M. & Permutt, M. A. Gene expression profiling in islet biology and diabetes research. *Diabetes Metab. Res. Rev.* **19**, 32–42 (2003).
158. Rafaeloff, R., Qin, X. F., Barlow, S. W., Rosenberg, L. & Vinik, A. I. Identification of differentially expressed genes induced in pancreatic islet neogenesis. *FEBS Lett.* **378**, 219–223 (1996).
159. Gao, N. *et al.* Foxa2 controls vesicle docking and insulin secretion in mature Beta cells. *Cell Metab.* **6**, 267–279 (2007).
160. Akpinar, P., Kuwajima, S., Krützfeldt, J. & Stoffel, M. Tmem27: a cleaved and shed plasma membrane protein that stimulates pancreatic beta cell proliferation. *Cell Metab.* **2**, 385–397 (2005).
161. Sachdeva, M. M. *et al.* Pdx1 (MODY4) regulates pancreatic beta cell susceptibility to ER stress. *Proc. Natl. Acad. Sci. U.S.A.* **106**, 19090–19095 (2009).
162. Garnett, K. E., Chapman, P., Chambers, J. A., Waddell, I. D. & Boam, D. S. W. Differential Gene Expression Between Zucker Fatty Rats and Zucker Diabetic Fatty Rats: A Potential Role for the Immediate-Early Gene Egr-1 in Regulation of Beta Cell

Proliferation. *J Mol Endocrinol* **35**, 13–25 (2005).
163. Ghanaat-Pour, H., Huang, Z., Lehtihet, M. & Sjöholm, Å. Global Expression Profiling of Glucose-Regulated Genes in Pancreatic Islets of Spontaneously Diabetic Goto-Kakizaki Rats. *J Mol Endocrinol* **39**, 135–150 (2007).
164. Gunton, J. E. *et al.* Loss of ARNT/HIF1beta mediates altered gene expression and pancreatic-islet dysfunction in human type 2 diabetes. *Cell* **122**, 337–349 (2005).
165. Dorrell, C. *et al.* Transcriptomes of the major human pancreatic cell types. *Diabetologia* **54**, 2832–2844 (2011).
166. Sanchez, J. C. *et al.* The mouse SWISS-2D PAGE database: a tool for proteomics study of diabetes and obesity. *Proteomics* **1**, 136–163 (2001).
167. Bergsten, P. Islet protein profiling. *Diabetes Obes Metab* **11 Suppl 4**, 97–117 (2009).
168. Christensen, U. B. *et al.* Islet protein expression changes during diabetes development in islet syngrafts in BB-DP rats and during rejection of BB-DP islet allografts. *Autoimmunity* **32**, 1–15 (2000).
169. Christensen, U. B. *et al.* Different islet protein expression profiles during spontaneous diabetes development vs. allograft rejection in BB-DP rats. *Autoimmunity* **39**, 315–321 (2006).
170. Karlsen, A. E., Sparre, T., Nielsen, K., Nerup, J. & Pociot, F. Proteome analysis--a novel approach to understand the pathogenesis of Type 1 diabetes mellitus. *Dis. Markers* **17**, 205–216 (2001).
171. Sparre, T. *et al.* IL-1beta induced protein changes in diabetes prone BB rat islets of Langerhans identified by proteome analysis. *Diabetologia* **45**, 1550–1561 (2002).
172. Yang, P. *et al.* Comparative analysis of the islet proteome between NOD/Lt and ALR/Lt mice. *Ann. N. Y. Acad. Sci.* **1150**, 68–71 (2008).
173. Sanchez, J.-C. *et al.* Effect of rosiglitazone on the differential expression of diabetes-associated proteins in pancreatic islets of C57Bl/6 lep/lep mice. *Mol. Cell Proteomics* **1**, 509–516 (2002).
174. Lu, H., Yang, Y., Allister, E. M., Wijesekara, N. & Wheeler, M. B. The identification of potential factors associated with the development of type 2 diabetes: a quantitative proteomics approach. *Mol. Cell Proteomics* **7**, 1434–1451 (2008).
175. Silva, D. & Petrovsky, N. Identification of key beta cell gene signaling pathways involved in type 1 diabetes. *Ann. N. Y. Acad. Sci.* **1037**, 203–207 (2004).
176. Jin, J. *et al.* Detection of differential proteomes of human beta-cells during islet-like differentiation using iTRAQ labeling. *J. Proteome Res.* **8**, 1393–1403 (2009).

# Chapter 3

## Regenerating Islet Derived (Reg) Gene Expression is Reduced in Failing Islets of Zucker Diabetic Fatty Rats

Cyrus F Khambatta*‡, Scott M Turner†‡, Matthew D Bruss*,
Ellen L Tsang†, Mei X Steele†, Songyuan Chen†, Pamela C Mejia*, Lindsay S Roberts*,
Marcy Dalidd*, and Marc K Hellerstein*

*Department of Nutritional Sciences and Toxicology,
University of California at Berkeley, Berkeley, California 94720
† Kinemed Inc, Emeryville, CA 94608
‡ These authors contributed to this work equally

### Abstract

#### Aims/Hypothesis

Insulin resistance and beta cell failure are the two central etiological processes underlying type 2 diabetes. The effect of insulin resistance and islet cell failure on islet cell proliferation and gene expression is of great interest. We systematically investigated the cell proliferative response gene expression profiles of islet cells in the settings of islet maintenance, hyperproliferation, and failure.

#### Methods

Five-week old male Zucker Diabetic Fatty rats (n=24) were randomized into three groups: 4 week rosiglitazone treatment (RT), rosiglitazone withdrawal (RW), or untreated controls (UT). Gene arrays were performed on isolated islets from heavy water ($^2H_2O$) labeled animals to measure the rate of islet cell proliferation and gene expression in the same animals *in vivo*.

#### Results

Two weeks of insulin resistance following the withdrawal of rosiglitazone promoted a rapid 3.2-fold increase in islet cell proliferation vs. insulin sensitive animals, followed by a sharp reduction in proliferation after 2 more weeks. In response to islet failure, the expression of regenerating islet-derived genes *Reg3a, Reg3b,* and *Reg3g* were significantly

downregulated, concomitant with reduced serum insulin. Both insulin resistance and islet failure significantly downregulated the expression of genes involved in insulin synthesis, secretion, peptide processing, and vesicular transport, including *Pdx-1, Nkx2.2, Nkx6.1, FoxA2, Pax6, Pcsk2, Rab27a, Tram1.* Insulin sensitization delayed islet cell failure by four weeks compared to untreated controls.

**Conclusions/Interpretation**

Islet cell failure in response to *in vivo* insulin resistance in ZDF rats is characterized by a unique gene expression profile in which the regenerating islet-derived *Reg* gene family is significantly downregulated. These genes may serve as candidate biomarkers of islet hyperproliferation and failure.

**Keywords**

Rosiglitazone, Microarray Analysis, Islet Cell Proliferation, Insulin Resistance In Vivo, Beta Cell Dysfunction, Beta Cell Compensation, Zucker Diabetic Fatty Rat, Gene Expression Profiling, Thiazolidinediones, TZDs

## Introduction

Type 2 diabetes is a disease of increasing global prevalence that affects an estimated 300 million individuals worldwide [1]. Insulin resistance and bell cell secretory failure are the two principal etiological roots of this metabolic condition, and the transition to type 2 diabetes from insulin resistance is characterized by the inability of the beta cells in the islets of Langerhans to respond to an increasing peripheral demand for insulin [2]. Therapeutic interventions that preserve the capacity for beta cell proliferation and insulin secretion are therefore of great interest.

A distinct set of circulating and intracellular signals regulate islet cell function in response to insulin sensitization, insulin resistance, and diabetes. Islet cells respond to systemic insulin resistance by increased proliferation in order to augment insulin production and prevent hyperglycemia [2–5]. In animal models of type 2 diabetes, prolonged insulin resistance leads to a failure of islet cells to secrete insulin, resulting in overt hyperglycemia [6,7]. Although these physiological responses of islet cells to insulin resistance have been studied, the genetic determinants of islet cell plasticity and failure are poorly understood. Therefore, understanding the regulation of gene expression in hyperproliferating and failing islet cells in response to insulin resistance is important in developing effective strategies to treat diabetes.

In this study, we used rosiglitazone as an experimental tool to synchronize the transition of Zucker Diabetic Fatty rats (ZDF, fa/fa) from insulin sensitive to compensated insulin resistance and diabetes. The ZDF rat model harbors a mutation in the leptin receptor, resulting in obesity, severe insulin resistance, and islet cell hyperplasia prior to the onset of diabetes at eight to twelve weeks of age [8]. In a recent study, it was shown that rosiglitazone treatment delayed type 2 diabetes disease progression, which then resumed at the normal rate once the drug was removed [9]. Accordingly, we treated ZDF rats with insulin sensitizing drug rosiglitazone, then removed it to initiate a synchronized transition to insulin resistance and diabetes in order to identify transcriptional signatures of islet cell maintenance, hyperproliferation, and failure.

We have developed a technique for measuring cell proliferation rates *in vivo*, based on non-toxic $^2H_2O$ labeling and mass spectrometric analysis, which has been applied to the measurement of the proliferation of numerous cell types in experimental animals and humans, including islet cell proliferation in rats [9,10]. This method is well suited for the measurement of cell proliferation in slow turnover tissues because $^2H_2O$ can be conveniently administered for long periods of time in drinking water without toxic effects, combined with the high sensitivity of mass spectrometric analysis of the deoxyribose (dR) moiety of DNA [11].

We sought to combine $^2H_2O$ labeling with microarray analysis to determine the temporal regulation of islet-specific genes in relation to islet cell proliferative capacity. To our knowledge there have been no studies that combine measurements of islet cell proliferation rates and islet cell gene expression profiling during insulin resistance and type 2 diabetes *in vivo*. Therefore, our objective in this study was to identify global changes in gene expression that correlate with islet cell maintenance, hyperproliferation, and failure in the same animals *in vivo*.

## Methods

### Animals

Five-week old ZDF (fa/fa) animals (n=24) were purchased from Charles River Laboratories (Wilmington, MA). Following 48 hours of acclimation, animals were randomized into one of three groups: 4 week rosiglitazone treated (RT), 2 week rosiglitazone withdrawal (RW), or untreated controls (UT). Rosiglitazone was administered in the diet as powdered Avandia tablets (3mg rosiglitazone/kg body weight) from weeks 5-9 in RT and RW animals, and removed from weeks 9-11 in RW animals only. Two weeks before euthanasia, animals in each group were labeled with an intraperitoneal injection of 100% $^2H_2O$ (0.35mL/10 g body weight) and were subsequently provided 8% $^2H_2O$ drinking water to maintain body $^2H_2O$ enrichments of approximately 5% [11]. Animals were euthanized at week 9 (RT), week 11 (RW), and week 13 (UT) under isoflurane anesthesia, followed by cervical dislocation. All experiments were performed under the approval of the Institutional Animal Use Committees of the University of California at Berkeley.

### Islet cell isolation and in vivo cell proliferation analysis

Pancreatic islets were isolated immediately following euthanasia according to a perfusion protocol that has been described previously [10]. DNA was extracted from islets using the DNeasy kit (Qiagen, Valencia, CA), and was enzymatically hydrolyzed to free deoxyribonucleosides by overnight incubation at 37°C with S1 nuclease and potato acid phosphatase. The dR moiety of the deoxyribonucleosides was derivatized to the pentane tetraacetate derivative as described previously [11], and was analyzed by positive chemical ionization GC/MS with a model 5973 mass spectrometer fitted with a model 6890 gas chromatograph (Agilent, Palo Alto, CA). Selected ion monitoring was performed on mass isotopomers with mass-to-charge (m/z) ratios of 245, 246 and 247, representing the $M_0$, $M_1$ and $M_2$ ions of the pentane tetraacetate

deoxyribonucleoside derivatives, respectively. The excess fractional $M_1$ enrichment ($EM_1$) of dR was calculated as follows:

$$EM_1 = \frac{(Abundance M_1)_{sample}}{(Abundance M_0 + M_1)_{sample}} - \frac{(Abundance M_1)_{standard}}{(Abundance M_0 + M_1)_{standard}}$$

The fractional synthesis rates (f) of islets were calculated by comparison to bone marrow cells from the same animal [11].

### RNA isolation and quality control

Total RNA was isolated from 20-30 mg of islets using the RNEasy kit according to the manufacturer's instructions (Qiagen, Valencia, CA). Equal amounts of RNA from each of 3 replicates were reverse transcribed to cDNA after the purity and concentration of RNA samples were determined from $OD_{260/280}$ readings using a dual beam UV spectrophotometer. RNA integrity was determined by capillary electrophoresis using the RNA 6000 Nano Lab-on-a-Chip kit and the Bioanalyzer 2100 (Agilent Technologies).

### cRNA synthesis and labeling

cRNA was synthesized and labeled with biotinylated UTP and CTP by in vitro transcription using the T7 promoter-coupled double stranded cDNA as template and the Bioarray™ HighYield™ RNA Transcript Labeling Kit (ENZO Diagnostics Inc.). The labeled cRNA was separated from unincorporated ribonucleotides by passing through a CHROMA SPIN-100 column (Clontech) and ethanol precipitated at –20°C for 1 hr to overnight.

### Oligonucleotide array hybridization and analysis

Labeled cRNA (15.0 ug) was fragmented by Magnesium ion-mediated hydrolysis and hybridized for 16hr at 45°C to Affymetrix GeneChip Rat Genome 230 2.0 arrays (Affymetrix, Santa Clara, CA). Arrays were washed and stained using an Affymetrix Fluidics Station 450. The arrays were stained with phycoerythrein-conjugated streptavidin (Invitrogen, Carlsbad, CA) and the fluorescence intensities were determined using a GCS 3000 7G high-resolution confocal laser scanner (Affymetrix). The scanned images were analyzed using programs resident in AGCC and Expression Console (Affymetrix). Quality control metrics for cRNA integrity, sample loading, and variations in staining were determined by MAS 5.0 statistical algorithms.

### Microarray data analysis

Signal values were generated by the RMA method and detection p-values were generated by MAS 5.0 [12,13]. Probe sets exhibiting significant differential expression were identified using GeneMaths XT (Applied Maths, Austin TX), based on the following criteria: (a) MAS5.0 detection p-values ≤ 0.05, (b) ANOVA p-value ≤ 0.05, (c) absolute signal log ratio ≥ 1.0 and independent t-test p-value ≤ 0.05 for at least one pair wise comparison versus the control group. Unsupervised hierarchical clustering and heat map generation were performed following row mean centering of $\log_2$ transformed RMA signal values. Gene annotation, gene ontology information and biochemical pathway information were obtained from the Database for Annotation, Visualization and Integrated Discovery (DAVID) v6.7 from the National Institute of Allergy and

Infectious Diseases (NIAID), at the National Institutes of Health (NIH) [14,15].

### Gene expression analysis by quantitative qRT-PCR

RNA was isolated from isolated islets using the RNeasy kit (Qiagen, Valencia, CA) and reverse transcribed with M-MulV reverse transcriptase (New England Biolabs). Next, 25 ng of diluted cDNA was run on an ABI 7500 Fast Real-Time PCR System using TaqMan gene expression master mix and probed with Fam-labeled primer-probe sets (Applied Biosystems, Carlsbad, CA).

## Results

### Food Intake and Body Weight

Following two weeks on their respective diets, RT and RW animals consumed an average of 9.7 $\pm$ 4.0 g/day ($p<0.001$) more food than UT animals, and removal of rosiglitazone from the diet decreased food intake to the levels of UT animals (Figure 1A). The body weights of rosiglitazone treated animals were also significantly higher than chow-fed animals (Figure 1B).

### Blood Glucose and Plasma Insulin

In this study, we used rosiglitazone as an experimental tool to synchronize the transition of ZDF rats from insulin sensitive to compensated insulin resistance and diabetes. We first measured the effect of rosiglitazone treatment and withdrawal on circulating glucose and insulin in ZDF rats (Figure 2A and B). At 9 weeks of age RT rats had normal blood glucose levels (102.0 $\pm$ 9.0 mg/dL), and normal fasting insulin levels (7.0 $\pm$ 1.4 ng/mL). In contrast, UT controls at the same age were already hyperglycemic (380.0 $\pm$ 32.0 mg/dL) and hypoinsulinemic (5.1 $\pm$ 1.0 ng/mL), and maintained this phenotype for the remainder of the study. Rosiglitazone withdrawal at 9 weeks led to a steady increase in blood glucose and a rapid but transient increase in fasting insulin. At 11 weeks of age, RW animals exhibited elevated blood glucose (163.0 $\pm$ 40.0 mg/dL) and insulin (15.0 $\pm$ 4.8 ng/mL). By 13 weeks, RW animals were frankly hyperglycemic (276.4 $\pm$ 47.1 mg/dL), and insulin concentrations had fallen to near baseline levels (8.0 $\pm$ 1.3 ng/mL). Taken together, these data demonstrate that rosiglitazone coordinated the progression of ZDF rats to diabetes, and acted as an effective insulin sensitizing agent. In addition, this treatment-and-withdrawal regimen highlights three relevant stages in the progression towards diabetes: (a) insulin sensitivity (RT at 9 weeks), (b) insulin resistance (RW at 11 weeks), and (c) diabetes (UT at 13 weeks).

### Islet Cell Proliferation

Next, we assessed how rosiglitazone treatment and withdrawal affected islet cell proliferation. At 9 weeks of age, RT insulin sensitive mice exhibited low islet cell proliferation (0.90 $\pm$ 0.09 % new cells per day) (Figure 3). Rosiglitazone withdrawal at 9 weeks led to a rapid increase in islet cell proliferation by 11 weeks (2.69 $\pm$ 0.25 % new cells per day) that paralleled the increase in circulating insulin, indicative of islet cell hyperproliferation in the face of insulin resistance (compensated insulin resistance).

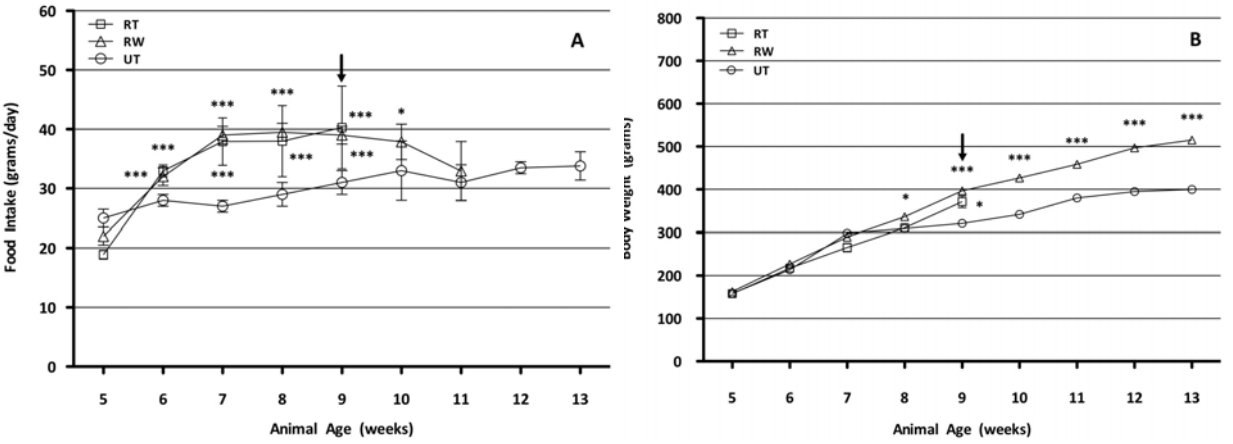


**Figure 1.** The effect of rosiglitazone treatment and removal on (A) mean daily food intake and (B) body weight in rosiglitazone treated (RT, open squares), rosiglitazone withdrawal (RW, open triangles), and untreated control (UT, open circles) ZDF rats. Values are means ± SEM, and significance was calculated by repeated measures ANOVA or a two-tailed student's t-test vs. UT animals (*, $p<0.05$; **, $p<0.01$; ***, $p<0.001$). Arrow indicates the time point at which animals in the RW group were switched to a chow diet devoid of rosiglitazone.

By 13 weeks, islet cell proliferation returned to baseline values (0.89 ± 0.09 % new cells per day), indicating islet cell failure. The progressive decline in islet cell proliferation in UT animals demonstrates progressive islet cell failure throughout the study. From 9 to 13 weeks, islet cell proliferation rates fell by over 70%, and at 13 weeks of age islet cell proliferation in the UT group was only 0.49% ± 0.11 new cells/day. Taken together with the glucose and insulin data, these results validate our experimental design and allow for the assessment of three distinct phases in the progression towards diabetes: (a) islet cell maintenance (RT at 9 weeks), (b) islet cell hyperproliferation (RW at 11 weeks), and (c) islet cell failure (UT at 13 weeks).

## Gene Expression Profiling

We then performed gene expression profiling in these three cohorts under the conditions of islet cell maintainence, hyperproliferation and failure. Total RNA was isolated from a subset of islets collected from RT, RW and UT animals. Affymetrix gene arrays (Rat 230 2.0) were used to evaluate changes in gene expression in response to islet cell failure and hyperproliferation in isolated islet cells (n=3 per group). Gene expression profiling identified 620 probe sets representing 401 known genes as being differentially expressed.

We performed four pair wise comparisons to determine the gene expression profiles that characterize islet cell failure (Table 1) and hyperproliferation (Table 2), and classify differentially expressed genes by function.

## Islet Cell Failure Gene Expression Profiling

We performed two pair wise comparisons (UT vs. RT and UT vs. RW) to determine the gene expression profiles unique to failed islet cells. In the first comparison we identified 228 probe sets representing 149 known genes as differentially expressed. There were 22 upregulated genes and 127 downregulated genes. In

the second comparison we identified 35 probe sets representing 23 known genes as differentially expressed, resulting in 17 upregulated genes and 6 downregulated genes (Table 1).

We identified 3 genes that were downregulated in both comparisons: *Reg3b*, *Reg3g*, and *TRH*. *Reg3b* expression was downregulated 2.30-fold and 2.94-fold, *Reg3g* expression was downregulated 14.00-fold and 14.92-fold, and *TRH* expression was downregulated 6.65-fold and 3.00-fold in comparison with RT and RW animals, respectively. We also identified 2 genes that were upregulated in both comparisons: *AldoB* and *Txnip*. *AldoB* expression was upregulated 21.10-fold and 13.85-fold, whereas *Txnip* was upregulated 2.80-fold and 2.71-fold in comparison with RT and RW animals, respectively. Of all the probe sets represented on the gene array, *AldoB* demonstrated the largest magnitude of downregulation.

Genes involved in islet cell proliferation, differentiation and migration were downregulated in UT animals in comparison with RT animals only. These genes include *Fos*, *Jun*, *Mapt*, and *Wif-1* and have well classified effects on promoting cellular proliferation and differentiation. In addition, pro-apoptotic genes including *Gch1*, *App*, *Nell1*, *Siva1*, *Kcnma1*, *Il1r1*, and *Dusp1*, as well as the anti-apoptotic genes *Dnajb9*, *Wfs1*, *Btg2*, *Nfkbia*, *Scg2* and *Hspa1b* were downregulated between 2.04 and 4.00-fold. Our data suggest that the gene expression profile of apoptotic genes does not correlate with functional pathway activity, and that the reduction in proliferation due to islet cell failure is a complex integrated balance between the expression of the proliferative and apoptotic genes identified here.

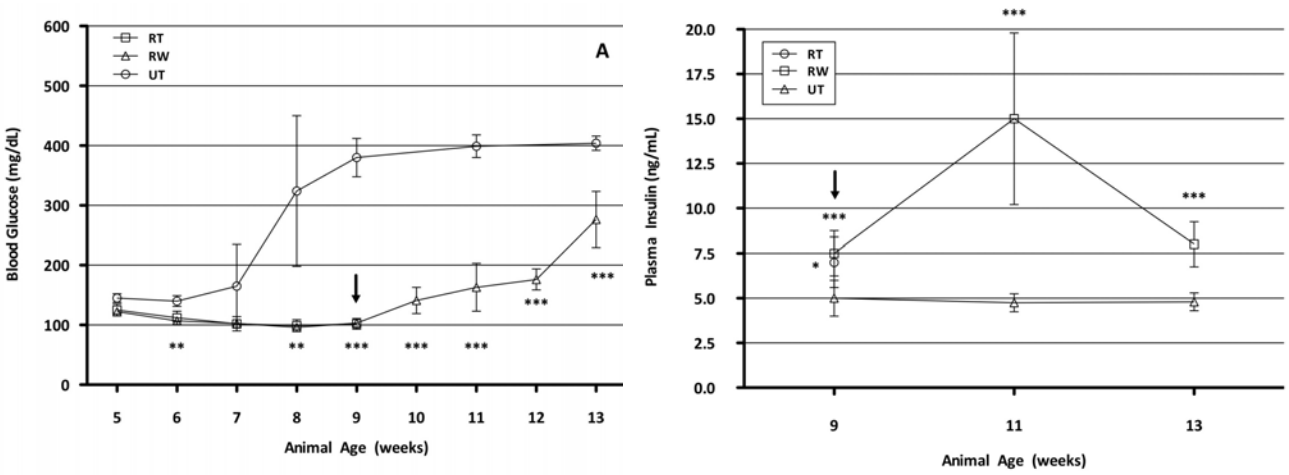


**Figure 2.** The effect of rosiglitazone treatment and removal on (A) blood glucose and (B) plasma insulin over time in rosiglitazone treated (RT, open squares), rosiglitazone withdrawal (RW, open triangles), and untreated control (UT, open circles) ZDF rats. Values are means ± SEM, and significance was calculated by repeated measures ANOVA or a two-tailed student's t-test vs. UT animals (*, $p<0.05$; **, $p<0.01$; ***, $p<0.001$). Arrow indicates the time point at which animals in the RW group were switched to a chow diet devoid of rosiglitazone. The RT group was euthanized at week 9.

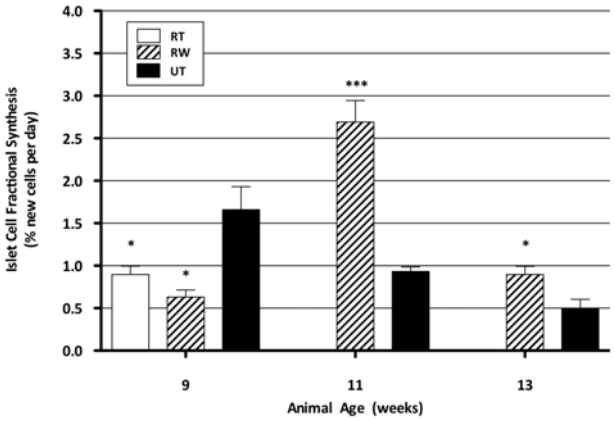


**Figure 3.** The effect of rosiglitazone treatment and removal on islet proliferation in rosiglitazone treated (RT, open squares), rosiglitazone withdrawal (RW, open triangles), and untreated control (UT, open circles) ZDF rats. Values are means ± SEM, and significance was calculated by repeated measures ANOVA or a two-tailed student's t-test vs. UT animals (*, $p<0.05$; **, $p<0.01$; ***, $p<0.001$). Animals in all groups were labeled for 2 weeks preceding euthanasia (n=3 animals/time point).

Similarly, genes involved in insulin secretion, peptide processing, and vesicular transport were downregulated in UT animals only in comparison with RT animals. The expression of this family of genes was downregulated between 2.1 and 6.65-fold, and includes *Gipr, Nnat, Pcsk2, P2ry1, Rab27a, Rab3b, Tram1, Spcs2*, and *Hspa1b*. In contrast to the increased expression of *AldoB*, genes involved in glucose metabolism including *Prkacb, Prkar1a,* and *Sst* were significantly downregulated in UT animals in comparison with RT animals.

### Islet Cell Hyperproliferation Gene Expression Profiling

We performed two pair wise comparisons (RW vs. RT and RW vs. UT) to determine the gene expression profiles common to hyperproliferating islet cells. In the first comparison we identified 357 probe sets representing 229 known genes as differentially expressed, resulting in 13 upregulated genes and 216 downregulated genes. In the second comparison we identified 35 probe sets representing 23 known genes as differentially expressed, resulting in 6 upregulated genes and 17 downregulated genes (Table 2).

Interestingly, we found that there were no genes in common to both comparisons, however genes grouped by functional pathway were coordinately regulated. We found that there was no significant change in the expression of the *Reg* family of genes in RW animals in comparison with RT animals, and that the expression of these genes was different only in comparison with UT animals.

Genes involved in proliferation, differentiation and migration, including *Fos, Jun, Mapt, Wif1, Atf4*, and *Ppm1b* did not reflect islet cell hyperproliferation. All genes in this group were downregulated between 2.01 and 3.34-fold. We also found a reduced expression of negative regulators of islet cell apoptosis in comparison with RT animals, between 2.03 and 2.38-fold. Genes in this family included *Vegfa, Dnajb9, Btg2, Nfkbia, Scg2, Hspa1b, Sod2,* and *Irak1.* In addition, 3 genes involved in the positive regulation of apoptosis were downregulated between 2.03 and 2.35-fold, including *Siva1, Il1r1,* and *Dusp1.* Taken together, these data indicate that while proliferative and apoptotic genes may play a role in regulating islet cell plasticity, expression levels of these genes are poor transcriptomic signatures of islet cell hyperplasia.

| Gene Symbol | Fold Change UT vs. RT | Fold Change UT vs. RW | Gene Name |
|---|---|---|---|
| **Pancreatic Regeneration and Inflammation** | | | |
| Reg3a | - | -2.36[b] | Regenerating islet-derived 3 alpha |
| Reg3b | -2.30 | -2.94[b] | Regenerating islet-derived 3 beta |
| Reg3g | -14.00 | -14.92[c] | Regenerating islet-derived 3 gamma |
| Nupr1 | -2.28[a] | - | Nuclear protein, transcriptional regulator, 1 |
| **Cell Proliferation, Differentiation and Migration** | | | |
| Fos | -4.14[b] | - | FBJ osteosarcoma oncogene |
| Jun | -2.64-3.08[b] | - | Jun oncogene |
| Mapt | -2.16[c] | - | Microtubule-associated protein tau |
| Wif1 | -2.20[a] | - | Wnt inhibitory factor 1 |
| Atf4 | - | - | Activating transcription factor 4 |
| Ppm1b | - | - | Protein phosphatase 1B, beta isoform |
| **Positive Regulation of Insulin Secretion, Peptide Processing, and Vesicular Transport** | | | |
| Gipr | -2.13[b] | - | Gastric Inhibitory Polypeptide Receptor |
| Nnat | -4.40[b] | - | Neuronatin |
| Serp1 | - | - | Stress-associated endoplasmic reticulum protein 1 |
| Snap25 | - | - | Synaptosomal-associated protein 25 |
| TRH | -6.65[b] | -3.00[b] | Thyrotropin releasing hormone |
| Apln | - | - | Apelin |
| Cadps | - | - | Calcium-dependent secretion activator |
| Pcsk2 | -2.15[b] | - | Proprotein convertase subtilisin/kexin type 2 |
| P2ry1 | -4.01[a] | - | Purinergic Receptor P2Y, G-protein coupled 1 |
| Rab27a | -2.40[b] | - | Rab27a, member RAS oncogene family |
| Rab3b | -2.35[b] | - | Rab3b, member RAS oncogene family |
| Tram1 | -2.10[b] | - | Translocation associated membrane protein 1 |
| Spcs2 | -2.10[b] | - | Signal peptidase complex subunit 2 homolog |
| Rapgef4 | - | - | Rap guanine nucleotide exchange factor 4 |
| Hspa1b | -4.00[b] | - | Heat shock 70kD protein 1B |
| Scfd1 | - | - | Sec family domain containing 1 |
| **Glucose Metabolism** | | | |
| AldoB | 21.10[c] | 13.85[c] | Aldolase B, fructose-bisphosphate |
| Prkacb | -2.30[c] | - | Protein kinase, cAMP dependent, catalytic, beta |

| | | | |
|---|---|---|---|
| Prkar1a | 2.01 | - | Protein kinase, cAMP dependent, regulatory, type 1 alpha |
| Sst | -2.44[b] | - | Somatostatin |
| **Positive Regulation of Apoptosis** | | | |
| Gal | 3.18[b] | - | Galanin proteptide |
| Txnip | 2.80[b] | 2.71[b] | Thioredoxin interacting protein |
| Gch1 | -2.04[b] | - | GTP cyclohydrolase 1 |
| App | -2.11[b] | - | Amyloid beta (A4) precursor protein |
| Nell1 | -2.12[b] | - | NEL-like 1 (chicken) |
| Siva1 | -2.23[a] | - | SIVA1, apoptosis-inducing factor |
| Kcnma1 | -2.25[b] | - | Potassium large conductance calcium-activated channel, subfamily M, alpha member 1 |
| Il1r1 | -2.29[b] | - | Interleukin 1 receptor, type 1 |
| Dusp1 | -2.32[b] | - | Dual specificity phosphatase 1 |
| **Negative Regulation of Apoptosis** | | | |
| Vegfa | 2.02[c] | - | Vascular endothelial growth factor A |
| Dnajb9 | -2.05[a] | - | DnaJ (Hsp40) homolog, subfamily B, member 9 |
| Wfs1 | -2.15[b] | - | Wolfram syndrome 1 homolog (human) |
| Btg2 | -2.26-2.42[b] | - | B-cell translocation gene 2 |
| Nfkbia | -2.43[c] | - | Nuclear factor of kappa light polypeptide gene enhancer in B-cells inhibitor, alpha |
| Scg2 | -2.44[b] | - | Secretogranin II |
| Hspa1b | -4.00[b] | - | Heat shock 70kD protein 1B |
| Sod2 | | | Manganese superoxide dismutase, mitochondrial |
| Irak1 | - | - | Interleukin-1 receptor-associated kinase 1 |

**Table 1. Gene Expression Profile in Failing Islet Cells.** The effect of islet cell failure on the expression of selected differentially expressed genes. A range of fold change values is presented for genes that were represented by multiple probes on the Affymetrix microarray. Positive values indicate upregulation in UT animals, and negative values indicate downregulation in UT animals as compared with the latter group in each pair wise comparison. Significance was calculated by a two-tailed student's t-test ([a], $p<0.05$; [b], $p<0.01$; [c], $p<0.001$).

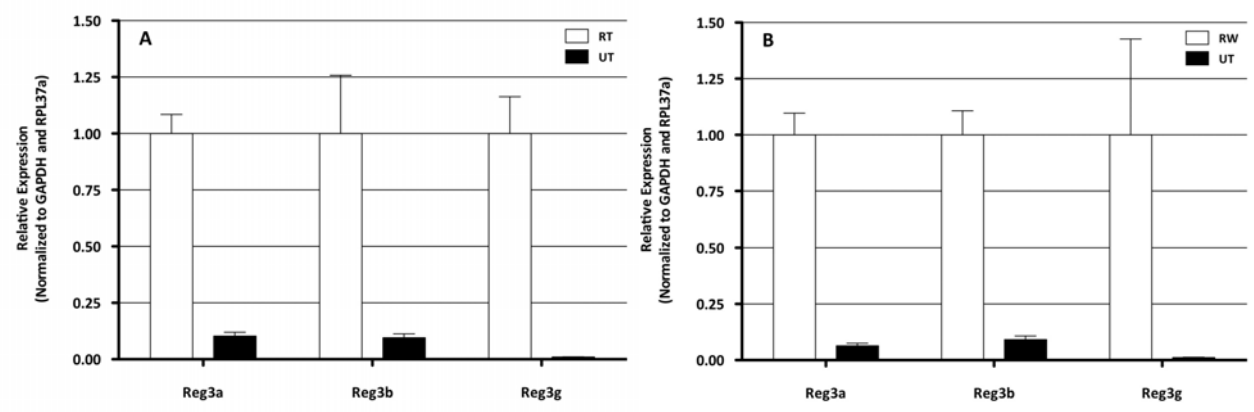


**Figure 4.** Quantitative PCR confirmation of Reg3a, Reg3b and Reg3g in response to (A) long-term islet cell failure (UT vs. RT), (B) acute islet cell failure (UT vs. RW), (C)???, and (D) ???. The normalized expression of each gene is corrected for the average expression of *GAPDH* and *RPL37a* and is expressed in arbitrary units. Values are means ± SEM, and significance was calculated by two-tailed student's t-test vs. the latter group in each comparison (*, $p<0.05$; **, $p<0.01$; ***, $p<0.001$).

We found that genes involved in the regulation of insulin secretion, peptide processing and vesicular transport displayed a consistent 2.0 to 2.7-fold downregulation in RW animals in comparison with RT animals, including *Serp1, Snap25, Cadps, Rapgef4, Scfd1*, and the previously identified genes *Gipr, Nnat, Pcsk2, P2ry1, Rab27a, Rab3b, Tram1*, and *Spcs2*. Additionally, master beta cell transcription factors *Pdx-1, Nkx2.2, Nkx6.1, FoxA2, Pax6*, and *NeuroD1* were downregulated between 2.0 and 2.7-fold. *Pdx-1* is an important transcription factor that promotes the expression of insulin, *Glut-2, Nkx-6.1, IAP*, and *Nkx-6.1*, while *Nkx-6.1* is a beta cell transcription factor which binds to the insulin promoter to initiate insulin gene expression [16,17].

In comparison with UT animals, RW animals displayed minor differences in the expression of genes involved in (a) islet cell proliferation, differentiation and migration, (b) positive regulation of insulin secretion, peptide processing and vesicular transport, (c) master islet cell transcription factors, (d) genes that promote apoptosis, and (e) genes that negatively regulate apoptosis. Interestingly, these data indicate that the gene expression profile of hyperproliferating islet cells closely matches that of failed islet cells despite significant differences in islet cell proliferative capacity.

### PCR Confirmation of Gene Targets

Given that gene expression profiling identified a significant downregulation of regenerating islet-derived genes, we confirmed the expression of all genes involved in pancreatic regeneration and inflammation, including *Reg3a, Reg3b, Reg3g*, and *Nupr1* using quantitative PCR. The selected gene expression followed microarray trends (Figure 4A-D). In addition, we confirmed the expression of selected genes from the functional pathways discussed above in order to validate microarray expression values (Figure 4E-X). IS THIS NECESSARY?

## Discussion

These data demonstrate a number of novel findings regarding islet cell physiology and gene expression in response to insulin resistance and diabetes. We show that the rosiglitazone treatment-and-withdrawal regimen was an effective tool to synchronize the transition of ZDF rats to compensated insulin resistance and diabetes. Removal of the insulin sensitizing agent rosiglitazone from the diet triggered acute onset insulin resistance, and a rapid increase in islet cell proliferation that persisted for only two weeks. This period of islet cell hyperproliferation is then followed by an immediate and sharp decline in islet cell proliferative capacity that marked the transition to diabetes. Together, these dynamic results suggest that islet cell hyperproliferation reveals an important physiological response to insulin resistance in that blood glucose values are maintained at the expense of large increases in islet cell mass and insulin secretion. Maintenance of insulin sensitivity preserved the capacity of islet cells to proliferate later in life in response to the emergence of insulin resistance. Our findings imply that the failure of islet cell proliferation is not a temporally programmed intrinsic feature of the ZDF phenotype, but is rather influenced by ambient insulin secretory burden. Thus, in ZDF rats early treatment of insulin resistance reduces the need for islet cell proliferation and prolongs the subsequent capacity for islet cell expansion, preserving the ability to adequately regulate glucose homeostasis at later stages of life. Most importantly, there appears to be a finite islet cell proliferative reserve.

Using genome-wide gene expression profiling, we demonstrated that the *Reg* family of genes (*Reg3a, Reg3b,* and *Reg3g*) are significantly downregulated in response to islet failure. We show that in diabetic animals, *Reg3b* and *Reg3g* are downregulated in comparison with both insulin sensitive and insulin resistant animals. This family of regenerating islet-derived genes encodes secretory proteins that play roles in recruiting macrophages to sites of inflammation in many organs, including the pancreas, bowel, liver, ovaries and heart, and are associated with islet cell regeneration and inflammation [18].

Previous studies have shown that the family of *Reg* genes encode secretory proteins of the endocrine and exocrine pancreas that act as growth stimulants to promote cell proliferation and neogenesis in response to stress in humans and in rodents [19]. Since the original discovery that *Reg* mRNA is increased in regenerating islets of depancreatized rats treated with the islet growth stimulant nicotinamide (okamoto, 1987), many studies have shown that *Reg* proteins regulate apoptosis, cell regeneration, cell proliferation, and inflammation in response to endocrine and exocrine cell damage [18,20]. Importantly, *Reg* gene products have been identified as important markers of beta cell stress and acute phase pancreatitis [21].

Expression of *Reg3a* is associated with islet cell expansion, and studies have shown that *Reg3a* transcript and protein levels are significantly increased in humans with type 1 or type 2 diabetes, and during pregnancy [21–24].

While the direct effect of *Reg3b* expression on beta cells has yet to be

established, the function of *Reg3b* in liver tissue closely resembles that of *Reg1* in stimulating pancreatic regeneration. It has been proposed that *Reg3b* promotes islet cell proliferation, cell survival, insulin secretion, and neogenesis [25,26].

Previous work has shown that islet cell proliferation and regeneration promotes an increased expression of *Reg* proteins [23] MORE REFS HERE, yet we are the first to show that the ensuing failure of islet cells downregulates *Reg* expression *in vivo*. Previous work has demonstrated that *Reg3a* is downregulated in human gastric carcinomas [27] MORE REFS HERE, yet to date a reduced expression of *Reg* genes in failing islets has not been reported.

In addition, we found that long-term islet failure reduced *Nupr1* gene expression by 2.28-fold, a beta cell nuclear protein that enhances islet cell growth, survival and function [26]. *Nupr1* was originally identified in acinar cells in response to acute pancreatitis, but has now been shown to regulate beta cell growth and apoptosis [28]. Our results support the finding that *Reg3b* and *Nupr1* participate in a coordinated two-way feedback [28].

*TRH* was found to be downregulated in response to islet failure by 6.65-fold in comparison with RT animals, and 3.0-fold in comparison with RW animals. Pancreatic *TRH* has two principal effects: (a) positive regulation of glucagon secretion, and (b) attenuation of exocrine secretion. *TRH* content in rat islets is high during growth and development and decreases into adulthood [29]. This hormone is localized and secreted with insulin, and is correlated with insulin secretory capacity of the islet cell [29,30]. Our data demonstrate that islet cell failure is coupled with a reduced *TRH* transcript level, supporting a role for *TRH* in regulating GSIS. These results provide evidence that *TRH* expression and insulin secretion play a coordinated role in maintaining beta cell function in the adult rat pancreas.

We found that *Pdx-1* expression was downregulated by insulin resistance, suggesting a pivotal role for this transcription factor in the regulation of GSIS. While *Pdx-1* primarily mediates the secretion of insulin, *Pdx-1* also plays a role in beta cell neogenesis, differentiation, and apoptosis [31,32]. *Pdx-1* is the principal regulator of GSIS, and is expressed in both insulin-producing beta cells and somatostatin-producing delta cells. Elevations in circulating glucose increase beta cell glycolytic flux which translocates *Pdx-1* to the nucleus where it regulates the transcription of genes involved in beta cell maturation, including *GLUT2, Gck, Sst, Iap,* and *MafA* [33–36]. These data support our findings that *Pdx-1* expression is downregulated by insulin resistance, supporting a central role for Pdx-1 in regulating the transcription of genes that promote islet cell function.

In this study, the emergence of insulin resistance stimulated a net downregulation of master islet cell transcription factors, including *Pdx-1, Nkx2.2, Nkx6.1, FoxA2, Pax6*, and *NeuroD1*. Specifically, we found that insulin resistance resulted in a 2.3-fold downregulation of *Nkx6.1*, a beta-cell specific gene that may function downstream of *Nkx2.2* [37,38]. Interestingly, *Nkx2.2* knockout mice develop severe hyperglycemia and die shortly after birth [39], while mutation of the *Nkx6.1* gene eliminates beta cell neogenesis and results

| Gene Symbol | Fold Change RW vs. RT | Fold Change RW vs. UT | Gene Name |
|---|---|---|---|
| **Pancreatic Regeneration and Inflammation** | | | |
| Reg3a | - | 2.36[b] | Regenerating islet-derived 3 alpha |
| Reg3b | - | 2.94[b] | Regenerating islet-derived 3 beta |
| Reg3g | - | 14.92[c] | Regenerating islet-derived 3 gamma |
| Nupr1 | - | - | Nuclear protein, transcriptional regulator, 1 |
| **Cell Proliferation, Differentiation and Migration** | | | |
| Fos | -3.34[a] | - | FBJ osteosarcoma oncogene |
| Jun | -2.18-2.52[a] | - | Jun oncogene |
| Mapt | -2.03[c] | - | Microtubule-associated protein tau |
| Wif1 | -2.57[b] | - | Wnt inhibitory factor 1 |
| Atf4 | -2.12[b] | - | Activating transcription factor 4 |
| Ppm1b | -2.01[b] | - | Protein phosphatase 1B, beta isoform |
| **Positive Regulation of Insulin Secretion, Peptide Processing, and Vesicular Transport** | | | |
| Gipr | -2.02[b] | - | Gastric Inhibitory Polypeptide Receptor |
| Nnat | -2.93[b] | - | Neuronatin |
| Serp1 | -2.12[b] | - | Stress-associated endoplasmic reticulum protein 1 |
| Snap25 | -2.14[c] | - | Synaptosomal-associated protein 25 |
| TRH | - | 3.0[b] | Thyrotropin releasing hormone |
| Apln | 2.06[b] | - | Apelin |
| Cadps | -2.00[c] | - | Calcium-dependent secretion activator |
| Pcsk2 | -2.1[b] | - | Proprotein convertase subtilisin/kexin type 2 |
| P2ry1 | -2.26 | - | Purinergic Receptor P2Y, G-protein coupled 1 |
| Rab27a | -2.07[b] | - | Rab27a, member RAS oncogene family |
| Rab3b | -2.26[b] | - | Rab3b, member RAS oncogene family |
| Tram1 | -2.1[c] | - | Translocation associated membrane protein 1 |
| Spcs2 | -2.2[c] | - | Signal peptidase complex subunit 2 homolog |
| Rapgef4 | -2.30[b] | - | Rap guanine nucleotide exchange factor 4 |
| Hspa1b | - | - | Heat shock 70kD protein 1B |
| Scfd1 | -2.24[b] | - | Sec family domain containing 1 |
| **Master Islet Cell Transcription Factors** | | | |
| Pdx-1 | -2.1[c] | - | Pancreatic and duodenal homeobox 1 |
| Nkx2.2 | -2.1[c] | - | NK2 homeobox 2 |

| | | | |
|---|---|---|---|
| Nkx6.1 | -2.3[c] | - | NK6 homeobox 1 |
| FoxA2 | -2.0[b] | - | Forkhead box A2 |
| Pax6 | -2.7[b] | - | Paired box 6 |
| NeuroD 1 | -2.3[c] | - | Neurogenic differentiation 1 |
| Slc2a2 | -2.01[c] | - | Solute carrier 2 (facilitated glucose transporter), member 2 (Glut-2) |
| **Glucose Metabolism** | | | |
| AldoB | - | -13.85[c] | Aldolase B, fructose-bisphosphate |
| Prkacb | -2.12[c] | - | Protein kinase, cAMP dependent, catalytic, beta |
| Prkar1a | - | - | Protein kinase, cAMP dependent, regulatory, type 1 alpha |
| Sst | -3.80[c] | - | Somatostatin |
| **Positive Regulation of Apoptosis** | | | |
| Gal | - | - | Galanin proteptide |
| Txnip | - | -2.71[b] | Thioredoxin interacting protein |
| Gch1 | - | - | GTP cyclohydrolase 1 |
| App | - | - | Amyloid beta (A4) precursor protein |
| Nell1 | - | - | NEL-like 1 (chicken) |
| Siva1 | -2.03[a] | - | SIVA1, apoptosis-inducing factor |
| Kcnma1 | - | - | Potassium large conductance calcium-activated channel, subfamily M, alpha member 1 |
| Il1r1 | -2.09[b] | - | Interleukin 1 receptor, type 1 |
| Dusp1 | -2.35[b] | - | Dual specificity phosphatase 1 |
| **Negative Regulation of Apoptosis** | | | |
| Vegfa | -2.07-2.09[c] | - | Vascular endothelial growth factor A |
| Dnajb9 | -2.38[c] | - | DnaJ (Hsp40) homolog, subfamily B, member 9 |
| Wfs1 | - | - | Wolfram syndrome 1 homolog (human) |
| Btg2 | -2.01-2.27[a] | - | B-cell translocation gene 2 |
| Nfkbia | -2.03[b] | - | Nuclear factor of kappa light polypeptide gene enhancer in B-cells inhibitor, alpha |
| Scg2 | -2.05[c] | - | Secretogranin II |
| Hspa1b | -2.52 | - | Heat shock 70kD protein 1B |
| Sod2 | -2.16[a] | | Manganese superoxide dismutase, mitochondrial |

| | | | |
|---|---|---|---|
| Irak1 | -2.04[b] | - | Interleukin-1 receptor-associated kinase 1 |

**Table 2. Gene Expression Profile in Hyperproliferating Islet Cells.** The effect of islet cell hyperproliferation on the expression of selected differentially expressed genes. A range of fold change values is presented for genes that were represented by multiple probes on the Affymetrix microarray. Positive values indicate upregulation in RW animals, and negative values indicate downregulation in RW animals as compared with the latter group in each pair wise comparison. Significance was calculated by a two-tailed student's t-test ([a], $p<0.05$; [b], $p<0.01$; [c], $p<0.001$).

in a complete loss of beta cell precursor cells [40]. In addition, *FoxA1* and *FoxA2* play distinct roles in the secretion of many endocrine hormones in tissues including the pancreas [41,42]. We found that acute induction of insulin resistance stimulated a 2-fold downregulation of *FoxA2*, likely contributing to insulin secretion abnormalities. In addition, it has been demonstrated that *Pax6* controls the transcription of *Pcsk2* and *NeuroD1*, genes involved in the transactivation of insulin expression [43,44]. Mutation of *NeuroD1* causes MODY6 in humans, and severe glucose intolerance in mice [44], indicating that *NeuroD1* is required for proper beta cell maturation. In the present study, we demonstrate that islet cell hyperplasia is coincident with a 2.7-fold downregulation of *Pax6*, a 2.1-fold downregulation of *Pcsk2*, and a 2.3-fold downregulation of *NeuroD1*. These findings are consistent with previous studies that identify *Pdx-1, Nkx2.2, Nkx6.1, FoxA2, Pax6*, and *NeuroD1* as crucial determinants of beta cell maturation and the reprogramming of extrapancreatic tissue to glucose-responsive insulin-producing cells [45].

One limitation of this study is whether the transcriptional effects of islet cell hyperproliferation and failure are due to rosiglitazone withdrawal and the inactivation of *PPAR-gamma*. A growing body of evidence supports a direct effect of *PPAR-gamma* agonists on beta cell function in humans and in rodents [46–48]. In a recent study, it was shown that beta cell-specific *PPAR-gamma* deletion blunted increases in beta cell mass in insulin resistant mice, suggesting that beta cell *PPAR-gamma* is required for beta cell proliferation [49]. In another pancreatic-specific *PPAR-gamma* knockout mouse model, isolated islets were not hyperplastic, and showed blunted GSIS and downregulation of the genes *Pdx-1* and *GLUT2*, highlighting the role of *PPAR-gamma* in mediating islet cell maturation [50].

In line with this reasoning, we found that genes involved in the regulation of insulin secretion, peptide processing, and vesicular transport were downregulated only in comparison with RT animals. We observed that in UT and RW animals, these genes were downregulated between 2.00 and 6.65-fold, suggesting that this family of genes is sensitive to rapid alterations in islet cell metabolism induced by either insulin resistance or diabetes. These data suggest that the direct effects of *PPAR-gamma* deactivation may be responsible for our observed gene expression results. The inactivation of beta cell *PPAR-gamma* has been shown to result in a number of pro-apoptotic beta cell mechanisms, including the activation of endoplasmic reticulum stress pathways [51], oxidative stress [52], and

lipotoxicity [53]. Collectively, our study supports the idea that *PPAR-gamma* deactivation results either in the direct transcriptional reprogramming of beta cells or in the evolution of insulin resistance, resulting in profound islet cell abnormalities and the eventual ablation of insulin secretion.

In summary, this experimental approach provided insight into the pattern of gene expression that regulates both the hyperplastic and failure mechanisms. By combining physiological data with transcriptional profiling, we demonstrated for the first time important changes in gene expression in response to islet cell hyperproliferation and failure in the same animals *in vivo*. The genes identified here play a role in the response of islets to increased demand for insulin secretion, and are involved in the regulation of islet cell maintenance, hyperproliferation, and failure. *Reg3a, Reg3b,* and *Reg3g* proteins are exciting candidate biomarkers of islet cell hyperplasia and failure, and further studies are needed to clarify the potential regulatory role of *Reg3* gene products in directing islet cell proliferation in response to insulin resistance.

## Acknowledgements

The authors would like to recognize the efforts of Larry Thompson, Olga O'Connor, Antonio Moreno**,** Airlia Thompson, Matthew Bruss, Simply Floracruz, Deona Villegas and the staff of the Northwest Animal Facility at UC Berkeley, including Julio Gonzalez, Bob Williams, Bennie Mitchell, and Joan Wallace. These people are being recognized for their outstanding behind-the-scenes work at making this research possible. In addition, the authors would like to thank Robert J. Rooney, PhD at Genome Explorations, Inc (Memphis, TN) for his invaluable assistance and patience in performing bioinformatic analysis.

## Contribution Statement

C.K. and S.T. wrote and reviewed the manuscript, C.K. researched data, S.T. helped design the experiment, E.T. performed islet cell proliferation analysis and edited the manuscript, M.S. performed islet cell proliferation analysis and edited the manuscript, S.C. performed islet cell proliferation analysis and reviewed the manuscript, P.M. helped design the experiment and edited the manuscript, L.R. performed background research and reviewed the manuscript, M.D. performed background research and edited the manuscript, and M.H. designed the experiment, developed the tracer techniques, maintained quality assurance of the laboratory processes, and reviewed the manuscript.

## Duality of Interest

Authors affiliated with Kinemed, Inc. disclose a conflict of interest in that products/services of this company are directly related to the treatment of type 2 diabetes. The authors with this affiliation receive financial support for employment (S.T., E.T), board membership (M.H.), consultancy (M.H), stock options (M.H., S.T., E.T.), and travel accommodations (M.H., S.T.).

## Literature Cited


1. Danaei, G. *et al.* National, regional, and global trends in fasting plasma glucose and diabetes prevalence since 1980: systematic analysis of health examination surveys and epidemiological studies with 370 country-years and 2·7 million participants. *The Lancet* **378**, 31–40 (2011).
2. Kloppel, G., Lohr, M., Habich, K., Oberholzer, M. & Heitz, P. U. Islet pathology and the pathogenesis of type 1 and type 2 diabetes mellitus revisited. *Surv Synth Pathol Res* **4**, 110–25 (1985).
3. Lingohr, M. K., Buettner, R. & Rhodes, C. J. Pancreatic beta-cell growth and survival--a role in obesity-linked type 2 diabetes? *Trends Mol Med* **8**, 375–384 (2002).
4. Bonner-Weir, S. Islet growth and development in the adult. *J. Mol. Endocrinol.* **24**, 297–302 (2000).
5. Bruning, J. C. *et al.* Development of a novel polygenic model of NIDDM in mice heterozygous for IR and IRS-1 null alleles. *Cell* **88**, 561–72 (1997).
6. Pick, A. *et al.* Role of apoptosis in failure of beta-cell mass compensation for insulin resistance and beta-cell defects in the male Zucker diabetic fatty rat. *Diabetes* **47**, 358 –364 (1998).
7. Unger, R. H. & Orci, L. Diseases of liporegulation: new perspective on obesity and related disorders. *FASEB J.* **15**, 312–321 (2001).
8. Finegood, D. T. *et al.* Beta-cell mass dynamics in Zucker diabetic fatty rats. Rosiglitazone prevents the rise in net cell death. *Diabetes* **50**, 1021–1029 (2001).
9. Busch, R., Neese, R. A., Awada, M., Hayes, G. M. & Hellerstein, M. K. Measurement of cell proliferation by heavy water labeling. *Nat Protoc* **2**, 3045–3057 (2007).
10. Chen, S. *et al.* Measurement of pancreatic islet cell proliferation by heavy water labeling. *Am. J. Physiol. Endocrinol. Metab.* **293**, E1459–1464 (2007).
11. Neese, R. A. *et al.* Measurement in vivo of proliferation rates of slow turnover cells by 2H2O labeling of the deoxyribose moiety of DNA. *Proc. Natl. Acad. Sci. U.S.A.* **99**, 15345–15350 (2002).
12. Hubbell, E., Liu, W. M. & Mei, R. Robust estimators for expression analysis. *Bioinformatics* **18**, 1585–92 (2002).
13. Irizarry, R. A., Wu, Z. & Jaffee, H. A. Comparison of Affymetrix GeneChip expression measures. *Bioinformatics* **22**, 789–94 (2006).
14. Huang da, W., Sherman, B. T. & Lempicki, R. A. Systematic and integrative analysis of large gene lists using DAVID bioinformatics resources. *Nat Protoc* **4**, 44–57 (2009).
15. Dennis, G. *et al.* DAVID: Database for Annotation, Visualization, and Integrated Discovery. *Genome Biol* **4**, P3 (2003).
16. Harmon, J. S. *et al.* In vivo prevention of hyperglycemia also prevents glucotoxic effects on PDX-1 and insulin gene expression. *Diabetes* **10.2337/diabetes.48.10.1995**,
17. Moibi, J. A. *et al.* Peroxisome proliferator-activated receptor-gamma regulates expression of PDX-1 and NKX6.1 in INS-1 cells. *Diabetes* **10.2337/db06-0948**,
18. Viterbo, D. *et al.* Pancreatitis-associated protein 2 modulates inflammatory responses in macrophages. *J. Immunol.* **181**, 1948–1958 (2008).
19. Watanabe, T. *et al.* Pancreatic beta-cell replication and amelioration of surgical diabetes by Reg protein. *Proc. Natl. Acad. Sci. U.S.A.* **91**, 3589–3592 (1994).
20. Li, B., Wang, X. & Liu, J.-L. Pancreatic acinar-specific overexpression of Reg2 gene offered no protection against either experimental diabetes or pancreatitis in

mice. *Am. J. Physiol. Gastrointest. Liver Physiol.* **299**, G413–421 (2010).
21. Marselli, L. *et al.* Gene expression profiles of Beta-cell enriched tissue obtained by laser capture microdissection from subjects with type 2 diabetes. *PLoS ONE* **5**, e11499 (2010).
22. Shervani, N. J. *et al.* Autoantibodies to REG, a beta-cell regeneration factor, in diabetic patients. *Eur. J. Clin. Invest.* **34**, 752–758 (2004).
23. Xue, Y. *et al.* Study on pancreatic islet adaptation and gene expression during pregnancy in rats. *Endocrine* **37**, 83–97 (2010).
24. Gurr, W., Shaw, M., Li, Y. & Sherwin, R. RegII is a beta-cell protein and autoantigen in diabetes of NOD mice. *Diabetes* **56**, 34–40 (2007).
25. Okamoto, H. The Reg gene family and Reg proteins: with special attention to the regeneration of pancreatic beta-cells. *J Hepatobiliary Pancreat Surg* **6**, 254–62 (1999).
26. Xiong, X. *et al.* Pancreatic islet-specific overexpression of Reg3β protein induced the expression of pro-islet genes and protected the mice against streptozotocin-induced diabetes mellitus. *Am. J. Physiol. Endocrinol. Metab.* **300**, E669–680 (2011).
27. Choi, B. *et al.* Downregulation of regenerating islet-derived 3 alpha (REG3A) in primary human gastric adenocarcinomas. *Exp. Mol. Med.* **39**, 796–804 (2007).
28. Päth, G., Opel, A., Knoll, A. & Seufert, J. Nuclear protein p8 is associated with glucose-induced pancreatic beta-cell growth. *Diabetes* **53 Suppl 1**, S82–85 (2004).
29. Ebiou, J. C., Bulant, M., Nicolas, P. & Aratan-Spire, S. Pattern of thyrotropin-releasing hormone secretion from the adult and neonatal rat pancreas: comparison with insulin secretion. *Endocrinology* **130**, 1371–9 (1992).
30. Luo, L. G. & Jackson, I. Thyrotropin releasing hormone (TRH) may preserve pancreatic islet cell function: potential role in the treatment of diabetes mellitus. *Acta Biomed* **78 Suppl 1**, 216–21 (2007).
31. Jonsson, J., Carlsson, L., Edlund, T. & Edlund, H. Insulin-promoter-factor 1 is required for pancreas development in mice. *Nature* **371**, 606–9 (1994).
32. Shao, S., Fang, Z., Yu, X. & Zhang, M. Transcription factors involved in glucose-stimulated insulin secretion of pancreatic beta cells. *Biochem Biophys Res Commun* **384**, 401–4 (2009).
33. Waeber, G., Thompson, N., Nicod, P. & Bonny, C. Transcriptional activation of the GLUT2 gene by the IPF-1/STF-1/IDX-1 homeobox factor. *Mol Endocrinol* **10**, 1327–34 (1996).
34. Raum, J. C. *et al.* FoxA2, Nkx2.2, and PDX-1 regulate islet beta-cell-specific mafA expression through conserved sequences located between base pairs -8118 and -7750 upstream from the transcription start site. *Mol Cell Biol* **26**, 5735–43 (2006).
35. Petersen, H. V. *et al.* Glucose stimulates the activation domain potential of the PDX-1 homeodomain transcription factor. *FEBS Lett* **431**, 362–6 (1998).
36. Lebrun, P., Montminy, M. R. & Van Obberghen, E. Regulation of the pancreatic duodenal homeobox-1 protein by DNA-dependent protein kinase. *J Biol Chem* **280**, 38203–10 (2005).
37. Bernardo, A. S., Hay, C. W. & Docherty, K. Pancreatic transcription factors and their role in the birth, life and survival of the pancreatic beta cell. *Mol Cell Endocrinol* **294**, 1–9 (2008).
38. Sander, M. *et al.* Homeobox gene Nkx6.1 lies downstream of Nkx2.2 in the major pathway of beta-cell formation in the pancreas. *Development* **127**, 5533–40 (2000).
39. Sussel, L. *et al.* Mice lacking the homeodomain transcription factor

Nkx2.2 have diabetes due to arrested differentiation of pancreatic beta cells. *Development* **125**, 2213–21 (1998).
40. Nelson, S. B., Schaffer, A. E. & Sander, M. The transcription factors Nkx6.1 and Nkx6.2 possess equivalent activities in promoting beta-cell fate specification in Pdx1+ pancreatic progenitor cells. *Development* **134**, 2491–500 (2007).
41. Friedman, J. R. & Kaestner, K. H. The Foxa family of transcription factors in development and metabolism. *Cell Mol Life Sci* **63**, 2317–28 (2006).
42. Gao, N. *et al.* Foxa1 and Foxa2 maintain the metabolic and secretory features of the mature beta-cell. *Mol Endocrinol* **24**, 1594–604
43. Gosmain, Y. *et al.* Pax6 controls the expression of critical genes involved in pancreatic {alpha} cell differentiation and function. *J Biol Chem* **285**, 33381–93
44. Gu, C. *et al.* Pancreatic beta cells require NeuroD to achieve and maintain functional maturity. *Cell Metab* **11**, 298–310
45. Ferber, S. *et al.* Pancreatic and duodenal homeobox gene 1 induces expression of insulin genes in liver and ameliorates streptozotocin-induced hyperglycemia. *Nat Med* **6**, 568–72 (2000).
46. Cavaghan, M. K., Ehrmann, D. A., Byrne, M. M. & Polonsky, K. S. Treatment with the oral antidiabetic agent troglitazone improves beta cell responses to glucose in subjects with impaired glucose tolerance. *J. Clin. Invest.* **100**, 530–537 (1997).
47. Gupta, D., Kono, T. & Evans-Molina, C. The role of peroxisome proliferator-activated receptor gamma in pancreatic beta cell function and survival: therapeutic implications for the treatment of type 2 diabetes mellitus. *Diabetes Obes Metab* **12**, 1036–47
48. Kim, H. I. & Ahn, Y. H. Role of peroxisome proliferator-activated receptor-gamma in the glucose-sensing apparatus of liver and beta-cells. *Diabetes* **10.2337/diabetes.53.2007.S60**,
49. Rosen, E. D. *et al.* Targeted elimination of peroxisome proliferator-activated receptor gamma in beta cells leads to abnormalities in islet mass without compromising glucose homeostasis. *Mol. Cell. Biol.* **23**, 7222–7229 (2003).
50. Gupta, D. *et al.* In vivo and in vitro studies of a functional peroxisome proliferator-activated receptor gamma response element in the mouse pdx-1 promoter. *J Biol Chem* **283**, 32462–70 (2008).
51. Schroder, M. & Kaufman, R. J. ER stress and the unfolded protein response. *Mutat Res* **569**, 29–63 (2005).
52. Li, N., Frigerio, F. & Maechler, P. The sensitivity of pancreatic beta-cells to mitochondrial injuries triggered by lipotoxicity and oxidative stress. *Biochem Soc Trans* **36**, 930–4 (2008).

# Chapter 4

## The Effect of Insulin Resistance and Diabetes on Islet Cell Protein Dynamics: A Combination of Dynamic and Quantitative Proteomics

Cyrus F. Khambatta*‡, Matthew D. Bruss†‡, John C. Price#,
Marcy Dalidd*, Lindsay S. Roberts*, William E. Holmes#
Kelvin E. Lee#, Scott M. Turner#, and Marc K. Hellerstein*

‡ These authors contributed to this work equally

*Department of Nutritional Sciences and Toxicology,
University of California at Berkeley, Berkeley, California 94720
†Department of Biochemistry, University of Wisconsin-Madison, Madison, WI, 53706
# KinemedInc, Emeryville, CA 94608

**Abstract**

Insulin resistance and islet cell failure are the two fundamental processes underlying type 2 diabetes. Alterations in mitochondrial protein turnover have been implicated in the pathology of type 2 diabetes, however the specific effect of insulin resistance and diabetes on the intracellular dynamic islet proteome have yet to be described. In this study, we investigated the effects of insulin resistance and diabetes on the synthesis of proteins from isolated rat islets for the first time, using both $^2H_2O$ (heavy water) labeling and SILAM quantitative proteomics. Using this approach, we measured fractional and absolute synthesis rates of cytoskeletal, glycolytic, mitochondrial, ER, and ribosomal proteins, the principal pathways responsible for glucose stimulated insulin secretion (GSIS). We found that insulin resistance increased the fractional synthesis rates (FSR) of 97% of all measured islet proteins, and the subsequent transition to diabetes resulted

in the selective impairment of ribosomal protein synthesis. Absolute synthesis rates followed the same trend; insulin resistance increased absolute turnover rates, and islet failure reduced this effect. Our findings suggest that the rapid rate of islet cell proliferation due to insulin resistance is accompanied by increased fractional and absolute synthesis of critical GSIS proteins, and that the failure of islets results mainly in impaired ribosomal pathway flux, independent of alterations in mitochondrial metabolism.

**Keywords**

Insulin Resistance, Diabetes, Protein turnover, Proteome Dynamics, Glucose Stimulated Insulin Secretion, Ribosomal Protein Synthesis, Isotopic Labeling.

## Introduction

Type 2 diabetes (T2D) is a condition of increasing global prevalence, which affected nearly 150 million people worldwide in the year 2000, and is estimated to grow to 300 million individuals by the year 2025[1]. The physiological basis of T2D includes two principal etiologies: insulin resistance (IR) and beta cell secretory failure[2]. In the early stages of the disease process, IR in peripheral tissues stimulates the proliferation of pancreatic islet cells to increase insulin biosynthesis and maintain normoglycemia[2–5]. The subsequent transition from IR to T2D is marked by the failure of islet cells to secrete insulin altogether, resulting in overt hyperglycemia[6–9]. Although the proliferative response of islet cells to IR and subsequent failure in diabetes has been well characterized, the underlying cellular mechanisms that differentiate the proliferative and failure states are poorly understood[2,10]. Therefore, understanding the molecular determinants of each is important in developing effective strategies to treat and prevent T2D.

It is commonly known that dysfunctions in protein turnover are associated with a number of age-related diseases, including diabetes, cancer, hypertension, cardiovascular disease, and Parkinson's disease[11,12]. An increasingly large body of evidence has shown that impairments in protein replacement result in the accumulation of misfolded proteins, cross-linked aggregates, and a reduced ability to degrade damaged proteins, resulting in aberrant cell behavior[13]. In insulin secreting beta cells, the ubiquitin-proteasome pathway mediates the expression of genes involved in glucose stimulated insulin secretion (GSIS)[14], providing an important connection between protein replacement and the regulation of glucose metabolism.

While microarray studies have uncovered key transcriptional regulators of IR-mediated islet cell dysfunction and failure[15–17], few studies have investigated the effect of IR on the islet cell proteome. More importantly, this is the first study to investigate the kinetics of islet cell protein synthesis and replacement, two integral processes which are critical indicators of islet cell health.

Both relative and quantitative proteomics have been applied to the study of diabetic mouse islet cells, identifying altered expression of proteins involved in insulin secretion, the unfolded protein response, ER-associated protein degradation, cytoskeletal remodeling, cell proliferation, and mitochondrial metabolism[18–20]. To this effect, an increasing body of evidence suggests that defects in mitochondrial

metabolism may play a central role in islet cell dysfuntion[21–27].

In this study, we combined *in vivo* stable isotope metabolic labeling using $^2H_2O$ (heavy water)[28] with exogenously labeled standards (SILAM)[29–31] to measure both fractional and absolute protein synthesis rates. This approach resulted in the calculation of synthesis and breakdown rates of many islet cell proteins using LC-MS/MS. The objective of this study was to employ a novel combination of dynamic and quantitative proteomics in order to determine fractional and absolute protein turnover rates across a large spectrum of the islet cell proteome in response to IR and diabetes for the first time. To study the effect of IR on islet cell protein turnover, we compared prediabetic insulin resistant Zucker Diabetic Fatty rats (7 week old ZDF) with Zucker Lean control rats (ZLC). To determine the effect of diabetes on islet cell protein turnover, we compared diabetic rats (15 week old ZDF) with Zucker Lean control rats (ZLC).

We found that IR significantly increased the fractional replacement rates of 97% of all measured islet proteins (75/77), including those involved in the endoplasmic reticulum, glycolysis, cytoskeletal remodeling, mitochondrial metabolism, and ribosomal protein synthesis, concomitant with a 2.8-fold increase in islet cell proliferation and severely diminished insulin sensitivity in comparison with control animals. In addition, we found that diabetes reversed this effect; protein fractional synthesis was significantly decreased in 48% of all measured islet proteins (39/80), and islet cell proliferation was decreased by 30% in comparison with control animals.

These findings demonstrate that peripheral IR (a) stimulates rapid increases in the rate of islet cell proliferation, (b) increases ribosomal pathway flux, responsible for the synthesis of both intracellular and secreted proteins, and (c) diabetes results in impaired islet cell proliferation and ribosomal pathway flux, independent of mitochondrial metabolism. Our data support the hypothesis that islet cell proteome dynamics are highly responsive to the levels of circulating glucose and insulin.

## Materials and Methods

### Animals

Four groups of animals were purchased from Charles River (Wilmington, MA): seven week old prediabetic ZDF rats (ZDFp), seven week old Zucker Lean Controls (ZLC), fifteen week old diabetic ZDF rats (ZDFd), and fifteen week old Zucker Lean Controls (ZLC). Following one week of acclimation, animals in each group were labeled with an intraperitoneal injection of isotonic 100% $^2H_2O$ (0.35mL/10g body weight), and were subsequently provided 8% $^2H_2O$ drinking water for the remainder of the study to maintain body $^2H_2O$ enrichments of approximately 5%, as described previously[32]. For dynamic proteomics experiments, animals were sacrificed following either 12 hours, 2 days or 5 days of $^2H_2O$ labeling (Figure 1B), and for SILAM quantitative proteomics all animals remained unlabeled (Figure 1A). Body weights and blood glucose were measured at the time of metabolic labeling and at the time of euthanasia. Animals were sacrificed via $CO_2$ asphyxiation followed by cervical dislocation and cardiac puncture. All

experiments were performed under the approval of the Institutional Animal Care and Use Committees of the University of California at Berkeley (IACUC).

### Islet Cell Isolation

Islet cells were isolated according to a pancreatic perfusion protocol that has been previously described[33]. Briefly, animals were euthanized by $CO_2$ asphyxiation and cervical dislocation. A clamp was placed at the distal end of the pancreatic duct at the entrance to the duodenum, and the pancreas was then perfused with 15mL HBSS (Sigma, St. Louis, MO) containing 2 mg/mL BSA (Sigma, St. Louis, MO) and 0.5 mg/mL collagenase Type X (Sigma, St. Louis, MO). Following perfusion, the pancreas was excised, removed from surrounding viscera, digested by shaking in a hot water bath 37°C and 160 rpm. Islet cells were then isolated by hand under microscopic visualization, and immediately frozen at -20°C until further analysis.

### Measurement of $^2H$ Enrichment in Body Water

Enrichment of $^2H_2O$ in body water (blood) was measured by IRIS. Briefly, whole blood was centrifuged at 6000g for 10 minutes at 4°C, and the plasma supernatant was removed and distilled at 45°C overnight. The plasma distillate (water) was then collected, and was then analyzed for $^2H/^{18}O$ isotopic enrichment by IRIS.

### Glucose Disposal Test and Measurment of Whole Body Glycolysis

Animals were given a 500uL intraperitoneal bolus injection of 10% $H_2{}^{18}O$ (Cambridge Isotopes, Andover, MA) to determine the total body water pool volume by dilution. Two hours later, animals were given an oral gavage of 10% [6,6-$^2$H]glucose (Cambridge Isotopes, Andover, MA) at a dose of 1g/kg body weight. Blood was sampled via tail vein bleed at baseline and 10 min post gavage and the blood was sampled directly into microcapillary tubes for the determination of $^2H_2O$ isotopic enrichment (25uL, Sarstedt 16.446.100) and plasma insulin concentrations (25uL, Sarstedt 16.444.100). Blood for isotopic enrichment was subsequently distilled at 45°C for two hours, and the distilled water was then analyzed for $^2H/^{18}O$ isotopic enrichment by IRIS. Insulin concentrations were assayed in duplicate using an ultrasensitive rat insulin ELISA kit (Crystal Chem, Downers Grove, IL). Blood glucose was taken at baseline (0 min), 10 min, 30 min, and 60 min post gavage using a hand held blood glucose monitor (Contour Ascencia, Bayer Corp.). Insulin sensitivity was calculated by the following equation:

$$SI=\Delta D_2O\ (\%)*GlucoseAUC^{-1}*InsulinAUC^{-1}$$

where $\Delta D_2O$ (%) represents the change in $D_2O$ isotopic enrichment (IE) in blood between the 0 and 60 minute time points; GlucoseAUC represents the integral of the glucose tolerance curve between 0 to 60 minutes; and InsulinAUC represents the integral of the insulin secretion curve between 0 to 60 minutes. Glucose and Insulin area under the curves (AUC) were calculated using the trapezoidal method.

### Immunohistochemistry

Whole pancreas was snap frozen in liquid $N_2$ in OCT (Sakura Finetek, Netherlands) and stored at -80°C until further analysis. Cryosections were cut at a thickness of 10um at -24°C and placed onto frostless

glass slides, and immediately transferred to -80°C. Slides were allowed to thaw for 2 minutes at room temperature, fixed in ice cold acetone for 60 seconds, then blocked for 1 hour in TBS-T containing 5% goat serum at room temperature. Slides were then incubated in rabbit monoclonal anti-insulin primary antibody (C27C9, Cell Signaling) at a dilution of 1:400 at 4C overnight. Slides were then incubated in an AlexaFluor 546 goat anti-rabbit secondary antibody (A1101, Invitrogen) at a dilution of 1:500 for 2 hours at room temperature. Images were taken using a Zeiss Axioimager M2 fluorescent microscope fitted with a digital color camera (Hamamatsu, Bridgewater, NJ) at a magnification of 1:400 using iVision software. Fluorescence intensity was quantified using ImageJ version 1.46 (NIH, Bethesda, MD).

### In Vivo Cell Proliferation

DNA was extracted from 50-200 islet cells using the DNeasy kit (Qiagen, Valencia, CA), and was enzymatically hydrolyzed to free deoxyribonucleosides by overnight incubation at 37°C with S1 nuclease and potato acid phosphatase. Hydrolysates were reacted with pentafluorobenzyl hydroxylamine and acetic acid and then acetylated with acetic anhydride and 1-methylimidazole. Dichloromethane extracts were dried, resuspended in ethyl acetate, and analyzed by gas chromatography-mass spectrometry on a DB-17 column with negative chemical ionization, using He as carrier and $CH_4$ as reagent gas. The fractional molar isotope abundances at m/z 435.2 ($M_0$ mass isotopomer) and 436.2 ($M_1$) of the pentafluorobenzyl triacetyl derivative of purine dR were quantified using ChemStation software. Excess fractional $M_{+1}$ enrichment ($EM_1$) was calculated as:

$$EM_1 = \frac{(AbundanceM_1)_{sample}}{(AbundanceM_0 + M_1)_{sample}} - \frac{(AbundanceM_1)_{standard}}{(AbundanceM_0 + M_1)_{standard}}$$

where sample and standard refer to the analyzed sample and an unenriched pentafluorobenzyl triacetyl purine dR derivative standard, respectively. The fractional replacement rate (f) was calculated by a comparison of $EM_1$ to the theoretical maximum $EM_1$ of a fully turned over tissue at the measured body water enrichment according to the following equation:

$$f = \frac{EM_{1\,sample}}{EM_{1\,maximum}}$$

### Protein Isolation and In-Gel Trypsin Digestion

Protein was isolated by tissue homogenization in RIPA buffer containing 0.1% SDS, 1uM DTT, PhosStop, 1nM trichostatin A, 1mg/mL leupeptinin, 1mg/mL pepstatin, 2mg/mL aprotinin, 100nM PMSF, and 100nM nicotinamide using a TissueLyser (Qiagen, Germantown, MD), followed by centrifugation at 10,000g for 10 minutes at 4 °C. The supernatant contained soluble proteins whereas the cell pellet was used for cell proliferation analysis. Protein from prepared homogenates was uniformly reduced by incubation in 10 mM DTT and SDS-PAGE sample loading buffer for 7 min at 95°C. The reduced samples were then alkylated by incubating in 15 mM iodoacetamide for 1 hour at room temperature in the dark. Proteins were then fractionated by SDS-PAGE.

Using in-gel molecular weight markers, each sample was divided into molecular weight regions and subjected to overnight trypsin digestion at 37°C (Trypsin Gold, Promega, Madison, WI).

### LCMS Data Acquisition

The trypsin-digested peptides were analyzed on an Agilent 6550 QToF with Chip Nano source and 1200 series nanoflow and capillary HPLC pumps (Agilent Technologies, Santa Clara, CA). Each sample was injected twice per analysis using a Polaris HR chip (Agilent #G4240-62030) consisting of a 360 nL enrichment column and a 0.075 x 150 mm analytical column, both packed with Polaris C18-A stationary phase (3um particle size). Mobile phase for the nano LC was 3% v/v acetonitrile, 0.1% formic acid, in 18MΩ water (Solvent A) and 95% acetonitrile, 0.1% formic acid in 18MΩ water (Solvent B). Samples were eluted at a flow rate of 350 nL/min with an 18 min gradient (5% to 30% B in 10 min, 50% B in 3 min, 90% B in 0.1 min, 5 min hold at 90% B). During the first injection, data dependent MSMS fragmentation spectra were collected with the instrument set to collect 6 MS scans per second, 4 MSMS spectra per second, and up to 12 precursors per cycle. During the second injection, no MSMS fragmentations were performed and a longer dwell time (1 spectrum per second) was used in the full scan acquisition. The longer dwell time increased the signal to noise ratio for the observed isotopomer patterns. MSMS fragmentation data were analyzed using Spectrum Mill MS Proteomics Workbench (version B.04.00, Agilent Technologies, Santa Clara, CA) using the Swiss-Prot rat database (08/2010) with a global false discovery rate of 1%. Fixed modifications (carbamidomethylation of cysteine) and variable modifications (oxidized methionine, pyroglutamic acid) were enabled and up to two missed cleavages allowed. Results validated at the peptide and protein level were searched again allowing for non-specific cleavage of the protein. A list of peptides with scores greater than 11 and scored peak intensities greater than 50% was exported from Spectrum Mill and collapsed into a non-redundant peptide formula database using Excel. This database, containing peptide elemental composition, mass, and retention time, was used to extract peptide isotopomer abundances (containing kinetic information) of each peptide from corresponding MS-only acquisition files with the Find-by-Formula algorithm in Mass Hunter (version B.05.00, Agilent Technologies, Santa Clara, CA).

### Extraction of Kinetic Labeling Information

MSMS fragmentation data was analyzed using Spectrum Mill (Agilent, Palo Alto, CA) and protein identifications were based on the Uniprot/Swissprot database (08/2010) where species=rat, trypsin digest, and carbamidomethylation of cysteine were used as restrictions on the search. Isotopomer patterns were extracted from the MS scan data using the MassHunter software package from Agilent. The peptide list with calculated neutral mass, elemental formula, and retention time was used to filter the observed isotope clusters. A visual basic application was used to calculate peptide elemental composition from lists of peptide sequences and calculate isotopomer patterns over a range of precursor body $^2H_2O$ enrichments ($\boldsymbol{p}$), for

the number (***n***) of C-H positions actively incorporating H/D from body water. Subsequent data handling was performed using Microsoft Excel.

**Calculation of Turnover Rate**

Fractional replacement (***f***) is the proportion of newly synthesized proteins in a population, expressed as a fraction of the total pool. The kinetic interpretation of the time-dependent replacement of pre-existing protein molecules by newly synthesized molecules requires an knowledge of the mass isotope pattern of newly-synthesized species as compared to unlabeled species[32,34]. The mass isotopomer pattern of peptides synthesized in the presence of a stable-isotope enriched precursor pool can be calculated based on the elemental composition of the peptide. Each protein (and by extension, each tryptic peptide) acquires isotopic enrichment from the precursor pool at the rate of protein turnover (***k***), the $^2$H-isotopic enrichment in the body water (***p***), and the number of sites in the peptide capable of incorporating H/D from water(***n***). Therefore, ***p*** and ***n*** must both be known to calculate ***k***. In these experiments, we have measured ***p*** directly. At the $^2$H enrichments used in this study the mass spectra of newly synthesized protein will occupy the same m/z range as the unlabeled species, but knowing ***p*** and ***n*** we can deconvolute the isotopomer patterns.

For a ***f*** between 0-100% (i.e. a mixed protein pool), deconvoluting the two subpopulations is carried out by treating each peptide as a biochemical polymer and calculating quantitative changes in the relative isotopic abundance pattern using the Mass Isotopomer Distribution Analysis (MIDA)[35]. As described previously[34], the mass isotopomer of each peptide was normalized to the total intensity of the isotopomer envelope, typically 4 masses ($M_0$-$M_3$). Peptides with a mass greater than ~2,400 Da exhibit a larger isotopomer envelope, so 5 masses ($M_0$-$M_4$) were used. We have based our calculations of ***f*** on the change in intensity of the normalized monoisotopic peak ($EM_0$). We find that the signal to noise is most favorable for $EM_0$, because of the larger change in fractional abundance for this isotopomer ($EM_0$ decreases while labeled species distribute from $EM_1$ to $EM_4$). Peptides which met our criteria for inclusion had signal intensity >30,000 counts, an RMS error against the theoretical natural abundance spectra of less than 1.5% for the day 0 (unlabeled) sample, and had a LC elution time within 30 seconds of the unlabeled control. The ***f*** of each peptide was calculated using the ***n*** specific for that sequence and the ***p*** measured for the mouse. Each peptide was considered as a replicate measurement of the fractional replacement for the protein of origin. Therefore the protein ***f*** in each mouse was calculated as the median ***f*** of the peptide population from that protein. A time-dependent fractional replacement curve was constructed for each protein, by plotting the protein ***f*** for the each mouse in each feeding regime against the time of exposure to $^2H_2O$. Proteins which were observed in fewer than 3 mice were removed from the data set. The rate constant ***k*** for each protein was calculated using a regression fit for the single pool model ($f=1-e^{(-kt)}$) in the Prism software package (Graph Pad, La Jolla CA). A coefficient of variation (%CV) was calculated for each protein as the ratio of

standard deviation reported for the regression over the rate constant. Proteins which had a %CV of more than 30% for either the CR or AL feeding regime were removed from the data set.

### Stable Isotope Labeling in Mammals (SILAM) Quantitation

SILAM was performed using the "spike-in" method, in which 100ug of a protein homogenate isolated from labeled INS-1E rat insulinoma cells *in vitro* was mixed with 100ug of islet cell protein homogenates from unlabeled animals. Rat INS-1E cells were grown in custom made RPMI-1640 SILAC media containing 11mM glucose, HEPES, and Glutamax (AthenaES, Baltimore, MD), enriched with 99% $^{13}C_6$-Leucine (CLM-2262, Cambridge Isotopes, Andover, MA) and $^{13}C_6$-Lysine (CLM-2247, Cambridge Isotopes, Andover, MA).

Protein was then isolated from INS-1E cells and islet cells from unlabeled animals as described above, and mixed together in a 1:1 ratio prior to reduction and alkylation. Alkylated protein homogenates were then fractionated by SDS-PAGE, then divided into molecular weight regions and subjected to overnight trypsin digestion at 37°C (Trypsin Gold, Promega, Madison, WI). Ratios of heavy:light peptides were calculated using two algorithms: (a) the XPRESS algorithm included in the Trans Proteomic Pipeline[36,37], and (b) extracted MS data scans using the MassHunter software package from Agilent. Ratios of heavy:light peptides were combined with fractional synthesis data in order to calculate control-corrected absolute protein replacement rates according to the equation:

*Control-Corrected Absolute Protein Synthesis Rate (%/day) = %f (%/day)*Q(heavy:light experimental)/Q(heavy:light control)*

### Gene Ontology and Pathway Analysis

Gene annotation, gene ontology and biochemical pathway information were obtained from the Database for Annotation, Visualization and Integrated Discovery (DAVID) v6.7 from the National Institute of Allergy and Infectious Diseases (NIAID), at the National Institutes of Health (NIH)[38,39]. Network analysis was performed using MetaCore (GeneGo V6.11).

## Results

The body weights of all animals are shown in Figure 2. Insulin resistant animals weighed significantly less than controls (188.5 vs. 344.6 g, $p<0.001$), and diabetic animals weighed significantly more than controls (408.5 vs. 344.6 g, $p<0.001$).

### Glucose Homeostasis

First, we performed a series of glucose disposal tests (GDT) to quantify (a) whole-body glycolysis, (b) circulating insulin, (c) glucose tolerance, and (d) insulin sensitivity[40]. Diabetic animals had significantly higher circulating glucose at all time points following an oral glucose challenge in comparison with insulin resistant and control animals (Figure 3A). Insulin resistant animals had significantly higher circulating insulin at all time points following glucose challenge vs. diabetic and control animals (Figure 3B). Whole-body glycolysis was highest in control animals at 10, 30, and 60 minutes as determined by the production of $^2H_2O$ (Figure 3C).

Insulin sensitivity was lowest in diabetic animals (0.18% vs. controls), and significantly reduced in prediabetic animals (0.34% vs. controls) (Figure 3D). Taken together, these results verify three distinct phases of glucose homeostasis: (a) insulin resistant ZDF rats (ZDFp), (b) diabetic ZDF rats (ZDFd), and (c) insulin sensitive controls (ZLC).

### Immunohistochemistry

Next, we performed immunohistochemistry on serial sections from each experimental group in order to verify morphological changes in islet cells in response to insulin resistance and diabetes. Islet cells in control animals showed a distinct clustered morphology, were numerous, and were structurally distinct from surrounding exocrine tissue (Figure 4A). Islet cell fluorescence intensity was increased by 86% in ZDFp animals vs. controls, suggesting islet cell hyperplasia (Figure 4B). Islet cells in diabetic animals showed a diffuse staining pattern and irregular shape.

### Islet Cell Proliferation

Next, we measured the rate of islet cell proliferation in response to insulin resistance and diabetes. Following euthanasia, islet cells were isolated by hand following pancreatic perfusion under microscopic visualization and were clearly distinguishable from acinar and ductal tissue (Figure 5A). Control animals proliferated at a rate of 1.15% new cells/day, in agreement with previous observations[33]. In insulin resistant animals, islet cell proliferation was 2.8-fold higher than in control animals ($p<0.001$), at a rate of 3.27% new cells/day. Islet cells in diabetic animals proliferated at a rate of 0.80% new cells/day, a 30% reduction in the rate of new cell synthesis vs. controls (Figure 5B).

### Islet Cell Proteome Dynamics

Animals were labeled for 12 hours (n=3 per group), 2 days (n=3 per group), and 5 days (n=3 per group) in order to identify rapid, moderate, and long turnover proteins using a target body water enrichment of 5% (Figure 1B). Following LC-MS/MS measurement of peptide spectra, we used five stringent selection criteria to remove low confidence kinetic data: (a) peptide signal intensity less than 30,000 counts, (b) RMS error for unlabeled peptide mass isotopomer abundance measurements must be less than 1.5% compared with natural abundance, (c) observation of the parent protein in at least 2 rats per experimental group, (d) a coefficient of variation of the one-phase exponential association curve fit less than 30%, and (e) an $r^2$ curve fit value greater than 0.7. (Figure S1). We identified 3042, 3418, and 4162 peptides, corresponding to 243, 167, and 138 proteins in insulin resistant, diabetic, and control animals, respectively (Figure S3).

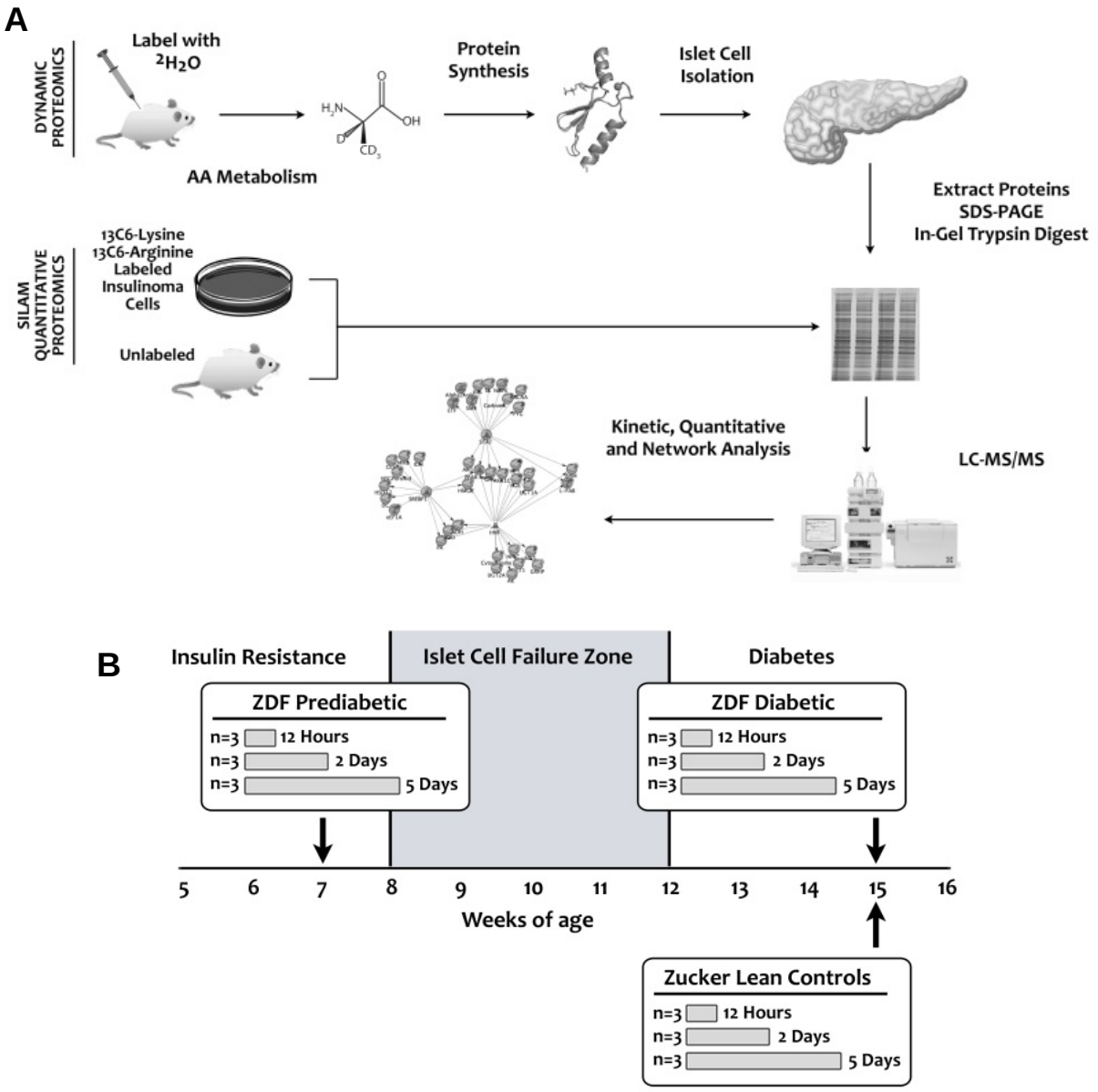


**Figure 1. Dynamic Proteomics Workflow and Experimental Design**. (A) Dynamic proteomics was performed by labeling rats with $^2H_2O$ at a target enrichment of 5%, followed by *in vivo* protein synthesis, islet cell isolation, SDS-PAGE protein separation, in-gel trypsinization, and LCMS analysis. Quantitative proteomics was performed by growing INS-1E rat insulinoma cells *in vitro* in the presence of heavy lysine ($^{13}C_6$-K) and heavy leucine ($^3C_6$-L), then using this protein lysate as the spike-in standard for unlabeled protein isolated from unlabeled rats, followed by SDS-PAGE protein separation, in-gel trypsinization, and LCMS analysis. (B) Three groups of animals were studied: insulin resistant ZDF prediabetic rats at 7 weeks of age, ZDF diabetic rats at 16 weeks of age, and ZLC controls at 16 weeks of age.

### Fractional and Absolute Protein Synthesis Rates in Insulin Resistant Rats

Insulin resistance increased the FSR of 97% of measured islet cell proteins as compared with controls (Figure 6A). Of the 93 proteins common to both groups, 75 proteins showed increased FSR (ZDFp/ZLC > 1.1), 16 proteins showed no change (0.9 < ZDFp/ZLC < 1.1), and 2 change (0.9 < ZDFp/ZLC < 1.1), and 2 proteins showed decreased FSR (ZDFp/ZLC < 0.9) as compared with controls (Figure 6A). Mean protein fractional synthesis was increased by 26.5% due to insulin resistance. We performed a gene ontology analysis to determine the localization of the proteins that were affected by insulin resistance

Interestingly, insulin resistance increased the FSR of proteins across many pathways involved in GSIS, including the TCA cycle, oxphos, glycolysis, ER-mediated protein processing and folding, cytoskeletal remodeling, and ribosomal protein synthesis (Figure 6B-G). Insulin resistance increased the FSR of proteins in each pathway, independent of their distribution between organelles. The ribosome contained the largest number of measured proteins (n=26), and insulin resistance increased the FSR by 19% (12.7% $day^{-1}$ vs. 10.7% $day^{-1}$), corresponding to a decrease in mean half-life of 1.0 days (5.4 days vs. 6.4 days) (Figure 6G).

Next, we performed quantitative proteomics (SILAM) in order to determine absolute protein synthesis rates in response to IR. In order to generate exogenous labeled proteins, we grew rat INS-1E cells *in vitro* in custom made media enriched with 99% $^{13}C_6$-Leucine and $^{13}C_6$-Lysine, as previously described[41]. For labeling experiments, it is crucial to appropriately select the heavy amino acids in order to achieve a high degree of labeled peptides following trypsin digestion. It is well known that in INS-1E cells, arginine can be converted into proline, introducing a bias into the downstream quantification[41]. Therefore, we cultured INS-1E cells in media enriched with 99% $^{13}C_6$-Leucine and $^{13}C_6$-Lysine given that leucine is an abundant amino acid in cellular proteins, and lysine corresponds to the trypsin cleavage site. According to this strategy, we reasoned that the islet proteome would achieve more than 98% enrichment following 6 doubling times (%enrichment = $(1-(1/2)^6)$).

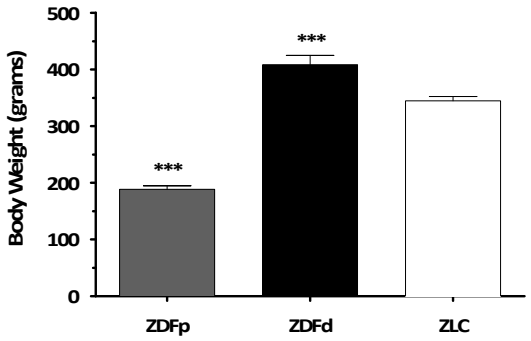


**Figure 2.** ZDF prediabetic rats weighed significantly less than both diabetic and control rats at 16 weeks of age. ZDF diabetic rats weighed significantly more than ZLC controls at 16 weeks of age. Significance was calculated by one-way ANOVA vs. ZLC animals (*, p<0.05; **, p<0.01; ***, p<0.001).

We found that insulin resistance increased the absolute synthesis rates of 88% of identified proteins (15/17 proteins), and that these proteins were not clustered into any specific gene ontology. Absolute synthesis fold-changes ranged from 0.6 to 1.6 in comparison with

control animals (Table S1). The protein with the largest increase in absolute synthesis was High mobility group protein B1 (Hmgb1, 1.6-fold increased vs. controls), a DNA-binding protein that has been associated with chronic inflammation as well as type 1 and type 2 diabetes[42–44].

Beta cells are the body's primary glucose sensors, and optimal secretion of insulin in response to elevations in circulating glucose is a tightly regulated process that heavily depends on many pathways in the beta cell, including glycolysis, the TCA cycle, oxidative phosphorlation, cytoplasmic ATP translocation, and the protein biosynthetic apparatus. In this study, we uncovered a number of novel kinetics that had not been previously described in the literature. First, we found that IR increased the fractional synthesis of cytoskeletal, glycolytic, mitochondrial, and ribosomal proteins in comparison with controls, and that the transition to diabetes resulted in the selective decrease in ribosomal proteins.

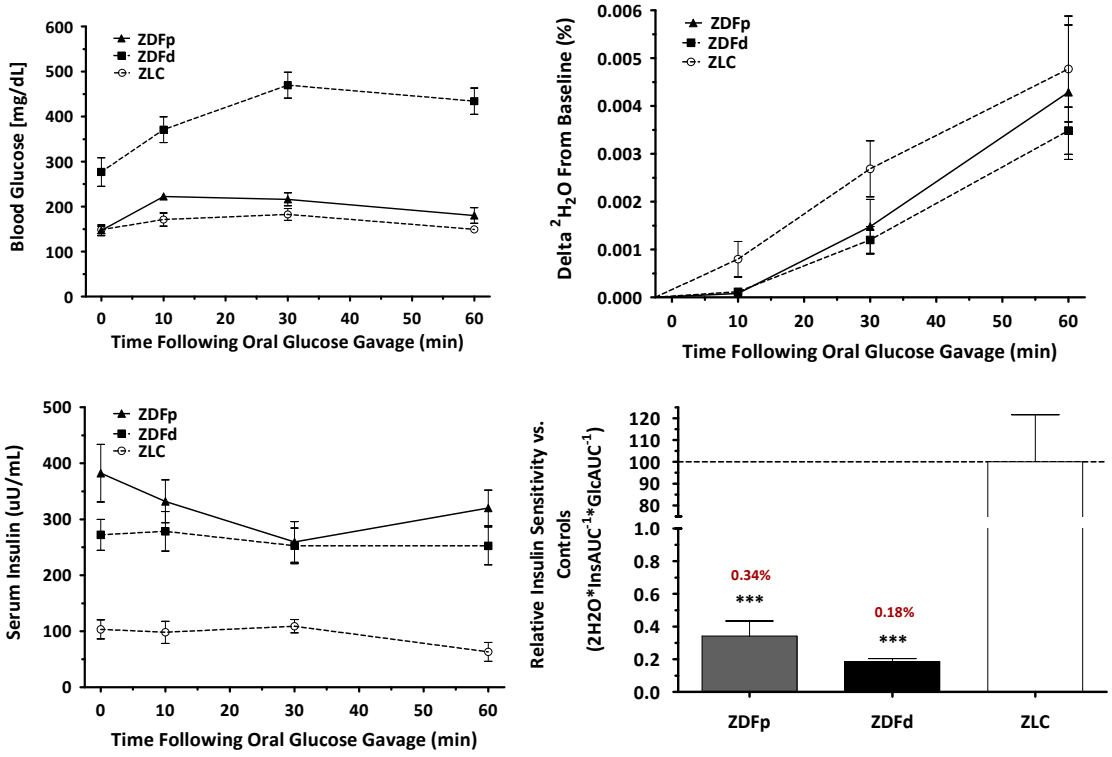


**Figure 3. Altered Glucose Homeostasis in Insulin Resistant and Diabetic Rats.** (A) Blood glucose values following an oral glucose gavage (1mg/g body weight); 16 week ZDF rats show significantly elevated circulating glucose at all time points vs. ZLC controls and 7 week ZDF rats are not different than ZLC controls. (B) Insulin concentrations in response to an oral glucose gavage show that both 7 and 16 week old ZDF rats are hyperinsulinemic at all time points vs. ZLC controls. (C) $^2H_2O$ production following an oral glucose gavage containing 6,6-$^2$H-glucose shows suppressed glycolytic disposal of glucose in 7 week and 16 week ZDF animals vs. ZLC controls. (D) Insulin sensitivity is significantly reduced in 7 week and 16 week animals vs. ZLC controls. Significance was calculated by one-way ANOVA vs. ZLC animals (*, $p<0.05$; **, $p<0.01$; ***, $p<0.001$).

IR increased the absolute synthesis rates of 88% (15/17 proteins), distributed throughout many cellular compartments and signaling pathways.

Next, we found that diabetes selectively decreased fractional synthesis of ribosomal proteins, and did not significantly change the fractional synthesis of glycolytic, TCA cycle, oxphos, or cytoskeletal proteins from their expression levels in the IR state. In addition, we found that diabetes decreased the absolute synthesis rate of 39% (7/18 proteins), involved in many pathways throughout the cell.

By combining $^{2}H_2O$ labeling and exogenously labeled standards (SILAM) with high-resolution LC/MS analysis of tryptic peptides, we were able to quantify both fractional and absolute protein replacement rates *in vivo* in insulin resistant and diabetic islets for the first time. Others have applied quantitative proteomics to the measurement of protein abundance in both insulin resistant and diabetic islets using label-free quantitation and iTRAQ, in order to describe the identities as well as the relative expression levels of beta cell-specific proteins[20,18,22,48,49]. In this study, we have used a new quantitative approach wherein absolute protein synthesis and breakdown rates are measured *in vivo* in hundreds of proteins across the islet proteome simultaneously. The technique is operationally simple, involving the administration of $^{2}H_2O$ for specific durations, followed by a rigorous solution to the major technical barrier that has long confounded the measurement of isotopically labeled peptides, namely the direct measurement of isotopic enrichment in the true *in vivo* precursor pool by use of mass isotopomer patterns inherent to the peptides themselves (MIDA). We recently showed that using this technique we can measure protein turnover in humans[34] and in mice[50], and others have shown similar approaches *in vivo*[51]. Using both exogenously labeled proteins from labeled INS-1E cells in culture ($^{13}C_6$-Lysine and $^{13}C_6$-Leucine), in combination with metabolically labeled proteins ($^{2}H_2O$), we were able to measure the synthesis and breakdown rates of hundreds of islet-specific proteins for the first time.

We also found that the protein with the highest absolute synthesis due to IR was also the protein with the lowest absolute synthesis due to diabetes (Hmgb1). This protein may serve as a biomarker for IR and diabetes, given that its absolute synthetic is inversely related to islet cell proliferation in both states[42]. High-mobility-group box-1 protein is an activator of Toll-like receptors (TLR) and the receptor for advanced glycation end products (RAGE). Hmgb1, TLR and RAGE form a triplex that mediates inflammation, promoting the production and secretion of pro-inflammatory cytokines in diabetes[43]. Hmgb1 plays a critical role in mediating islet cell injury, and activation of Hmgb1 triggers NF-kB activity, resulting in a pro-inflammatory state that has been associated with both type 1 diabetes and type 2 diabetes[44].

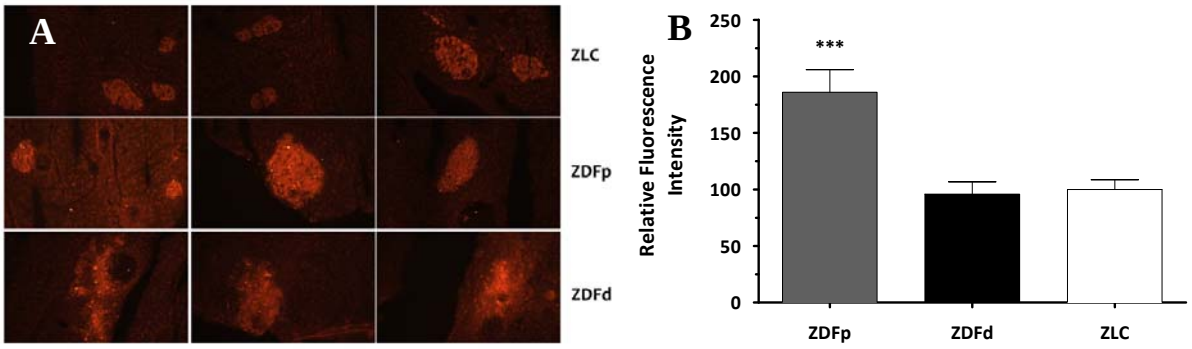


**Figure 4. Immunohistochemical Staining of Islets.** (A) Pancreatic sections were stained for insulin in order to determine the beta cell content and morphopogical islet cell changes in response to insulin resistance and diabetes. In comparison with ZLC islets (top), insulin resistant prediabetic ZDF islets (middle) are larger and show increased staining intensity, suggesting hyperproliferation and increased insulin content. ZDF diabetic islets (bottom) show an irregular shape and reduced staining intensity vs. ZLC control islets. (B) Normalized fluorescence intensity in comparison with ZLC control rats. Significance was calculated by one-way ANOVA vs. ZLC animals (*, $p<0.05$; **, $p<0.01$; ***, $p<0.001$).

The literature confirms that the expression and abundance of islet cell proteins is highly dependent on the glucose concentration in the circulating milieu. In an elegantly designed study, Martens et. al found that primary rat islet cells exposed to 7.5mM glucose increased the expression of glycolytic and ribosomal proteins without significant alteration to TCA cycle, beta oxidation, or oxidative phosphorlyation (oxphos) mitochondrial proteins[48]. In agreement with our study, they found that many 40S and 60S ribosomal proteins were more abundant in response to elevated glucose, as well as the glycolytic enzymes Eno1, Eno2, Eno3, Pgam1, Pgk1, Gapdh, Mdh1, and Tpi1. Interestingly, they found that elevated glucose did not significantly alter the molar abundance of TCA cycle enzymes Mdh2, Idh2, Aco2, or subunits of the oxphos F0-F1 ATPase complex ATP5a1, ATP5b, ATP5c1, ATP5d, ATP5o. We found that Atp5o fractional synthesis was 1.6-fold increased due to IR, however ATP5a1 and ATP5h synthesis was unchanged.

Waanders et. al found that single primary mouse islets cultured in 16.7mM glucose for 24 hours increased the abundance of proteins involved in glycolysis, TCA cycle, and ATP translocation[20]. In addition, hyperglycemic conditions resulted in a 1.7-fold increase in $Mn^{2+}$-superoxide dismutase (Sod1), in agreement with our measurement of a 1.4-fold increase in Sod1 fractional synthesis in response to IR. Lu et. al also found that the expression of Sod2 was decreased in response do diabetes, suggesting that increased production of antioxidant defense proteins in response to oxidative stress may be a critical determinant in preventing the transition to diabetes[52,53]. We found that the synthesis of Sod1 did not decrease following the transition to islet failure and diabetes, suggesting that the ability of the beta cells to constitutively upregulate other antioxidant enzymes including the mitochondrial Sod2 may tightly control the transition from insulin resistance to diabetes.

In addition, Waanders et. al found that hyperglycemic conditions resulted in reduced insulin content per islet, most likely resulting from constitutive insulin secretion. Our findings agree with these results; Park7 (DJ-1) was increased 2-fold in response to hyperglycemic conditions *in vitro*, and increased in synthetic rate by 1.28-fold *in vivo*. Park7 is a protein that has been implicated in Parkinson's disease, and mutations in Park7 cause mitochondrial dysfunction that a also associated with excessive oxidative stress[54]. Together, these findings suggest that acute hyperglycemic conditions affect the islet cell proteome by upregulation of proteins involved in integral pathways of GSIS.

Lu et. al demonstrated that diabetic MKR mice harboring a mutation in the IGF-1 gene in skeletal muscle show gross functional impairments in mitochondria, including a smaller number of hyperplastic mitochondria, reduced insulin granule content, reduced mitochondrial oxygen consumption, and reduced membrane hyperpolarization[22]. At the protein level, Lu et. al found that 95% of identified mitochondrial proteins were decreased in diabetic MKR mice, including proteins involved in the TCA cycle, fatty acid metabolism, and oxidative phosphorylation[18,22]. These proteins include members of the NADH dehydrogenase complex (Ndufa9), cytochrome b-c1 complex (Uqcrh), cytochrome c oxidase complex (mt-Co2, Cox4i1, Cox5a), ATP synthase complex (Atp5j2), and the ADP/ATP translocase (Slc25a5). Our analysis revealed that mitochondrial proteins were increased in fractional synthesis due to insulin resistance (100%, 9/9 proteins) and that this effect persisted following the transition to diabetes (78%, 7/9 proteins). We identified members of the electron transport chain (Etfa, Atp5a1, Atp5h, Atp5o), the phosphate carrier protein Slc25a3, the beta-oxidation enzyme Hadh, the mitochondrial oxidoreductase Prdx1, a ketone body synthesis enzyme (Acat1), and a membrane channel protein Vdac1.

The discrepancy between these results and those of Lu et. al reveal a fundamental

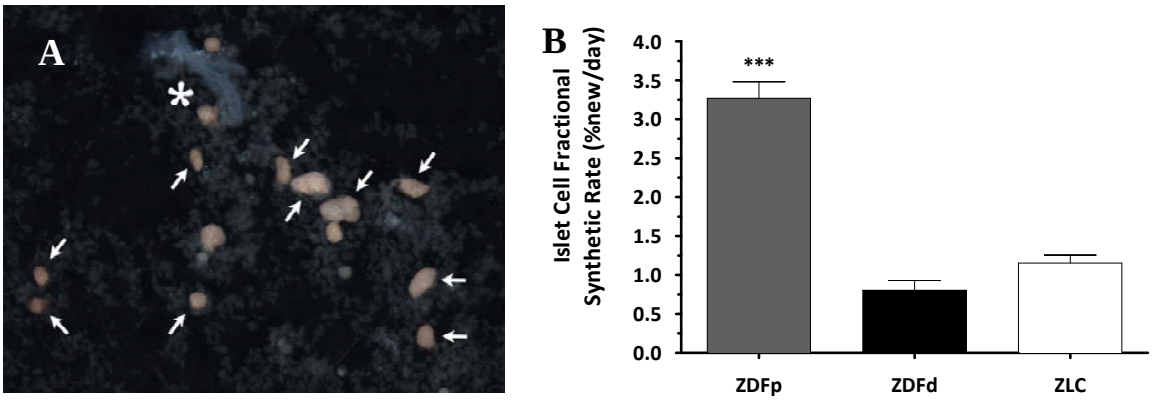


**Figure 5. Insulin Resistance Promotes Islet Hyperproliferation.** (A) Islet cells were isolated by hand following pancreatic perfusion under microscopic visualization, and were clearly distinguishable from acinar and ductal tissue. (B) Cell proliferation analysis following $^2H_2O$ labeling revealed that insulin resistance results in a 2.8-fold increase in islet cell proliferation vs. ZLC. Diabetes results in a 30% decrease in islet cell proliferation vs. ZLC controls. Significance was calculated by one-way ANOVA vs. ZLC animals (*, $p<0.05$; **, $p<0.01$; ***, $p<0.001$).

difference between quantitative (abundance) and dynamic proteomics (synthesis) in that increased protein synthetic rates, when matched by increased protein degradation rates, do not affect the size of the resultant protein pool. Instead, $^{2}H_2O$ labeling combined with SILAM exposes (a) the rate at which proteins are being synthesized, by the measurement of $^{2}H$ incorporation into amino acids in proteins ($^{2}H_2O$ labeling), and (b) the resultant effect on relative molar abundance (SILAM). Together, these metrics can be combined to calculate the absolute synthesis rate of identified peptides, providing a holistic picture of the regulation of hundreds of proteins simultaneously. These integral components of proteostasis are masked by the measurement of molar abundance by itself[50]. Given the results of Lu et. al, our measurement of increased fractional synthesis of mitochondrial proteins suggests that degradation rates are also increased in order to maintain protein pool size. In addition, these results also suggest that islet proteome dynamics may show differential effects in various animal models of T2D, and may highly depend on species and strain.

Contrary to our findings, Lu et. al found that islet dysfunction in the diabetic state was characterized by an increased molar abundance of proteins involved in protein biosynthesis and folding, including eukaryotic initiation factors (EIFs) and elongation factors (eEIFs). Our analysis showed that more than 92% of ribosomal proteins (23/25) were decreased in fractional synthetic rate, suggesting that islet failure is associated not only with an inability to manufacture and secrete an adequate quantity of insulin, but is characterized by a global dysfunction of the protein biosynthetic apparatus as a network of coordinated enzymes. The findings of Lu et. al also highlight the possibility of significantly increased ribosomal protein degradation in the diabetic state, reducing the molar abundance of the resultant protein pool.

Diabetic MKR islets also demonstrated increased abundance of ER stress proteins and protein-folding proteins, in accordance with our findings. We found that protein-folding proteins, including Hyou1, Ppib, Pdi6 were increased in fractional synthesis, whereas only Pdia3 was decreased. In addition, we found an increase in the synthesis of the ER stress response protein Erp29. Proteins of this family are involved in the formation of disulfide bonds, and mediate protein folding by functioning as oxidoreductases within the ER[49,55,56].

Lu et. al also found that 46% of differentially regulated islet proteins show discordant mRNA expression levels, suggesting that (a) the measurement of transcript abundance is a poor indicator of proteome alterations[57,58], and (b) that much of the activity within the islet proteome may be regulated at the post-translational level.

Insulin resistance promotes islet hyperplasia, resulting in enlarged islets[18] and increased cell proliferation[33]. We found that IR stimulated a 2.8-fold increase in islet cell proliferation, consistent with literature findings. Increased islet cell mass can occur via a number of mechanisms, which include replication of preexisting islet cells, neogenesis of islet cell precursors[59–61], and inhibition of islet cell apoptosis[62]. It still remains unclear which of these mechanisms results in increased islet cell mass in response to IR, however the net

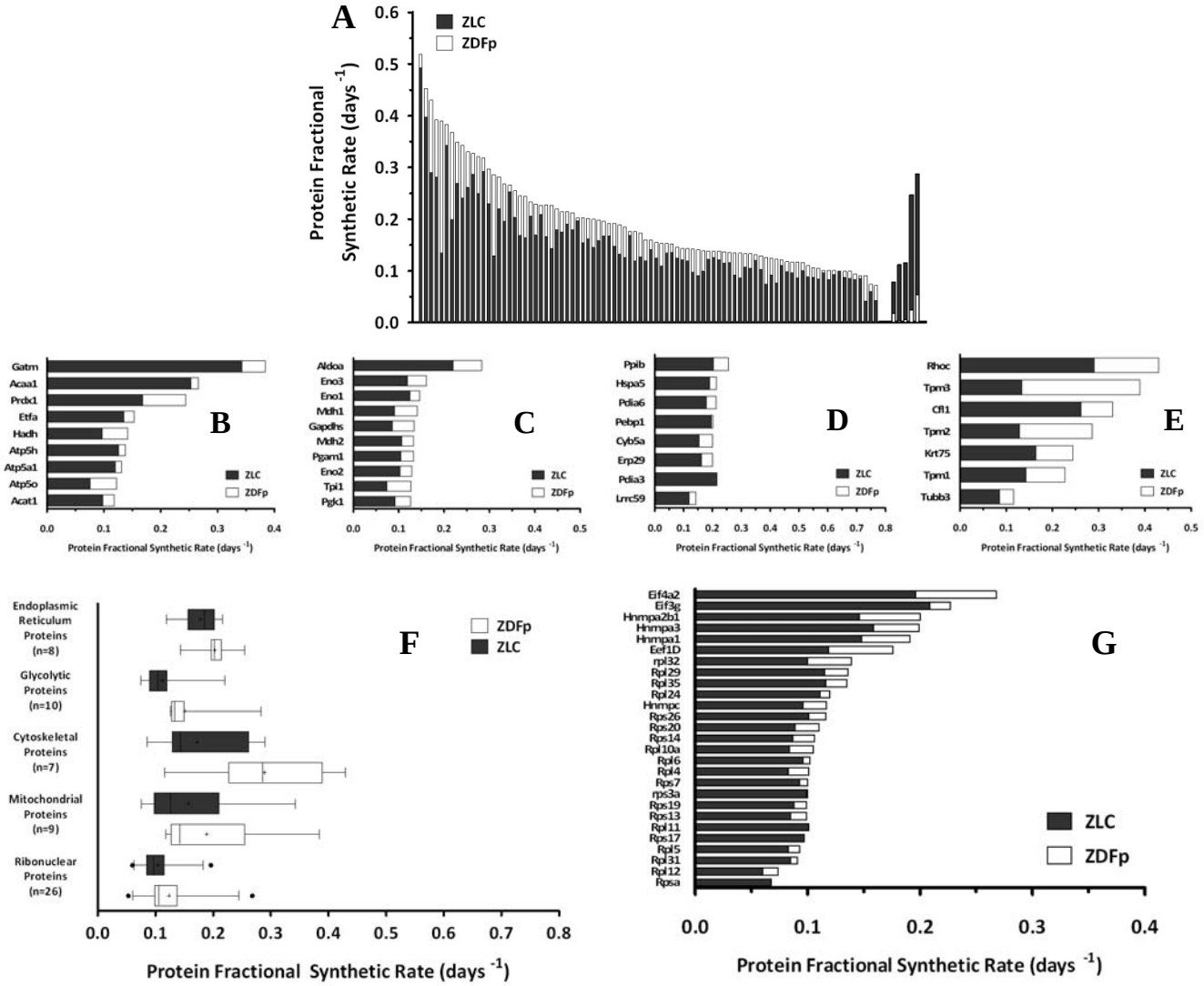


**Figure 6. Insulin Resistance Increases Global Protein Fractional Synthesis**. (A) Insulin resistance increased the fractional synthetic rate of 97% of identified proteins vs. ZLC controls. Proteins involved in the regulation of (B) mitochondrial metabolism (n=9), (C) glycolysis (n=10), (D) the endoplasmic reticulum (n=8), (E) cytoskeletal remodeling (n=7), and (G) the ribosome (n=26) showed increased fractional synthesis vs. ZLC controls. (F) Box plot indicating the interquartile range (IQR) for FSRs; bars extend from 5% to 95% of the data; outliers shown as individual points. Ribonuclear proteins were the most affected by insulin resistance.

effect results in 2 to 5-fold elevations in islet cell mass and insulin production[63].

Diabetes however, resulted in a 30% reduction in the rate of islet cell proliferation as compared with control animals. Whether decreased cell proliferation is a cause or an effect of diabetes remains to be definitively determined, however the decline in cell synthesis closely matches the decline in ribosomal protein synthesis, suggesting that impaired GSIS is coordinately linked with the rate of islet cell replication. Studies show that islet proliferation in ZF rats far exceeds those of ZLC rats in response to IR, suggesting that resistance to T2D originates from an ability to increase islet mass via either preexisting islet cell proliferation or by islet neogenesis[64–66,6,67–69].

In agreement with these findings, we found that cytoskeletal remodeling proteins were strongly increased by IR, providing a link between dynamic protein synthesis and islet hyperplasia. Three members of the tropomyosin family of proteins showed increased FSR in response to insulin resistance (Tpm1, Tpm2, Tpm3), as were cofilin-1 (Cfl1) and tubulin beta 3 chain (Tubb3). Diabetes reduced the FSR of Tpm1 and Tpm2 despite the fact that they remained elevated in comparison with controls animals.

An inherent limitation of this study is that protein degradation rates are difficult to determine in a tissue whose mass is increasing over time. At steady state, the calculation of protein degradation rates is easily performed, as we showed recently[50]. Given that insulin resistance promoted a 2.8-fold increase in islet cell proliferation, calculation of protein degradation rates can only be inferred from fractional and SILAM data.

In conclusion, we measured fractional and absolute synthesis rates of cytoskeletal, glycolytic, mitochondrial, ER, and ribosomal proteins, the principal pathways responsible for glucose stimulated insulin secretion (GSIS). We found that insulin resistance increased the fractional synthesis rates (FSR) of 97% of all measured islet proteins, and the subsequent transition to diabetes resulted in the selective impairment of ribosomal protein synthesis. Absolute synthesis rates followed the same trend. Taken together, these data suggest that the rapid rate of islet cell proliferation due to insulin resistance is accompanied by increased fractional and absolute synthesis of critical GSIS components, and that the failure of islet cells in diabetes results mainly in impaired ribosomal pathway flux, independent of alterations in mitochondrial protein metabolism.

## Contributions

CK, MB, and MH wrote the manuscript; CK, JC, and MH designed the experiment; CK, JC, and WH performed mass spectrometry; LR and MD performed islet isolation, SILAM, and sample processing prior to LC-MS/MS peptide analysis; CK and RM performed data analysis.

## Acknowledgements

The authors would like to thank Antonio Moreno, Larry Thompson, Bob Williams, Julio Gonzalez, Bennie Mitchell, and XXX for their outstanding behind the scenes work at making this research possible. Their contributions to this research are indispensible.

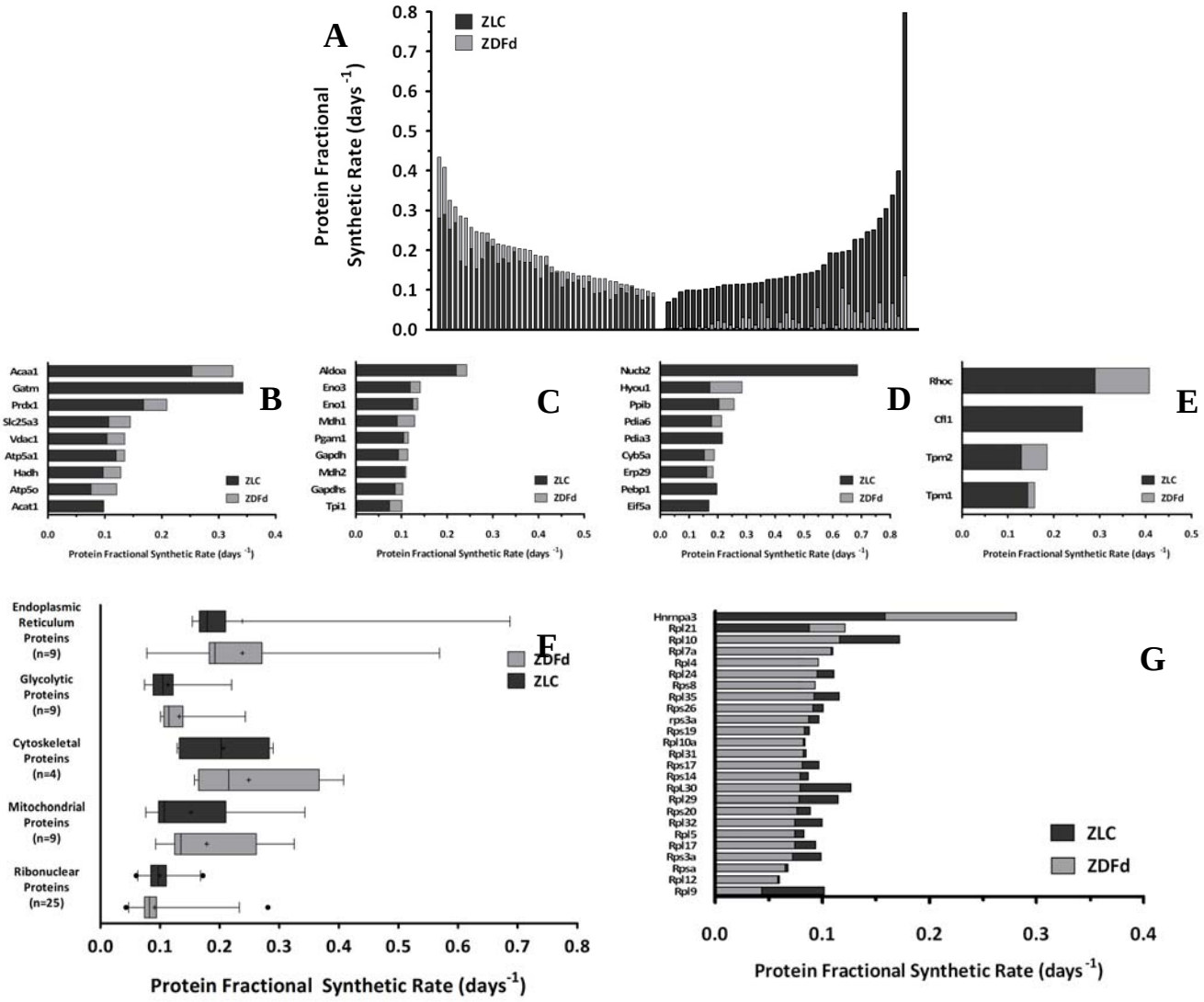


**Figure 7. Diabetes Selectively Reduces Ribosomal Protein Fractional Synthesis**. (A) In diabetic animals, the fractional synthetic rate was increased in 44% (35/80), and decreased in 24% (24/80) of identified proteins vs. ZLC controls. Proteins involved in the regulation of (B) mitochondrial metabolism (n=9), (C) glycolysis (n=9), (D) the endoplasmic reticulum (n=9), and (E) cytoskeletal remodeling (n=4) showed increased FSR vs. ZLC controls. (G) Ribosomal protein FSR was increased in 2/25 proteins and decreased in 23/25 proteins. (F) Box plot indicating the interquartile range (IQR) for FSRs; bars extend from 5% to 95% of the data; outliers shown as individual points.

## Literature Cited


1. Zimmet, P., Alberti, K. G. & Shaw, J. Global and societal implications of the diabetes epidemic. *Nature* **414**, 782–787 (2001).
2. Klöppel, G., Löhr, M., Habich, K., Oberholzer, M. & Heitz, P. U. Islet pathology and the pathogenesis of type 1 and type 2 diabetes mellitus revisited. *Surv Synth Pathol Res* **4**, 110–125 (1985).
3. Brüning, J. C. *et al.* Development of a novel polygenic model of NIDDM in mice heterozygous for IR and IRS-1 null alleles. *Cell* **88**, 561–572 (1997).
4. Bonner-Weir, S. Islet growth and development in the adult. *J. Mol. Endocrinol.* **24**, 297–302 (2000).
5. Lingohr, M. K., Buettner, R. & Rhodes, C. J. Pancreatic beta-cell growth and survival--a role in obesity-linked type 2 diabetes? *Trends Mol Med* **8**, 375–384 (2002).
6. Pick, A. *et al.* Role of apoptosis in failure of beta-cell mass compensation for insulin resistance and beta-cell defects in the male Zucker diabetic fatty rat. *Diabetes* **47**, 358 –364 (1998).
7. Unger, R. H. & Orci, L. Diseases of liporegulation: new perspective on obesity and related disorders. *FASEB J.* **15**, 312–321 (2001).
8. Kahn, B. B. Type 2 diabetes: when insulin secretion fails to compensate for insulin resistance. *Cell* **92**, 593–596 (1998).
9. Leahy, J. L. Pathogenesis of type 2 diabetes mellitus. *Arch. Med. Res.* **36**, 197–209 (2005).
10. Gunton, J. E. *et al.* Loss of ARNT/HIF1beta mediates altered gene expression and pancreatic-islet dysfunction in human type 2 diabetes. *Cell* **122**, 337–349 (2005).
11. Kirkwood, T. B. L. A systematic look at an old problem. *Nature* **451**, 644–647 (2008).
12. Hekimi, S. & Guarente, L. Genetics and the specificity of the aging process. *Science* **299**, 1351–1354 (2003).
13. Lee, J., Giordano, S. & Zhang, J. Autophagy, mitochondria and oxidative stress: cross-talk and redox signalling. *Biochemical Journal* **441**, 523–540 (2012).
14. Ehehalt, F. *et al.* Impaired insulin turnover in islets from type 2 diabetic patients. *Islets* **2**, 30–36 (2010).
15. Garnett, K. E., Chapman, P., Chambers, J. A., Waddell, I. D. & Boam, D. S. W. Differential Gene Expression Between Zucker Fatty Rats and Zucker Diabetic Fatty Rats: A Potential Role for the Immediate-Early Gene Egr-1 in Regulation of Beta Cell Proliferation. *J Mol Endocrinol* **35**, 13–25 (2005).
16. Homo-Delarche, F. *et al.* Islet Inflammation and Fibrosis in a Spontaneous Model of Type 2 Diabetes, the GK Rat. *Diabetes* **55**, 1625–1633 (2006).
17. Ghanaat-Pour, H., Huang, Z., Lehtihet, M. & Sjöholm, Å. Global Expression Profiling of Glucose-Regulated Genes in Pancreatic Islets of Spontaneously Diabetic Goto-Kakizaki Rats. *J Mol Endocrinol* **39**, 135–150 (2007).
18. Lu, H., Yang, Y., Allister, E. M., Wijesekara, N. & Wheeler, M. B. The identification of potential factors associated with the development of type 2 diabetes: a quantitative proteomics approach. *Mol. Cell Proteomics* **7**, 1434–1451 (2008).
19. Petyuk, V. A. *et al.* Characterization of the mouse pancreatic islet proteome and comparative analysis with other mouse tissues. *J. Proteome Res.* **7**, 3114–3126 (2008).
20. Waanders, L. F. *et al.* Quantitative proteomic analysis of single pancreatic islets. *Proc. Natl. Acad. Sci. U.S.A.* **106**, 18902–18907 (2009).
21. Olsson, A. H. *et al.* Decreased expression of genes involved in oxidative

phosphorylation in human pancreatic islets from patients with type 2 diabetes. *Eur. J. Endocrinol.* **165**, 589–595 (2011).
22. Lu, H., Koshkin, V., Allister, E. M., Gyulkhandanyan, A. V. & Wheeler, M. B. Molecular and metabolic evidence for mitochondrial defects associated with beta-cell dysfunction in a mouse model of type 2 diabetes. *Diabetes* **59**, 448–459 (2010).
23. Liu, Y. Q., Jetton, T. L. & Leahy, J. L. beta-Cell adaptation to insulin resistance. Increased pyruvate carboxylase and malate-pyruvate shuttle activity in islets of nondiabetic Zucker fatty rats. *J. Biol. Chem.* **277**, 39163–39168 (2002).
24. Maassen, J. A. *et al.* Mitochondrial diabetes and its lessons for common Type 2 diabetes. *Biochem. Soc. Trans.* **34**, 819–823 (2006).
25. Anello, M. *et al.* Functional and morphological alterations of mitochondria in pancreatic beta cells from type 2 diabetic patients. *Diabetologia* **48**, 282–289 (2005).
26. MacDonald, M. J. *et al.* Decreased levels of metabolic enzymes in pancreatic islets of patients with type 2 diabetes. *Diabetologia* **52**, 1087–1091 (2009).
27. Jitrapakdee, S., Wutthisathapornchai, A., Wallace, J. C. & MacDonald, M. J. Regulation of insulin secretion: role of mitochondrial signalling. *Diabetologia* **53**, 1019–1032 (2010).
28. Price, J. C., Guan, S., Burlingame, A., Prusiner, S. B. & Ghaemmaghami, S. Analysis of proteome dynamics in the mouse brain. *Proc. Natl. Acad. Sci. U.S.A.* **107**, 14508–14513 (2010).
29. Aebersold, R. & Mann, M. Mass spectrometry-based proteomics. *Nature* **422**, 198–207 (2003).
30. Pandey, A. & Mann, M. Proteomics to study genes and genomes. *Nature* **405**, 837–846 (2000).
31. Wu, C., MacCoss, M., Howell, K., Matthews, D. & Yates, J. Metabolic labeling of mammalian organisms with stable isotopes for quantitative proteomic analysis. *Anal. Chem.* **76**, 4951–4959 (2004).
32. Neese, R. A. *et al.* Measurement in vivo of proliferation rates of slow turnover cells by 2H2O labeling of the deoxyribose moiety of DNA. *Proc. Natl. Acad. Sci. U.S.A.* **99**, 15345–15350 (2002).
33. Chen, S. *et al.* Measurement of pancreatic islet cell proliferation by heavy water labeling. *Am. J. Physiol. Endocrinol. Metab.* **293**, E1459–1464 (2007).
34. Price, J. C. *et al.* Measurement of human plasma proteome dynamics with (2)H(2)O and liquid chromatography tandem mass spectrometry. *Anal. Biochem.* **420**, 73–83 (2012).
35. Busch, R., Neese, R. A., Awada, M., Hayes, G. M. & Hellerstein, M. K. Measurement of cell proliferation by heavy water labeling. *Nat Protoc* **2**, 3045–3057 (2007).
36. Deutsch, E. W. *et al.* A guided tour of the Trans-Proteomic Pipeline. *Proteomics* **10**, 1150–1159 (2010).
37. Han, D. K., Eng, J., Zhou, H. & Aebersold, R. Quantitative profiling of differentiation-induced microsomal proteins using isotope-coded affinity tags and mass spectrometry. *Nat. Biotechnol.* **19**, 946–951 (2001).
38. Huang, D. W., Sherman, B. T. & Lempicki, R. A. Systematic and integrative analysis of large gene lists using DAVID bioinformatics resources. *Nat Protoc* **4**, 44–57 (2009).
39. Huang, D. W., Sherman, B. T. & Lempicki, R. A. Bioinformatics enrichment tools: paths toward the comprehensive functional analysis of large gene lists. *Nucleic Acids Res.* **37**, 1–13 (2009).

40. Beysen, C. *et al.* Whole-body glycolysis measured by the deuterated-glucose disposal test correlates highly with insulin resistance in vivo. *Diabetes Care* **30**, 1143–1149 (2007).
41. Schvartz, D., Couté, Y., Brunner, Y., Wollheim, C. B. & Sanchez, J.-C. Modulation of neuronal pentraxin 1 expression in rat pancreatic β-cells submitted to chronic glucotoxic stress. *Mol. Cell Proteomics* **11**, 244–254 (2012).
42. Maillard-Lefebvre, H. *et al.* Soluble receptor for advanced glycation end products: a new biomarker in diagnosis and prognosis of chronic inflammatory diseases. *Rheumatology (Oxford)* **48**, 1190–1196 (2009).
43. Nogueira-Machado, J. A., Volpe, C. M. de O., Veloso, C. A. & Chaves, M. M. HMGB1, TLR and RAGE: a functional tripod that leads to diabetic inflammation. *Expert Opin. Ther. Targets* **15**, 1023–1035 (2011).
44. Zhang, S., Zhong, J., Yang, P., Gong, F. & Wang, C.-Y. HMGB1, an innate alarmin, in the pathogenesis of type 1 diabetes. *Int J Clin Exp Pathol* **3**, 24–38 (2009).
45. Prentki, M. New insights into pancreatic beta-cell metabolic signaling in insulin secretion. *Eur. J. Endocrinol.* **134**, 272–286 (1996).
46. Ashcroft, F. M. & Rorsman, P. ATP-sensitive K+ channels: a link between B-cell metabolism and insulin secretion. *Biochem. Soc. Trans.* **18**, 109–111 (1990).
47. Finegood, D. T. *et al.* Beta-cell mass dynamics in Zucker diabetic fatty rats. Rosiglitazone prevents the rise in net cell death. *Diabetes* **50**, 1021–1029 (2001).
48. Martens, G. A. *et al.* Protein markers for insulin-producing beta cells with higher glucose sensitivity. *PLoS ONE* **5**, e14214 (2010).
49. Dowling, P. *et al.* Proteomic screening of glucose-responsive and glucose non-responsive MIN-6 beta cells reveals differential expression of proteins involved in protein folding, secretion and oxidative stress. *Proteomics* **6**, 6578–6587 (2006).
50. Price, J. C. *et al.* The effect of long term calorie restriction on in vivo hepatic proteostatis: a novel combination of dynamic and quantitative proteomics. *Mol. Cell Proteomics* (2012).doi:10.1074/mcp.M112.021204
51. Kim, T.-Y. *et al.* Metabolic Labeling Reveals Proteome Dynamics of Mouse Mitochondria. *Mol. Cell Proteomics* (2012).doi:10.1074/mcp.M112.021162
52. Pi, J. & Collins, S. Reactive oxygen species and uncoupling protein 2 in pancreatic β-cell function. *Diabetes Obes Metab* **12 Suppl 2**, 141–148 (2010).
53. Pi, J. *et al.* ROS signaling, oxidative stress and Nrf2 in pancreatic beta-cell function. *Toxicol. Appl. Pharmacol.* **244**, 77–83 (2010).
54. Finsterer, J. Parkinson's syndrome and Parkinson's disease in mitochondrial disorders. *Mov. Disord.* **26**, 784–791 (2011).
55. Mori, K. Tripartite management of unfolded proteins in the endoplasmic reticulum. *Cell* **101**, 451–454 (2000).
56. Ferrari, D. M. & Söling, H. D. The protein disulphide-isomerase family: unravelling a string of folds. *Biochem. J.* **339 ( Pt 1)**, 1–10 (1999).
57. Jin, J. *et al.* Detection of differential proteomes of human beta-cells during islet-like differentiation using iTRAQ labeling. *J. Proteome Res.* **8**, 1393–1403 (2009).
58. Maziarz, M., Chung, C., Drucker, D. J. & Emili, A. Integrating global proteomic and genomic expression profiles generated from islet alpha cells: opportunities and challenges to deriving reliable biological inferences. *Mol. Cell Proteomics* **4**, 458–474 (2005).
59. Bonner-Weir, S., Baxter, L. A., Schuppin, G. T. & Smith, F. E. A second pathway for regeneration of adult exocrine and

endocrine pancreas. A possible recapitulation of embryonic development. *Diabetes* **42**, 1715–1720 (1993).
60. Bonner-Weir, S. Life and death of the pancreatic beta cells. *Trends Endocrinol. Metab.* **11**, 375–378 (2000).
61. Finegood, D. T., Scaglia, L. & Bonner-Weir, S. Dynamics of beta-cell mass in the growing rat pancreas. Estimation with a simple mathematical model. *Diabetes* **44**, 249–256 (1995).
62. Lee, S.-H., Hao, E. & Levine, F. β-Cell replication and islet neogenesis following partial pancreatectomy. *Islets* **3**, 188–195 (2011).
63. Zhou, Y. P., Cockburn, B. N., Pugh, W. & Polonsky, K. S. Basal insulin hypersecretion in insulin-resistant Zucker diabetic and Zucker fatty rats: role of enhanced fuel metabolism. *Metab. Clin. Exp.* **48**, 857–864 (1999).
64. Bray, G. A. The Zucker-fatty rat: a review. *Fed. Proc.* **36**, 148–153 (1977).
65. Cleary, M. P., Phillips, F. C. & Morton, R. A. Liver, serum and adipose tissue fatty acid composition in suckling Zucker rats. *Lipids* **29**, 753–758 (1994).
66. Phillips, M. S. *et al.* Leptin receptor missense mutation in the fatty Zucker rat. *Nat. Genet.* **13**, 18–19 (1996).
67. Takaya, K. *et al.* Molecular cloning of rat leptin receptor isoform complementary DNAs--identification of a missense mutation in Zucker fatty (fa/fa) rats. *Biochem. Biophys. Res. Commun.* **225**, 75–83 (1996).
68. Truett, G. E., Walker, J. A. & Harris, R. B. S. A developmental switch affecting growth of fatty rats. *American Journal of Physiology - Regulatory, Integrative and Comparative Physiology* **279**, R1956 –R1963 (2000).
69. Williams, G. *et al.* The hypothalamus and the control of energy homeostasis: different circuits, different purposes. *Physiol. Behav.* **74**, 683–701 (2001).

## Supplemental Tables and Figures

| Gene Symbol | Protein Name | ZDFp Kinetics (%/day) | ZLC Kinetics (%/day) | ZDFp SILAM | ZLC SILAM | ZDFp Abs (%/day) | ZLC Abs (%/day) | ZDFp/ZLC Abs |
|---|---|---|---|---|---|---|---|---|
| **Hmgb1** | High mobility group protein B1 | 0.153 | 0.109 | 1.524 | 1.332 | 0.175 | 0.109 | 1.606 |
| **Uchl1** | Ubiquitin carboxyl-terminal hydrolase isozyme L1 | 0.189 | 0.132 | 1.416 | 1.291 | 0.207 | 0.132 | 1.576 |
| **Hnrnpa2b1** | Heterogeneous nuclear ribonucleoproteins A2/B1 | 0.200 | 0.146 | 2.265 | 2.032 | 0.223 | 0.146 | 1.527 |
| **Mdh2** | Malate dehydrogenase, mitochondrial | 0.133 | 0.107 | 1.271 | 1.061 | 0.159 | 0.107 | 1.494 |
| **Atp5h** | ATP synthase subunit d, mitochondrial | 0.138 | 0.126 | 0.984 | 0.724 | 0.187 | 0.126 | 1.488 |
| **Hnrnpc** | Heterogeneous nuclear ribonucleoprotein C | 0.117 | 0.096 | 1.482 | 1.284 | 0.135 | 0.096 | 1.409 |
| **Park7** | Protein DJ-1 | 0.138 | 0.123 | 0.440 | 0.385 | 0.158 | 0.123 | 1.281 |
| **Cdc37** | Hsp90 co-chaperone Cdc37 | 0.343 | 0.241 | 1.021 | 1.162 | 0.302 | 0.241 | 1.249 |
| **Tubb3** | Tubulin beta-3 chain | 0.116 | 0.086 | 1.098 | 1.207 | 0.106 | 0.086 | 1.237 |
| **Prdx1** | Peroxiredoxin-1 | 0.244 | 0.168 | 1.345 | 1.590 | 0.207 | 0.168 | 1.232 |
| **Rps17** | 40S ribosomal protein S17 | 0.095 | 0.097 | 0.823 | 0.657 | 0.118 | 0.097 | 1.219 |
| **Eno2** | Gamma-enolase | 0.129 | 0.103 | 0.925 | 0.955 | 0.125 | 0.103 | 1.216 |
| **Acat1** | Acetyl-CoA acetyltransferase, mitochondrial | 0.118 | 0.098 | 0.185 | 0.190 | 0.115 | 0.098 | 1.167 |
| **Ywhab** | 14-3-3 protein beta/alpha | 0.229 | 0.170 | 0.982 | 1.152 | 0.196 | 0.170 | 1.148 |
| **Tagln2** | Transgelin-2 | 0.297 | 0.230 | 0.660 | 0.745 | 0.263 | 0.230 | 1.142 |
| **M6pr** | Cation-dependent mannose-6-phosphate receptor | 0.327 | 0.287 | 1.075 | 1.120 | 0.314 | 0.287 | 1.093 |
| **Nme1** | Nucleoside diphosphate kinase A | 0.144 | 0.121 | 1.250 | 1.355 | 0.132 | 0.121 | 1.092 |
| **Ywhaz** | 14-3-3 protein zeta/delta | 0.160 | 0.141 | 1.007 | 1.062 | 0.152 | 0.141 | 1.077 |
| **Ube2n** | Ubiquitin-conjugating enzyme E2 N | 0.192 | 0.167 | 0.740 | 0.800 | 0.177 | 0.167 | 1.065 |

| Gene Symbol | Protein Name | ZDFp Kinetics (%/day) | ZLC Kinetics (%/day) | ZDFp SILAM | ZLC SILAM | ZDFp Abs (%/day) | ZLC Abs (%/day) | ZDFp/ZLC Abs |
|---|---|---|---|---|---|---|---|---|
| **Nsfl1c** | NSFL1 cofactor p47 | 0.214 | 0.175 | 1.872 | 2.189 | 0.183 | 0.175 | 1.045 |
| **Gapdhs** | glyceraldehyde-3-phosphate dehydrogenase, spermatogenic | 0.134 | 0.086 | 1.441 | 2.251 | 0.086 | 0.086 | 1.001 |
| **Cyb5a** | Cytochrome b5 | 0.201 | 0.154 | 0.640 | 0.840 | 0.153 | 0.154 | 0.998 |
| **Eif4a2** | Eukaryotic initiation factor 4A-II | 0.268 | 0.196 | 0.754 | 1.073 | 0.196 | 0.196 | 0.998 |
| **Etfa** | Electron transfer flavoprotein subunit alpha, mitochondrial | 0.153 | 0.135 | 0.585 | 0.665 | 0.134 | 0.135 | 0.996 |
| **Eno1** | Alpha-enolase | 0.146 | 0.125 | 1.034 | 1.285 | 0.117 | 0.125 | 0.935 |
| **Atp5a1** | ATP synthase subunit alpha, mitochondrial | 0.131 | 0.120 | 1.245 | 1.483 | 0.110 | 0.120 | 0.914 |
| **Rps3a** | 40S ribosomal protein S3a | 0.100 | 0.099 | 0.755 | 0.835 | 0.091 | 0.099 | 0.914 |
| **Dctn2** | Dynactin subunit 2 | 0.204 | 0.250 | 1.011 | 1.040 | 0.198 | 0.250 | 0.790 |
| **Pdia3** | protein disulfide isomerase family A, member 3 | 0.195 | 0.216 | 0.603 | 0.900 | 0.131 | 0.216 | 0.606 |

**Table S1. Proteome Wide Normalized Absolute Synthesis Rates In Response to Insulin Resistance.** Absolute synthesis rates were calculated for proteins that were identified by (a) kinetics in ZDFp and ZLC animals, and by (b) calculation of the heavy:light ratio from either the TPP suite of software tools or using the in-house algorithm for the identification and quantitation of SILAM peptide pairs.

| Gene Symbol | Protein Name | ZDFd Kinetics (%/day) | ZLC Kinetics (%/day) | ZDFd SILAM | ZLC SILAM | ZDFd Abs (%/day) | ZLC Abs (%/day) | ZDFd/ZLC Abs |
|---|---|---|---|---|---|---|---|---|
| **Hnrnpa3** | Heterogeneous nuclear ribonucleoprotein A3 | 0.281 | 0.159 | 1.370 | 1.011 | 0.381 | 0.159 | 2.390 |
| **Atp5a1** | ATP synthase subunit alpha, mitochondrial | 0.135 | 0.120 | 2.349 | 1.483 | 0.214 | 0.120 | 1.777 |
| **Vdac1** | Voltage-dependent anion-selective channel protein 1 | 0.135 | 0.119 | 1.339 | 0.963 | 0.189 | 0.119 | 1.587 |
| **Ywhab** | 14-3-3 protein beta/alpha | 0.202 | 0.170 | 1.368 | 1.152 | 0.240 | 0.170 | 1.409 |
| **Ywhaq** | 14-3-3 protein theta | 0.206 | 0.196 | 1.765 | 1.340 | 0.272 | 0.196 | 1.388 |
| **Ybx1** | Nuclease-sensitive element-binding protein 1 | 0.204 | 0.173 | 2.401 | 2.038 | 0.240 | 0.173 | 1.386 |
| **Mdh2** | Malate dehydrogenase, mitochondrial | 0.110 | 0.107 | 1.277 | 1.028 | 0.136 | 0.107 | 1.278 |
| **Aldoa** | Fructose-bisphosphate aldolase A | 0.243 | 0.220 | 1.235 | 1.189 | 0.253 | 0.220 | 1.149 |
| **Pebp1** | Phosphatidylethanolamine-binding protein 1 | 0.181 | 0.189 | 1.403 | 1.168 | 0.216 | 0.189 | 1.141 |
| **Nme1** | Nucleoside diphosphate kinase A | 0.1202 | 0.1202 | 1.21 | 1.355 | 0.120 | 0.107 | 1.120 |
| **Ywhag** | 14-3-3 protein gamma | 0.163 | 0.166 | 1.078 | 0.960 | 0.183 | 0.166 | 1.103 |
| **Ywhaz** | 14-3-3 protein zeta/delta | 0.127 | 0.141 | 1.220 | 1.062 | 0.146 | 0.141 | 1.032 |
| **Cdc37** | Hsp90 co-chaperone Cdc37 | 0.183 | 0.212 | 1.338 | 1.162 | 0.211 | 0.212 | 0.997 |
| **Prdx4** | Peroxiredoxin-4 | 0.434 | 0.434 | 0.61 | 0.585 | 0.434 | 0.453 | 0.959 |
| **Gapdh** | Glyceraldehyde-3-phosphate dehydrogenase | 0.114 | 0.093 | 1.483 | 1.920 | 0.088 | 0.093 | 0.940 |
| **Park7** | Protein DJ-1 | 0.1167 | 0.1167 | 0.41 | 0.385 | 0.117 | 0.124 | 0.939 |
| **Gapdhs** | Glyceraldehyde-3-phosphate dehydrogenase, testis-specific | 0.103 | 0.086 | 1.748 | 2.251 | 0.080 | 0.086 | 0.931 |
| **Cyb5a** | Cytochrome b5 | 0.1878 | 0.1878 | 0.915 | 0.84 | 0.188 | 0.205 | 0.918 |
| **Nucb2** | Nucleobindin-2 | 0.5687 | 0.5687 | 0.625 | 0.57 | 0.569 | 0.624 | 0.912 |
| **Pdia3** | protein disulfide isomerase family A, member 3 | 0.192 | 0.204 | 0.856 | 0.900 | 0.183 | 0.204 | 0.898 |
| **Eif4a2** | Eukaryotic initiation factor 4A-II | 0.156 | 0.196 | 1.410 | 1.281 | 0.172 | 0.196 | 0.877 |
| **Cfl1** | Cofilin-1 | 0.245 | 0.262 | 1.386 | 1.497 | 0.226 | 0.262 | 0.865 |
| **Ube2n** | Ubiquitin-conjugating | 0.1561 | 0.1561 | 0.925 | 0.8 | 0.156 | 0.180 | 0.865 |

| Gene Symbol | Protein Name | ZDFd Kinetics (%/day) | ZLC Kinetics (%/day) | ZDFd SILAM | ZLC SILAM | ZDFd Abs (%/day) | ZLC Abs (%/day) | ZDFd/ZLC Abs |
|---|---|---|---|---|---|---|---|---|
| | enzyme E2 N | | | | | | | |
| **Eno1** | Alpha-enolase | 0.136 | 0.125 | 1.026 | 1.285 | 0.108 | 0.125 | 0.863 |
| **Prdx1** | Peroxiredoxin-1 | 0.209 | 0.188 | 1.020 | 1.374 | 0.159 | 0.188 | 0.841 |
| **Hmgb1** | High mobility group protein B1 | 0.082 | 0.109 | 1.282 | 1.332 | 0.079 | 0.109 | 0.723 |

**Table S2. Proteome Wide Normalized Absolute Synthesis Rates In Response to Diabets.** Absolute synthesis rates were calculated for proteins that were identified by (a) kinetics in ZDFd and ZLC animals, and by (b) calculation of the heavy:light ratio from either the TPP suite of software tools or using the in-house algorithm for the identification and quantitation of SILAM peptide pairs.

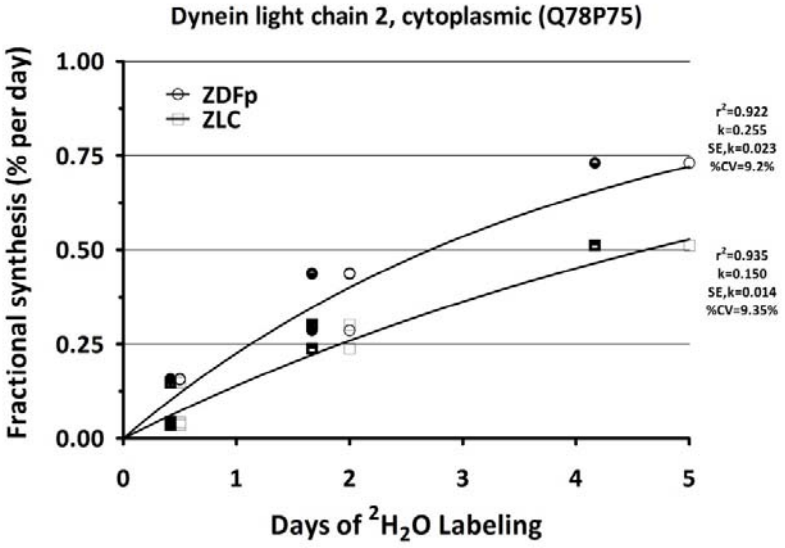


**Figure S1. One-Phase Exponential Protein Curve Fit Reveals Protein Synthetic Rate.** Proteins common to a particular analysis (ZLC-ZDFp or ZLC-ZDFd) are fit with a one-phase exponential association according to the equation $f=1-e^{(-kt)}$ with a $Y_{max}=1$. Proteins were removed from analysis if any of the following criteria were determined to be true: (a) peptide signal intensity less than 30,000 counts, (b) RMS error for unlabeled peptide mass isotopomer abundance measurements greater than 1.5% compared with natural abundance, (c) observation of the parent protein in less than 2 rats per experimental group, (d) a coefficient of variation of the one-phase exponential association curve fit greater than 30%, and (e) an $r^2$ curve fit value less than 0.7. The rate constant (k) was determined for each fit, and used for subsequent downstream calculations.

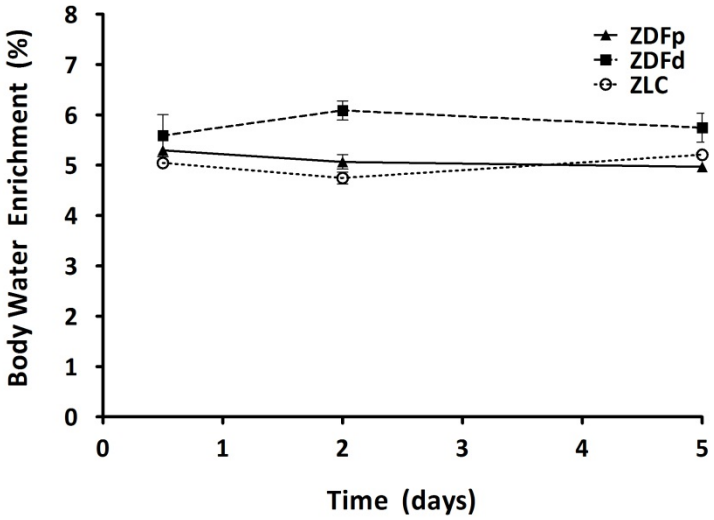


**Figure S2. Body Water Enrichments Over Time.** Animals in each group were labeled with an intraperitoneal injection of 100% $^2H_2O$ (0.35mL/10g body weight), and were provided 8% $^2H_2O$ drinking water for the remainder of the study to maintain target body $^2H_2O$ enrichments of approximately 5%. Actual body $^2H_2O$ enrichments of each animal are used to determine the theoretical peptide enrichments in the calculation of FSR.


**Figure S3. Common Proteins Used In Each Analysis.** (A) Proteins common to ZLC and ZDFp animals were used for the analysis of the effect of insulin resistance on the dynamic islet proteome. (B) Proteins common to ZLC and ZDFd animals were used for the analysis of the effect of diabetes on the dynamic islet proteome.